geodiversitas

2020 • 42 • 30

Cranial anatomy of *Andinodelphys cochabambensis*, a stem metatherian from the early Palaeocene of Bolivia

Christian de MUIZON &
Sandrine LADEVÈZE

art. 42 (30) — Published on 31 December 2020
www.geodiversitas.com

PUBLICATIONS SCIENTIFIQUES

MUSÉUM NAL HIST NATURELLE

COUVERTURE / *COVER*:
Life reconstruction of *Andinodelphys cochabambensis* by Charlène Letenneur: on the left is a complete animal (natural size) grasping on a branch and on the right, on the foreground, is a lateral view of the head.

Geodiversitas est indexé dans / Geodiversitas *is indexed in:*
– Science Citation Index Expanded (SciSearch®)
– ISI Alerting Services®
– Current Contents® / Physical, Chemical, and Earth Sciences®
– Scopus®

Geodiversitas est distribué en version électronique par / Geodiversitas *is distributed electronically by:*
– BioOne® (http://www.bioone.org)

Les articles ainsi que les nouveautés nomenclaturales publiés dans *Geodiversitas* sont référencés par /
Articles and nomenclatural novelties published in Geodiversitas *are referenced by:*
– ZooBank® (http://zoobank.org)

Geodiversitas est une revue en flux continu publiée par les Publications scientifiques du Muséum, Paris
Geodiversitas *is a fast track journal published by the Museum Science Press, Paris*

Les Publications scientifiques du Muséum publient aussi / *The Museum Science Press also publish:* ***Adansonia***, ***Zoosystema***, ***Anthropozoologica***, ***European Journal of Taxonomy***, ***Naturae***, ***Cryptogamie*** **sous-sections** ***Algologie***, ***Bryologie***, ***Mycologie, Comptes Rendus Palevol***

Diffusion – Publications scientifiques Muséum national d'Histoire naturelle
CP 41 – 57 rue Cuvier F-75231 Paris cedex 05 (France)
Tél. : 33 (0)1 40 79 48 05 / Fax : 33 (0)1 40 79 38 40
diff.pub@mnhn.fr / http://sciencepress.mnhn.fr

ISSN (imprimé / *print*) : 1280-9659/ ISSN (électronique / *electronic*) : 1638-9395

Cranial anatomy of *Andinodelphys cochabambensis*, a stem metatherian from the early Palaeocene of Bolivia

Christian de MUIZON
Sandrine LADEVÈZE
CR2P (CNRS, MNHN, Sorbonne Université),
Département Origines et Évolution, Muséum national d'Histoire naturelle,
case postale 38, 57 rue Cuvier, F-75231 Paris cedex 05 (France)

Submitted on 25 November 2019 | accepted on 31 March 2020 | published on 31 December 2020

urn:lsid:zoobank.org:pub:DA30F7AF-FA14-4007-8999-F61BBDDD6772

Muizon C. de & Ladevèze S. 2020. — Cranial anatomy of *Andinodelphys cochabambensis*, a stem metatherian from the early Palaeocene of Bolivia. *Geodiversitas* 42 (30): 597-739. https://doi.org/10.5252/geodiversitas2020v42a30. http://geodiversitas.com/42/30

ABSTRACT

Andinodelphys cochabambensis Marshall & Muizon, 1988 is one of the best preserved metatherian species from the early Palaeocene fauna of Tiupampa (Bolivia). It is represented by five almost complete skulls, three of them being securely associated to sub-complete to partial skeleton. Four skulls could be extracted from a block including several intermingled skeletons. The present paper provides a thorough description of the dental, cranial, and dentary anatomy of *A. cochabambensis*. The cranial anatomy of *A. cochabambensis* is similar to that of *Pucadelphys andinus*. The skull of *Andinodelphys* however differs from that of *Pucadelphys* in its larger size and proportionally longer rostrum. Other differences include the presence, in *Andinodelphys,* of large anteriorly protruding I1s, small palatal vacuities, a transverse canal, and a small hypotympanic sinus. *Andinodelphys* has the same dental formula as *Pucadelphys* (I 5/4, C 1/1, P 3/3, M4/4), the plesiomorphic condition for metatherians. Furthermore, both genera share the lack a tympanic process of the alisphenoid, a deep groove for the internal carotid artery at the anterior apex of the promontorium, a small prootic canal perforating the lateral edge of the petrosal and opening laterally in the deep sulcus for the prootic sinus, and a vestigial anterior lamina of the petrosal. Dentally *Andinodelphys* closely resembles *Pucadelphys*, the two genera differing in the larger size of the former and in the inconstant presence in the former of a twinned stylar cusp C. Although 25% smaller, the cheek teeth of *Andinodelphys* closely resemble those of *Itaboraidelphys camposi* from the early Eocene of Itaboraí (Brazil). As far as dental morphology is concerned, both genera are likely to have diverged from a direct common ancestor, probably *Andinodelphys*-like, with *Itaboraidelphys* displaying more derived dental structures. Two isolated petrosal from Itaboraí (Type 2 petrosals) are morphologically close to those of *Andinodelphys* but distinctly larger. In this paper, a previous interpretation including the teeth of *Itaboraidelphys* and these petrosals in the same taxon is followed. A phylogenetic analysis retrieved *Itaboraidelphys* as a sister taxon of the clade *Pucadelphys* + *Andinodelphys*, thus lending support to inclusion of the former in the Pucadelphyidae. Three sets of parsimony analyses were performed. A first set of analyses (with all characters) retrieved a strict

consensus tree with a clade as follows: (pucadelphyids, (deltatheroidans (stagodontids, Gurlin Tsav skull-GTS), sparassodonts)). An implied weighting analysis with the same data matrix placed the stagodontids in an early diverging position but retained a clade (pucadelphyids, (deltatheroidans, (GTS, sparassodonts))), the deltatheroidans, being therefore inserted in the pucadelphydans. This result implies an independent arrival of pucadelphyids and sparassodonts to South America, which consequently must have been present in North America in the Late Cretaceous. Possible North American sparassodonts could be the poorly known genera *Atokatheridium* and *Olklatheridium* (currently referred to deltatheroidans) and the pucadelphyids may have been present in the Late Cretaceous of North America with the genus *Aenigmadelphys*. However, this hypothesis is less parsimonious (with regard to palaeobiogeography) than a single southward migration of an ancestral Pucadelphyda (Pucadelphyidae + Sparassodonta). Because the result of this first set of analyses may have been induced by heavily homoplastic dental characters related to hypercarnivory, a second set of analyses was performed excluding all the dental characters. The strict consensus is poorly resolved but retains monophyletic Marsupialia and Sparassodonta. An implied weighting analysis retrieved a monophyletic Pucadelphyda but split the deltatheroidans, the polyphyly of which is regarded as a possible artefact related to the lack of dental characters. The GTS is sister taxon to Pucadelphyda. Because the polyphyly of deltatheroidans contradicts all previous hypotheses, a third set of analyses has been performed excluding only those molar characters that supported the close relationships of the hypercarnivorous clades (deltatheroids, stagodontids, and sparassodonts). The strict consensus tree retrieved monophyletic deltatheroidans, Marsupialia and sparassodonts. An implied weighting analysis resulted in deltatheroidans forming a paraphyletic stem assemblage of Metatheria and monophyletic Pucadelphyda. The GTS was no longer related to sparassodonts but was the sister taxon of a clade including the North American taxa of the data matrix, *Asiatherium*, and Marsupialia. This topology, which is favoured here, supports (as well as that of the second set of analyses) a single pucadelphydan southward migration, probably in the Late Cretaceous, with a Tiupampian radiation of South American carnivorous metatherians.

KEY WORDS
Mammalia,
Metatheria,
Pucadelphyidae,
cranial anatomy,
phylogeny,
Early Palaeocene,
Bolivia.

RÉSUMÉ
*Anatomie cranienne d'*Andinodelphys cochabambensis*, un stem-métathérien du Paléocène inférieur de Bolivie.*
Andinodelphys cochabambensis Marshall & Muizon, 1988 est l'une des espèces de métathériens les mieux conservées de la faune du Paléocène inférieur de Tiupampa (Bolivie). Elle est représentée par cinq crânes presque complets, trois d'entre eux étant associés à des squelettes sub-complets ou partiels. Le présent travail fournit une description détaillée de l'anatomie des dents, du crâne et du dentaire d'*Andinodelphys cochabambensis*. L'anatomie crânienne d'*A. cochabambensis* est semblable à celle de *Pucadelphys andinus*. Toutefois, le crâne d'*Andinodelphys* diffère de celui de *Pucadelphys* par sa taille plus grande et son rostre proportionnellement plus long. D'autre différences incluent la présence, chez *Andinodelphys*, de I1s plus grandes que les autres incisives et projetées antérieurement, de petites fenêtres maxillopalatines, d'un canal transverse et d'un sinus hypotympanique. *Andinodelphys* a la même formule dentaire que *Pucadelphys* (I 5/4, C 1/1, P 3/3, M4/4), qui constitue la condition plésiomorphe pour les métathériens. De plus, les deux genres partagent l'absence de processus tympanique de l'alisphénoïde, un profond sillon pour la carotide interne à l'apex antérieur du promontoire, un petit canal prootique perforant le bord latéral du pétreux et s'ouvrant latéralement dans le profond sillon pour le sinus prootique et une lame antérieure vestigiale du pétreux. Sur le plan dentaire *Andinodelphys* ressemble étroitement à *Pucadelphys,* les deux genres différant par la taille plus grande du premier et par la présence inconstante, chez le premier, d'une cuspide stylaire C dédoublée. Bien que 25% plus petites, les dents jugales d'*Andinodelphys* ressemblent beaucoup à celles d'*Itaboraidelphys camposi* de l'Eocène inférieur d'Itaboraí (Brésil). Du point de vue de leur morphologie dentaire, les deux genres ont très probablement divergé d'un morphotype ancestral de type *Andinodelphys*, avec *Itaboraidelphys* présentant une condition plus dérivée. Deux pétreux isolés d'Itaboraí (pétreux de type 2) sont morphologiquement très semblables à ceux d'*Andinodelphys*, mais nettement plus grands. Dans ce travail, une interprétation suggérée antérieurement, incluant les dents d'*Itaboraidelphys* et ces deux pétreux dans le même taxon, est entérinée. Une analyse phylogénétique résulte en un placement d'*Itaboraidelphys* comme taxon frère du clade *Andinodelphys* + *Pucadelphys*, supportant de ce fait le placement du premier parmi les Pucadelphyidae. Trois séries d'analyses de parcimonie ont été réalisées. Une première série d'analyses (avec tous les caractères) a produit un consensus strict avec un clade comme suit : (pucadelphyidés (deltathéroïdes (stagodontidés, crâne de Gurlin Tsav – GTS) sparassodontes)). Une analyse avec pondération implicite (Implied Wheighting) des caractères utilisant la même matrice de données a fait diverger les stagodontidés plus tôt sur l'arbre mais a maintenu le clade (pucadelphyidés, (deltathéroïdes (GTS, (sparassodontes))), les

deltathéroïdes étant donc insérés dans les Pucadelphyda (Pucadelphyidae + Sparassodonta). Ce résultat implique une arrivée en Amérique du Sud, indépendante, des pucadelphyidés et des sparassodontes qui, en conséquence, doivent avoir été présent en Amérique du Nord au Crétacé supérieur. De possible sparassodontes nord-américains pourraient être les genres mal connus que sont *Atokatheridium* et *Oklatheridium* (actuellement rapportés aux deltathéroïdes) et les pucadelphyidés étaient peut-être représentés dans le Crétacé supérieur nord-américain par le genre *Aenigmadelphys*. Toutefois, cette hypothèse est paléobiogéographiquement moins parcimonieuse qu'une seule migration vers le sud d'un Pucadelphyda ancestral. Comme le résultat de ce premier jeu d'analyse a peut-être été induit par des caractères dentaires liés à l'hypercarnivorie, bien connus pour être fortement homoplastiques, une deuxième série d'analyses a été réalisée en excluant tous les caractères dentaires. Le consensus strict obtenu est mal résolu, mais conserve la monophylie des Marsupialia et des Sparassodonta. Une analyse avec pondération implicite des caractères a produit des Pucadelphyda monophylétiques mais a éclaté les deltathéroïdes dont la polyphylie est considérée comme un artéfact probable dû à l'absence de caractères dentaires. La polyphylie des deltathéroïdes étant en contradiction avec toutes les hypothèses antérieures, une troisième série d'analyses a été réalisée en excluant seulement les caractères des molaires qui soutenaient les relations étroites des clades hypercarnivores (deltathéroïdes, GTS, stagodontidés et sparassodontes). L'arbre de consensus strict obtenu soutient la monophylie des deltathéroïdes, des Marsupialia et des sparassodontes. Une analyse avec pondération implicite résulte en une position des deltathéroïdes en groupe paraphylétique basal aux métathériens et soutient la monophylie des Pucadelphyda. Le GTS n'est plus apparenté aux sparassodontes mais constitue le taxon frère d'un clade incluant les taxons nord-américains de la matrice de données, *Asiatherium* et les Marsupialia. Cette topologie, qui est privilégiée ici, soutient (tout comme celle résultant de la deuxième série d'analyses) la possibilité d'une migration unique vers le sud des Pucadelphyda, probablement au Crétacé supérieur, avec une radiation tiupampienne de métathériens carnivores sud-américains.

MOTS CLÉS
Mammalia,
Metatheria,
Pucadelphyidae,
anatomie crânienne,
phylogénie,
Paléocène inférieur,
Bolivie.

INTRODUCTION

The early evolutionary history of metatherians is poorly known, especially because most of the taxa in the Cretaceous and early Tertiary are represented by isolated teeth or, at the best, by jaws. Skulls and skeletons are extremely rare and the few ones known are generally badly crushed or very incomplete. Until recently *Sinodelphys szalayi* from the Early Cretaceous of the Yixian Formation of China (Luo *et al.* 2003) was regarded as the oldest metatherian. However, the recent analysis by Bi *et al.* (2018) resulted in including *Sinodelphys* within the Eutheria. Be that as it may, it is noteworthy that, although remarkably complete, the holotype and single known specimen of *S. szalayi* is extremely crushed and does not provide information on its cranial anatomy and little on its dental anatomy. *Asiatherium reshetovi* Trofimov & Szalay, 1994 and *Deltatheridium pretrituberculare* Gregory & Simpson, 1926 from the late Cretaceous of Mongolia are more informative but are known from specimens whose skulls are either crushed (the former, Szalay & Trofimov 1996) or very incomplete (the latter, Rougier *et al.* 1998). In their description of *Asiatherium*, Szalay & Trofimov (1996: fig. 22) illustrate the remarkably well-preserved undistorted skull of a metatherian from Mongolia. Although still undescribed, this skull is clearly the best-preserved and most complete metatherian skull from the Cretaceous. As a matter of fact, it is commonly included in metatherian phylogenies and is currently referred to as "the Gurlin Tsav skull". Recently, two remarkable discoveries have been published, which provide a welcome information on the cranial evolution of Late Cretaceous metatherians. The first specimen is a complete skull of a new deltatheroidan from the Henan province of China (Bi *et al.* 2015) referred to a new taxon, *Lotheridium mengi*. The second discovery concerns sub-complete and partial skulls of the North American Late Cretaceous stagodontid *Didelphodon vorax* (Wilson *et al.* 2016). So far, no other metatherian skull has been described from the Late Cretaceous, but it is noteworthy that the discovery of skulls of *Alphadon halleyi* from the late Cretaceous of Montana has been mentioned by Brannick *et al.* (2016), although their description is still in progress. Well-preserved and complete metatherian remains from the early Tertiary are not common either. The oldest known metatherian skulls and skeleton from the Cenozoic are from the basal Palaeocene (*c.* 65 Ma, see Muizon *et al.* 2015, 2018, and below) of Tiupampa (Bolivia). The Tiupampa metatherian skulls and skeletons are the only ones known in Palaeocene deposits; partial metatherian skulls are known in the early Eocene of Brazil (Paula Couto 1952a; Beck 2017) and Argentina (Pascual 1980, 1981). The locality of Tiupampa has yielded at least 15 species of metatherians among which three are represented by uniquely complete skulls and skeletons. The most abundant taxon is by far *Pucadelphys andinus*, a *Dromiciops*-sized metatherian, which is known by 35 complete or partial skulls and skeletons (Marshall & Muizon 1988, Marshall *et al.* 1995; Ladevèze *et al.* 2011), some of them exceptionally preserved. The second most abundant taxon represented by skulls and skeletons is *Andinodelphys cochabambensis*. This taxon was first described on the basis of an upper molar (holotype) and

a referred lower molar (Marshall & Muizon 1988) (Fig. 1), but during the 1996 field season at Tiupampa, five partial or sub-complete skulls and skeletons have been recovered (Muizon *et al.* 1997) (Figs 2, 3). A third taxon, *Mayulestes ferox*, is an early sparassodont known by an almost complete (but dorsoventrally crushed) skull associated to a partial skeleton (Muizon 1994, 1998). Some other taxa are known by nearly complete or partial skulls such as the sparassodont *Allqokirus australis*, that has been recently described (Muizon *et al.* 2018), and five other specimens referred to *Mizquedelphys pilpinensis* Marshall & Muizon, 1988 (two sub-complete skulls and two partial skulls) and *Incadelphys antiquus* Marshall & Muizon, 1988 (one partial skull) currently under study by the authors. The other metatherians of Tiupampa are known by jaws and teeth only (Muizon 1992). The anatomy of the skull and postcranial skeleton of *Pucadelphys andinus*, *Mayulestes ferox,* as well as that of the skull of *Allqokirus australis* have been thoroughly described in earlier works (Marshall & Muizon 1995; Muizon 1998; Muizon *et al.* 2018). In contrast, only a preliminary description of the skulls of *Andinodelphys cochabambensis* has been provided by Muizon *et al.* (1997), although isolated petrosals have been described by Ladevèze & Muizon (2007). In the present paper, we intend to comprehensively describe the skull and dentition of *Andinodelphys cochabambensis* and to perform parsimony analyses in order to evaluate its phylogenetic affinities and to address the relationships of the major groups of American carnivorous metatherians. In particular, potential close relationships of *Andinodelphys* with the Itaboraian genus *Itaboraidelphys,* as suggested by Marshall & Muizon (1988) and Muizon *et al.* (2018), will be investigated.

AGE OF THE TIUPAMPA MAMMAL FAUNA

The Tiupampa fauna was discovered in 1982 by a French-US-Bolivian paleontological expedition in the Vila-Vila outcrop, a large exposure of red-beds in Mizque Province (Cochabamba Department, Bolivia). These red beds were initially referred to the El Molino Formation, which was correlated to the Late Cretaceous (Marshall *et al.* 1983; Muizon *et al.* 1983). Consequently, the mammals collected at Tiupampa were initially given a Late Cretaceous age (Maastrichtian) (Marshall *et al.* 1983, 1985; Marshall & Muizon 1988; Muizon *et al.* 1984). Subsequent studies brought to light the fact that the Vila Vila outcrop also included beds of the Santa Lucía Formation, which are considered to be Palaeocene (Sempere *et al.* 1997) and which yielded the Tiupampa mammal fauna. Although a Palaeocene age is now commonly accepted for the Tiupampa fauna, interpretations diverge on the age of the fauna within the Palaeocene. Marshall *et al.* (1997) and Sempere *et al.* (1997), on the basis of sedimentological and palaeontological (but see below) arguments, concluded that the Tiupampa mammal bearing beds correspond to the middle to late Santa Lucía Formation, and are included in a single reversed magnetostratigraphic series, which they correlated to Chron 26r. This Chron corresponds to the early Selandian (*c.* 58 Ma to 60 Ma), i.e. the early middle Palaeocene. Sempere *et al.* (1997) also reported the mammal fauna of Punta Peligro (Chubut Province, Patagonia, Argentina) to be older than that of Tiupampa and referred the former to the earliest Selandian or latest Danian (*c.* 62 to 60 Ma). This interpretation was followed by Pascual & Ortiz-Jaureguizar (2007: table 1), although these authors implicitly concluded that the Punta Peligro therians feature a South American cachet, whereas the Tiupampa fauna mainly retains a North American hallmark.

A different interpretation was given by Gelfo *et al.* (2009), Woodburne *et al.* (2014a, b), and Muizon *et al.* (2015, 2018), who considered the Tiupampa mammal fauna to be early Palaeocene (Danian) and older than the Punta Peligro fauna. Gelfo *et al.* (2009) employed two different methods, a cluster analysis and a parsimony analysis based on the Parsimony Analysis of Endemicity (PAE; Rosen 1988) and the Cladistics Analysis of Distribution and Endemism (CADE; Porzecanski & Cracraft 2005). Gelfo *et al.* (2009) concluded that the Tiupampa mammal fauna predated the Punta Peligro assemblage. Because the Tiupampa beds are included in a single reversed magnetostratigraphic series (following Sempere *et al.* 1997), Gelfo *et al.* (2009) correlated the Tiupampa beds with polarity Chron 28r, equivalent to the Puercan 3 (*c.* 64 to 64.5 Ma) of North America at that time (see Gelfo *et al.* [2009] and below for discussion on the referral of the Tiupampa mammal-bearing beds to Chron 28r rather than to Chron 26r as suggested by Sempere *et al.* [1997]). However, new calibration of the early Palaeocene NALMAs (Sprain *et al.* 2015, 2018) modified the age and position of Chron 28r relative to the NALMAs. According to Sprain *et al.* (2018: fig. 12) the lower limit of Chron 28r is bracketed between 65.075 Ma and 64.868 Ma (Fig. 4). The Torrejonian 1 spans the period from 65.041 Ma (Sprain *et al.* 2018) to *c.* 63.5 Ma (Vandenberghe *et al.* 2012; Flynn *et al.* 2020). On the basis of the calibrations of Sprain *et al.* (2015), which are very similar to those of Sprain *et al.* (2018), Muizon *et al.* (2015) correlated the mammal-bearing beds at Tiupampa, to the base of Torrejonian 1 and evaluated an age of approximately 65 Ma for the Tiupampa mammals, an interpretation followed here. Therefore, the longevity of the Tiupampa mammals probably does not exceed 0.2 Ma (the approximate duration of Chron 28r according to Sprain *et al.* 2018; see Fig. 4). Consequently, the time span of the Tiupampan in Woodburne *et al.* (2014a and b: fig. 2) and in Goin *et al.* (2016: fig. 7.2) should be significantly shortened.

Nevertheless, the age of the Tiupampa mammal fauna is still considered to be controversial by Eldridge *et al.* (2019), although these authors do not provide arguments in support of their conclusion. Eldridge *et al.* (2019) accepted the Danian age of the Punta Peligro fauna (Argentina) suggested by Sempere *et al.* (1997) but did not discuss the evidence provided by others (Gelfo *et al.* 2009; Muizon *et al.* 2015, 2018), who consider that the Tiupampa mammal fauna is older than that of Punta Peligro (therefore, early Danian in age). It is noteworthy that the latter interpretation is now commonly accepted by most authors (e.g., Rose 2010; Goin *et al.* 2012; Oliveira & Goin 2012; Woodburne *et al.*

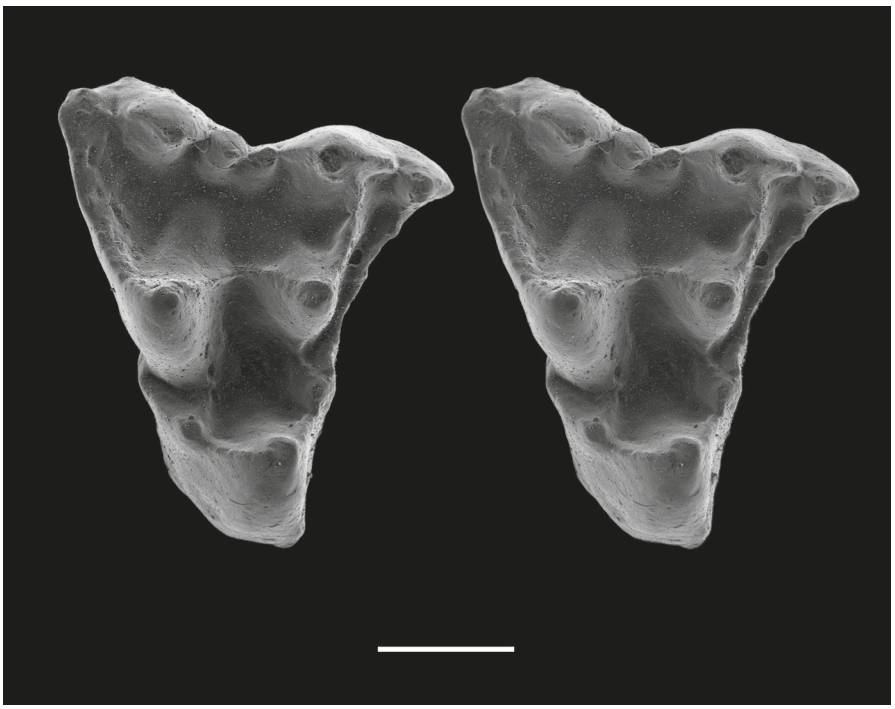

Fig. 1. — *Andinodelphys cochabambensis* (YPFB Pal 6192). SEM stereophotograph of the holotype: a right M2. Scale bar: 1 mm.

2014a, b; Reguero *et al.* 2014; Forasiepi *et al.* 2015; Goin *et al.* 2016; Babot *et al.* 2017; Carneiro 2018; Carneiro *et al.* 2018; Bauzá *et al.* 2019), who were not cited, however, by Eldridge *et al.* (2019). Croft *et al.* (2020) also followed the same interpretation.

Recently, Zimicz *et al.* (2020) went back to the paleomagnetic correlation arguments of Sempere *et al.* (1997), whom they followed, considering that the Tiupampa beds and fauna correlate with Chron 26r. Moreover, Zimicz *et al.* (2020: 8) further stated that there is a "[...] large amount of recent geological evidence reinforcing the Sempere's correlation of Santa Lucía beds with Chron 26r (e.g. Horton *et al.* 2001; DeCelles & Horton 2003; Demouy *et al.* 2012; Rak *et al.* 2017; Calle *et al.* 2018)." However, it is noteworthy that, most of these papers did not discuss directly the age of the Tiupampa fauna. Horton *et al.* (2001) and DeCelles & Horton (2003) mentioned the age of the Santa Lucía Formation, but without a critical reconsideration. Horton *et al.* (2001) did not provide new data on the problem or did not present arguments different from those of Gelfo *et al.* (2009). They simply cited Sempere *et al.* (1997) as the source of the referral of the Santa Lucía Formation to Chron 26r. Furthermore, considering the lithostratigraphic correlations established by Sempere *et al.* (1997) to justify their interpretation of the age of the Santa Lucía Formation at Tiupampa, Horton *et al.* (2001: 1389) stated that: "Despite successful dating of the Santa Lucía in several Bolivian locales, regional lithostratigraphic correlations over hundreds of kilometers remain tentative". DeCelles & Horton (2003) do not provide either new evidence concerning the age of the Santa Lucía Formation and its referral to Chron 26r, but only refer, in this respect, to Sempere *et al.* (1997). However, interestingly DeCelles & Horton (2003: fig. 13) illustrate the stratigraphic extension of the Santa Lucía Formation as approximately spanning the period 59 to 65 Ma, thereby, extending the lower limit of the formation to the lower Danian. Demouy *et al.* (2012) did not even mention the Santa Lucía Formation nor any polarity Chron for it and Rak *et al.* (2017) and Calle *et al.* (2018), did not comment on the correlation of Santa Lucía beds to Chron 26r. In fact, the "large amount of geological evidences" mentioned by Zimicz *et al.* (2020) are simply references to the interpretation of Sempere *et al.* (1997) with no critical discussion or new data. Therefore, *in essence*, the new interpretation of Zimicz *et al.* (2020) is based only on the argument of Sempere *et al.* (1997) to suggest a younger age for the Tiupampa beds, because the five geological references they mentioned are inappropriate to support their argument. Furthermore, Zimicz *et al.* (2020) provided neither new geological data nor critical discussion based on new paleontological arguments (see below for comments on their interpretation of the presence of *Peradectes* at Tiupampa and on the primitive morphologies that characterize the Tiupampa fauna). In this context, it is worth recalling that Sempere *et al.* (1997) based the main evidence justifying their assignment and their conclusions on: 1) paleontological arguments and 2) correlation of the Tiupampa profile to the one at La Palca, where the El Molino and Santa Lucía units are better exposed. However, as is concluded by Sempere *et al.* (1997: 718, 719): "A simple one-to-one correlation of the La Palca polarity zonation to the geomagnetic polarity time scale is not evident (Fig. 10). The correlation shown in Figures 10 and 11 is our preferred interpretation because it is corroborated by the paleontologic data and agrees with a number of facts discussed below." Therefore, Sempere *et al.*

FIG. 2. — *Andinodelphys cochabambensis*. Block containing intermingled bones referred at least to six individuals.

(1997) implicitly admitted that there are alternative interpretations. It is therefore unclear why Zimicz *et al.* (2020) dismissed most of the paleontological evidence provided by Gelfo *et al.* (2009) (but see comments below), which was, in fact, the same kind of evidence (but with a larger faunal sample per locality) that led Sempere *et al.* (1997), in partial view of the knowledge of the Tiupampa fauna by that time, to assign Santa Lucía and the upper part of the El Molino Formation to Chron 26r.

To conclude, because of the controversy mentioned by Eldridge *et al.* (2019) and the comments of Zimicz *et al.* (2020), and because paleontological data were regarded by Sempere *et al.* (1997) as partly supporting their interpretation, we consider it useful to review here the paleontological data that can, in the light of the new paleontological discoveries and studies since the publication of the Sempere *et al.* (1997) paper, support the anteriority of the Tiupampa mammal fauna relative to that of Punta Peligro and its correlation to the early Danian as advocated here.

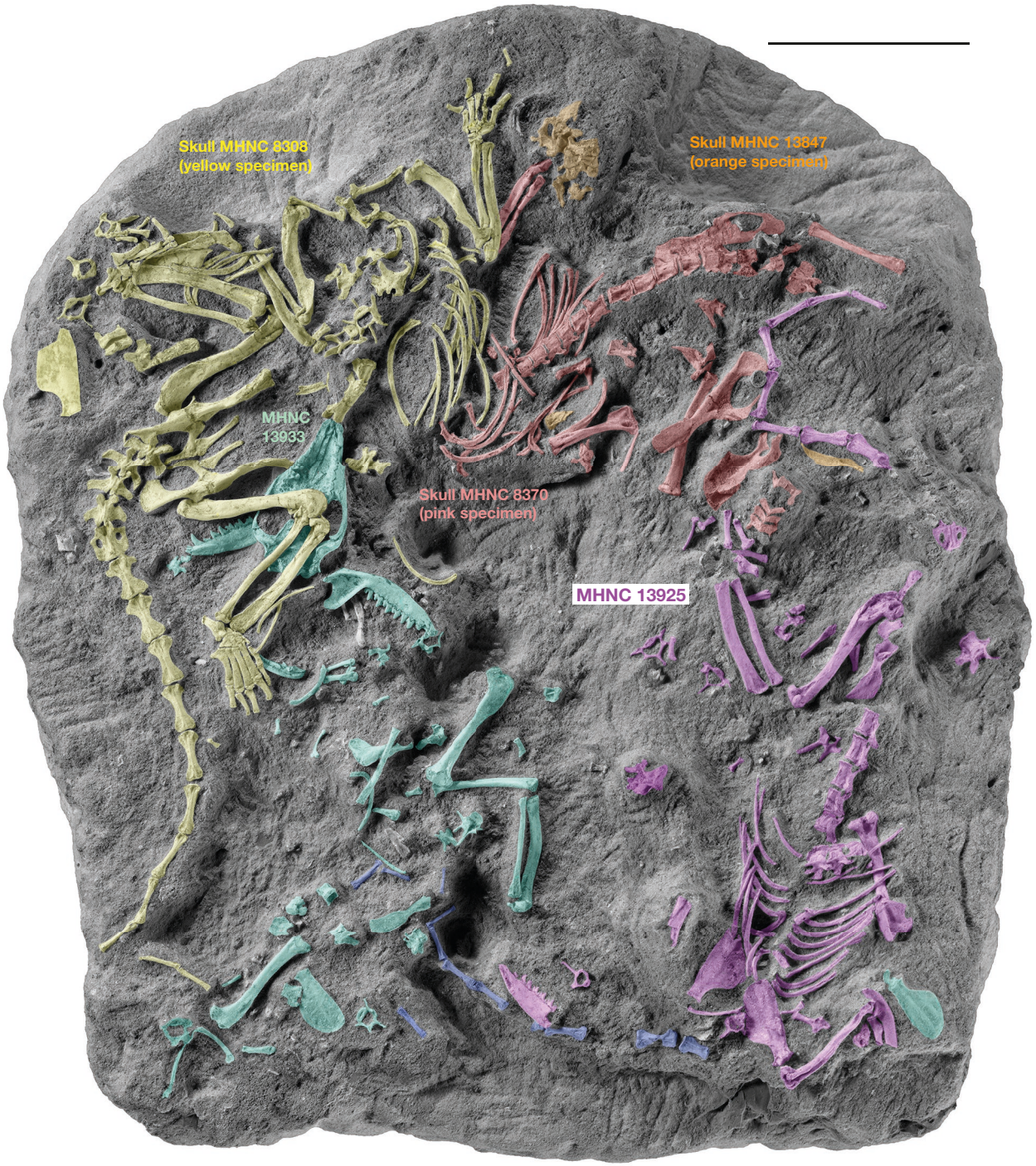

FIG. 3. — *Andinodelphys cochabambensis*. The same specimen as on Fig. 2 highlighting four major sets of bones (yellow, pink, purple, and green) probably referred each one to the same partial skeleton. Scale bar: 5 cm.

Because no direct radiometric dates are available at Tiupampa or at Punta Peligro and because magnetostratigraphic studies are inconclusive (Tiupampa beds are included in a single reversed magnetostratigraphic series), comparison of the evolutionary grades of the two faunas is the only criterion on which to base their relative ages and provide information on their absolute age (Gelfo *et al.* 2009). It is clear that the conclusions of such a comparison in the case of a small number of taxa could be questioned. However, in the case of taxonomically abundant faunas, if all (or most of) the species provide the same convergent information, the conclusions are obviously more reliable. Therefore, the Tiupampa mammal fauna (exclusively therians) with 22 described species (plus two undescribed ones) and the Punta Peligro fauna, which includes at least 9 therian species, can be compared with some degree of confidence.

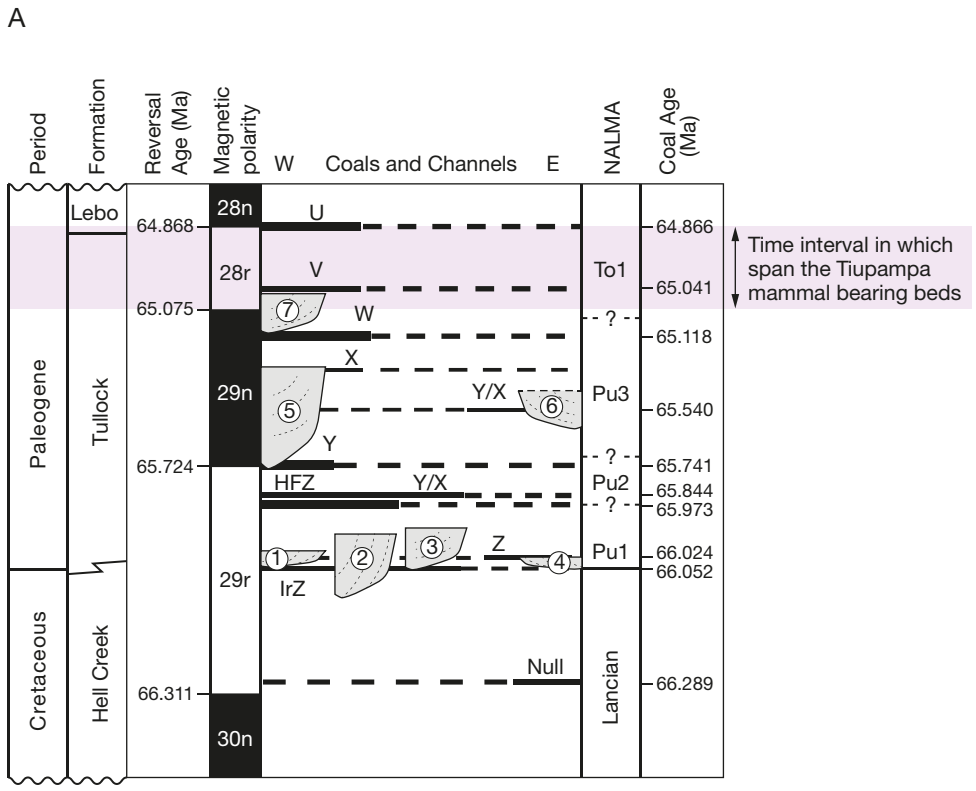

FIG. 4. — **A**, Reproduction of figure 12 of Sprain *et al.* (2018), modified, showing the calibration and correlations of Chrons 30n to 28n with NALMAs from Lancian to Torrejonian 1, to which have been superimposed (pink) the probable age span of the Tiupampa mammal-bearing beds relative to the early Palaeocene NALMAs.

The comments by Zimicz *et al.* (2020: 8) employed to refute such an analysis are discussed here. Concerning the primitive morphologies that characterize the Tiupampa mammal fauna, these authors expressed that: "the 'primitiveness' of the taxa present in the Tiupampan fauna could be explained by ecological factors, latitudinal effects or insularity (Ortiz-Jaureguizar *et al.*, 1999; Pascual and Ortiz-Jaureguizar, 2007; Ortíz-Jaureguizar and Pascual, 2011), without the necessity to invoke the 'evolutionary state of taxa'". They may be correct… or not. Nevertheless, given the dramatically poor record of the therian mammal faunas securely referred to the Palaeocene in South America (five localities/faunas [Grenier Farm tooth, Tiupampa, Punta Peligro, and Mealla Formation faunas and *Carodnia* faunal zone] and approximately 38 species [of which 22 are from Tiupampa] spanning 10 million years), the statement by Zimicz *et al.* (2020) is highly speculative and cannot be taken seriously especially given that these authors do not provide any factual element to support their suggestion. Furthermore, concerning the ecological factors that could explain the faunistic differences between Tiupampa and the higher latitudes of Punta Peligro, the paleoclimatic interpretations are noteworthy. At Punta Peligro, the alligatorids and chelids associated with the mammal fauna (Bonaparte *et al.* 1993) indicate a warm, probably subtropical climate, since the presence of crocodiles indicated a mean annual temperature equal to or higher than 14.2°C (Markwick 1998). This estimation is reinforced by the mean annual temperature estimation of 14.1 ± 2.6°C, based on the leaf analyses of the megaflora, which underlies the BNI ("Banco Negro Inferior") (Iglesias *et al.* 2007). These paleoclimatic conditions are not so different from those present in Tiupampa, where the occurrence of dyrosaurids is an indication of warm intertropical conditions (Jouve *et al.* 2020). Therefore, because, the paleoclimatic environments at Punta Peligro and Tiupampa were probably similar, they are inadequate to explain the "primitiveness" of the Tiupampa fauna as compared to that of Punta Peligro.

Now, the critical issue of the present discussion is to determine whether the Tiupampa beds are included in Chron 26r (as concluded by Sempere *et al.* 1997) or in Chron 28r (following Gelfo *et al.* 2009). In this debate, it is essential to evaluate the relative age of the Tiupampa and Punta Peligro faunas, since the latter is apparently now well-calibrated.

Punta Peligro is located in San Jorge Gulf, 40 km northeast of Comodoro Rivadavia city, Chubut Province, Argentina. The faunistic assemblage came from the so-called "Banco Negro Inferior" (BNI) i.e. lower black level, of the marine Salamanca Formation. The first estimation suggested an age of 62.6 ± 5.0 Ma for a tuff at the top of the Salamanca Formation (Andreis 1977, and recalculated following Dalrymple 1979, *sensu* Iglesias *et al.* 2007). On the basis of paleomagnetic evidence, Marshall *et al.* (1981) estimated an age of 62 Ma for the BNI. A reinterpretation of this data led Bonaparte *et al.* (1993) to suggest an age between 63 and 61.8 Ma for the BNI. Other attempts to interpret paleomagnetic information of the BNI in order to infer the age of the fauinistic assemblage were carried out by Somoza *et al.* (1995) who proposed

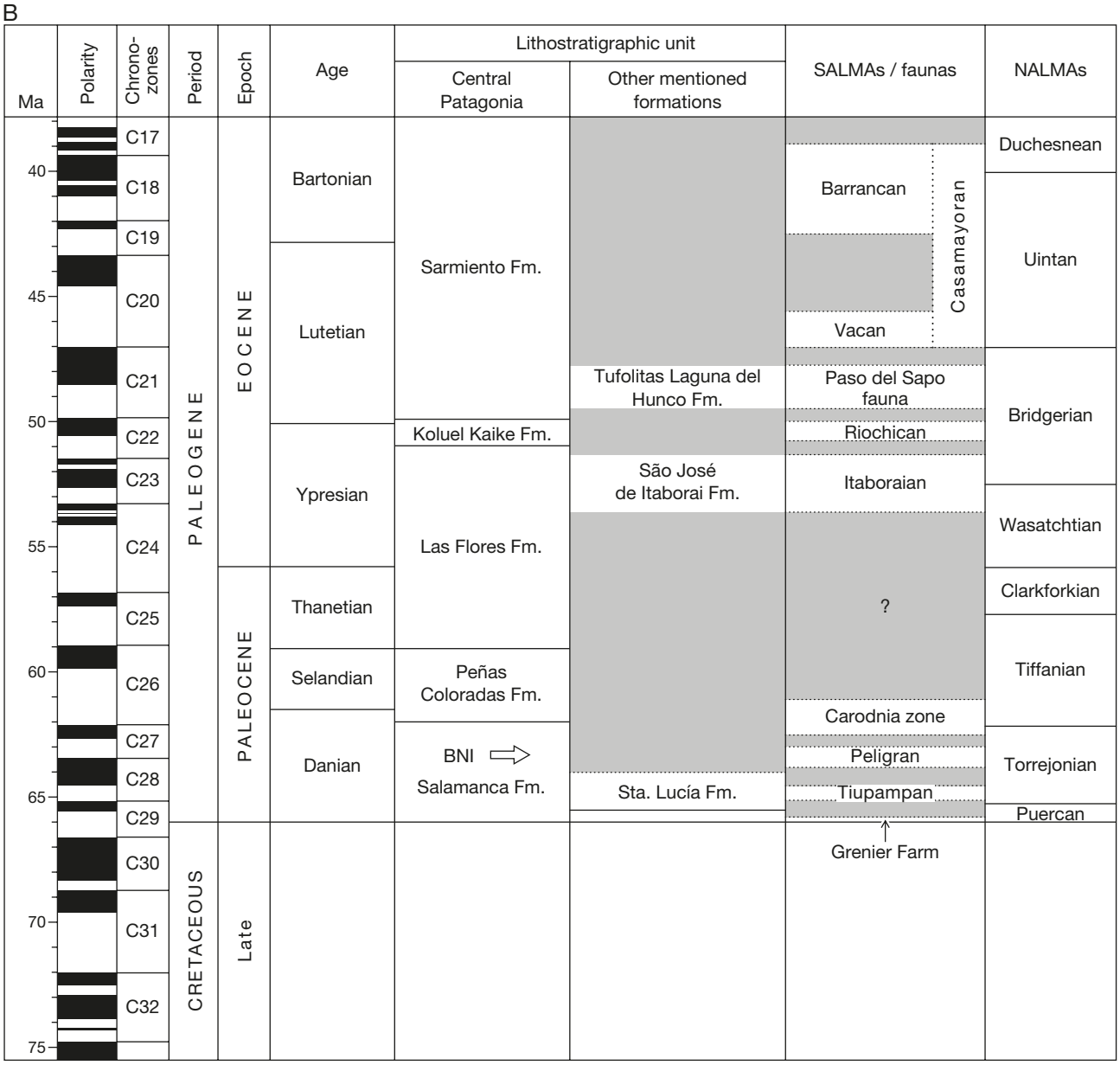

FIG. 4. — **B**, Chronostratigraphic diagram showing the correlation between the Tiupampa fauna and the absolute and magnetostratigraphic calibration, the general stratigraphic timetable, the North American Land Mammal Ages (NALMA) and the South American Land Mammal Ages (SALMA) (Modified from Gelfo *et al.* [2009], taking into account the new calibration of the Chron 28r in Gradstein *et al.* [2012] and Sprain *et al.* [2018], the new radiometric dating of Clyde *et al.* [2014] and Woodburne *et al.* [2014a]).

an age between 61.9 and 61.5 Ma; and lastly by Gelfo *et al.* (2009) and Woodburne *et al.* (2014a) who suggested a span between 61.7 to 60.8 Ma.

According to Clyde *et al.* (2014), the BNI, which has yielded the Punta Peligro fauna, is referred to Chrons 27r and 28n. More precisely, Clyde *et al.* (2014: 301 and fig 10) concluded that the BNI "is progradational from West to East and correlates to the top of Chron C28n near Sarmiento [in Ormaechea] and to the base of Chron C27r (63.49 Ma) along the coast", i.e. at Punta Peligro. Therefore, the Punta Peligro mammal fauna is Danian (*c.* "middle" Danian) in age.

Furthermore, another indication of the age of the Tiupampa beds can be obtained in the light of the undeniable North American affinities of the Tiupampa fauna. Therefore, an attempt to correlate the Tiupampan SALMA with the very precisely calibrated Palaeocene NALMAs must also be considered on the basis of a careful comparison of the Tiupampa mammal fauna with those of the Late Cretaceous and Palaeocene of North America.

The Punta Peligro fauna includes metatherian taxa such as *Derorhynchus* and *Didelphopsis,* which are also present in the early Eocene of Itaboraí and in the middle Eocene of Antarctica (*Derorhynchus)* (Marshall 1987; Goin *et al.* 1999; Oliveira & Goin 2012; Gelfo *et al.* 2007, 2019). In this respect, it is worth noting that the specimen DGM 803-M (a maxillary fragment with M1-M2 from Itaboraí), referred by Marshall (1987) to

Carolopaulacoutoia itaboraiensis, has been referred by Oliveira & Goin (2012) to *Derorhynchus singularis*, an interpretation followed here. Furthermore, bonapartheriid polydolopimorphs are present at Punta Peligro and are also recorded in the early Eocene of the Lumbrera Formation and in the middle Eocene of the Geste Formation of Northwestern Argentina (Pascual 1980, 1981; Goin *et al.* 1998; Pascual & Ortiz-Jaureguizar 2007; Gelfo *et al.* 2007; Woodburne *et al.* 2014a; Babot *et al.* 2017) as well as in the early Eocene of Brazil at Itaboraí (Beck 2017). These taxa from Punta Peligro (*Derorhynchus*, *Didelphopsis,* Bonapartheriidae) are relevant to the debate because the groups to which they belong ("Didelphimorphia" and Polydolopimorphia) are represented at Tiupampa by species that clearly exhibit more plesiomorphic features. The derived robust crushing molars, the large P3 (based on alveoli) and the large and inflated p3 of *Didelphopsis* are absent in any of the Tiupampa metatherians. Furthermore, several dental characters of *Derorhynchus* are more derived than in any of the Tiupampa "didelphimorphs". They are, for instance, in *Derorhynchus,* the greater size difference between the paracone and metacone, the lack of ectoflexus, the greater size of the stylar cusp C, the lower trigonid, the talonid of M2-3 wider than the trigonid and the larger entoconid, which is higher than the hypoconid. Furthermore, it is noteworthy that Gelfo *et al.* (2007) referred the Derorhynchidae recorded at Punta Peligro to *Derorhynchus* aff. *D. minutus*, a species present in the middle Eocene of Antarctica (Goin *et al.* 1999; Gelfo *et al.* 2019).

Polydolopimorphians are represented at Tiupampa by the basal polydolopiform *Roberthoffstetteria*, which is unknown in any other faunal assemblage. As noted by Goin *et al.* (2003) and Case *et al.* (2005), *Roberthoffstetteria* more closely resembles *Ectocentrocristus* from the Late Cretaceous of North America than any other South American polydolopimorphians. However, Chornogubsky & Goin (2015) have re-evaluated this statement providing a new interpretation of the molar morphology of the polydolopimorph *Sillustania quechuense*, from the late Palaeocene-early Eocene of Laguna Umayo (Peru). The holotype of *S. quechuense* (UMC-CHU33) is an isolated, incomplete, heavily worn, and somewhat eroded left M2. We can agree with their new interpretation of the identification of the cusps of *S. quechuense*, which follows that of Goin *et al.* (2003) concerning *Roberthoffstetteria*. In their phylogenetic analysis, Chornogubsky & Goin (2015) retrieved a sister group relationship of *Sillustania* and *Roberthoffstteteria*, which we provisionally accept. However, given these relationships we question the attribution to *Sillustania* of the m1 (UMC-CHU34) described by Crochet & Sigé (1996) because of the position of the paraconid, anteriorly projected and well-separated from the metaconid, which differs strongly from the condition in *Robersthoffstetteria,* in which these cusps are closely appressed one against the other and the paraconid does not project anteriorly. The morphology of the paraconid of UMC-CHU34 is also barely compatible with the very large metaconule, which has the size and position of a pseudohypocone, since, as stated by Jernvall (1995), the presence of well-developed hypocone or pseudohypocone is generally concomitant with a reduced paraconid appressed against the metaconid or a totally absent paraconid. Therefore, we consider here that the hypodigm of *Sillustania quechuense* should restricted to its holotype only (the M2). The similarities between the M2 of *Sillustania* and *Roberthoffstetteria* are noteworthy, but do not favour the possible contemporaneity of these taxa. On the contrary, as far as can be observed on the poorly preserved holotype of *Sillustania*, this taxon appears more derived than *Roberthoffstetteria* in, for instance, the larger stylar cusp C, the straight labial edge of the tooth (lack of ectoflexus), the much smaller paraconule, and the functional pseudohypocone (i.e. the metaconule) larger and more distinctly separated from the protocone, a condition that indicates an increased specialization in the crushing function of the cusp. In other respects, given the large dimensions and position of the metaconule, conspicuously separated from the protocone, relationships with the Caenolestoidea should be investigated. Furthermore, it is noteworthy that the holotype of *Sillustania* does not feature the labiolingual compression of the protocone observed in *Roberthoffstetteria* and *Ectocentrocristus*. Unfortunately, *Roberthoffstetteria*-like or *Sillustania-like* species are absent at Punta Peligro, which prevents comparison with these taxa. To conclude, even if similarities exist between *Roberthoffstetteria* and *Sillustania*, it is noteworthy that the poor preservation of the single upper molar known of *Sillustania* (the holotype) requires extreme caution in any character comparison with other morphologically similar taxa and casts doubts on any conclusion retrieved from such a comparison. The discovery of more complete and better preserved specimens of *Sillustania* (especially with premolars) is required to establish a reliable comparison. Considering the presence of enlarged sectorial premolars in polidolopimorphs (except *Roberthoffstetteria*), the discovery of such teeth in *Sillustania* is a critical issue. Be that as it may, *Roberthoffstetteria,* the single polydolopimorphian known at Tiupampa, retains more plesiomorphic dental characters than all other South American polydolopimorphs and in particular, does not present the enlarged sectorial P2 and/or P3-p3 observed in all the other taxa of the order. Furthermore, because of the transverse compression of its protocone combined with an alignment of this cusp with the conules, it strongly resembles *Ectocentrocristus* of North America, although it is more derived in the bunoid morphology of its cusps (Case *et al.* 2005). It is noteworthy that other studies (Williamson *et al.* 2012, 2014 and Eberle *et al.* 2019) recovered a sister group relationship of *Roberhoffstetteria* with *Glasbius*, whereas *Ectocentrocristus* is included in the Herpetotheriidae (but see Goin *et al.* 2016: 215). The results of Williamson *et al.* (2012, 2014 and Eberle *et al.* 2019) would therefore support a close relationship between *Glasbius* and *Roberthoffstetteria* as suggested by Goin *et al.* (2003). Therefore, both interpretations (Case *et al.* [2005] on the one hand and Williamson *et al.* [2012, 2014] and Eberle *et al.* [2019] on the other) suggest close affinities between *Roberthoffstetteria* and some North American taxa.

Polydolopimorphians recorded at Punta Peligro are referred to a new genus and species of Bonapartheriidae and to a new genus and species of an indeterminate polydolopimorphian

(Gelfo *et al.* 2007; Woodburne *et al.* 2014a; Babot *et al.* 2017). Bonapartheriidae are much more derived than the Tiupampa polydolopimorph, *Roberthoffstetteria,* from which they differ, for example, in the remarkable increase in size of the P3 and or P2 and p3 (which are sectorial), in the loss of the plesiomorphic metatherian molars pattern (which is clearly recognizable in *Roberthoffstetteria* in spite of the bunoid morphology of the cusps), and in the extreme reduction of P2 and p2 (absent in *Bonapartherium*) as well as M4 and m4. Bonapartheriidae are absent at Tiupampa but are present (in addition to Punta Peligro) in the early Eocene of Itaboraí (Beck 2017), and in Eocene Formations of Argentina (Lumbrera, Mealla, and Geste formations) (Goin *et al.* 1998; Woodburne *et al.* 2014a).

Although pucadelphyids are unknown at Punta Peligro, the Tiupampa pucadelphyids provide interesting elements for this debate because, as stated by Case *et al.* (2005), they represent an excellent morphological intermediate between a basal Late Cretaceous North American "peradectoid" stock and the more advanced Itaboraí opossum-like metatherians. The problem of the origin of the Tiupampa pucadelphyids is discussed below and we suggest that the North American *Aenigmadelphys archeri* from the Campanian of the Kaiparowits Formation is probably morphologically the closest North American metatherian to *Pucadelphys* and *Andinodelphys* (see below – p. 694 – for characters that support this statement). Furthermore, in our phylogenetic analyses below, the Tiupampa pucadelphyids (e.g., *Pucadelphys, Andinodelphys*) have been regarded as closely related to the Itaboraian pucadelphyid, *Itaboraidelphys camposi* (as suggested by Muizon *et al.* 2018). However, *Pucadelphys* and *Andinodelphys* are more plesiomorphic than *Itaboraidelphys* in, for instance, the more pronounced ectoflexus (almost absent in *Itaboraidelphys*), the shorter labial edge of M2-3 as related to labiolingual width, the smaller size difference (in volume and height) between paracone and metacone, the less V-shaped centrocrista, the larger stylar cusp C, the mesiodistally broader protocone, the much smaller size (in length and height) of p3 as compared to m1, the slightly more mesially projected trigonid, the smaller size difference (in volume and height) between paraconid and metaconid, the slightly shorter talonid as compared to trigonid, especially on m4, the smaller entoconid, and possibly their much smaller size. Therefore, the Tiupampa pucadelphyids are morphologically intermediate between the North American *Aenigmadelphys* and the Itaboraian *Itaboraidelphys*.

Furthermore, the discovery of a partial skull of *Incadelphys antiquus* (currently under study by the authors) has revealed the complete dental anatomy of this taxon. It appears that *I. antiquus* features remarkable similarities with pucadelphyids but also with *Aenigmadelphys archeri* from which it differs significantly only in the relative size of the paracone and metacone. The paracone is larger than the metacone in *Aenigmadelphys* and the condition is reversed in *Incadelphys*. The notable similarity between the two taxa is probably related to close phylogenetic affinities.

Zimicz *et al.* (2020: 8) have questioned that the presence of *Peradectes* (a genus also present in the NALMA Puercan3, included in Chrons 29n and 28r) at Tiupampa could be an argument to support correlation of the Tiupampa beds to the Chron28r (as advocated by Gelfo *et al.* [2009]), since, as suggested by Williamson *et al.* (2012), this genus is likely paraphyletic. Therefore, Zimicz *et al.* (2020) regard the affinities of the Tiupampa "*Peradectes*" as uncertain. Given the result of Williamson *et al.* (2012), we agree that the single upper molar from Tiupampa referred to *Peradectes* cf. *austrinum* may not belong to the genus *Peradectes*. However, as expressed below (p. 693), paraphyly is a very unstable condition especially in morphological matrices including a majority of taxa known only by dental characters, which are well-known to be highly homoplastic, because of strong selective pressures for feeding (Muizon & Lange-Badré 1997; Springer *et al.* 2007; Solé & Ladevèze 2017). As a matter of fact, Williamson *et al.* (2012: 632) mention that the paraphyly of Peradectidae retrieved in the strict consensus of their analysis is "a labile result" and state that "future studies may likely recover a more inclusive phylogenetically-defined Peradectidae (which may also include many of the species that fall into the polytomy in our strict consensus, many of which do group with *P. elegans* and *P. californicus* in many of the individual most parsimonious trees)". Be that as it may, the tooth from Tiupampa referred to *Peradectes* cf. *austrinum* by Muizon (1992) presents greater similarities with many of the paraphyletic peradectids of Williamson *et al.* (2012) (e.g., *P. elegans* and *P. californicus*) than with any other South American metatherian except the holotype of *Peradectes austrinum* from Laguna Umayo (Peru). Similarities between the Tiupampa and Laguna Umayo specimens strongly suggest that they belong to the same genus, but because of the size and age difference existing between the Tiupampa specimen and the holotype from Laguna Umayo, Muizon (1992) considered that the two specimens may belong to different species. However, because of the poor preservation of the two specimens and the scarcity of the material (two incomplete upper molars), Muizon (1992: 580), expressed reluctance to refer the Tiupampa specimen to a new species based on a single incomplete molar. Therefore, Muizon (1992) cautiously referred the *Peradectes* tooth from Tiupampa to *P.* cf. *austrinum* (*contra* Marshall & Muizon 1988), stating that the affinities of the two specimens had to be confirmed by the discovery of better preserved and more complete fossils.

The Tiupampa fauna includes a microbiotherian, *Khasia cordillerensis*, which is known from upper and lower molars and partial upper jaws. *Khasia* presents characteristic features of the Microbiotheriidae such as a reduced stylar shelf, stylar cusps B, C, and D very reduced to absent, a straight centrocrista, a preparacrista that ends at the anterolabial angle of the tooth, reaching stylar cusp A, and very reduced to absent cingula/cingulids (Marshall & Muizon 1988; Muizon 1992). It is noteworthy that *Khasia* has been referred by Goin *et al.* (2016) to the North American family Pediomyidae. However, pediomyids differ from *Khasia* in having: 1) well-developed cingulids and a precingulum, whereas they are reduced to almost absent in *Khasia*; 2) a trigon basin that is generally larger and more broadly excavated than in *Khasia*; 3) a well-developed posterior part of the stylar shelf (the anterior is absent) with large styles (especially StD), whereas *Khasia*

has a very narrow posterior stylar shelf, if any (the anterior is absent) and is lacking StB, C and D; 4) a postprotocrista and a postmetaconule crista that extend labial to the metacone and reach the posterolabial angle of the molar forming a true metacingulum, whereas in *Khasia* the postmetaconule crista remains above the lingual edge of the metacone. The condition of these four characters in *Khasia* is similar to that observed in microbiotherians. As a matter of fact, it is noteworthy that the upper molars of *Khasia* are more similar to those of *Dromiciops* than to those of the other fossil microbiotherians known by upper molars (e.g. *Microbiotherium, Woodburnodon*). Therefore, we do not fully endorse the interpretation of Goin *et al.* (2016) and rather suggest that *Khasia* should probably be retained as an early member of the South American family Microbiotheriidae. However, as expressed below, (p. 703) this debate may simply reveal an indication of close relationships (even possibly sister group relationships) between microbiotherians and pediomyoids (as suggested by Marshall 1987 and Muizon 1992). However, the latter are unknown in the Punta Peligro fauna and, therefore, do not provide an indication on the relative age of the Peligran and Tiupampan faunas. In other respect, although Carneiro *et al.* (2018) have recently described a pediomyoid from Brazil, we do not follow their interpretation and consider that, so far, representatives of this superfamily are absent in South America (see comments in Appendix 1). Therefore, if our interpretation is correct, the fact that the Tiupampa microbiotherian, *Khasia*, presents similarities with pediomyids (and possibly close phylogenetic relationships) could indicate that micobiotherians may have originated in North America from a pediomyid stock and recently (i. e. early in the Palaeocene) dispersed to South America. This hypothesis however appears plausible only if microbiotherians are sister group to all Australasian marsupials (= Eomarsupialia), following the latest robust molecular analysis of Duchêne *et al.* (2018), (see also Mitchell *et al.* 2014 and Nilsson *et al.* 2010), a hypothesis which implies one single dispersal event of australidelphian marsupials from western Gondwana to Australasia.

Therefore, as already stated by Gelfo *et al.* (2009) and Goin *et al.* (2016: 219), the metatherian fauna of Punta Peligro exhibits clearly more derived morphologies than the Tiupampa fauna, and "compare(s) well with Eocene taxa even at generic level". Furthermore, although inconclusive as far as the relatives ages of the Tiupampa and Punta Peligro faunas are concerned, the fact that several metatherians from Tiupampa (pucadelphyids, *Incadelphys*, *Roberthoffstetteria, Khasia*) feature morphological similarities with North American taxa from the Late Cretaceous is probably an indication of a short period of differentiation in South America due to the recent arrival in the subcontinent, thus suggesting a relatively basal age within the Palaeocene for these taxa.

The "condylarths" of Tiupampa (the Kollpaniinae) are related to the North American mioclaenid stock and differ from the endemic South American didolodontids and Notonychopidae, which are present at Punta Peligro. Although the mioclaenid affinities of the kollpaniines have been questioned by Williamson & Carr (2007), it is noteworthy that the strict consensus trees in their phylogenetic analyses are strongly unresolved and provide little information about the phylogenetic affinities of the kollpaniines. Similarly, the position of *Molinodus* retrieved by Halliday *et al.* (2017) is irrelevant to the mioclaenid affinities of *Molinodus*, since no other mioclaenid is considered in their analysis. In contrast, the Peligran "condylarths" are related to the South American family didolodontids and are represented by the genera *Escribania* and *Raulvacia* (Bonaparte *et al.* 1993; Gelfo 2007; Gelfo *et al.* 2007). Much smaller than the latter, the Tiupampa kollpaniines retain a more primitive morphology than the Punta Peligro didolodontids in lacking a conspicuous hypocone, a structure well-developed in the latter. However, as brought to light by Muizon *et al.* (2019), in *Molinodus*, a pseudohypocone is clearly in process of individualization by duplication of the protocone, a process also present in *Raulcaccia* but at a more advanced stage.

The endemic South American order Litopterna has not been discovered at Tiupampa but is undoubtedly represented at Punta Peligro by the notonychopid *Requisia vidmari* (Bonaparte & Morales 1997).

The orders "Proteutheria" and Pantodonta are abundant in North America and have not been recorded elsewhere than Tiupampa in South America.

The "proteutherian" *Cimolestes* is represented at Tiupampa by a lower m2 or m3 and is recorded in North America from the Maastrichtian to the late Puercan NALMA (Pu3) (Lofgren *et al.* 2004). "Proteutherians" have not been recorded elsewhere in South America.

Comparison of the Tiupampa pantodont, *Alcidedorbignya inopinata*, to North American taxa allows better estimation of the absolute age of the Tiupampa fauna. As mentioned by Gelfo *et al.* (2009) and Muizon *et al.* (2015), the morphology of *A. inopinata* is compatible with an evolutionary grade that clearly predates *Pantolambda bathmodon* from the Torrejonian 2 of New Mexico (Lofgren *et al.* 2004). *A. inopinata* is approximately 60% smaller than *P. bathmodon* and is, with *Crustulus fontanus,* from the Puercan 3 of Montana (Clemens 2017), the smallest American pantodont. *A. inopinata* is dentally less derived than *P. bathmodon* in lacking a mesostyle (formed by a marked labial inflexion of the centrocrista), a structure present in all the post-Puercan North American pantodonts. The description of the remarkably complete pantodont specimens from Tiupampa (Muizon & Marshall 1992; Muizon *et al.* 2015) clearly indicates that the entire skeletal and dental anatomy of *A. inopinata* more closely resembles that of *P. bathmodon* than that of any other North American pantodont (but see below for comparison with the recently described upper molar of *Crustulus*). However, it is distinctly more generalized than *Pantolambda* in all its cranial and postcranial morphology and could represent an almost perfect morphological ancestor for this taxon. The skull of *Alcidedorbignya* shows a set of primitive characters with respect to *Pantolambda*, such as the presence of a lower dorsal edge of the narial opening, posteriorly wider nasals bones, and angular process smaller and hook-like. Furthermore, in contrast to *Pantolambda* and all other North American pantodonts, *Alcidedorbignya* shows a primitive postcranial skeleton with no trace of graviportal

tendencies. This could be inferred, among others, from the morphology of the astragalus which has a strong condyloid head with a well-defined neck and from the gracility of its limb bones. In fact, the general morphology of the limbs of *Alcidedorbignya* is more similar to that of the mioclaenid condylarths of Tiupampa than to those of the other pantodonts (Muizon *et al.* 1998 and unpublished data from posterior limb bones referred to *Tiuclaenus*). Therefore, the morphology of *Alcidedorbignya*, which is considerably more primitive than that of *Pantolambda* (see Muizon *et al.* [2015] for a thorough comparison), except for the presence of single rooted P2 and p2, an autapomorphy of *Alcidedorbignya,* is likely to predate that of *Pantolambda*. In other words, an *Alcidedorbignya*-like morphological ancestor of *Pantolambda* is likely to have existed in North America, in beds older than *Pantolambda bathmodon*. This latter species is from the medial Torrejonian NALMA (=To2), which is correlated with Chron 27r (Leslie *et al.* 2018; Flynn *et al.* 2020). Because the beds of the Santa Lucia Formation at Tiupampa were referred to a single reversed Chron by Marshall *et al.* (1997) and because comparison of *Alcidedorbignya* with *Pantolalmba* suggests an older age for the former, the Tiupampa beds yielding *Alcidedorbignya* should be correlated to Chron 28r, which approximately corresponds to To1 (see above). This age is approximately 2 to 3 million years older than the *Pantolambda* bearing beds (To2) as suggested by Muizon (1998) and Muizon & Cifelli (2000). It is noteworthy that the To2, which corresponds to the Chron 27r, is similar in age to the Punta Peligro beds, which are referred to the same Chron (Clyde *et al.* 2014).

Interestingly, a recent study (Clemens 2017) described an isolated M2 referred to a new pantodont (*Crustulus fontanus*) from the latest Puercan (Pu3) of North America. The specimen (M1 or M2) is very similar to *Alcidedorbignya* but differs in the narrower stylar shelf (possibly plesiomorphic?), the larger conules (plesiomorphic), the convex labial edge of the para-, meta-, and protocone (whereas it is flat to concave in *Alcidedorbignya*) (plesiomorphic), the larger parastyle (plesiomorphic), and the slightly more developed postcingulum with a distinct medial cuspule (apomorphic). Given the scarcity of the material (a single upper molar) it is difficult to evaluate whether *Crustulus* could represent a potential morphological ancestor for *Alcidedorbignya* (probably not, as stated by Clemens 2017), but it clearly brings to light that a dental pattern remarkably close to that of *Alcidedorbignya* existed in North America in pre-Torrejonian beds. This occurrence reinforces the suggestion that the *Alcidedorbignya* morphology should predate that of *Pantolambda* and lends support to a To1-equivalent age for the former, i.e. between To2 (*Pantolambda*) and Pu3 (*Crustulus*).

The Tiupampa beds have yielded a single upper molar referred to the order Notoungulata (Muizon *et al.* 1984; Marshall & Muizon 1988, Muizon 1992; Muizon *et al.* 2019). This molar is poorly preserved since it is relatively worn and missing most of its ectoloph. In a recent analysis of some Tiupampa eutherians, it has been referred to cf. Henricosborniidae (Muizon *et al.* 1984; Muizon 1992; Muizon *et al.* 2019). However, similarities of the Tiupampa notoungulate to Henricosborniidae probably represent plesiomorphic features and, given its state of preservation, this single tooth may be too incomplete to be identified at a level lower than ordinal. As stated by Bauzá *et al.* (2019: 597) the phylogenetic relationships of this specimen need to be confirmed. Therefore, the Tiupampa notoungulate should probably be referred to Notoungulata indet. The Tiupampa notoungulate is the only evidence of the presence at Tiupampa of a typical South American Native Ungulate. However, the discovery of better preserved remains (at least a complete upper or lower molar) is required to establish its presence more securely.

The faunal comparison presented here has listed a set of paleontological data, which, taken jointly, clearly suggest (or are neutral in the case of the notoungulate) that: 1) the Tiupampa mammal fauna displays more plesiomorphic characters than that of Punta Peligro and appears to be less clearly specialised toward the South American mammalian faunal endemism pattern than that of Punta Peligro, 2) the Tiupampa mammal fauna still retains numerous remarkable morphological affinities with the North American faunas of the Late Cretaceous and early Palaeocene, and 3) the Tiupampa mammal fauna is likely to be anterior to the Torrejonian 2 NALMA. In brief, the Tiupampa mammal fauna exhibits an evolutionary grade that is intermediate between those of the North American Late Cretaceous-earliest Palaeocene (Puercan) faunas and the Punta Peligro fauna, the latter already being distinctly characterized by a conspicuous South American mammalian endemism. Furthermore, comparison with North American earliest pantodonts (*Pantolambda* and *Crustulus*) suggests that the Tiupampa pantodont is probably no older (but no younger either) than the To1, which is approximately correlated with Chron 28r and the base of Chron 28n. To conclude, the Tiupampa fauna (which is correlated to a single reversed magnetostratigraphic Chron) is referred to Chron 28r as demonstrated by Gelfo *et al.* (2009). Taking into account the new calibration of Chron 28r (Sprain *et al.* 2015, 2018), the Tiupampa mammal fauna is early Paleocene, probably early Danian and its absolute age is likely to be close to 65 Ma (Fig. 4). The Punta Peligro fauna is correlated to Chron 27r and is therefore no more than 2 to 3 million years younger than that of Tiupampa. It is noteworthy however that the Tiupampa beds do not contain the earliest Tertiary mammals of South America because the polydolopimorphian *Cocatherium lefipanum*, from the Lefipan Formation at the Grenier Farm (Chubut, Argentina) is regarded by Goin *et al.* (2006) to be earliest Danian in age. This taxon is known from a single lower molar, which was discovered a few metres above the K-T boundary and is probably older than the Tiupampa fauna.

Finally, although we definitely favor an early Danian age for the Tiupampa mammal fauna on the basis of the combination of the paleontological arguments expounded above, it is clear that only radiometric dating at Tiupampa would provide a definitive answer to the question of the age of the Tiupampa mammal-bearing beds. Unfortunately, so far, numerous field seasons at Tiupampa seem to indicate that no tuff or volcanic ashes are present in the Santa Lucía beds on this site.

MATERIAL AND METHODS

Specimens, description, and comparison

Andinodelphys cochabambensis was named on the basis of a single upper molar (right ?M2) (Fig. 1) to which was referred a lower molar (left ?m3) (Marshall & Muizon 1988). The skulls described below bear well-preserved teeth, mostly complete dental series, and four of the five skulls known are associated to their mandibles. Therefore, their referral to the holotype and referred lower molar is securely established (Muizon *et al.* 1997).

The specimens described below have been discovered as a tangle of bones including at least seven individuals. In the block illustrated by Muizon & Argot (2003), which is part of the skeleton association (Figs 2, 3), at least five specimens are recognizable, three of them being still partially articulated skeletons. One specimen is especially complete with most of the bones, including sub-complete foot and hand. This specimen (MHNC 8308, yellow on Fig. 3), is that of an adult with almost fully ossified bones, while the other two are sub-adult individuals (pink and purple on Fig. 3) and their postcranial bones are often missing their epiphyses although the pink specimen (MHNC 8370) has fully erupted M4s. One specimen (the green one MHNC 13933) is notably disarticulated but still preserves complete skull and mandibles. Of the five skulls available, two are almost complete and preserve the basicranium with the two petrosals, the basioccipital and exoccipitals (MHNC 8264 and 8308). MHNC 8264 (which was found close to the block but not in it) is almost undistorted but is missing the right premaxilla and MHNC 8308 (yellow specimen on Fig. 3) has suffered some transverse distortion and the left side of the dorsal face of the braincase is crushed and smashed. The skull of one specimen (pink specimen, MHNC 8370) is seriously distorted transversely and preserves disarticulated basioccipital + exoccipitals and left petrosal, but is missing the right petrosal; this specimen lacks the right mandible. MHNC 13847 (orange specimen) is lacking elements of the basicranium (right petrosal, basioccipital and, exoccipitals) and its left maxilla is disarticulated; both mandibles are missing. The fifth skull (green specimen on Fig. 3) is not convenient for description because it is still on the block and extremely difficult to extract because several bones are closely appressed against it, especially the left hind limb of MHNC 8308. CT scanning is not easy either because of the size of the block and the fragility of the fossil bones. However, if technically possible, a scanning of the block presented on Fig. 2 will be undertaken in the future at the ESRF (European Synchrotron Radiation Facilities, Grenoble, France) in order to perform a virtual preparation of one the skeletons presented below (Fig. 3, yellow specimen MHNC 8308). This project is in progress by the authors and F. Goussard.

Therefore, the following description will refer almost exclusively to the four isolated skulls (MHNC 8264 8308, 8370, and 13847). The petrosal of *Andinodelphys* has been described by Ladevèze & Muizon (2007) and the description of this bone will concern other specimens but, when necessary, will refer to this paper. Comparisons will be made with the closely related Tiupampian genus *Pucadelphys* and, if useful, to *Mayulestes* and *Allqokirus* (in Appendix 2 we provide photos of the upper and lower premolars and molars of *Mayulestes*, which are of better quality than figures 2-4 in Muizon [1998]). Comparisons with *Pucadelphys* will be based on the description by Marshall & Muizon (1995) but also on the numerous specimens discovered since this publication (see Ladevèze *et al.* 2011). Comparisons with *Mayulestes* and *Allqokirus* will be based on the original specimens (respectively MHNC 1249 and 8267). Some comparisons will be made with the undescribed skulls from Tiupampa referred to *Mizquedelphys pilpinensis* (MHNC 13917). These skulls are approximately 50% smaller than *Andinodelphys* and 30% smaller than *Pucadelphys* and coincides in dental morphology and size to the holotype of *M. pilpinensis* (a maxilla bearing P3-M3). Following the description, a comparison section will consider some dental and cranial characters of *Andinodelphys* differing from *Pucadelphys* (or not considered by Marshall & Muizon 1995) and discuss their distribution and, when relevant, the state present in *Andinodelphys*. The comparison presented below does not pretend to represent an exhaustive study of all metatherians characters but rather to intend to make a survey of some interesting features found in basal metatherians and to briefly discuss their potential distribution within Theria.

Phylogenetic analysis

The phylogenetic analysis performed here used the data matrix of Muizon *et al.* (2018). Comments on and justification of the construction of this data matrix (which originated from that of Forasiepi 2009) are presented in Muizon *et al.* (2018: 366, 367). The character list is a slightly revised version of that of Muizon *et al.* (2018: 439-455).

Our dataset comprises a total of 364 osteological characters (102 dental, 16 mandibular, 124 cranial, 122 postcranial), examined in six outgroup and 45 ingroup taxa (fossil and extant metatherians). The revised character list is given in Appendix 3. The outgroup includes three more taxa than in Muizon *et al.* (2018). The outgroup taxa include one stem therian (the zatherian *Vincelestes*) and five fossil eutherians, the sister group to Metatheria. The outgroup eutherians include *Prokennalestes* from the Early Cretaceous of Mongolia, which is known from upper and lower postcanine teeth, dentaries, and one petrosal (Kielan-Jaworowska & Dashzeveg 1989; Sigogneau-Russell *et al.* 1992; Wible *et al.* 2001). Furthermore, in a recent monograph Lopatin & Averianov (2017) described and illustrated a remarkably abundant new material of *Prokennalestes* including several hundreds of upper and lower jaws and teeth from the locality of Khovoor in the Gobi Desert of Mongolia. Other outgroup eutherian taxa are *Maelestes*, represented by the skull, mandible, anterior vertebrae, and partial left forelimb, *Zalambdalestes,* and *Asioryctes*, both represented by several complete skulls and skeletons

from the Late Cretaceous of Mongolia (Wible *et al.* 2004, 2009; Kielan-Jaworowska 1977, 1981). Another outgroup eutherian taxon is *Leptictis* represented by very complete cranial and post cranial material (Butler 1956; Novacek 1986; Rose 2006) from the early Oligocene of Wyoming. Ingroup taxa include metatherians that belong to different lineages. They include 17 sparassodonts, mostly represented by well-preserved material, and other, well-preserved fossil metatherians (pucadelphyids, stagodontids, peradectids, alphadontids, *Pediomys*, herpetotheriids, deltatheroidans, *Kokopellia*, and *Asiatherium*). Because it shares many similarities with *Andinodelphys* we included the Itaboraian genus *Itaboraidelphys* represented by dental remains (Marshall & Muizon 1984) and two petrosals (Type II petrosal of Ladevèze 2004) that Muizon *et al.* (2018) referred to this taxon (see below). We also added to Muizon *et al.* (2018)'s matrix the so called "Gurlin Tsav Skull" (GTS), a remarkably complete (but undescribed yet) metatherian skull from the Late Cretaceous of Mongolia (Szalay & Trofimov 1996). *Varalphadon*, an early Cretaceous genus of North America, which has been regarded by Carneiro (2018) as the earliest sparassodont, has also been included in our ingroup. Selected extant marsupials amongst the least derived clades (didelphids, *Dromiciops*, dasyurids, and *Thylacinus*) are also included in the matrix.

The taxon/character states matrix was analysed using heuristic parsimony searches implemented by PAUP* (Swofford 2002). Each heuristic parsimony search employed 100 replicates of random taxon addition with TBR branch swapping, saving up to 10 trees. The phylogenetic tree with morphological character state optimisations was generated by PAUP* (Swofford 2002) and Winclada v.1.00.08 (Nixon 2008). Polymorphic taxa were coded with multiple character state entries. Most multistate characters were treated as unordered, but 57 of them were considered as additive because previous studies have assumed they are morphoclines or because we suspected them to be (see list of characters, Appendix 3). Branch support was assessed by calculating the Bremer index (Bremer 1988) with PAUP* (Swofford 2002) (heuristic searches with 100 replications, saving up to 10 trees, TBR branch swapping). The results of the parsimony analysis will be presented and discussed.

Terminology, measurements, and taxon list and material

Anatomical terminology for the skull essentially follows Wible (2003, 2008, 2011) and Wible & Spaulding (2013) unless specified. Vessels and nerves terminology and passageways refer to MacPhee (1981), Wible (1990, 1993, 2008, 2009, 2010, 2011, 2012), Wible & Spaulding (2013), and Evans & de Lahunta (2013). Most of this terminology corresponds to anglicized terms of NAV (2005). Dental terminology follows Marshall & Muizon (1995). Lower incisor homology follows Hershkovitz (1982, 1995). Dental measurements follow Gheerbrant (1992: fig. 4). Internal edge of the teeth (i.e. on the side of the mouth and tongue) will be designated as lingual and external edge (i.e. on the side of the vestibulum, lips or cheeks), will be designated as labial, although the last molars are generally bordered by the cheek rather than the lip.

Appendix 4 provides a list of the taxa and material available to us (original specimen with catalogue numbers, casts, photos, CT data, publications). The list of generic and specific taxa cited in the text with authorship and date of publication is given on Appendix 5.

Institutional abbreviations

AMNH	American Museum of Natural History, New York;
BMNH	Beijing Museum of Natural History, Beijing;
DGM	Divisão de Geología e Mineralogía do Departamento Nacional da Produção Mineral , Rio de Janeiro;
UMC	Palaeontological collections of the Université Montpellier 2, Montpellier;
FMNH	Field Museum of Natural History, Chicago, Illinois;
IEEUACG	Instituto de Ecología y Evolución, Universidad Austral de Chile, Valdivia;
MACN	Museo Argentino de Ciencias Naturales "Bernardino Rivadavia", Buenos Aires;
MB.Ma	Museum für Naturkunde, Berlin, Berlin;
MHNC	Museo de Historia Natural "Alcide d'Orbigny", Cochabamba;
MNHN	Muséum national d'Histoire naturelle, Paris;
MNRJ	Museu Nacional e Universidade Federal do Rio de Janeiro, Rio de Janeiro;
NDGS	North Dakota Geological Survey, State Fossil Collection at the North Dakota Heritage Center State Museum, Bismarck, North Dakota;
OMNH	Oklahoma Museum of Natural History, Norman, Oklahoma;
PIMUZ	Paläontologisches Institute und Museum Zürich;
PIN	Paleontological Institute of the Russian Academy of Sciences, Moscow;
PSS-MAE	Paleontological and stratigraphy Section (Geological Institute), Mongolian Academy of Sciences, Ulaan Baatar, Mongolia;
RH	Robert Hoffstetter collection of Recent vertebrates, in the MNHN;
SC	Sierra CollegeNatural History Museum; Rocklin, California;
SMF	Senckenberg, Museum of Natural History, Frankfurt;
SMP-SMU	Shuler Museum of Paleontology, Southern Methodist University, Dallas;
STM	Tianyu Museum of Nature, Linyi, Shandong Province, China;
UCMP	Museum of Paleontology, University of California, Berkeley;
USNM	United States National Museum, Smithsonian Institution, Washington;
UWBM	University of Washington, Burke Museum of natural history and Culture, Seatle, Washington;
YPFB	Yacimientos Petrolíferos Fiscales de Bolivia, Santa Cruz;
YPM-PU	Princeton University collection housed in the Yale Peabody Museum, Yale University, New Haven, Connecticut;
ZPAL	Paleontological Institute of the Polish Academy of Sciences, Warsaw.

SUPPLEMENTARY DATA

Supplementary data are available at the following address: NEXUS file of the data matrix: http://sciencepress.mnhn.fr/sites/default/files/documents/fr/andinodelphys-data-matrix.nex

SYSTEMATIC PALAEONTOLOGY

Infraclass METATHERIA Huxley, 1880

Superorder PUCADELPHYDA Muizon, Ladevèze, Selva, Vignaud, Goussard, 2018

Remark
The Pucadelphyda includes the order Sparassodonta and the family Pucadelphyidae (see Muizon *et al.* 2018).

Order indet.

Family Pucadelphyidae Muizon, 1998

Included genera. — *Pucadelphys* Marshall & Muizon, 1988; *Andinodelphys* Marshall & Muizon, 1988; *Mizquedelphys* Marshall & Muizon, 1988, *Itaboraidelphys* Marshall & Muizon, 1984.

Genus *Andinodelphys* Marshall & Muizon, 1988

Type Species. — *Andinodelphys cochabambensis* Marshall & Muizon, 1988 by original designation.

Diagnosis. — Because the genus is monospecific, its diagnosis is that of the type species.

Andinodelphys cochabambensis Marshall & Muizon, 1988

Holotype. — An isolated right M2 (YPFB Pal 6192)

Hypodigm. — **Holotype**. YPFB Pal 6194, isolated m3 (Marshall & Muizon 1988: fig. 6 A and B); MHNC 8264: sub-complete cranium (missing right premaxilla and anterior part of right nasal) bearing all teeth except incisors, with mandibles bearing all teeth except left i3-1 and crown of left canine; MHNC 8306: isolated right mandible with p1 isolated and p2-m4 in situ; MHNC 8308: sub-complete skeleton with slightly transversely distorted cranium with posterior left part of the roof crushed and smashed; all upper teeth are preserved except right I2, I4-5 and crowns of left I3 and I5, both mandibles, all lower teeth are preserved except right i1-4 and crown of left i2 (Fig. 3 yellow elements); MHNC 8370: partial skeleton including sub-complete skull, transversely distorted, with disarticulated basioccipital and exoccipitals (bones are fused) and left petrosal, most of teeth are preserved except right I3-1, left I1, I3-5 right P2-3, left mandible with I1, P2-M4, and partial postcranial skeleton (Fig. 3 pink elements); MHNC 8371: isolated right petrosal; MHNC 13847: partial cranium lacking most of basicranium but the left petrosal; the specimen is transversely compressed and the right maxilla is detached, canines and incisors are missing and three premolars and a pterygoid are free; a left scapula found in close contact with the left maxilla is also referred to this specimen; furthermore, a set of six cervical vertebrae (atlas-C6) and an isolated right jugal are possibly part of the same individual (Fig. 3 orange elements); MHNC 13912: left distal humerus; MHNC 13925: set of bones possible referred to the same individual and including right mandible, right petrosal and most of postcranial skeleton (Fig. 3 purple elements); MHNC 13926: isolated left humerus; MHNC 13933: sub-complete cranium and mandibles still imbedded on the large block of Fig. 2, and lacking exoccipitals, upper incisors, right canine, M3-4, the left P3, probably associated with a set of non-articulated bones (Fig. 3, green elements); MHNC 13934: 14 caudal vertebrae almost all of them being articulated; MHNC 13935: isolated left femur lacking the epiphyses of the head and distal extremity; MHNC 13936: left femur lacking proximal epiphyses and distal extremity; MHNC 13937: left ulna lacking distal epiphysis and radius lacking both epiphyses; MHNC 13938: right fibula; MHNC 13939: left calcaneus; MHNC 13940: right calcaneus lacking extremity of the tuber; MHNC 13941: right metacarpus (McII-V); MHNC 13942: right radius lacking epiphyses; MHNC 13943: right astragalus; MHNC 13944: left metacarpus (McI-IV) with first phalanges; MHNC 13945: axis lacking atlas intercentrum; MHNC 13946: left illium; MHNC 13947: right ischiopubis; MHNC 13948: right humerus lacking proximal epiphysis; MHNC 13949: left humerus lacking epiphyses.

Emended diagnosis. — Dental formula I5/i4, C/c, P3/p3, M4/m4. Large Pucadelphyidae approximately 35% larger in skull length and 20% in bizygomatic width than *Pucadelphys andinus*, and 60% larger than *Mizquedelphys pilpinensis* in skull length; approximately 10% smaller than *Mayulestes ferox*, and approaching the size of *Allqokirus australis* in skull length.
Andinodelphys cochabambensis differs from *Pucadelphys andinus* in the following characters: I1 larger and ventrally projecting below the other incisors; stylar cusp C on the upper molars conspicuously smaller and variably twined (always single in *Pucadelphys*); rostrum and (correlatively) dentary proportionally longer; small palatal vacuity in the maxilla (lacking in *Pucadelphys*); small transverse canal (absent in *Pucadelphys*); hypotympanic sinus present posterolateral to the foramen ovale (absent in *Pucadelphhys*).
Andinodelphys cochabambensis differs from *Itaboraidelphys camposi* in the following characters: size 25% smaller in comparable linear tooth dimensions; molars less bulbous in overall appearance; less V-shaped centrocrista; p2 distinctly smaller than p3; protoconid of p2-3 more asymmetrical in lateral view; trigonid higher as compared to talonid; narrower talonid; smaller entoconid.
Andinodelphys cochabambensis differs from *Mayulestes ferox* and *Allqokirus australis* in the following characters: larger and mesiodistally longer protocone; paracone and metacone separated at base; slightly V-shaped centrocrista; preparacrista of M4 forms an angle close to 90° with the para-metacone axis; lateral edge of protoconid not inflated and strongly convex at mid-height; metaconid much larger in height and volume than paraconid; metaconid and paraconid adjoined at base; paracristid lacking a carnassial notch; moderate increase in size of molars (m1-m3) posteriorly (great in *Mayulestes* and *Allqokirus*); dentary shallower below molars and more slender; lower incisors more procumbent and mandibular symphysis more slanted; small palatal vacuity present on maxilla; transverse canal; frontal-maxilla articulation on the dorsolateral aspect of the rostrum; distinct and sharp supraorbital process of the frontal.
Andinodelphys cochabambensis differs from deltatheroidans in the following characters: larger and mesiodistally longer protocone, paracone smaller than metacone (paracone larger than metacone in deltatheroidans), paracone and metacone separated at base; slightly V-shaped centrocrista; preparacrista of M3 slightly shorter than postmetacrista (much longer in deltatheroidans); metaconid much larger in height and volume than paraconid; metaconid and paraconid adjoined at base; paracristid lacking a carnassial notch; larger entoconid; m4 not significantly reduced as compared to m3; moderate increase in size of molars (m1-m3) posteriorly (marked in deltatheroidans); dentary lower, below molars and more slender; lower incisors more procumbent and mandibular symphysis more slanted; longer and narrower rostrum; small palatal vacuity present on maxilla; frontal-maxilla articulation on the dorsolateral aspect of the rostrum.

Geological setting and age. — The *Andinodelphys* skulls and skeletons are from beds of the Santa Lucía Formation at Tiupampa

and have been discovered in 1996 in the locality called "the Quarry" by Gayet *et al.* (1992) and Marshall & Muizon (1995). As discussed above (p. 600-609) and elsewhere (Gelfo *et al.* 2009; Muizon *et al.* 2015, 2018), the age of the Tiupampa beds is regarded as early Danian in age (*c.* 65 Ma).

COMPARATIVE DESCRIPTION

The description below is based on the skulls of the specimens included in the block of intermingled skeletons illustrated in Figures 2 and 3. All the specimens included in the hypodigm, except the holotype, the referred m3 (YPFB Pal 6194), and MHNC 13912, have been discovered in, or close to, this block. These individuals were probably buried in a single catastrophic event as has also been suggested in the case of the accumulation of nearly complete skulls and skeletons of *Pucadelphys andinus* from the same locality, which have been regarded as belonging to the same population (Ladevèze *et al.* 2011). Consequently, because the specimens described here have undergone similar taphonomic conditions, they are also regarded as belonging to the same population of *Andinodelphys cochabambensis*. Therefore, the morphological differences observed between the specimens, especially concerning dental morphology, are regarded here as related to individual variation within the species *A. cochabambensis*. They could also be related to sexual dimorphism, although our sample does not present morphological arguments favouring this hypothesis.

Dentition

As mentioned above two almost complete skulls are known (Figs 5, 6), but all the teeth of *Andinodelphys* are well preserved on the four prepared skulls and the two isolated mandibles, which provides an excellent knowledge of the dental anatomy. The dental formula is the plesiomorphic pattern for metatherians: I5/i4, C1/c1, P3/p3, M4/m4 (Kielan-Jaworowska *et al.* 2004). Upper dentition will be described first, followed by lower dentition.

Upper dentition

Upper Incisors. (Fig. 7) Both I1 are preserved on MHNC 8308. They are relatively slender with a conical crown, which is at least twice as high as wide, although it may be more because the boundary between enamel and dentine is difficult to observe precisely. The crown is elevated relative to the other upper incisors and the part of the root external to the alveolus is approximately 50% to 100% higher than on the other teeth. As a consequence, the I1 projects farther ventrally than the other incisors. The I1s are closely appressed one against each other at their apices and diverge at their base. Because of this layout, they appear slightly oriented medially. The relative proportion and layout of the I1 clearly resemble the condition observed in Recent didelphids but also in *Mayulestes* as mentioned by Muizon *et al.* (1997). As observed on MHNC 8308, I2 is much smaller than I1 and approaches the size of I5 (preserved only on the right premaxilla of MHNC 8370). The crown of I2 is much lower than that of I1. It is triangular, approximately as wide as high and slightly compressed labiolingually. I3 and I4 are morphologically similar to I2 but are larger, I3 being in turn larger than I4. The three teeth have a clearly lower crown than that of I1. I5 is not preserved on MHNC 8308. On MHNC 8370, I5 is a tiny tooth with a peg-like crown that is not distinctly triangular as on I2-4 and not compressed labiolingually. The edges of the alveoli of I1-3 are on the same level, while that of I4 is slightly more dorsal. The alveolus of I5 is much more dorsal, facing distinctly posteroventrally at the anterior edge of the paracanine fossa for the lower canine. A small diastema separates I1 and I2 as is observed in Recent didelphids and a large one separates I5 from the canine.

Upper Canine. (Figs 7-10) The upper canine is a large tooth similar in size (as compared to the skull length) to the condition observed in *Didelphis* and *Caluromys*. It is slightly larger proportionally than in *Philander* and *Marmosa* and much larger than in *Thylamys* and *Metachirus* (Table 1). As compared to the other Tiupampa metatherians, the upper canine of *Andinodelphys* is slightly smaller than that of the only known specimen of *Mayulestes* but falls within the range of the variation observed in *Pucadelphys*. In the latter genus, the wide range of variation of the size of the upper canine (Table 1) is related to sexual dimorphism (Ladevèze *et al.* 2011). In the available sample for *Andinodelphys* (3 specimens) no such variation is observed since the maximum variation of the ratio canine height/skull length is 0.006 whereas in *Pucadelphys* it is eight times as much (0.048). Therefore, the size variation of the upper canine, which has been regarded as related to sexual dimorphism in *Pucadelphys*, may be only related to individual variation in *Andinodelphys*. However, it is also possible that, because of its small size, our sample of *Andinodelphys* skulls may not include specimens allowing identification of sexual dimorphism. The upper canine of *Andinodelphys* is pointed and arcs posteriorly so that the apex of the crown is approximately ventral to the posterior edge of the crown base. The cross section of the canine is oval-shaped without anterior or posterior carina and the edges of the tooth are slightly flattened transversely. At the base of the crown the section of the tooth is more than twice longer than wide (2.93 mm x 1.28 mm on MHNC 8308).

Upper Premolars. (Figs 8-11) The three upper premolars are double-rooted and distinctly increase in size from P1 to P3. The crown of P2 is distinctly higher than that of P1 but is only slightly lower than that of P3. The same observation is made for the mesiodistal length and transverse width as observed on the means calculated on Table 2 for the three measurements. The three premolars are single cusped with anterior and posterior heels. P1 is closely appressed against the canine. On the four skulls, the anterior root is distinctly lateral to the posterolateral edge of the canine. As a consequence, the tooth is set obliquely in the tooth row its axis being oriented anterolaterally-posteromedially. The crown of P1 is lower than long and its apex is ventral to the posterior edge of the anterior root. As a consequence, the anterior keel of the main cusp is much shorter than the posterior one. The

FIG. 5. — **A**, **B**, *Andinodelphys cochabambensis* (MHNC 8264) stereophotos of the cranium: **A**, dorsal view; **B**, ventral view. Scale bar: 10 mm.

anterior base of the crown bears a small heel, which is lower than that observable at the posterior angle of the crown. In occlusal view the crown is ovoid, the lingual edge being more convex than the labial one. P2 is approximately twice as large as P1 but morphologically similar. Its crown is higher and its apex is less anterior than that of P1. In labial view the crown

Fig. 5. — **C**, **D**, *Andinodelphys cochabambensis* (MHNC 8264) stereophotos of the cranium: **C**, lateral view; **D**, occipital view. Scale bar: 10 mm.

appears less asymmetrical than P1 and the anterior edge of the main cusp is only slightly shorter than the posterior one. The crown is roughly triangular and slightly lower than long. Mesially, a small cuspule is present at the base of the crown and distally a significant heel extends the tooth posteriorly. In occlusal view the lingual edge of the crown is inflated above the anterior edge of the posterior root. Consequently, in occlusal view the crown forms a low triangle with the apex in a distolingual position. The P3 is elevated and robust being much larger than P2. It is only slightly longer than P2 but 33% higher (mean in Table 2). It is approximately 50% higher than long. In labial view the tooth is slightly asymmetrical and the apex of the main cusp is shifted posteriorly being ventral to the anterior edge of the posterior root. As a consequence, the mesial edge of the crown is longer than the distal one in contrast with the condition on P1 and P2. At the mesial base of the crown the condition varies. On MHNC 8370 a small cuspule, larger than on P2, is present. On MHNC 8264, there is no real cuspule as on P2 but a small cingulum surrounds the mesial edge of the crown base and on MHNC 8308 the mesial edge of the crown passes smoothly to the mesial root. Lingually the distolingual inflation is more accentuated than on P2 and is ventral to the whole length of the distal root. At the distal base of the crown a well-cuspated heel is present. Distally this cusp closely contacts the stylar cusp A of M1. The mesial edge of the main cusp is a thick and rounded ridge from base to apex, whereas the distal edge of the main cusp is a relatively sharp crista, straight or slightly concave distally.

Upper Molars. (Figs 8-11) The upper molar anatomy of *Andinodelphys* has been described by Marshall & Muizon (1988) on the basis of the holotype of *A. cochabambensis*, an M2 or M3 (more likely an M2). The measurements of the holotype (L = 2.9 mm; W = 3.2 mm) better fit the measurements range

TABLE 1. — Size of the upper canine as compared to the length of the cranium (ratio canine height/cranium length) in pucadelphydans and didelphids. Abbreviations: Cah, canine height; Skl, cranium length (condylobasal). Allqokirus australis, the other sparassodont from Tiupampa, has not been included in this table because the only skull known of this species is that of a sub-adult individual with a canine that is not fully erupted.

Taxon	Cah	Skl	Cah/Skl
Andinodelphys cochabambensis (MHNC 8264)	6.94	47.99	0.144
Andinodelphys cochabambensis (MHNC 8308)	6.74	47.30	0.142
Andinodelphys cochabambensis (MHNC 8370)	5.83	42.2	0.138
Andinodelphys cochabambensis **(mean)**			**0.141**
Pucadelphys andinus (MHNC 8266)	4.54	33.34e	0.136
Pucadelphys andinus (MHNC 8381)	5.12	31.73e	0.161
Pucadelphys andinus (MHNC 8382)	5.40e	34.29e	0.157
Pucadelphys andinus (MHNC 8378)	3.12	27.65e	0.113
Pucadelphys andinus **(mean)**			**0.142**
Mayulestes ferox (MHNC 1249)	8.15	53.12	0.153
Didelphis virginiana MNHN-ZM-2007-7	20.55	115.65	0.177
Didelphis virginiana (Coll SL uncat.)	18.66	118	0.158
Didelphis albiventris (MNHN-RH 120)	12.78	99.17	0.129
Didelphis pernigra MNHN-ZM-MO-1920-250	14.3	95.9	0.149
Didelphis marsupialis MNHN-ZM-2007-8	12.15	101.10	0.12
Didelphis marsupialis MNHN-ZM-MO-1900-581	16.3	105.75	0.154
Didelphis marsupialis MNHN-ZM-MO-1932-3003	10.11	100.63	0.100
Didelphis marsupialis MNHN-ZM-MO-1900-583	16.21	110.1	0.147
Caluromys philander (MNHN uncat – 15J)	8.6	57.41	0.150
Caluromys philander (MNHN uncat – 17L)	8.00	56.13	0.133
Caluromys philander (MNHN uncat – 17F)	7.67	57.58	0.133
Caluromys lanatus MNHN-ZM-MO-1929-651	7.75	57.21	0.135
Caluromys lanatus MNHN-ZM-MO-1929-652	8.29	56.21	0.147
Caluromys lanatus MNHN-ZM-MO-1929-650	7.75	55.78	0.139
Philander opossum (MNHN-ZM-2012-21)	8.74	87.96	0.099
Philander opossum (MNHN-ZM-MO-2000-215)	9.46	74.14	0.127
Philander opossum (MNHN-ZM-MO-1998-2264)	7.42	73.76	0.100
Philander opossum (MNHN-ZM-2003-153)	7.44	73.63	0.101
Marmosa murina (MNHN-RH 82)	4.45	41.36	0.107
Metachirus nudicaudatus MNHN-ZM-MO-1985-1803	3.17	57.22	0.055
Metachirus nudicaudatus MNHN-ZM-2004-316	3.02	56.02	0.054
Metachirus nudicaudatus (MNHN-RH 81)	5	54.61	0.091
Metachirus nudicaudatus (Coll CM uncat)	4.85	63.94	0.076
Metachirus nudicaudatus (MNHN-Coll Filhol uncat)	3.59	47.89	0.075
Thylamys sp. (Coll CM uncat)	2.29	27.21	0.084

obtained for the M2 (2.45 mm < L < 3.06 mm; 3.03 mm < W < 3.56 mm) than for the M3 (2.62 mm < L < 3.19 mm; 3.25 mm < W < 3.84 mm) as well as the means for M2 (L= 2.82 mm; W = 3.29 mm) and M3 (L = 2.85 mm; W = 3.57 mm) obtained from the four skulls described here (Table 2). Furthermore, the morphology of the six M2s described from the new sample presented here closely matches that of the holotype. Therefore, there is no doubt that these cranial remains belong to the same taxon as the holotype and can be safely referred to *Andinodelphys cochabambensis*.

However, on the five new specimens described here, the four molars are preserved on both sides, which provide a much more complete knowledge of *Andinodelphys* upper molar anatomy and variation. In length and width (see Table 2 for definition of Length and Width of upper molars) M1<M2<M3>M4. This comparison is based on four specimens, which preserve both right and left molars, giving 8 values per tooth and per measurements. The first three molars are slightly wider than long. This condition is more pronounced on M4, which is mesiodistally shorter than the other molars. The mesial edge of the first three molars is roughly perpendicular to the mesiodistal axis of the molar row (i.e. approximately the paracone-metacone axis), while the distal edge is distinctly oblique. Because the first three molars more resemble each other than the last one, they will be first described jointly before M4.

Upper M1-3 (Figs 8-11). On the labial border of M1-3, the stylar cusp A- stylar cusp E axis is approximately parallel to the mesiodistal axis of the tooth row whereas it is oblique on M4, being mesiolabially-distolingually oriented. On M1-3 the protocone is the largest cusp of the tooth. It is a large and massive cusp, triangular in occlusal view. On M1-2 it is as long as wide, while on M3 it is slightly shorter than wide. It is moderately elevated being as high as the paracone but clearly lower than the metacone. In occlusal view, the apex of the protocone is shifted mesially; in other words, the mesial face of the protocone is subvertical and the distal face slopes distally. Similarly, the lingual rounded keel of the protocone is deflected mesially so that the mesial face of the protocone is roughly transverse and the distal face is distinctly oblique. As a consequence of its asymmetry, the protocone appears

TABLE 2. — Measurements of the teeth of *Andinodelphys cochabambensis*. Abbreviations: **L** (for canines and premolars), maximum length of the tooth; W (for canines and premolars), maximum width of the tooth; L (for molars), maximum length of the tooth measured parallel to the paracone-metacone axis; W (for molars), maximum width of the tooth perpendicular to length; Lab, length of the tooth along the labial alveolar border; Ltr, length of the trigonid; Ltl, length of the talonid; Wtr, maximum width of the trigonid; Wtl, maximum width of the talonid; H, height of the tooth; Htr, height of the trigonid; Htl, height of the talonid. Measurements are in mm.

	MHNC 8264		MHNC 8308		MHNC 8370		MHNC 13847		MHNC	MHNC	
specimen	L	R	L	R	L	R	L	R	8306	13925	Mean
L C	3.05	2.88	2.93	2.93	2.37	2.32	–	–	–	–	2.74
W C	1.52	1.34	1.29	1.25	1.39	1.43	–	–	–	–	1.37
H C	6.49	6.39	6.4	6e	5.88	5.62	–	–	–	–	6.13
L P1	1.27	1.53	1.33	1.44	1.55	1.32	1.30	1.35	–	–	1.38
L P2	2.27	2.12	2.10	2.04	2.13	–	2.46	2.34	–	–	2.21
L P3	2.21	2.21	2.25	2.68	2.38	–	2.58	2.46	–	–	2.39
W P1	0.59	0.69	0.65	0.60	0.74	0.69	0.66	0.61	–	–	0.65
W P2	0.95	1.02	0.95	1.01	0.97	–	0.93	1.09	–	–	0.99
W P3	1.18	1.42	1.44	1.41	1.30	–	1.18	1.13	–	–	1.29
H P1	0.69	0.76	1.00	0.84	0.74	1.04	0.86	1.02	–	–	0.87
H P2	1.52	1.74	1.7e	1.82	1.68	–	1.76	1.66	–	–	1.70
H P3	2.17	2.10	2.12	2.22e	2.27	–	2.69	2.27	–	–	2.26
L M1	2.81	2.81	2.73	2.79	2.53	2.54	2.83	2.70	–	–	2.71
L M2	3.06	2.80e	3.00	2.94	2.45	2.68	2.85	2.79	–	–	2.82
L M3	3.09	3.19	2.95	2.83	2.62	2.63	2.75	2.78	–	–	2.85
L M4	2.54	2.57	2.47	2.53	2.02	2.04	2.22	1.95	–	–	2.29
Lab M1	2.85	2.91	2.71	2.78	2.50	2.60	2.89	2.76	–	–	2.75
Lab M2	3.08	2.88e	3.08	2.94	2.54	2.70	2.75	2.66	–	–	2.82
Lab M3	3.09	3.21	2.92	2.81	2.72	2.69	2.76	2.77	–	–	2.87
Lab M4	2.79	2.78	2.83	2.59	2.27	2.17	2.48	2.40	–	–	2.53
W M1	2.72	3.14	3.01	2.62	2.78	2.80	2.86	3.19	–	–	2.89
W M2	3.30	3.50	3.37	3.11	3.38	3.10	3.03	3.56	–	–	3.29
W M3	3.73	3.71	3.50	3.38	3.52	3.25	3.64	3.84	–	–	3.57
W M4	3.45	3.42	3.47	3.13	3.35	3.27	3.26	3.62	–	–	3.37
L c	–	2.88	2.83	2.49	–	–	–	–	–	–	2.73
W c	–	1.16	1.01	1.31	–	–	–	–	–	–	1.16
H c	–	5.28	4.71e	–	–	–	–	–	–	–	4.99
L p1	1.57	1.14	1.59	1.60	–	–	–	–	1.36	1.38	1.44
L p2	2.21	2.23	2.25	2.26	2.16	–	–	–	2.30	1.92	2.23
L p3	2.53	2.35	2.58	2.38	2.32	–	–	–	2.44	2.48	2.44
W p1	0.68	0.59	0.55	0.60	–	–	–	–	0.72	0.62	0.63
W p2	0.88	0.94	0.92	0.96	0.93	–	–	–	1.00	0.95	0.94
W p3	0.88	1.00	1.13	1.14	1.00	–	–	–	1.09	1.00	1.03
H p1	0.98	0.92	1.02	1.01	–	–	–	–	0.96	1.08	0.99
H p2	1.71	1.87	1.84	1.66	1.76	–	–	–	2	1.94	1.82
H p3	2.20e	2.30e	2.33	2.89	2.30	–	–	–	2.2	2.54	2.39
L m1	2.72	2.64	2.69	2.64	2.74	–	–	–	2.62	2.36	2.63
L m2	2.94	2.77	2.87	3.05	3.00	–	–	–	2.89	2.76	2.89
L m3	3.04	2.92	2.91	3.20	3.05	–	–	–	2.97	2.92	3.00
L m4	3.20	2.93	3.08	3.11	3.06	–	–	–	2.91	3.12	3.05
Ltr m1	1.80	1.60	1.79	1.62	1.81	–	–	–	1.50	1.35	1.64
Ltrm2	1.96	1.75	1.92	1.72	1.90	–	–	–	1.74	1.55	1.79
Ltr m3	1.96	1.70	1.97	2.00	1.93	–	–	–	1.74	1.59	1.84
Ltr m4	1.96	1.65	1.89	1.84	1.95	–	–	–	1.71	1.60	1.80
Ltl m1	1.24	1.10	1.20	1.03	1.03	–	–	–	0.89	1.00	1.07
Ltl m2	1.31	1.18	1.38	1.18	1.22	–	–	–	1.08	1.05	1.20
Ltl m3	1.29	1.16	1.20	1.09	1.14	–	–	–	1.23	1.14	1.18
Ltl m4	1.33	–	1.25	1.12	1.16	–	–	–	1.16	1.39	1.23
Wtr m1	1.29	1.30	1.28	1.42	1.39	–	–	–	1.46	1.39	1.36
Wtr m2	1.60	1.77	1.37	1.79	1.63	–	–	–	1.67	1.52	1.62
Wtr m3	1.79	1.80	1.80	1.75	1.81	–	–	–	1.83	1.68	1.78
Wtr m4	1.72	1.81e	1.62	1.76	1.75	–	–	–	1.78	1.68	1.72
Wtl m1	1.34	1.03	1.34	1.31	1.31	–	–	–	1.28	1.26	1.26
Wtl m2	1.61	1.41	1.52	1.44	1.43	–	–	–	1.51	1.33	1.46
Wtl m3	1.56	1.50	1.51	1.44	1.41	–	–	–	1.53	1.39	1.48
Wtl m4	1.23	1.22	1.37	1.30	1.08	–	–	–	1.12	1.17	1.21
Htr m1	2.23	–	2.18	–	–	–	–	–	2.09	2.21	2.17
Htr m2	2.23	2.41	2.22	2.23	2.45	–	–	–	2.32	2.35	2.31
Htr m3	2.31	2.50	2.22	2.30	2.61	–	–	–	2.60	2.43	2.42
Htr m4	2.35	–	2.35	2.51	2.52	–	–	–	2.72	–	2.49
Htl m1	1.22	1.11	1.24	–	–	–	–	–	1.23	1.35	1.23
Htl m2	1.32	–	1.29	1.36	1.15	–	–	–	1.44	1.51	1.34
Htl m3	1.41	–	1.33	1.38	1.35	–	–	–	1.50	1.37	1.39
Htl m4	1.09	–	1.11	1.01	1.17	–	–	–	1.13	1.10	1.10

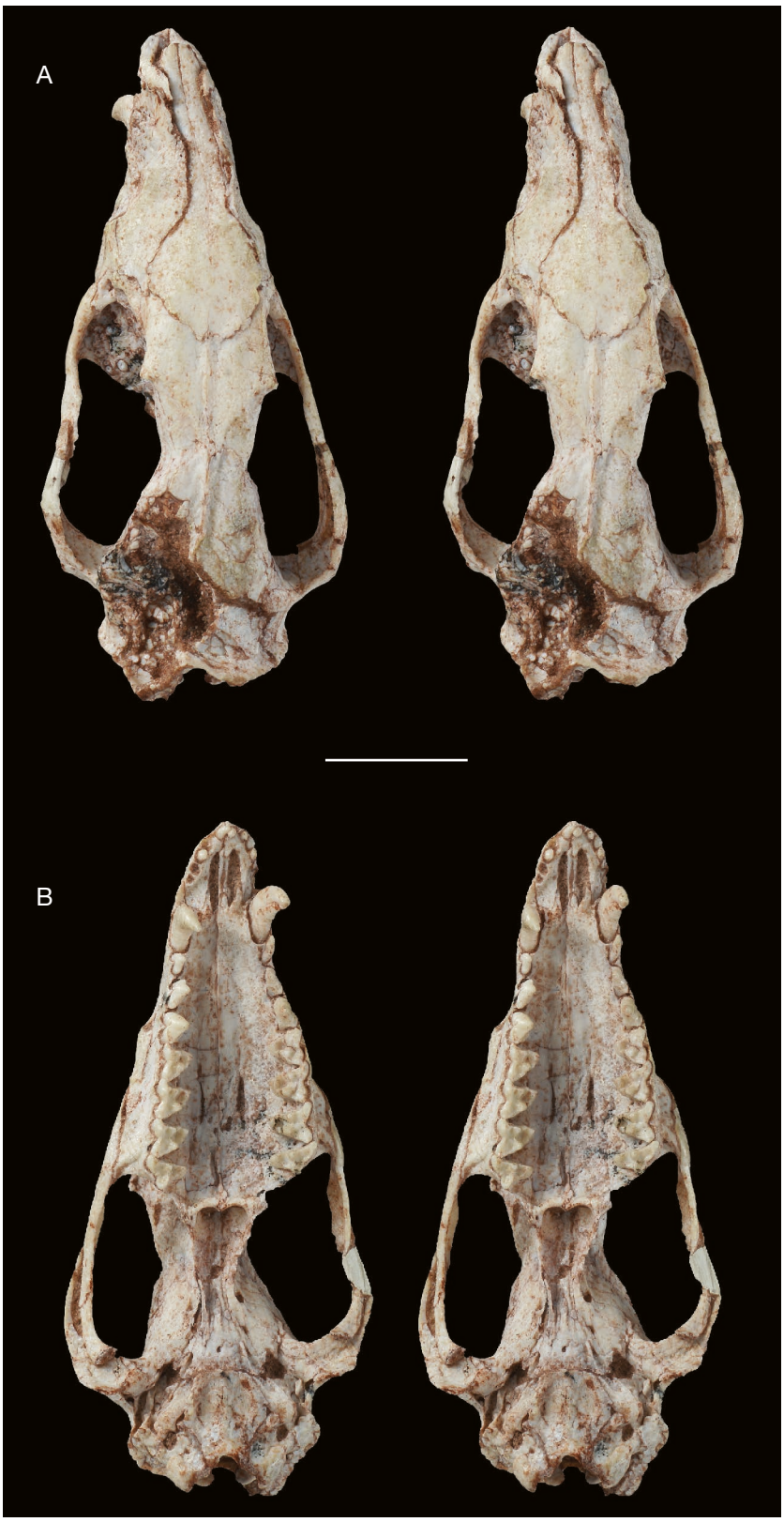

Fig. 6. — *Andinodelphys cochabambensis* (MHNC 8308) stereophotos of the cranium: **A**, dorsal view; **B**, ventral view. Scale bar: 10 mm.

inflated on its distobasal edge. The asymmetry of the protocone is also present in the relative size of the protocristae, the preprotocrista being shorter than the postprotocrista. At their labial extremity, the protocristae bear well-developed para- and metaconules, which are subequal in size. When present the postparaconule and premetaconule cristae are very weak and

FIG. 7. — *Andinodelphys cochabambensis* (MHNC 8308), **A**, right lateral view of the anterior region of the rostrum; **B**, left lateral view of the anterior region of the rostrum; **C**, upper incisors and canines in anterior view; **D**, upper incisors and canines in ventral view; **E**, upper incisors and canines in anteroventrolateral view; Scale bar: 5 mm.

low. In contrast, the conules extend disto- and mesio-dorsally in well-developed preparaconule and postmetaconule cristae. The preparaconule crista extends labially along the base of the paracone and form a well-developed paracingulum, which reaches the stylar cusp A. The postmetaconule crista extends distodorsally but remains at the mesiolingual base of the metacone and does not extend labially towards the stylar cusp E. The trigon basin is deep and wide and extends labially between the para- and metacone. These cusps are widely separated at their bases as is observed in *Pucadelphys*. They are not adjoined at their bases in contrast to the condition observed in the basal sparassodonts, *Mayulestes, Allqokirus* or *Patene*. The paracone is distinctly lower and subequal to slightly less voluminous (in occlusal view) than the metacone. The postparacrista and premetacrista are moderately developed. They extend from the apices of their respective cusp dorsally and labially. As a consequence, their point of contact is located more labial than the apices of the cusps so that, in occlusal view, the centrocrista (postparacrista + premetacrista) is slightly V-shaped with the apex of the V pointing labially. In labial view the centrocrista is V- shaped to U-shaped and wide open as is observed in *Pucadelphys.* It differs from the condition in *Mayulestes, Allqokirus*, and *Patene*, in which the V- shaped angle formed by the centrocrista in labial view is narrower and more closed. The part of the cusps lingual to the centrocrista is voluminous and strongly convex, while the labial part is reduced and only slightly convex. The preparacrista and postmetacrista are also

Fig. 8. — *Andinodelphys cochabambensis* (MHNC 8370), upper canine and cheek teeth series: **A**, ventromedial view of left canine and cheek teeth (C-M4); **B**, occlusal view of left canine and cheek teeth (C-M4); **C**, ventrolateral view of right molars. Scale bar: 5 mm.

in a slightly labial position as is the centrocrista. As a consequence, in occlusal view the paracone and metacone have a roughly triangular section. However, because of the slight inflation of the labial aspect of the paracone and metacone, this condition is not as marked as in extant didelphids. Lingually, the bases of the paracone and metacone are just labial to the conules. Labially, the slightly convex ridge of the cusps is more developed on the metacone than on the paracone. Both ridges cross the stylar shelf and converge labially toward the stylar cusp C. The stylar shelf is large, wide and deep. It occupies approximately the labial 40% of the tooth in width and occlusal area. Its morphology varies from M1 to M3. On M1 it is distinctly narrower mesially than distally, a condition that reduces on M2 and even more on M3, on which this width difference is less pronounced. From M1 to M3 the stylar shelf is roughly constant in length but it increases in width. The stylar cusps are large and massive. Stylar cusp A is well developed and extends mesially in a salient parastylar lobe, which overlaps the distolabial angle of the preceding tooth being closely appressed against it and generally labial to it. Stylar cusp B is voluminous being almost as large as the paracone on M1-2. It is connected to the paracone by a salient preparacrista, which increases in length from M1 to M3. The preparacrista attaches to the mesiolingual region of the stylar cusp B. In occlusal view stylar cusp B is oval shaped, being longer than wide. Stylar cusp C is located in the middle region of the labial edge of the tooth in the ectoflexus. The morphology, size and number of this cusp are extremely variable on our sample. On MHNC 8370 and 13847 stylar cusp C is a single well-developed, transversely flattened

FIG. 9. — *Andinodelphys cochabambensis* (MHNC 8308) upper canine and cheek teeth series: **A**, ventromedial view of left and labial view of right tooth row; **B**, occlusal view of right and ventromedial view of left tooth row. Scale bar: 5 mm.

Fig. 10. — *Andinodelphys cochabambensis* (MHNC 8264) upper canine and cheek teeth series (C-M4): **A**, occlusal view of left and labial view of right tooth row; **B**, labial view of left and occlusal view of right tooth row. Scale bar: 5 mm.

cusp, which approximates the size of the stylar cusp A and is much smaller than stylar cusps B and D. On MHNC 8264 stylar cusp C is a single cusp on M1-2 but is reduced to a thickened cingulum on M3. On MHNC 8308, it is a small cusp on M1, and a thickened cingulum on left M2 and M3. On right M2 it is twinned in a pair of two small cusps as is

FIG. 11. — *Andinodelphys cochabambensis* (MHNC 13847): stereophotographs of the left upper premolar (P1-P2) and molar (M1-M4) series. Scale bar: 5 mm.

observed on the holotype (YPFB Pal 6192). Furthermore, on MHNC 8370 stylar cusp C is twinned on the right M2 but is single cusp on the left M2. The same condition is also present on MHNC 13847 but reversed (left stylar cusp C of M2 only is twinned). Therefore, the twinned nature of stylar cusp C observed on the holotype is apparently highly variable within our sample. Stylar cusp D is slightly smaller than stylar cusp B (but sometimes subequal to it) and transversely compressed. Stylar cusp D is slightly posterolabial to the metacone. Stylar cusp E is distinctly present but is the smallest cusp of the tooth. It is sometimes connate to stylar cusp D and linked to the metacone by a long mesially concave postmetacrista. The ectoflexus is very shallow to absent on M1 but increase in depth from M1 to M3. The first three upper molars have a similar pattern but differ in their proportions and relative size of some of their elements. From M1 to M3 they increase in overall size and width. The preparacrista increases in length correlatively to the increase in width of the stylar shelf. Stylar cusp A, B, and D slightly increase in size from M1 to M3. The ectoflexus deepens from M1 to M3. No pre- or postcingula are present.

Upper M4 (Figs 8-11). The M4 is significantly different from the other three anterior molars, which justifies a separate description. The major differences of M4 relatively to M1-3 result from the strong reduction of the metacone, which is much lower and less voluminous. The metacone is also clearly smaller in height and volume than the paracone. As a consequence, the premetacrista is almost sub-horizontal in some specimens and the postmetacrista is greatly shortened. The paracone is similar in size to that of M3 and the preparacrista is longer. The protocone and conules are slightly smaller than on the preceding molars. The stylar cusp A is slightly larger than on M3. In contrast, stylar cusp B is much smaller to barely present. Stylar cusp C is tiny (sometimes twinned) and stylar cusps D and E are absent. As a consequence, the distolabial angle of the tooth is greatly reduced, the stylar shelf strongly narrows distally and the labial alveolar edge of M4 is strongly oblique being oriented distolingually-mesiolabially. In contrast, the parastylar lobe is greatly developed being slightly larger than on M3. As on the other molars, the preparacrista is markedly transverse and forms an angle close to 90°-100° with the centrocrista (or paracone-metacone axis). This con-

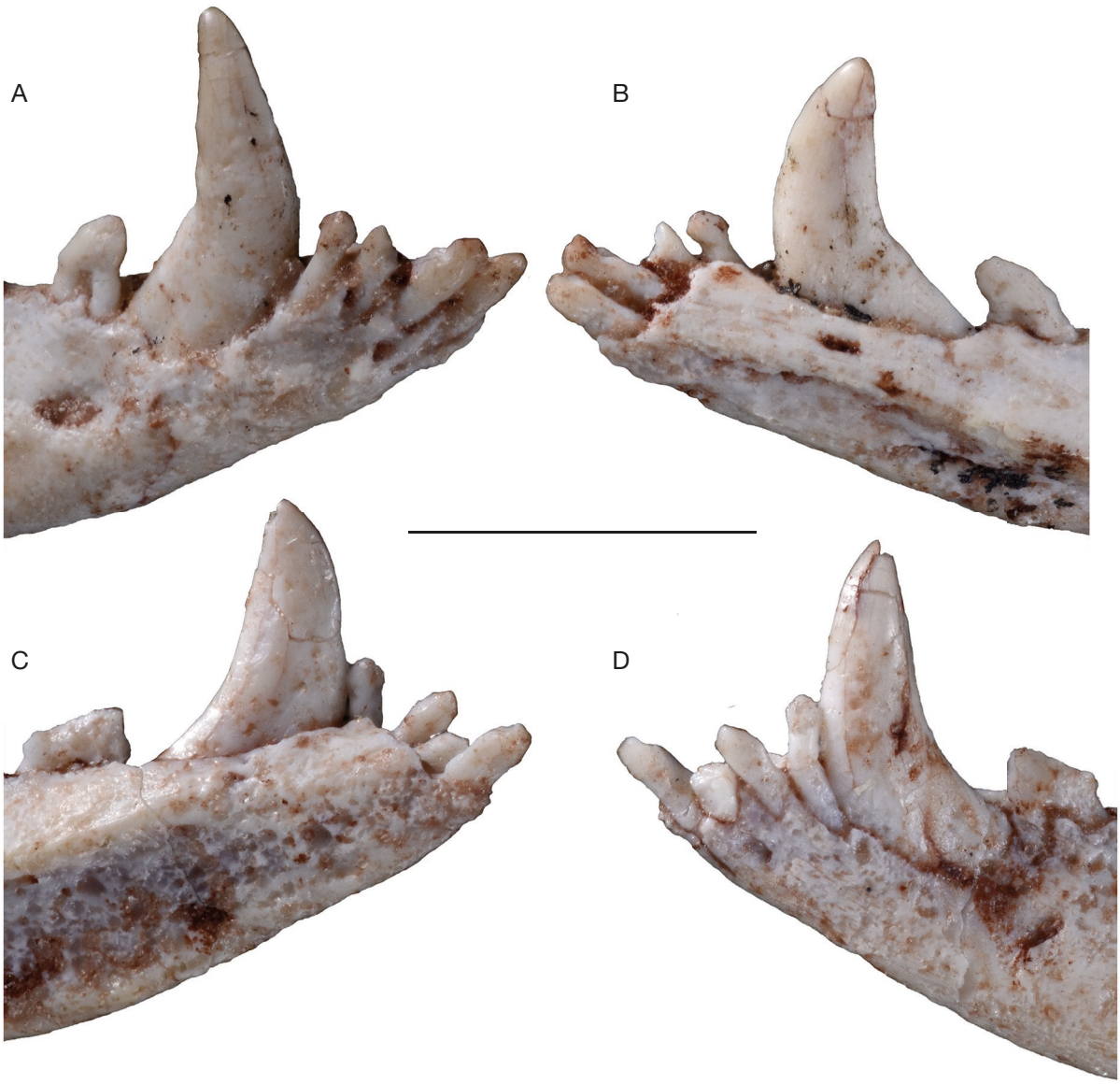

Fig. 12. — *Andinodelphys cochabambensis*, lower incisors and canine: **A**, right anterolabial view of MHNC 8264; **B**, right anterolingual view of MHNC 8264; **C**, left anterolingual view of MHNC 8308; **D**, left anterolabial view of MHNC 8308. Scale bar: 5 mm.

dition is also observed on the M4 of *Pucadelphys* and in most extant didelphids (in which the M4 is not drastically reduced). This condition differs from that observed in *Mayulestes* and *Allqokirus*, in which the cristae are at an angle of *c.* 130°. A similar angle is observed in *Patene simpsoni* and is even greater in later sparassodonts in which the cristae are still observable (e.g. *Sallacyon*, *Sipalocyon*) (see discussion below). As a whole, the M4 is mesiodistally shorter than the other molars.

Lower dentition

Lower incisors. (Figs 12, 13) Four incisors are present. In the description below, we follow the interpretation of Hershkovitz (1982, 1995), that the four lower incisors of metatherians are serially homologous to i2-i5. The crowns of i2, i3, and i5 are preserved on MHNC 8264 and the crowns of i2, i4, and i5 are preserved on MHNC 8308. The i2-4 are roughly subequal in size and i5 is slightly smaller than the other incisors. The i3 is distinctly staggered as indicated by the buttress visible on the anterolabial edge of the dentary just ventral to the labial aspect of the tooth on MHNC 8308. In dorsal view the dorsal shift of the root of i3 is clearly visible between the roots of i2 and i4. The crowns of i2 and i3 are spatulate and slightly compressed labiolingually. They are roughly triangular being only slightly higher than long. The i4 of MHNC 8308, which is unworn is pointed apically and its root is slightly thicker than those of i2-3. The i5 is distinctly smaller with a lower crown, approximately as long as high.

Lower canine. (Figs 12, 13) The lower canine is a large tooth, although consistently smaller than the upper canine. It is pointed at apex and curved (from the alveolar border) dorsally but not posteriorly. In other words, the apex of the tooth does not

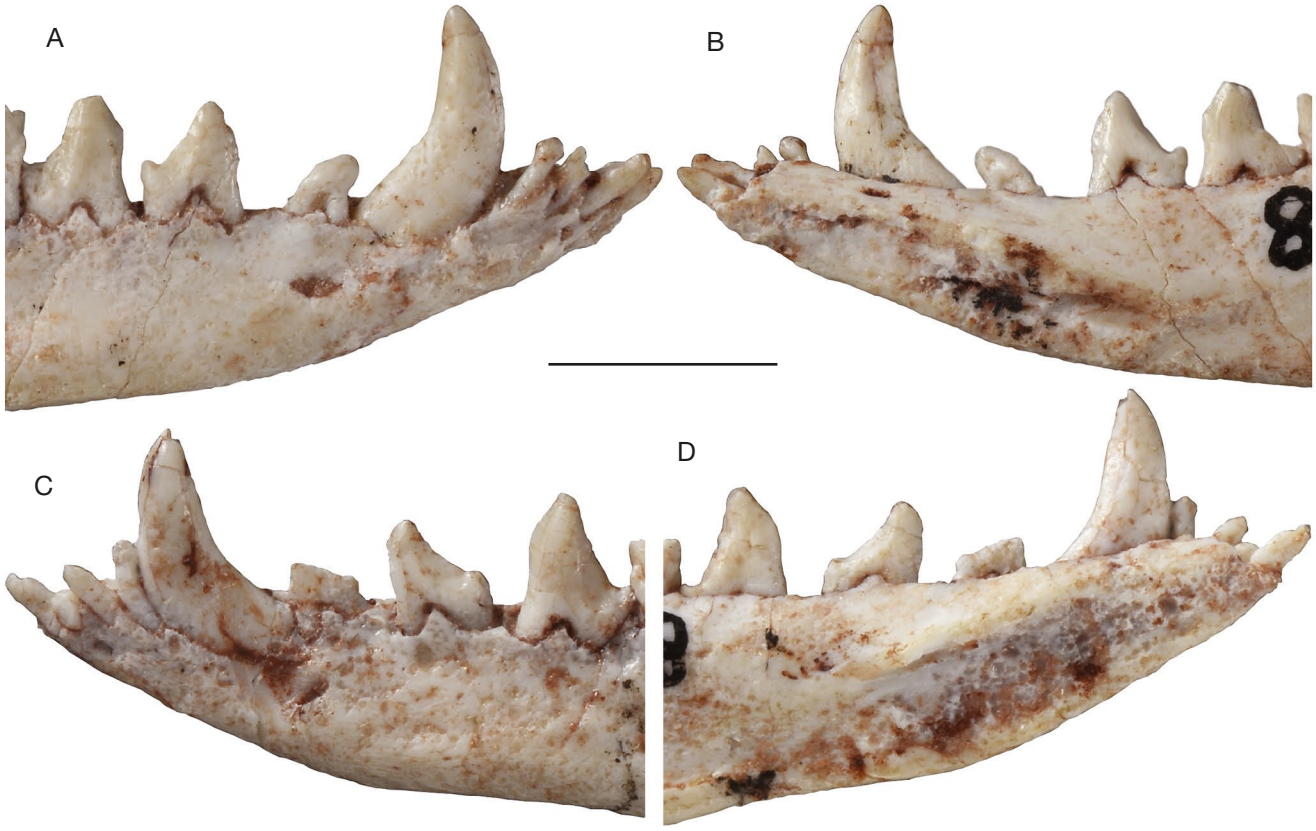

Fig. 13. — *Andinodelphys cochabambensis* anterior part of the dentary with i1-p3: **A**, right labial view of MHNC 8264; B, right lingual view of MHNC 8264; **C**, left labial view of MHNC 8308; **D**, left lingual view of MHNC 8308. Scale bar: 5 mm.

overhang the distal edge of the crown (Fig. 13). In cross-section the canine is oval-shaped, with the lingual face of the crown being slightly flattened or less convex than the labial face. At the alveolar border the section of the tooth is more than two times longer than wide (1.22 × 3.03 on MHNC 8264). The axis of the canine is set at a slightly oblique angle relative to the cheek tooth series, being mesiolabially-distolingually oriented.

Lower premolars. (Figs 13-Fig. 16) As observed on the upper premolars, p2 and p3 are closer to each other in the values of the three measurements presented in Table 2 (length, width and height) than are p1 and p2. In other words, the size difference between the p1 and p2 is more pronounced than between p2 and p3. All three lower premolars are double-rooted. They are distinctly premolariform and are composed of one single cusp. The p1 is very small and adjacent to the distal edge of the canine. In contrast, it is separated from p2 by a small diastema (*c.* 0.6 mm). In occlusal view p1 is ovoid and strongly compressed transversely. The p1 is set obliquely in the tooth row and its mesial root is distinctly distolabial to the distal edge of the canine. In labial view, the whole tooth is tilted anteriorly so that the alveolar border of the mesial root is ventral to that of the distal root. In labial view p1 is strongly asymmetrical and the apex of the crown is set above the mesial edge of the mesial root. In MHNC 8264 the mesial edge of the crown is even mesial to the mesial edge of the mesial root. As a consequence, the distal edge of the crown is at least three times longer than the mesial one. At the distal base of the crown is a tiny cuspule. The p2 is twice as large as p1. In occlusal view the crown is oval-shaped (wider posteriorly than anteriorly) with a lingual face less convex (almost flat or even slightly concave as in MHNC 8264 and 8370) than the labial one. The mesial edge of the crown is subvertical and slightly convex mesially. The apex of the crown is mesially placed above the mesial root. The distal ridge of the crown is two times longer than the mesial ridge, slightly concave distodorsally and gently sloping distoventrally. At the distal base of the crown is a small but distinct distal heel. The p3 is very similar to the P3. It is distinctly larger than p2, being slightly longer and much higher. It is set in an upright position to a greater extent than p2. Consequently, the apex of the crown is in a slightly more distal position than on p2, being dorsal to the distal edge of the mesial root (Fig. 13). In labial view, the mesial edge of the crown is convex but slightly sloping mesially (i.e. the apex of the crown is distal to its mesial base). The distal edge of the crown is straight to slightly concave. It is longer than the mesial edge although to a lesser extent than on p2. The distal base of the crown bears a well-developed heel. The apex of this small talon is in a lingual position so that its labial face is more extended and more sloping than its lingual side. None of the lower premolars bears any kind of cingulum. From p1 to p3 the lower premolars of *Andinodelphys* conspicuously shift from a mesially tilted to an upright position.

Fig. 14. — *Andinodelphys cochabambensis* (MHNC 8264) left lower premolars (p2-p3) and molars: **A**, labial view; **B**, occlusal view (stereophotos); **C**, lingual view. Scale bar: 5 mm.

FIG. 15. — *Andinodelphys cochabambensis* (MHNC 8308) left lower premolars and molars: **A**, labial view; **B**, occlusal view (stereophotos); **C**, lingual view. Scale bar: 5 mm.

Lower molars. (Figs 14-16) The four lower molars slightly increase in length distally (m1<m2<m3<m4). This comparison is based on the mean of five specimens, two of them including right and left molars (MHNC 8264, 8308), and therefore seven measurements. The trigonid of m1 is slightly lower than on the other molars but m2-m4 are subequal in trigonid height. The trigonid is slightly narrower than the talonid on m1, subequal on m2-3, and the trigonid is consistently wider than the talonid on m4. The trigonid of m1 is relatively long with a paraconid set mesiolabially (as compared to the other molars) so that the angle between the paracristid and protocristid is more open lingually. As a consequence, if the length of the trigonid is measured at the apices of paraconid and metaconid, the trigonid of m1 is distinctly longer than wide, while it is wider than long on m2-4. In contrast, if the length of the trigonid is measured from mesialmost point of the molar to distobasalmost point of the metaconid, the trigonid is longer than wide on the four molars. The protoconid is the highest of the trigonid cusps, but it is only slightly higher than the metaconid. In width, it occupies approximately half of the talonid width. In occlusal view, the protoconid is triangular in section, while the metaconid is roughly ovoid and less voluminous. In lingual view, the metaconid is subvertical and slightly increases in height distally. The paraconid is the smallest cusp of the trigonid. In lingual view, it is consistently tilted mesially and also increases in height distally. Paraconid and metaconid are connate at base and the vallid between them is higher than half of the metaconid height (measured from the lingual alveolar border). Because of this condition, the trigonid basin is elevated, well-excavated, and well-circumscribed lingually at least on m2-4. On these molars, the deepest point of the basin is at the level of, or lower than the uppermost point of the paraconid-metaconid vallid. This condition is similar to that observed in *Pucadelphys* but differs distinctly from that observed in the Tiupampa sparassodonts, *Mayulestes* and *Allqokirus*. In these taxa, the paraconid and metaconid are broadly separated and the vallid between them is wider and extends almost as far as the base of the crown lingually. As a consequence, the trigonid basin is broadly open lingually and is more a slope on the lingual side of the protoconid than a true depression. The paraconid of *Andinodelphys* is roughly triangular in occlusal section and its mesiolingual angle bears a salient paraconid ridge, which projects mesially. Labial to this ridge the mesial face of the paraconid is excavated by a shallow hypoconulid notch. The ridge and notch interlock with the hypoconulid of the preceding molar. When unworn, paracristid and protocristid are sharp but no carnassial notch is present on the paracristid, whereas a weak notch is present on the protocristid. The median point of the cristids (point of contact of the cusps) is slightly lower on the paracristid than on the protocristid, this condition being more marked on the anterior molars. The paracristid is strongly oblique relative to the axis of the tooth row, whereas the protocristid is distinctly transverse. The angle of the paracristid with the axis of the tooth row increases from m1 to m4 (Figs 14B-16B).

The talonid is distinctly basined. On m1-3, the hypoconid is the largest cusp in height and volume; the entoconid and the hypoconulid are subequal in height and volume. On m4 the hypoconulid is the highest cusp of the talonid. The hypoconid is large and occupies approximately half of the talonid volume on m1-2 and slightly less on m3-4. It is conspicuously larger than the other cusps of the talonid. In occusal view, it is triangular to V-shaped in appearance. At the mesial edge of the hypoconid, the cristid obliqua is well-developed and sharp. It extends mesiolingually and connects to the trigonid at the distolingual edge of the protoconid (i.e. slightly labial to the protocristid notch). On the distolingual edge of the hypoconid a strong posthypocristid connects to the hypoconulid. It is distolabially concave and deeply notched between the two cusps. The posthypocristid notch is located approximately at midline of the talonid. At the distolingual angle of the talonid the hypoconulid and entoconid are clearly approximated and twinned (i.e. set closer to each other than to the hypoconid). They are not distinctly connate. The hypoconulid is lingual to the midline of the talonid. The entoconid is a small but well-individualized cusp. It is somehow compressed transversely and bears, on its mesial edge, a marked entocristid, which connects the distal base of the metaconid. Therefore, the talonid is relatively well enclosed lingually. On m4 the hypoconulid is enlarged and elevated above the other talonid cusps. The entoconid is reduced and partially fused at base of the hypoconulid. A well-developed precingulid is present at the mesial base of the protoconid and extends on the mesiolabial base of the paraconid. A thick postcingulid is present on distal edge of m1-3 as a shelf extending ventrolabially from the apex of the hypoconulid to the distal edge of the hypoconid as far as its labial side. A postcingulid is absent on m4.

Bony skull

General features (Figs 6, 17-20)

Three complete skulls of *Andinodelphys* are known. MHNC 8264 is little distorted and measurements of the skull provide an acceptable approximation of its proportions. MHNC 8308 is slightly compressed transversely and the left side of the skull appears to have been more affected by transverse distortion than the right. Therefore, the measurement of the bizygomatic width of the skull can be estimated in multiplying by 2 the measurement taken for the right half of the skull width (see table below). MHNC 8370 is strongly distorted, with the right side more affected by the distortion and the right zygomatic arch completely crushed. The deformation of this specimen is severe and prevents to estimate rigorously its dimensions.

In general size and when compared to the length of the five *Pucadelphys* skulls measured in Table 3, the skull length of *Andinodelphys* is 28% (minimum length of *Andinodelphys* vs. maximum length of *Pucadelphys*) to 42% (maximum length of *Andinodelphys* vs. minimum length of *Pucadelphys*) larger (in absolute value) than that of *Pucadelphys*. Therefore, the skull of *Andinodelphys* is approximately one third longer than that of *Pucadelphys* (28 + 42/2 = 35). When comparing the means of the bizygomatic width of the two genera, the skull of *Andinodelphys* is 19.6% wider than that of *Pucadelphys*. Therefore, the significant difference observed in the two measurements shows that the skull of *Andinodelphys* is proportionally longer than

FIG. 16. — *Andinodelphys cochabambensis* (MHNC 8370) left lower premolars (p2-p3) and molars: **A**, labial view; **B**, occlusal view; **C**, lingual view. Scale bar: 5 mm.

that of *Pucadelphys*. Comparison of the mean of the width/length ratio obtained from the two complete skulls of *Andinodelphys* (0.520 + 0.497/2 = 0.508) with the mean obtained with 5 skulls of *Pucadelphys* ($\bar{X}$= 0.632) clearly indicates that the skull of the former is proportionally *c.* 24% longer than that of the latter. Comparison of the relative length of the palate and rostrum indicates that it is proportionally slightly longer in *Andinodelphys* than in *Pucadelphys*. In contrast, the relative length of the orbitotemporal fossa of *Andinodelphys* is not significantly larger (proportionally) than in *Pucadelphys*.

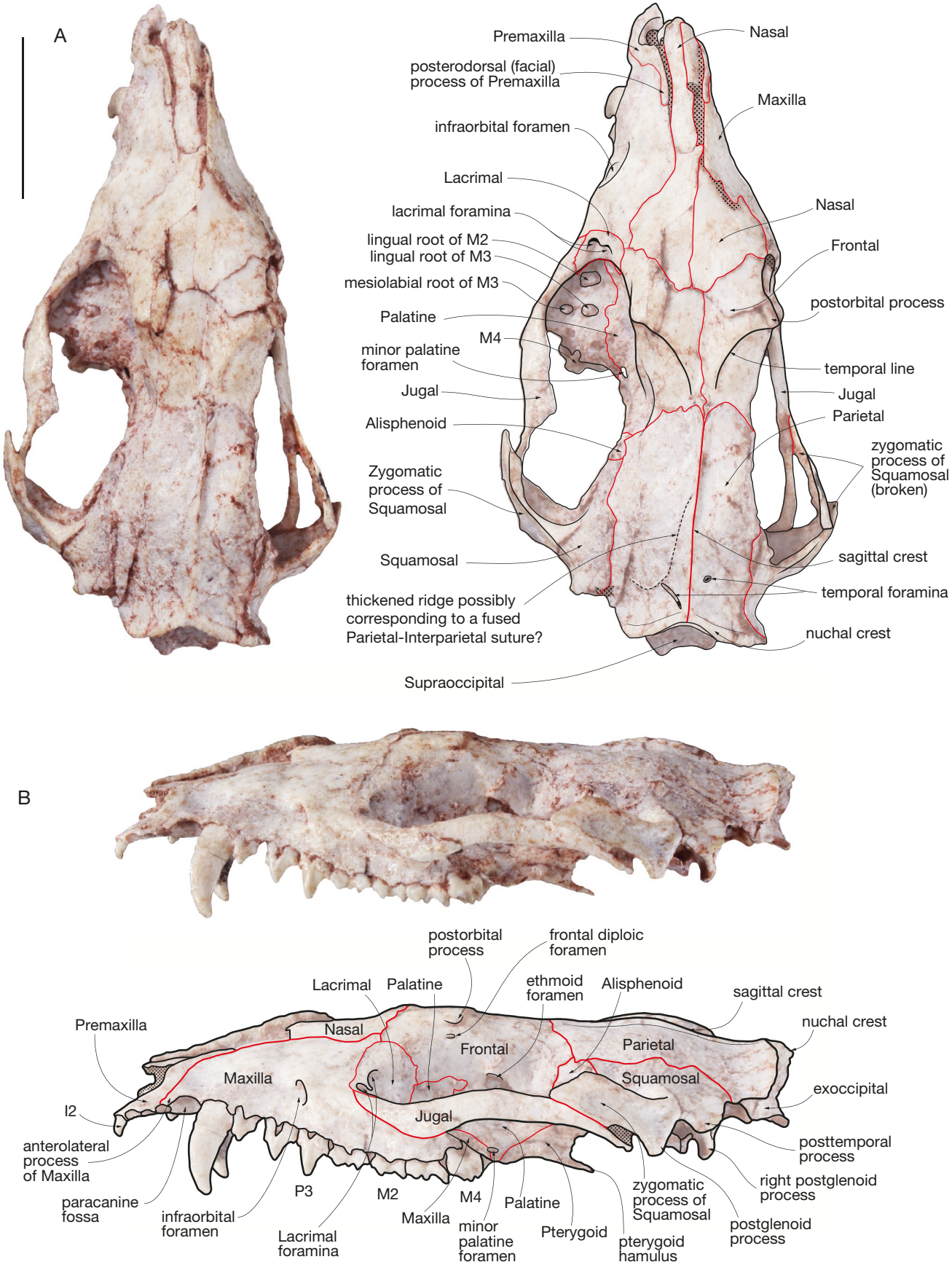

FIG. 17. — **A**, **B**, *Andinodelphys cochabambensis* (MHNC 8370), cranium: **A**, dorsal view; **B**, lateral view. Scale bar: 10 mm.

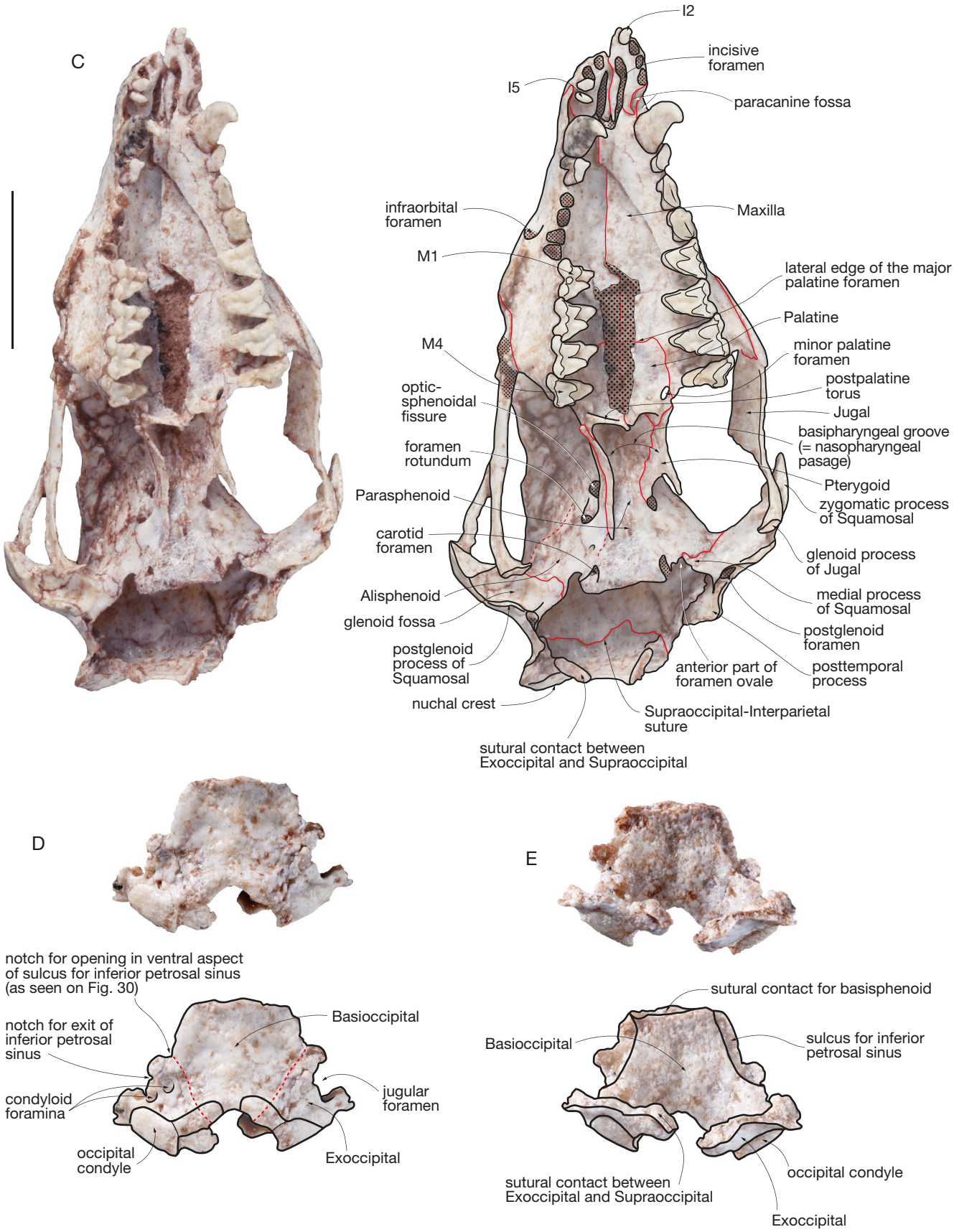

FIG. 17. — **C**-**E**, *Andinodelphys cochabambensis* (MHNC 8370), cranium: **C**, ventral view; **D**, basioccipital and exoccipitals in ventral view; **E**, basioccipital and exoccipitals in dorsal view. Scale bar: 10 mm.

TABLE 3. — Skull proportions in two specimens of *Andinodelphys cochabambensis* and five specimens of *Pucadelphys andinus.* Abbreviations: **Lft**, length of the orbitotemporal fossa measured dorsally; **Lpl**, length of the palate from the median palatine spine to the anterior end of the premaxilla; **Lr**, length of the rostrum from the anterior edge of the orbit to the anterior end of the premaxilla; **Lt**, condylobasal length; **Wbz**, bizygomatic width. Measurements are in mm.

	Lt	Wbz	L pl	Lr	Lft	Wbz/Lt	Lpl/Lt	Lr/Lt	Lft/Lt
Andinodelphys cochabambensis									
MHNC 8264	48.2	25.08	27.5	19.32	23.79	0.520	0.570	0.400	0.493
MHNC 8308	47.14	11.72 × 2 = 23.44e	27.45	20.75 + 19.31/2 = 20.03e	22.13	0.497	0.582	0.424	0.469
Mean *Andinodelphys*	47.67	24.26	27.47	19.67	22.96	0.508	0.576	0.412	0.481
Pucadelphys andinus									
MHNC 8266	33.03	18.30	17.9	12.47	15.68	0.554	0.542	0.377	0.474
MHNC 8278	28.2e	18.72	15.83	10.89 + 11.02/2 = 10.95e	13.02	0.664	0.561	0.388	0.462
MHNC 8382	34.01	19.61	18.17	12.92	16.56	0.576	0.534	0.380	0.487
MHNC 8381	31.61	20.69	17.30	12.61	14.38	0.654	0.547	0.399	0.455
YPFB Pal 6105 Holotype	28.32	10.09 × 2 = 20.18	15.6	10.08 + 11.89/2 = 10.90	13.22	0.712	0.550	0.384	0.466
Mean *Pucadelphys*	31.02	19.5	16.96	11.97	14.57	0.632	0.546	0.385	0.469

In general aspect, the skull of *Andinodelphys* is similar to that of the Recent didelphid *Metachirus*, although 15% to 30% smaller. Furthermore, the braincase of *Andinodelphys* is smaller than that of *Metachirus*, which is demonstrated by the fact that the anterior region of the braincase (the narrowest point of the skull) is posterior to the apex of the zygomatic process of the squamosal in *Andinodelphys*, whereas it is at the same level in *Metachirus* (i.e. more anterior than in *Andinodelphys*).

In dorsal view the zygomatic arches are not regularly and strongly convex as in the Recent didelphids. They diverge evenly from their anterior root, being only slightly convex and, at the level of the lateral edge of the glenoid fossa, they rapidly bend medially at an angle of almost 90° as is observed (generally) in *Pucadelphys* (Ladevèze *et al.* 2011) and *Mayulestes* (Muizon 1998). Posteriorly, the glenoid fossae, at the posterior roots of the zygomatic arches, project laterally in contrast to the condition observed in extant didelphids but resembling *Pucadelphys* in this respect. This condition is related to the morphology of the zygomatic arches exposed above.

A small but conspicuous sagittal crest is present, formed by the posterior junction of the weak temporal lines (= orbital crests). It starts at the posterior edge of the frontals, runs along the parietal and connects to the nuchal crest posteriorly. It is low and has the same elevation all along the parietal. It resembles the sagittal crest observed in *Pucadelphys* and *Monodelphis*, but is much lower than in *Didelphis*. It clearly differs from the condition observed in *Caluromys* and *Metachirus,* in which the temporal lines do not meet posteriorly (or join very posteriorly) and form two parasagittal crests, which extend almost until the nuchal crest or which join at a short distance beyond it. The nuchal crest of *Andinodelphys* is well developed and projects posteriorly above the occipital condyles. On the ventral side of the skull, the palate is long and narrow. The dental rows are rectilinear and diverge only slightly posteriorly.

As a whole, the general morphology of the skull of *Andinodelphys* is roughly similar (with the small differences mentioned above) to that of the extant didelphids especially *Metachirus* and *Monodelphis*.

In order to predict the body mass of *Andinodelphys*, we chose to follow the same equation as that used for *Pucadelphys* (Ladevèze *et al.* 2011). From the study of Myers (2001), we selected the dasyuromorphian model and, as tested on the *Didelphis virginiana pigra* specimens of known body mass, the most accurate equation is that based on the total skull length given in Myers (2001: 105). We therefore calculated the body masses for three specimens of *Andinodelphys cochabambensis,* in which the skull length can be measured (MHNC 8264, 3308, and 8370) from Myers' equation: log y = –3.465 + 3.436(log TSL), where TLS is the total length of the skull. We found a mean of 177 grams for *Andinodelphys* (Table 4), which is much more than the bodymass estimated for *Pucadelphys* (20 grams).

Premaxilla (Figs 7, 17-20)

In lateral view the premaxilla presents a long and narrow posterodorsal process (facial process), which is wedged between the nasal and the maxilla. The apex of the process extends posteriorly as far as approximately one third (MHNC 8308) to mid-length of the parallel-sided anterior portion of the nasal (MHNC 8264, 8370). On the lateral aspect of the rostrum, the premaxilla-maxilla suture is roughly sigmoid, being anterodorsally concave in its anterior portion and convex in its posterior portion. Anteroventrally the suture reaches the alveolar border between I4 and I5. In other words, a small anterolateral process of the maxilla covers the premaxilla in the area of the lateral alveolar border of I5 (see below). The dorsal edge of the premaxilla, viewed laterally, is also sigmoid being convex in its posterodorsal portion and concave in its anteroventral region. In its posterodorsal region the dorsal edge of the premaxilla articulates with the nasal. Anteriorly the dorsal edge bends ventrally, leaves the nasal and forms the lateral edge of the narial opening. In dorsal view, the anterior edge of the two premaxillae have a strongly convex shape (parabolic), with a small premaxillary tubercle at their anteromedial tip. This structure is consistently present on the specimens, which have a fully preserved anterior tip of the premaxillae (MHNC 8308, 8370, 13847). In ventral view, the premaxilla bears the five incisors anteriorly. The

TABLE 4. — Estimations of the body mass for the three skulls of *Andinodelphys*, in which the total length of the skull can be measured, from Myers' equation: log y = –3.465 + 3.436(log TSL).

Taxon	Total skull length	Body mass from Myers'equation: log y = –3.465 + 3.436(log TSL)
Andinodelphys cochabambensis (MHNC 8264)	47.99	204.8490606
Andinodelphys cochabambensis (MHNC 8308)	47.3	194.9049547
Andinodelphys cochabambensis (MHNC 8370)	42.2	131.6963024
Mean		177.1501059

two premaxillae form approximately the portion of the palate anterior to the anterior alveolar border of the canines with a small contribution of the anterolateral processes of the maxillae. On the palate, the premaxillae are pierced by the anterior two thirds of the elongated incisive foramina. The ventral view of the premaxilla shows two posteriorly oriented branches, which form the lateral and medial edges of the incisive foramina. These branches articulate posteriorly with the maxilla on the palate. The lateral branch of the premaxilla, which borders the incisive foramen laterally, has approximately the same width from I1 to the canine. It is approximately twice as wide (on MHNC 8264) as the incisive foramen. Its posterior extremity is located between the anterolateral and the anteromedian process of the maxilla (the latter being located between the anteromedial and anterolateral processes); (see above and below) (Figs 18B; 19B). The posterolateral branch of the premaxilla bears the medial two thirds of the paracanine fossa for the lower canine, which is located just anterior to the upper canine. This branch is rounded posteriorly and almost contacts the anteromedial edge of the alveolus of the canine, leaving only a very narrow strip of maxilla between it and the tooth posteriorly. In the anterior region of the paracanine fossa is the alveolus of the I5, while the fossa extends anteriorly as a narrow sulcus on the medial edge of the alveolar border of I5. In the posterior region of the paracanine fossa, the premaxilla-maxilla suture is U-shaped to V-shaped anteriorly. It enters the palate at the level of the posterolabial alveolar border of I5 (between the apex of the anterolateral process of the maxilla and the premaxilla), runs posteromedially from the lateral aspect of the rostrum, almost reaches the anteromedial edge of the canine alveolus, makes a U to V-turn, and extends further anteromedially as far as approximately the posterior third of the lateral edge of the incisive foramen. The medial branch of the premaxilla forms the medial edge of the incisive foramen for approximately 80% of its length anteriorly. Both medial branches of the premaxillae form the median bar, which separates the incisive foramina. This medial branch articulates posteriorly with a small anteromedial process of the maxilla and both structures slightly overlap anteroposteriorly. The medial branch is much narrower than the lateral one as the bar separating the incisive foramina (formed by the two medial branches) is two times narrower than the lateral branch. The incisive foramina are anteroposteriorly elongated and narrow. They are approximately five times narrower than long. They extend from a point medial to I3 anteriorly to a point medial to or slightly posterior to the anterior edge of the alveolus of the canine posteriorly.

Maxilla (Figs 17-24, 27)

The maxilla forms the lateral wall of the rostrum between the posterodorsal process of the premaxilla and the lacrimal (which represents the facial process). Ventrally, it forms most of the palate between the premaxilla anteriorly and the palatines posteriorly (which represents the palatal process). Anteriorly, the maxilla presents an anterolateral process, which forms the lateral wall of the paracanine fossa between I5 and the canine. Its medial edge is excavated and forms the lateral third part of the fossa. The anterolateral process of the maxilla overlaps the posterolateral edge of the premaxilla to a point labial to I5. Posterodorsally, the facial process of the maxilla is wedged between the lacrimal and the nasal and forms a narrow posterodorsal process, which has a short suture with the frontal. Ventral to the maxilla-frontal suture, the maxilla articulates with the lacrimal. From the maxilla-frontal suture the maxilla-lacrimal suture runs in an anterior direction and turns anteroventrally along the anterior rim of the orbit to contact the jugal at the lower edge of the orbit, just ventral to the ventral lacrimal foramen. This triple point, which connects the maxilla, the lacrimal and the jugal is dorsal to the posterior edge of M1 or anterior edge of M2. Posterior to this point the maxilla has a long suture with the jugal, which extends posteriorly along the ventral edge of the jugal on the lateral face of the skull. At the level of the anterior end of the orbitotemporal fossa the suture passes on the medial side of the zygomatic arch and delimitates a short and rounded zygomatic process of the maxilla. On the dorsal edge of the process the maxilla-jugal suture runs anteriorly slightly ventral to the ventral border of the orbit.

On the lateral aspect of the rostrum is a large anterior foramen of the infraorbital canal. It opens dorsal to P3 (dorsal to anterior edge of P3 on MHNC 8370 and 13847) and is at the level of the ventral lacrimal foramen dorsoventrally. The infraorbital foramen is dorsoventrally elongated, approximately three times higher than wide (height = 2.32 mm and width = 0.7 mm on MHNC 8264, left side) and its height approaches the length of the alveolar border of M1 (Table 2) as is observed in some didelphids (e.g. *Metachirus, Marmosa, Monodelphis*); this feature however is absent in other didelphids such as *Didelphis, Thylamys,* and *Caluromys,* in which the foramen is distinctly smaller. The posterior opening of the infraorbital canal, the maxillary foramen, opens in the orbit. It is large and transversely elongate. Its dorsal rim is formed by the lacrimal, its ventral and lateral rim by the maxilla and its ventromedial rim is formed by a narrow strip of the pala-

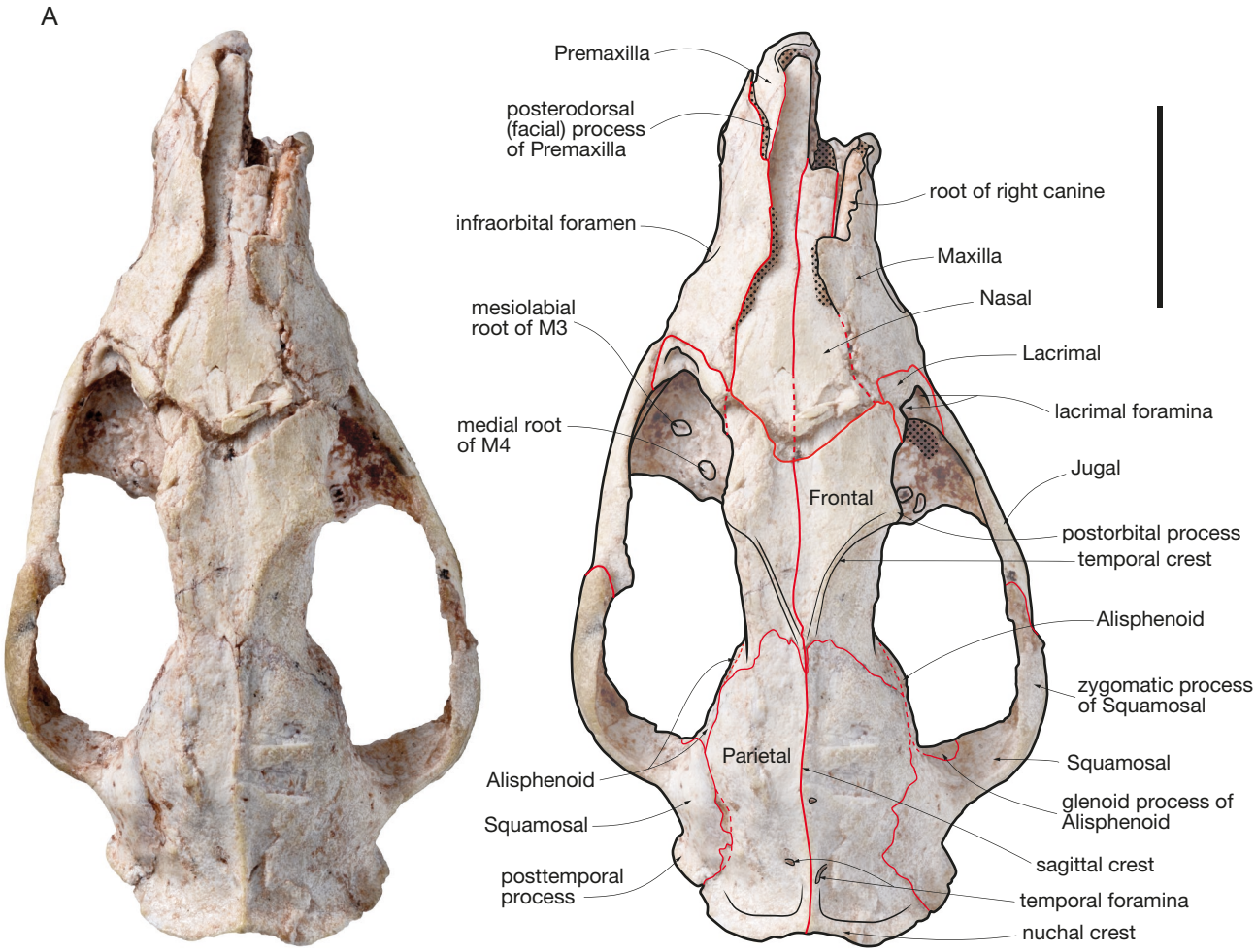

FIG. 18. — **A**, *Andinodelphys cochabambensis* (MHNC 8264), cranium, dorsal view. Scale bar: 10 mm.

tine, which penetrates the infraorbital canal (Figs 21-23). This condition is remarkably similar to that observed in *Pucadelphys* (Marshall & Muizon 1995: fig. 15). It is also present in most Recent didelphids (e.g. *Monodelphis, Metachirus, Caluromys, Philander*). The infraorbital canal transmits the infraorbital nerve (a branch of the V2) and the infraorbital artery, which innervate and supplies blood to the face respectively.

On the lateral aspect of the rostrum ventral to the maxilla-jugal suture and dorsal to the alveolar border of M1-M3 is an elongated fossa formed by two anteroposteriorly set depressions (Fig. 24). A similar fossa has been observed in *Allqokirus australis* (Muizon *et al.* 2018) and has been interpreted as the origin of the *levator labii superioris* muscle. Such a fossa is also present in *Mayulestes* and *Pucadelphys*. In extant didelphids, the fossa for the *zygomaticus* and *levator labii superioris* is generally deep and well developed on the anterolateral region of the jugal but does not excavate the maxilla anterior to the jugal-maxilla suture, although the muscles also originate in part on the maxilla (Turnbull 1970). Because the origin of the *levator labii superioris* in *Didelphis* is ventral to that of the *zygomaticus*, it is likely that the fossa observed in *Andinodelphys* and the other Tiupampa metatherians corresponds to the origin of the *levator labii superioris*, while the *zygomaticus* probably originated on the jugal as in *Didelphis,* although no fossa for this muscle is observed on the jugal of *Andinodelphys*.

Within the orbitotemporal fossa the maxilla forms the floor of the orbit (Figs 21-23). In the four specimens in which they are visible (MHNC 8264, 8308, 8370, and 13847), the roots of the molars are exposed on the floor of the orbit. The medial and posterolateral root of M4 are exposed on all specimens. The anterolateral root of M4, those of M3, and, in one case (MHNC 8370), those of M2 are variably exposed. The maxilla does not have an ascending process in the medial wall of the orbit. It has a long suture with the palatine, which runs along the ventromedial edge of the orbit and reaches the minor palatine foramen posteriorly. The maxilla has a very small participation to this foramen, barely forming its anterolateral quarter (Fig. 17B, C).

Ventrally the maxilla forms most of the palate from the incisive foramen anteriorly to the maxilla-palatine suture posteriorly. The anterior suture of the maxilla with the premaxilla has been treated in the premaxilla section. The suture with the palatine is a rough parabola, the apex of which is at the level of M2. Its branches diverge posteriorly, approach the alveolar border of posterior molars, and reach the anterior edge of the minor palatine foramen posteromedial to M4.

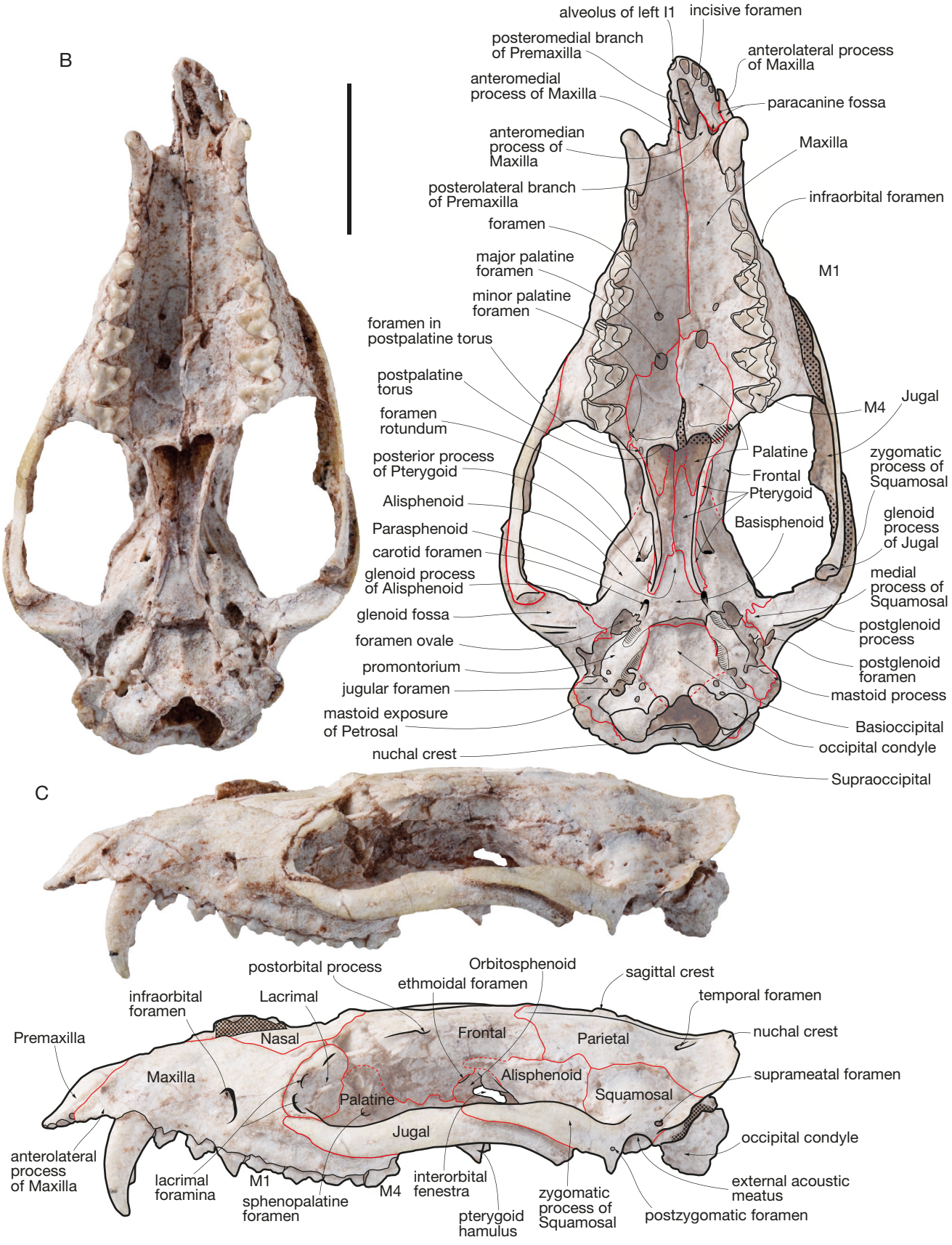

FIG. 18. — **B**, **C**, *Andinodelphys cochabambensis* (MHNC 8264), cranium: **B**, ventral view; **C**, lateral view. Scale bar: 10 mm.

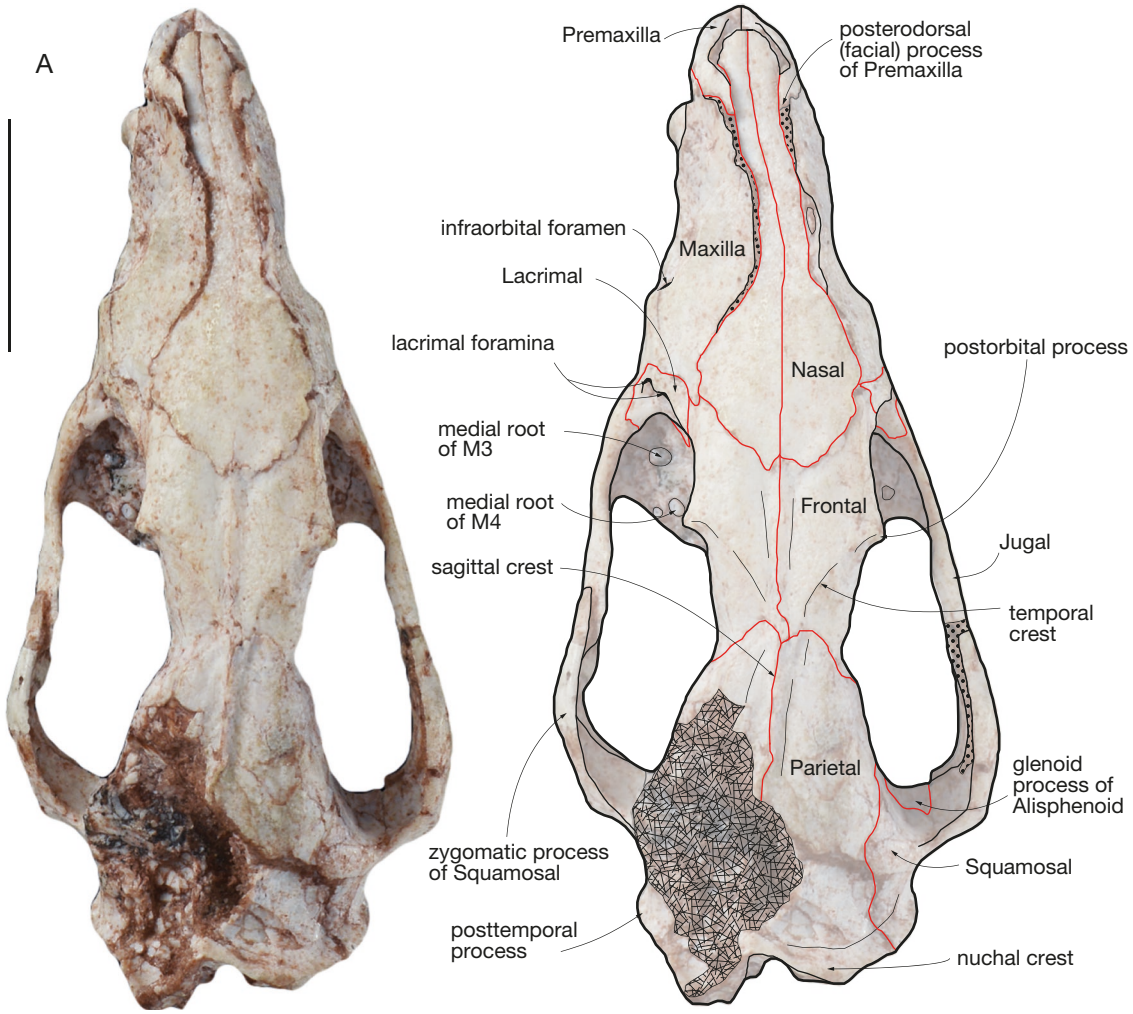

Fig. 19. — **A**, *Andinodelphys cochabambensis* (MHNC 8308), cranium, dorsal view. Scale bar: 10 mm.

Perforation of the palate varies. In MHNC 8264 a large major palatine foramen is present at the maxilla-palatine suture. This foramen is oval-shaped being slightly elongated anteroposteriorly. It is located at the level of the embrasure between M2 and M3 on the medial third of the palate width. On the right palatal process of the maxilla, well anterior to the major palatine foramen (at the level of the posterior edge of M1), is a small circular foramen approximately three times smaller than major palatine foramen. This foramen is present on the left side at the level of the embrasure between M1 and M2, but it is slightly compressed transversely because of post-mortem distortion. The anteroposterior position of this foramen corresponds to that of the anterior end of the maxillopalatal fenestra of the other specimens; it is labelled "foramen" on Fig. 18B. In MHNC 13847, the major palatine foramen is an elongated slit approximately four times longer than wide and which extends from the level of the metacone of M2 posteriorly to the level of the protocone of M1 anteriorly (Fig. 11). The foramen notches the palatine posteriorly along less than one fifth of its length, and the maxilla anteriorly on most of its length. A similar condition is observed in MHNC 8308 (Fig. 19B) and on MHNC 13933 (the partially unprepared skull on the block of Fig. 3). In MHNC 8370 although the palate is partly damaged it is possible to observe the lateral edge of an elongated palatine foramen on the left maxilla (Fig. 17C), and it is therefore likely that it was similar to the condition observed in MHNC 13847, and 8308. It is unclear whether or not this elongated major palatine foramen should be regarded as an incipiently developed palatal vacuity. The condition in MHNC 8264, in which the major palatine foramen is not strongly elongated but in which another small foramen is present in a position similar to the anterior end of the elongated palatine foramen in the other two specimens is noteworthy. It could represent a morphological stage leading from a single major palatine foramen to an elongated foramen, which in turn could represent a step toward a larger palatal vacuity as observed in some extant didelphids. In fact, the condition observed in *Andinodelphys* is reminiscent of the condition observed in some extant didelphids. However, it is noteworthy that the presence and morphology of the palatal vacuities are extremely variable in extant didelphids (Voss & Jansa 2009). They are generally absent in *Caluromys* and *Caluromysiops* (but see Voss & Jansa 2009: 94). They form an elongated slit at the maxilla-

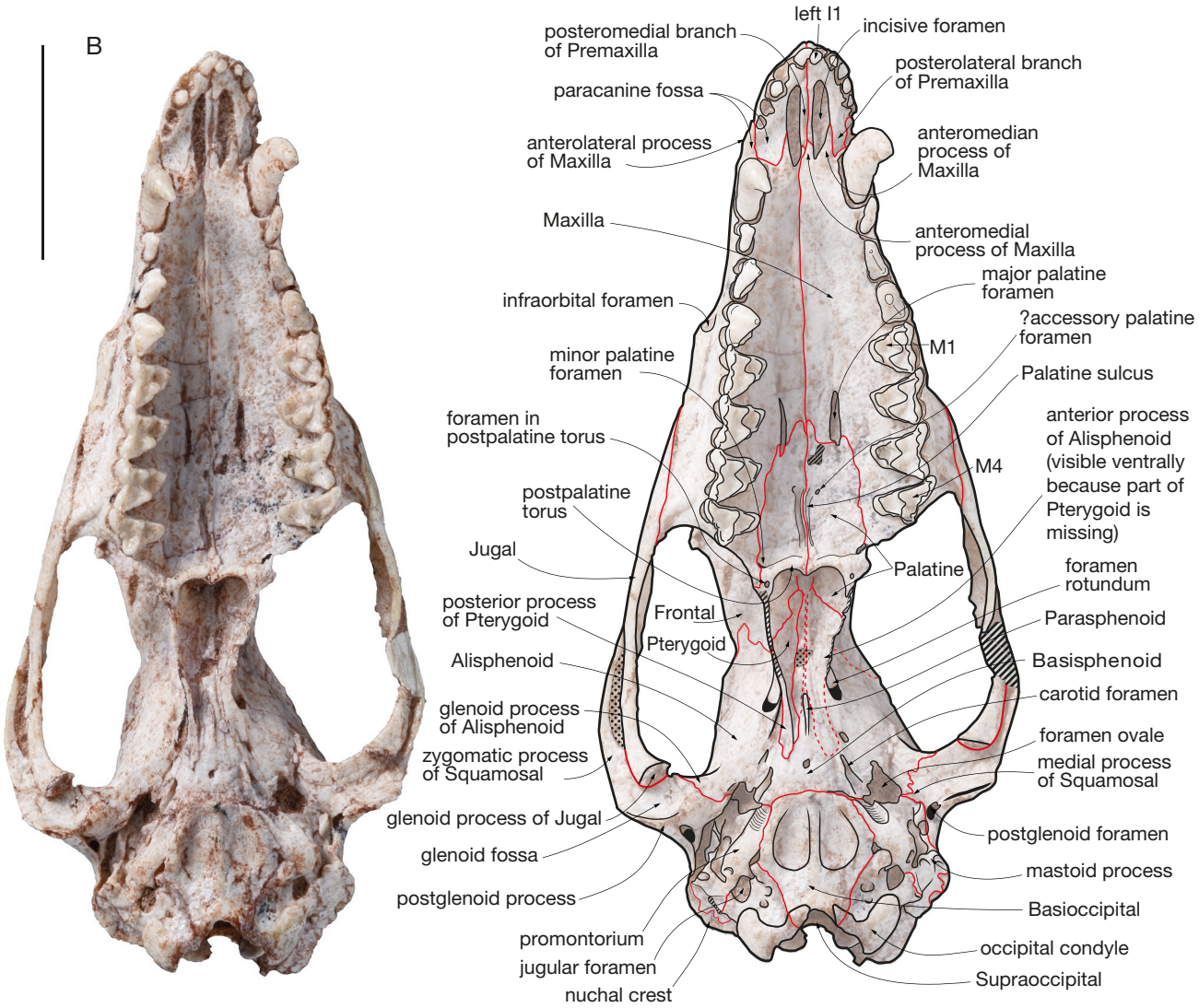

FIG. 19. — **B**, *Andinodelphys cochabambensis* (MHNC 8308), cranium, ventral view. Scale bar: 10 mm.

palatine suture as is observed on MHNC 13847 and 8308, but more elongated, in *Hyladelphys*, *Lutreolina*, *Lestodelphys*, *Philander*, *Marmosa*, *Marmosops*, and *Monodelphis* (although they are very small in *Monodelphis dimidiata* as noted by Pine *et al.* [1985: fig. 4] and Chemisquy [2015: fig. 1c]). They are longer and wider in *Metachirus*, *Chironectes*, *Didelphis, Gracilinanus* than in *Andinodelphys*. In *Andinodelphys* the elongated major palatine foramina are the only small palatal vacuities observed in our sample, whereas in some extant didelphids additional vacuities are present on the palatine or lateral to the major palatine foramina (e.g., *Didelphis, Philander, Thylamys, Lutreolina, Tlacuatzin, Cryptonanus, Gracilinanus*) (Voss & Jansa 2009). It is noteworthy that small elongated palatal vacuities, similar to those of *Andinodelphys* are present in *Sparassocynus derivatus* (Beck & Taglioretti 2019). The major palatine foramen transmits the major palatine artery and nerve to the ventral region of the secondary palate. On the posterolateral region of the palate, the maxilla meets the minor palatine foramen.

Lacrimal (Figs 17-24)

The lacrimal is relatively large. It forms the anterior edge of the orbit, although it is mainly internal to it. The facial process is crescent-like and narrow. It does not strongly extend on the face as it does in the basal metatherians, deltatheroidans and sparassodonts (including *Mayulestes*). It resembles the condition in *Pucadelphys* and extant didelphids. The internal portion of the lacrimal is three to four times larger than the facial process. As exposed above, the lacrimal has a long suture with the maxilla anteriorly, with the frontal dorsally and posterodorsally, with the palatine posteroventrally and ventrally, and a small one with the jugal ventrolaterally. On the anterior edge of the orbit, but internal to it, two lacrimal foramina open posteriorly. They are subequal in size and roughly circular to oval-shaped. They are positioned one above the other along a dorsomedial-ventrolateral axis; in other words, the ventral lacrimal foramen is ventrolateral to the dorsal one. Between the two lacrimal foramina is a circular thickening of the bone, which we regard as a small

lacrimal tubercle. This tubercle is clearly present on the two skulls of fully adult individuals (MHNC 8264 and 8308), while it is not really developed on the other two skulls of young adults (MHNC 8370 and 13847). A lacrimal tubercle similar to that of *Andinodelphys* is variably present in some extant didelphids (e.g., *Caluromys, Thylamys* – personal observations). It is absent in *Pucadelphys* and *Mayulestes*. Within the orbit, the lacrimal forms the dorsal edge of the maxillary foramen.

Nasal (Figs 17-Fig. 19)

The nasals are elongated bones, which are approximately 45% the condylobasal length. They are narrow with sub-parallel edges in their anterior two thirds and strongly widen in their posterior third. The anterior apices of the nasals are preserved on the four fully prepared skulls (the left only on MHNC 8264). The anterior edge of the two nasals protrudes anteriorly being distinctly rounded (semicircular to parabolic) and strongly convex anteriorly. Therefore, the medial side of the apex of each nasal is well anterior to its lateral side. Anteriorly, the nasals extend beyond the anteriormost point of the nasal-premaxilla suture and overhang the narial opening on more than half of its length: on MHNC 8308 the anteriormost point of the nasal is at the level of the posterior edge of I3. The nasal-maxilla suture is anteroposteriorly oriented up to the level of the infraorbital foramen. There, it turns laterally at approximately 45° and turns posteriorly just before contacting the maxilla-frontal small suture. Posterior to this suture the nasal contacts the frontal and the nasal-frontal suture turns medially at approximately 45° and meets the sagittal plane. The posterior suture of the nasals, with the frontals, is markedly convex posteriorly. It is not distinctly W-shaped as in *Pucadelphys* and in most didelphids (e.g., *Hyladelphys, Marmosa, Monodelphis, Metachirus, Didelphis, Lutreolina, Cryptonanus, Lestodelphys, Thylamys*). This posterior flared portion of the nasals is roughly square to diamond-shaped with one of the diagonals oriented anteroposteriorly. It is roughly as long as wide and differs from the condition in extant didelphids, in which this part of the nasals is distinctly longer than wide. Interestingly, this region of the nasals is conspicuously wider than long in *Deltatheridium*, a late Cretaceous metatherian from Mongolia (Rougier *et al.* 1998). In its lateralmost region the nasal is closely approximated to the lacrimal but does not contact it, in contrast to the condition in sparassodonts and deltatheroidans, in which the bones have a distinct suture. Posteriorly, the nasals extend approximately as far as mid-length of the orbit and remain well anterior to the supraorbital processes.

Jugal (Figs 20, 21)

Complete jugals are preserved on the four prepared skulls. It is a relatively slender bone as compared to extant didelphids but similar in this respect to that of *Pucadelphys*. In lateral view, it is consistently convex laterally and concave medially. It is gently sigmoid being dorsally concave anteriorly and convex posteriorly. Its anterior dorsally concave part forms the ventral edge of the orbit. In lateral view at its anterodorsal apex it has a short anterior suture with the lacrimal and a long (*c.* one third of its total length) and oblique anterior suture with the maxilla along its ventral edge as far as the anterior edge of the orbitotemporal fossa (in ventral view). As mentioned above, it receives the short zygomatic process of the maxilla on the medial aspect of its anterior region. The posterior dorsally convex portion of the jugal has a long dorsal suture with the zygomatic process of the squamosal on approximately 45% of its total length. In lateral view, the free part of the jugal (i.e. with no suture with the maxilla nor with the squamosal) is approximately 25% of the length of the bone. It very slightly increases in height posteriorly, the bone having its greatest depth just anterior to the jugal-squamosal suture. However, in this region of the jugal of *Andinodelphys* there is no conspicuous frontal process of the jugal as is observed in Recent didelphids and dasyurids, in which it marks the posterior limit of the orbit (Wible 2003; Voss & Jansa 2009). However, a very small elevation of the dorsal edge of the jugal, posterior to the concave anterior part, demarcates the posterior limit of the orbit and could be regarded as an incipient frontal process. The condition of *Andinodelphys* is apparently intermediate between that of extant didelphids and that of *Pucadelphys, Allqokirus* and *Mayulestes,* in which the transition between the ventral edge of the orbit and the posterior part of the jugal is notably smooth. This incipient frontal process of *Andinodelphys* is slightly posterior to level of the postorbital process and well anterior to the narrowest part of the intertemporal constriction. In extant didelphids the most elevated region of the jugal (the frontal process) is generally at the level of the postorbital process or slightly posterior to it. In some taxa, however, it is more posteriorly located, at the level of the intertemporal constriction (e.g. *Lestodelphys, Thylamys*).

However, the condition of *Andinodelphys* differs strongly from that in extant didelphids and dasyurids, in which the posterodorsal angle of the jugal extends posteriorly above the zygomatic process of the squamosal. As a consequence, the jugal-squamosal suture is bifurcated, a condition which is never observed in *Andinodelphys* nor in the other Tiupampa pucadelphydans (*Pucadelphys* and *Mizquedelphys*). The conditions observed in Figures 21-23 are artefacts due to a slight displacement of the two bones, which has modified the external aspect of the jugal-squamosal suture, a condition that has been enhanced by the oblique nature of the photographs. Figures 18C and 20 provide a better rendering of the actual jugal-squamosal suture in *Andinodelphys*.

From the anterior end of the jugal-squamosal suture, the jugal underlaps the zygomatic process of the squamosal, reducing in height posteriorly and thickening again at its posterior extremity. The posterior end of the jugal bears a conspicuous glenoid process, which articulates with the anterolateral edge of the glenoid fossa. This process bears a small ovoid articular facet for the mandibular condyle. It faces posteroventrally and its transverse width is approximately one third to one fourth the total width of the glenoid fossa of the squamosal.

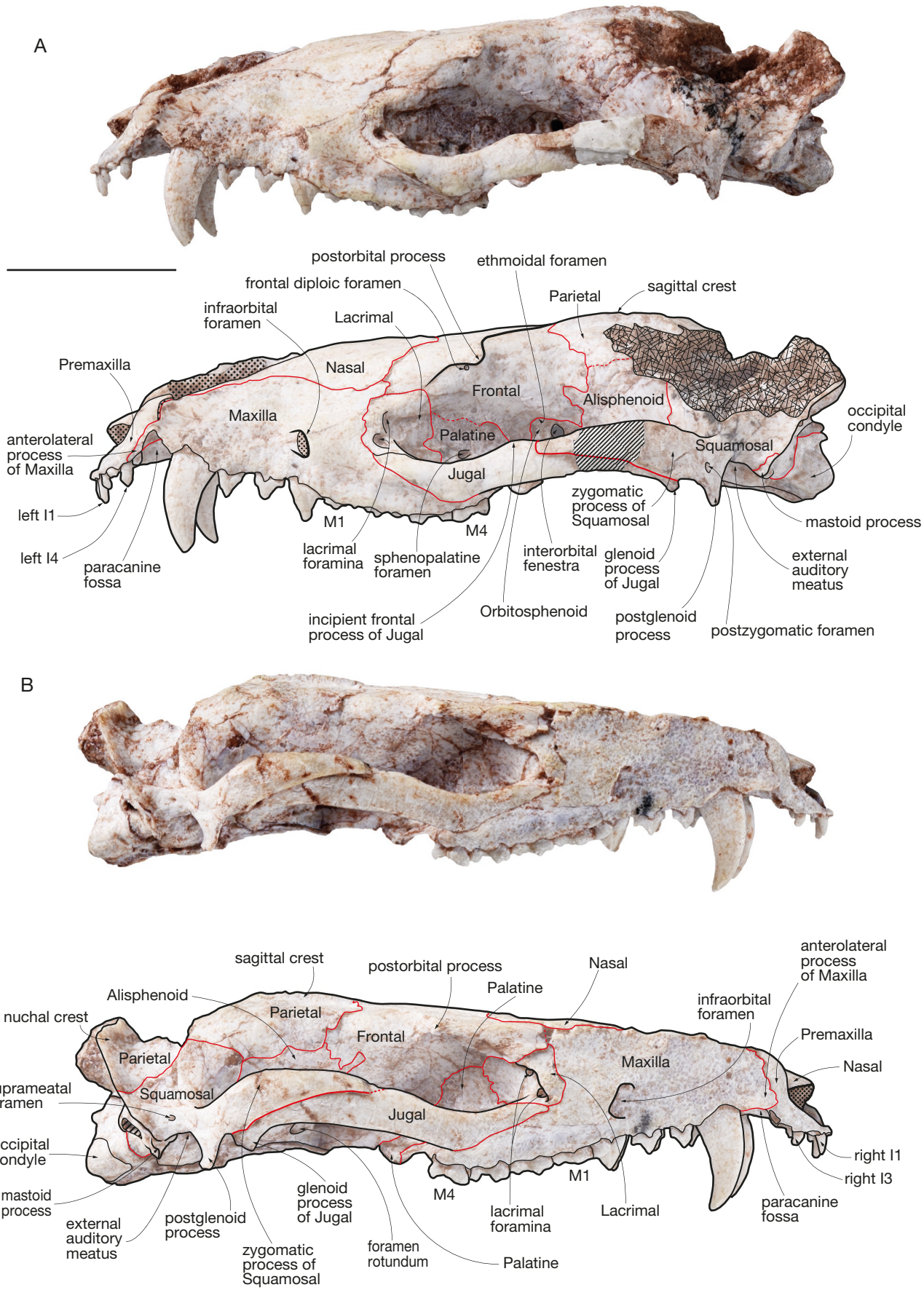

FIG. 20. — *Andinodelphys cochabambensis* (MHNC 8308), cranium: **A**, left lateral view; **B**, right lateral view. Scale bar: 10 mm.

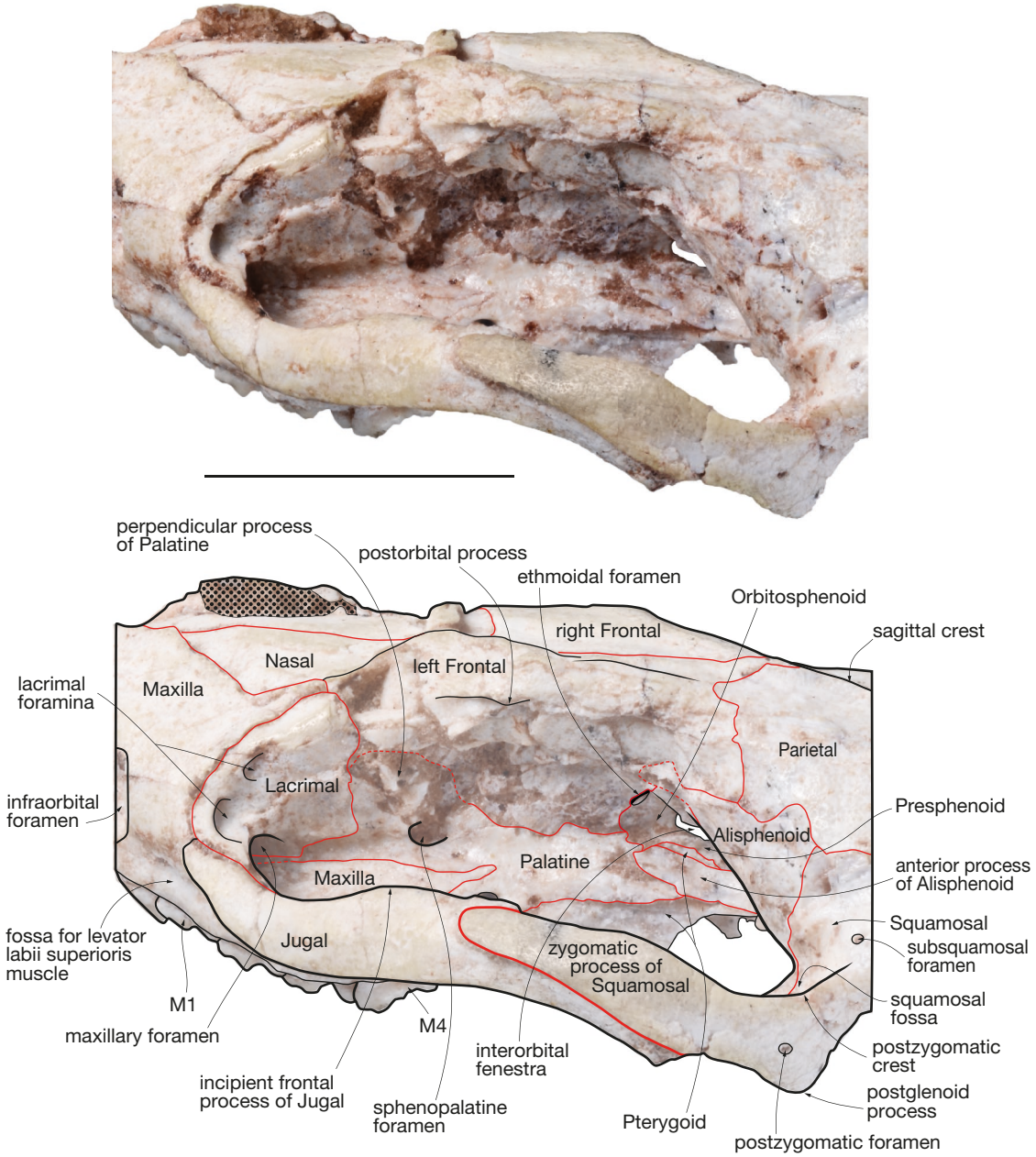

Fig. 21. — *Andinodelphys cochabambensis* (MHNC 8264): posterolateral view of the orbit. Scale bar: 10 mm.

Palatine (Figs 17-24)

The palatine occupies the posterior third to quarter of the length of the palate. In this region, the two bones form a parabolic suture, which penetrates the posterior edges of the palatal processes of the maxillae. The palatines do not contact the medial edge of the last molars posterolaterally, although they are very close to it. Such a contact has been observed in *Allqokirus*, but is apparently absent in *Mayulestes* and *Pucadelphys*. The palatines form the posterior region of the palate, which is distinctly deflected ventrally being concave and facing anteroventrally. In other words, the posterior end of the palate is in a much more ventral position than the anterior edge of the palatines.

On the ventral aspect of each palatine the medial edge of the bone bears a sharp ventrally projecting ridge, which borders the suture between the two bones. Just lateral to the medial crest is a narrow groove (palatine sulcus) running anteriorly on more than half of the palatine sagittal length in MHNC8308 and less in MHNC 8264. In MHNC 8308 in its anterior third, the palatine sulcus turns laterally on a very short distance and penetrates a small foramen, probably the accessory palatine foramen (= middle palatine foramen). This condition is especially clear on the left palatine. On the right palatine, the foramen is partly squashed (Fig. 19B). Palatine vacuities, posterior to the major palatine foramen, are absent on the four prepared specimens. Anterior palatal

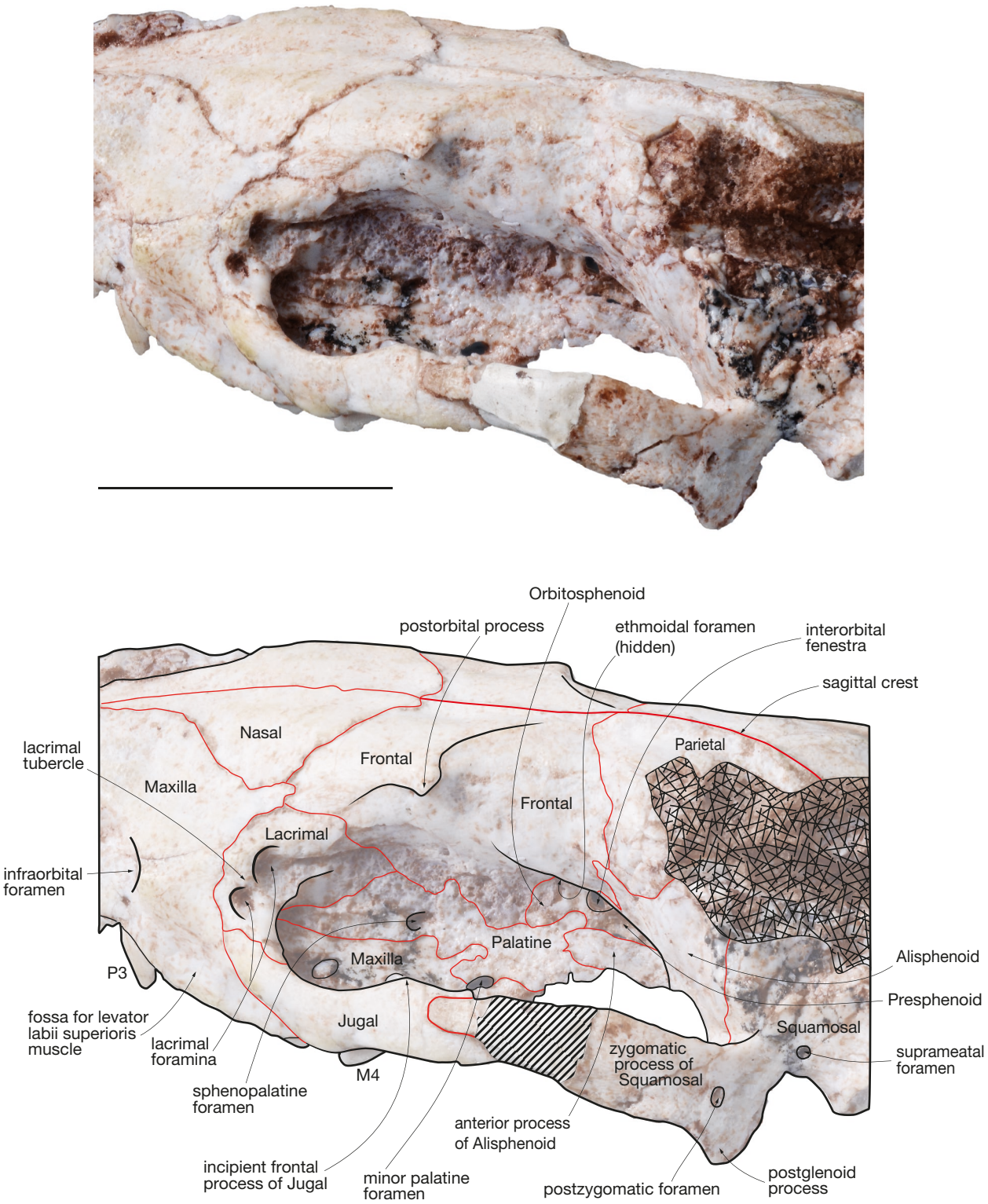

FIG. 22. — *Andinodelphys cochabambensis* (MHNC 8308): posterolateral view of the orbit. Scale bar: 10 mm.

vacuities resulting from the enlargement of the major palatine foramina have been discussed above in the maxilla section.

The posterior edge of the palatine is a thickened bar, the postpalatine torus, which forms the ventral edge of the choanae. The torus is posterior to the M4. It bears three spines on its posterior surface, a medial one at the point of contact of the two palatines and two lateral ones on the medial edge of the minor palatine foramina. The medial spine is formed by the junction of the contribution of each palatine. The torus has its maximum thickness at the level of the lateral spine, just posterior to the minor palatine foramen, which it encloses almost totally (see above). Because the medial palatine spine

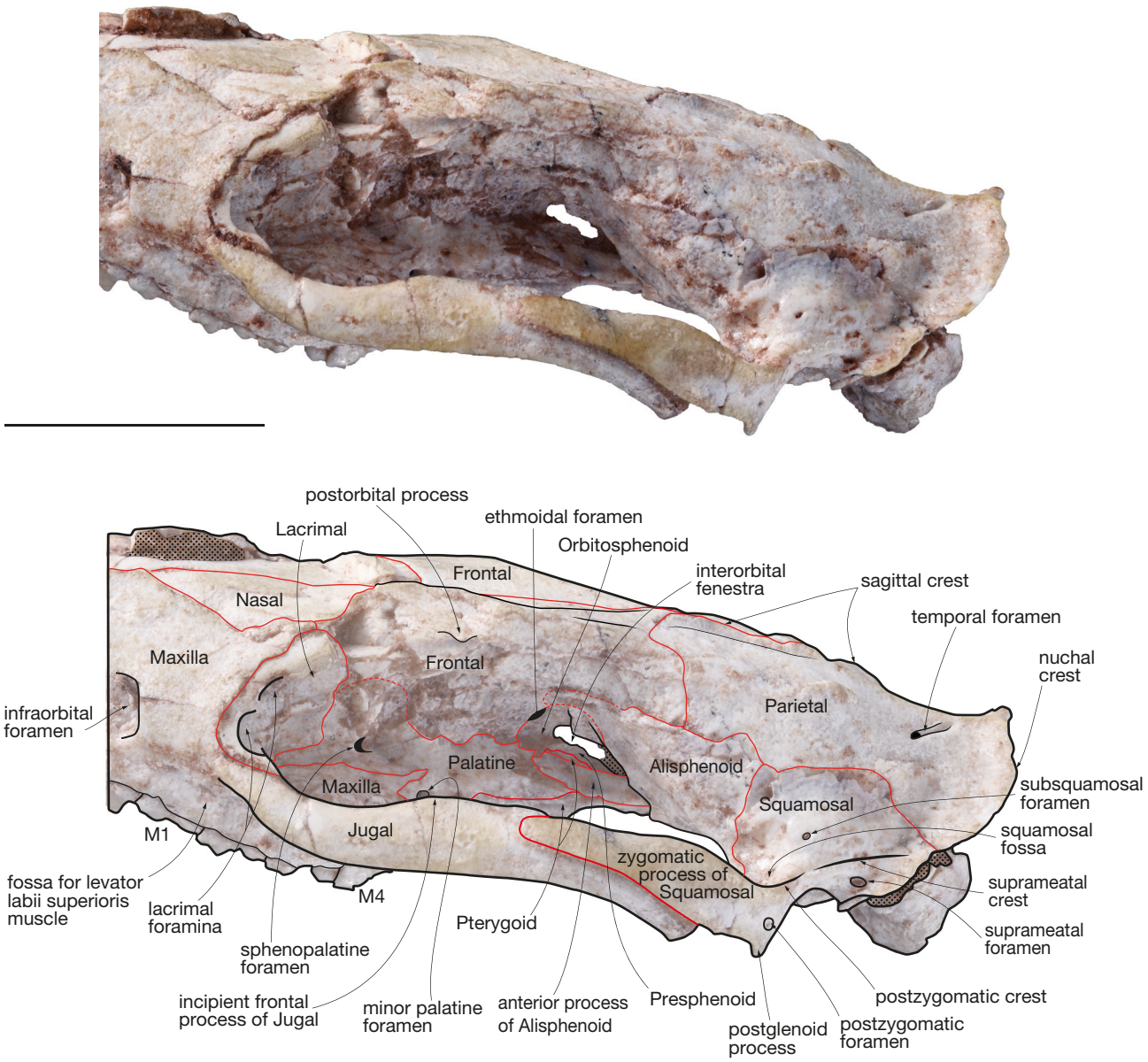

Fig. 23. — *Andinodelphys cochabambensis* (MHNC 8264): dorsolateral view of the orbitotemporal fossa. Scale bar: 10 mm.

is relatively well developed and protrudes posteriorly and posterodorsally, the posterior edge of each palatine is distinctly concave. Therefore, the ventral border of the choanae is markedly biconcave and has a rough m-shaped aspect (on MHNC 8264) as is observed in *Pucadelphys* (Marshall & Muizon 1995; Ladevèze *et al.* 2011, and personal observations). The minor palatine foramen is large and oval-shaped with its main axis oriented posteromedially-anterolaterally. The posterolateral edge of the foramen forms a thickened bar of bone, which extends from the lateral postpalatine spine to the posteromedial edge of M4. This bar is formed by the palatine posteromedially and by the maxilla anterolaterally. Because this bar and the postpalatine torus extend ventrally relative to the plane of the posterior region of the palate, the plane of the minor palatine foramen is subvertical and the foramen faces anteromedially. This condition is identical to that observed in *Pucadelphys*. The minor palatine foramen transmits the minor palatine artery and nerve to the ventral region of the secondary palate.

In the orbit the palatine has a long ventromedial suture with the maxilla, an anterodorsal suture with the lacrimal, and a long dorsal suture with the frontal (Figs 21-24). The anterior part of the palatine-frontal suture corresponds to a large roughly semicircular perpendicular process (also named, orbital, ascending or vertical process), which extends as far as mid-height of the orbit. At the base of the perpendicular process, slightly medial to the palatine-maxilla suture, in the ventromedial angle of the orbit, is a large sphenopalatine foramen. The foramen is elliptical, being at least twice as wide as high, and has a posterolaterally directed opening. It is located approximately at the anteroposterior level of the medial root of M4, thus well anterior to the minor palatine foramen. This

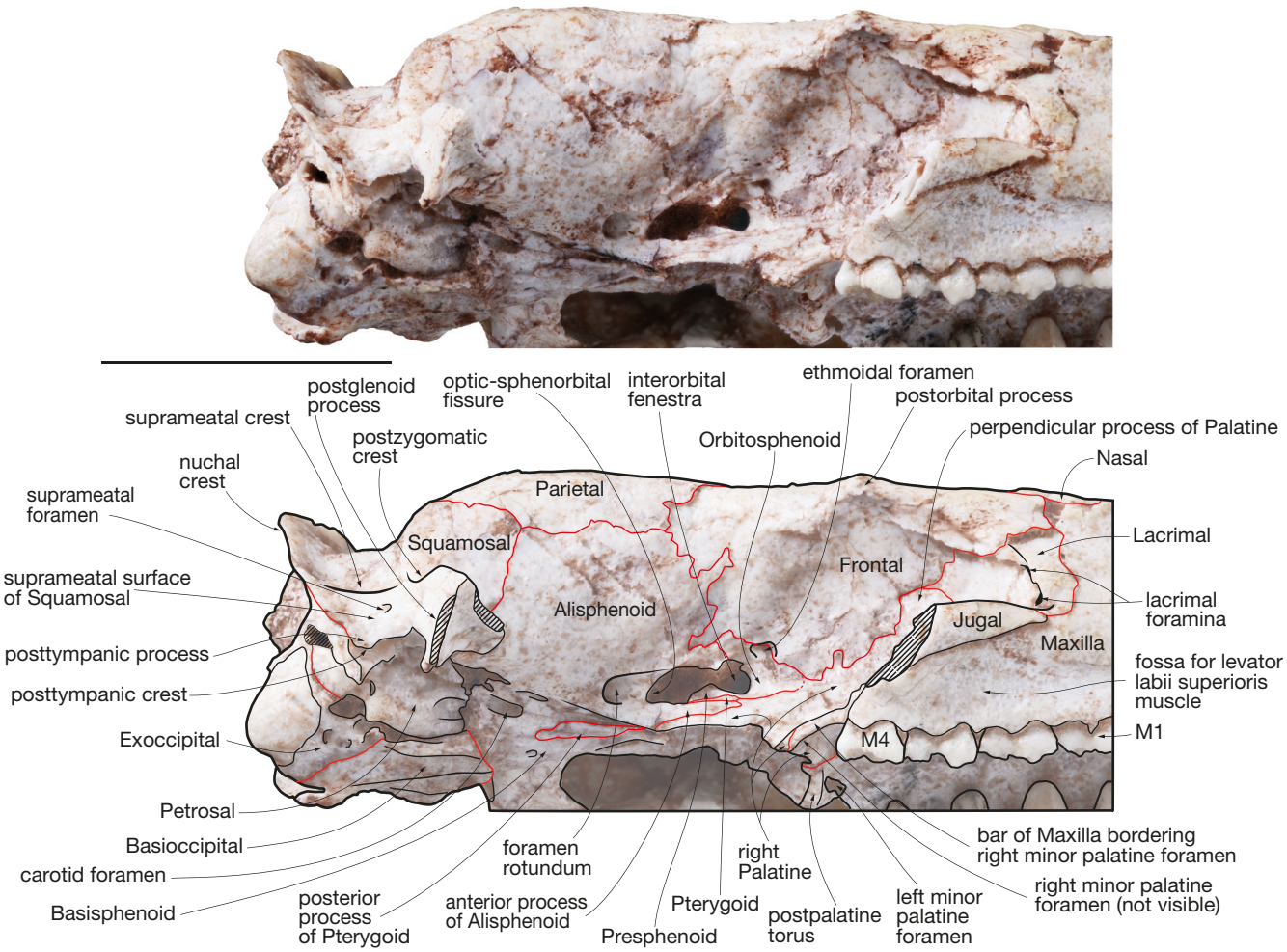

FIG. 24. — *Andinodelphys cochabambensis* (MHNC 8308): right ventrolateral view of the orbitotemporal fossa. Note: this photo has been possible because of an accidental breakage of the right zygoma which allowed a better view of the bone sutures of the lateral wall of the skull. Scale bar: 10 mm.

condition is similar to that observed in *Pucadelphys*. Anterior to the perpendicular process, the palatine extends as a narrow strip of bone wedged between the lacrimal dorsally and the maxilla ventrally. This small anterior extension of the palatine enters the maxillary foramen, of which it forms part of the medial border. Posteroventrally, the palatine forms the lateral wall of the basipharyngeal groove and is overlapped by the anterior process of the alisphenoid (Figs 19B; 24). Dorsal to this process the palatine borders the ventral edge of the orbitosphenoid. In the basipharyngeal groove (= nasopharyngeal passage), the palatine has an oblique suture with the pterygoid (Fig. 17C). The palatine forms the anterior part of the wall of the groove and the pterygoid the posterior part. The palatine extends posteriorly as far as the anterior edge of the Basisphenoid.

Pterygoid (Figs 18, 19, 24)

The pterygoids are preserved on the four skulls available but lack the hamular process in MHNC 8308. They are well developed relative to the condition in extant didelphids. The pterygoid forms most of the ventral edge of the wall of the basipharyngeal groove, from which it extends ventrally in a well-developed triangular blade. From this blade, a long finger-like hamular process projects posteriorly.

Internal to the basipharyngeal groove, the pterygoid forms most of the medial aspect of the wall. On this side, anteriorly, it forms a thin triangular blade of bone, which articulates with the palatine anteriorly and dorsally. Within the basipharyngeal groove the pterygoids expand dorsally and medially and contact in the sagittal plane, forming the roof of the groove. This dorsal blade of the pterygoid extends posteriorly as far as the anterior region of the basisphenoid, at the level of the rod-shaped eminence observed in the anterior midline of this bone.

From this point the pterygoids diverge from each other and extend on the lateral sides of the basipharyngeal groove forming a narrow posterior process that is slightly concave laterally (complete on MHNC 8264, but almost completely missing on the left side of MHNC 8308). This process underlies the basisphenoid but its lateral edge contacts the alisphenoid. Its dorsal face is relatively flat but its ventral aspect bears a sharp crest. The process extends posteriorly as far as the dorsal edge of the carotid foramen as clearly observed on the complete right pterygoid of MHNC 8264 (Figs 18B; 19B). The condi-

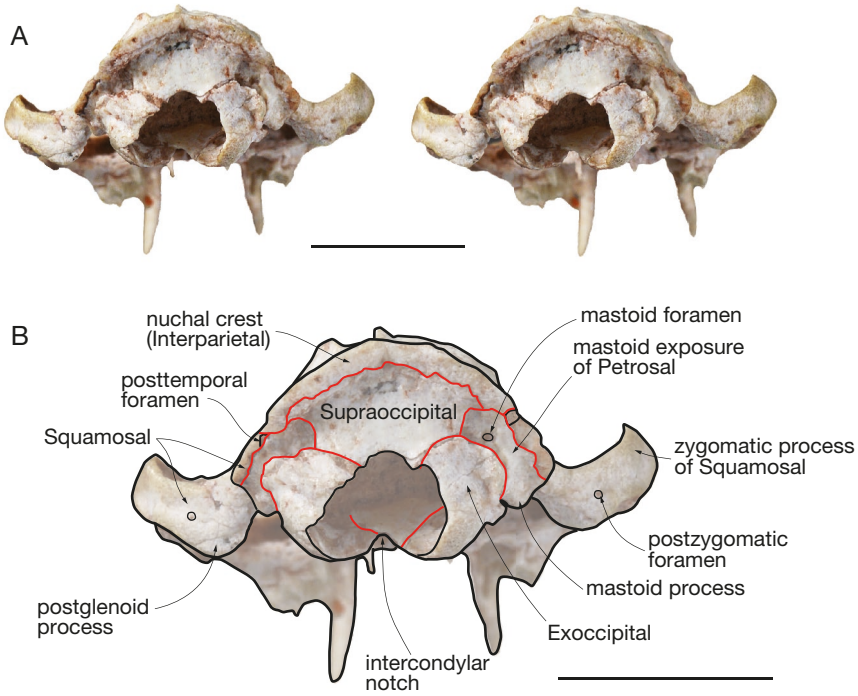

FIG. 25. — *Andinodelphys cochabambensis* (MHNC 8264): **A**, stereophotos of the cranium in occipital view; **B**, occipital view of the cranium showing the sutures of the bone of the occiput. Scale bar: 10 mm.

tion of the pterygoid of *Andinodelphys* shows the same pattern as in *Pucadelphys* and *Mayulestes*.

On the lateral side of the wall of the basipharyngeal groove, the pterygoid is partially covered by the palatine and the overlying anterior process of the alisphenoid (see below). Dorsal to this process, the pterygoid is still visible as a narrow strip of bone, which articulates with the presphenoid dorsally and with the palatine anteriorly (Figs 21, 23, 24). This lateral exposure of the pterygoid is present in extant didelphids and corresponds the "flat trapezoidal sliver of bone" described by Wible (2003: 149) in *Monodelphis.*

On the lateral edge of the posterior process of the pterygoid is a tiny slit and foramen in the suture between the pterygoid and the alisphenoid just anterior to the transverse canal foramen (see below in the alisphenoid section). This foramen is interpreted as the posterior opening of the pterygoid canal. It is observed on both sides of MHNC 8264 and on the right side of 8308. This position exactly corresponds to the observation of Wible (2003: fig. 6) in *Monodelphis*. The anterior opening of the pterygoid canal is probably the little slit observable in the suture between the dorsal edge of the dorsolateral exposure of the pterygoid mentioned above and the presphenoid on the anteroventral region of the optic-sphenorbital fissure on MHNC 8264. If this observation is correct, it has a similar position to that described by Wible (2003) in *Monodelphis*. In this genus, the anterior opening is in the suture between the pterygoid and the anterior process of the alisphenoid on the ventral edge of the optic-sphenorbital fissure; the dorsal edge of the anterior process of the alisphenoid bears a notch that forms the posterior and lateral rims of the opening.

Frontal (Figs 17-24)

In dorsal view, the frontal forms the interorbitotemporal bridge between the rostrum and the braincase. Its anteroposterior extension in the sagittal plane is short and represents only 15% to 20% of the total length of the skull. It articulates anteriorly with the nasal, the lacrimal and the maxilla and posteriorly with the parietal. Anterolaterally it has a large process wedged between the nasal and the lacrimal, which articulates with the narrow posterodorsal process of the maxilla. The anterior suture with the nasal is regularly convex posteriorly and no anterior process of the frontals is wedged between the nasals. At the widest region of the interorbitotemporal bridge, each frontal bears a small but distinct postorbital process. It is sharp and triangular and projects laterally. Anteroventral to the process is a small anteriorly-opening frontal diploic foramen (Figs 17B; 20). This foramen likely conveyed the frontal diploic vein, an emissary of the dorsal cerebral vein/dorsal sagittal sinus or a vein issued from the frontal diploe (Thewissen 1989; Evans & de Lahunta 2013; Wible *et al.* 2004). This foramen is called supraorbital foramen by Novacek (1986) and Marshall & Muizon (1995), the frontal foramen by Evans & de Lahunta (2013), the foramen for the frontal diploic vein by Wible & Rougier (2000), Wible (2003), Wible *et al.* (2009) and Wible (2011), and the frontal diploic foramen by Thewissen (1989). In this paper, we retain the terminology "frontal diploic foramen". Such a foramen is present in *Pucadelphys* and generally in Recent didelphids. From the supraorbital processes, low temporal lines (= orbital crest or temporal crests) converge posteriorly. They form laterally concave curves, which meet at the level of the frontal-parietal suture. At this point, they merge to form the sagittal crest. Posteriorly the two frontals

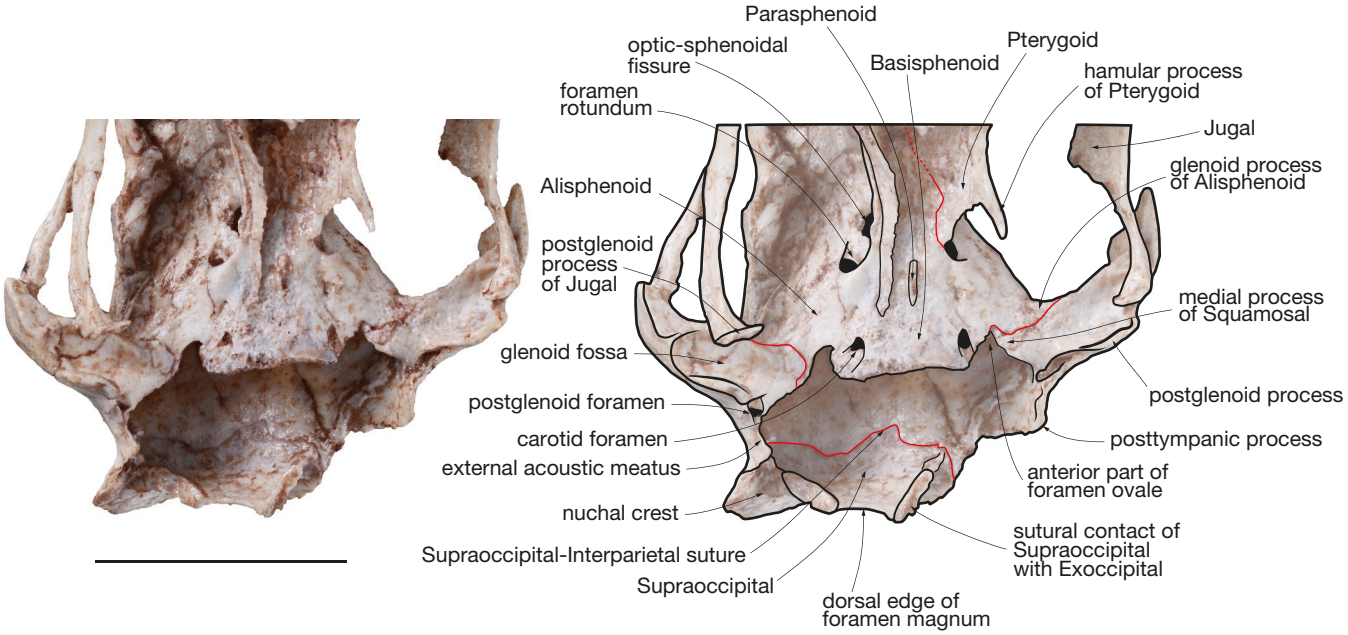

FIG. 26. — *Andinodelphys cochabambensis* (MHNC 8370): ventral view of the posterior region of the cranium showing the posterodorsal region of the endocranial cavity. Scale bar: 10 mm.

form a small spur-like sagittal process, which wedges between the parietals. From this point the frontal-parietal suture extends posteroventrally and meets the alisphenoid at the triple contact frontal-parietal-alisphenoid, approximately at mid-height of the braincase.

In the orbitotemporal fossa, the frontal forms most of the dorsomedial wall of the orbit. It has a large descending orbital process, which articulates with the lacrimal anterodorsally and with the palatine anteroventrally and ventrally. It reaches the level of the sphenopalatine foramen ventrally. From its ventralmost point, the frontal-palatine suture turns posterodorsally and has a short suture with the orbitosphenoid. An oval-shaped ethmoidal foramen is present in the suture. It opens ventrally to posteroventrally. The frontal forms its lateral wall (dorsally and anteriorly), and the orbitosphenoid, its medial wall, ventrally. The alisphenoid does not reach the posterior edge of the ethmoidal foramen, but is close to it. The condition of *Andinodelphys* closely resembles that observed in didelphids and dasyurids. There is no participation by the basisphenoid to the ethmoidal foramen as observed (erroneously) by Marshall & Muizon (1995) in *Pucadelphys*. From the posterodorsal edge of the ethmoidal foramen the frontal-alisphenoid suture runs posterodorsally until the triple contact with the parietal.

Parietal and Interparietal (Figs 17-27)

The two parietals form most of the roof of the braincase. They are roughly rectangular and articulate anteriorly with the frontal, anteroventrally with the alisphenoid, posteroventrally with the squamosal and posteriorly with the interparietal. The parietal is strongly convex reflecting the morphology of the underlying cerebral hemispheres. They bear various irregularities and scars for attachment of the temporalis muscle, especially on the left parietal of MHNC 13847. In the sagittal region both parietal unite and rise vertically forming a low but consistent sagittal crest, which does not extend on the frontals anteriorly.

Because of early fusion of the parietals with the interparietal, the bones are completely fused on the four available specimens and their suture is hardly discernible. However, on MHNC 8370 a thickened oblique irregular line in the posterior region of the left parietal may reveal a probable suture with the interparietal (Fig. 17A). Based on this indication the interparietal was probably roughly triangular with a conspicuous contact with the squamosals posterolaterally. A low interparietal sagittal crest is present medially, which extends the parietal sagittal crest as far as the nuchal crest. The latter is likely formed by the interparietal as is observed in *Monodelphis* and *Didelphis* (Toeplitz 1920; Clark & Smith 1993; Wible 2003). In occipital view the interparietal is clearly separated from the underlying supraoccipital by a distinct suture (Fig. 25). This suture is at the posterior base of the nuchal crest, a condition which corroborates the interpretation that it is completely formed by the interparietal. The suture extends laterally and contacts the squamosal and the mastoid exposure of the petrosal. Intracranially, as is observed on the two skulls that have lost their exoccipitals and basioccipital (MHNC 8370 and 13847), the suture runs along the posterior wall of the braincase and remains distinctly posterior to the vermis fossa on the skull roof (Figs 26, 27). Because of this position, it cannot be the parietal-interparietal suture which, in extant didelphids, is always located anterior to the vermis fossa. In these skulls, no suture is observed anterior to the vermis fossa, which indicates that the interparietal-parietal suture is totally fused. Therefore, the condition of *Andinodelphys* differs from that in most extant didelphids

(e.g. *Didelphis, Metachirus, Marmosa, Philander, Thylamys*), in which the supraoccipital-interparietal suture fuses very early in ontogeny (Clark & Smith 1993; Nesslinger 1956, Voss & Jansa 2009), whereas the interparietal-parietal suture remains unfused in adults. The condition is reversed in *Andinodelphys*. In contrast, the condition of *Andinodelphys* resembles that of *Allqokirus* (Muizon *et al.* 2018), and *Pucadelphys* (pers. observations on MHNC 8378, 8380, 8381).

The nuchal crest is extremely developed and extends posterodorsally overhanging the supraoccipital. However, it does not extend further posteriorly than the level of the occipital condyles. The size of the nuchal crest accommodates large temporal fossae on the roof of the skull for attachment of the *temporalis* muscle and a large occipital fossa for attachment of the nuchal muscles (e.g., *longissimus capitis, longissimus thoracis, obliquuus capitis, spinalis* and *semispinalis capitis, splenius, biventer, complexus*). The condition of *Andinodelphys* is very similar to that of *Pucadelphys*.

The parietals and interparietal bear small temporal foramina, which are variable in number and position. The foramina are generally associated to an elongated narrow groove. On MHNC 13847 four temporal foramina are present. Two are located posteriorly, close to the nuchal crest, at the base of the sagittal crest, and posteromedially-anterolaterally oriented, with the foramen located at the anterolateral extremity of the groove. The left foramen and groove are anterior to the right one. Anteriorly to those foramina are two other foramina and grooves, slightly posterior to the mid-length of the braincase, close to the sagittal crest and roughly transverse. The left foramen is located at the lateral extremity of the groove, while the right is at the medial end of the groove at the base of the sagittal crest. In this case, the left foramen and groove are posterior to the right one. On the right parietal in the anterolateral region of the braincase, are another foramen and a groove that is posterolaterally-anteromedially oriented. The foramen is at the posterolateral end of the groove.

The number of anterior parietal foramina are variable, since they are apparently absent in MHNC 8370. In contrast, this specimen bears two posterior foramina, the right foramen being anterior to the left one. A distinct oblique groove is present on the left side, with the foramen at the anterolateral end of the groove. No groove accompanies the foramen on the right side. In MHNC 8264, on the posterior region of the skull roof, are two posteromedially-anterolaterally oriented grooves, which bear at their anterolateral extremity a small temporal foramen. These grooves are posteriorly situated on the braincase and are at a distance of less than 3 mm from the nuchal crest. Their posteromedial end starts high on the braincase, just at the base of the sagittal crest. The left foramen is slightly anterior to the right one. Slightly posterior to mid-length of the braincase, probably on the right parietal (the parietal-interparietal suture is obliterated) is a small temporal foramen, located very close to the sagittal crest and associated with a very short groove that is almost transversely oriented. Anterior to this foramen on the left parietal, and very close to the sagittal crest, are two tiny foramina, which could also be temporal foramina although because of their small size they could also represent nutrient foramina. Foramina are not observable in MHNC 8308 because of the collapse of the roof of the braincase.

Thus, it appears that the anterior or parietal temporal foramina are quite variable in number and position. In contrast, the two posterior foramina with a posteromedially oriented groove are present in the three crania in which this region is well preserved. Although not mentioned by Marshall & Muizon (1995), similar foramina are constantly present in *Pucadelphys*. Such foramina are generally present in *Didelphis* and, when observed, they open either in the interparietal or in the interparietal-parietal suture. It is therefore likely that the posterior foramina perforate the interparietal and their position in *Andinodelphys* may represent an indication of the anterior extension of the interparietal and parietal-interparietal suture.

Alisphenoid (Figs 17-35)

The alisphenoid forms the ventrolateral wall of the braincase from the anterior edge of the posterior root of the zygomatic arch to the level of the interorbitotemporal constriction. It has a long dorsal subvertical suture with the squamosal posteriorly, a sub-horizontal one with the parietal dorsally, and an oblique suture with the frontal anteriorly. Anteriorly, the alisphenoid approaches the posterior edge of the ethmoidal foramen but does not reach it (Figs 21, 23, 24, 27). Posteriorly, the alisphenoid forms the medial angle of the posterior root of the zygomatic arch. There, the alisphenoid-squamosal suture passes ventrally and delimits a small glenoid process of the alisphenoid. From this process, on the ventral face of the skull, the alisphenoid-squamosal suture runs posteromedially and reaches the lateral edge of the large foramen ovale. The anterior half of this foramen is formed by the alisphenoid. As in *Pucadelphys* and *Mayulestes,* there is no tympanic process of the alisphenoid and the foramen ovale is a true primary foramen ovale (i.e. not a foramen pseudovale as in most Recent didelphids, in which the external exit of the mandibular nerve is fully enclosed in the alisphenoid), which transmits the mandibular branch of the trigeminal nerve (V3). On the anteromedial region of the rim of the foramen ovale, the alisphenoid bears a posteriorly directed short process, which defines medially a small notch separating the alisphenoid anteriorly and the petrosal posteriorly, with a possible participation of the basisphenoid medially. This structure was clearly described and figured in *Monodelphis* by Wible (2003: fig.6), who interpreted it as the exit of the greater petrosal nerve (foramen for the greater petrosal nerve) from the hiatus Fallopii on its way to the pterygoid canal (Figs 28-31). This condition is observed on MHNC 8264 and 8308 and is consistently present in the new specimens of *Pucadelphys* figured by Ladevèze *et al.* (2011), (see below).

From the medial edge of the foramen ovale, the alisphenoid extends anteriorly along the basisphenoid, to which it is tightly fused. However, most of the line of junction of the alisphenoid and the basisphenoid is hidden by the large underlying posterior process of the pterygoid (Fig. 28). Therefore, from the carotid foramen (see basisphenoid section below) the alisphenoid has a long contact with the posterior process of the

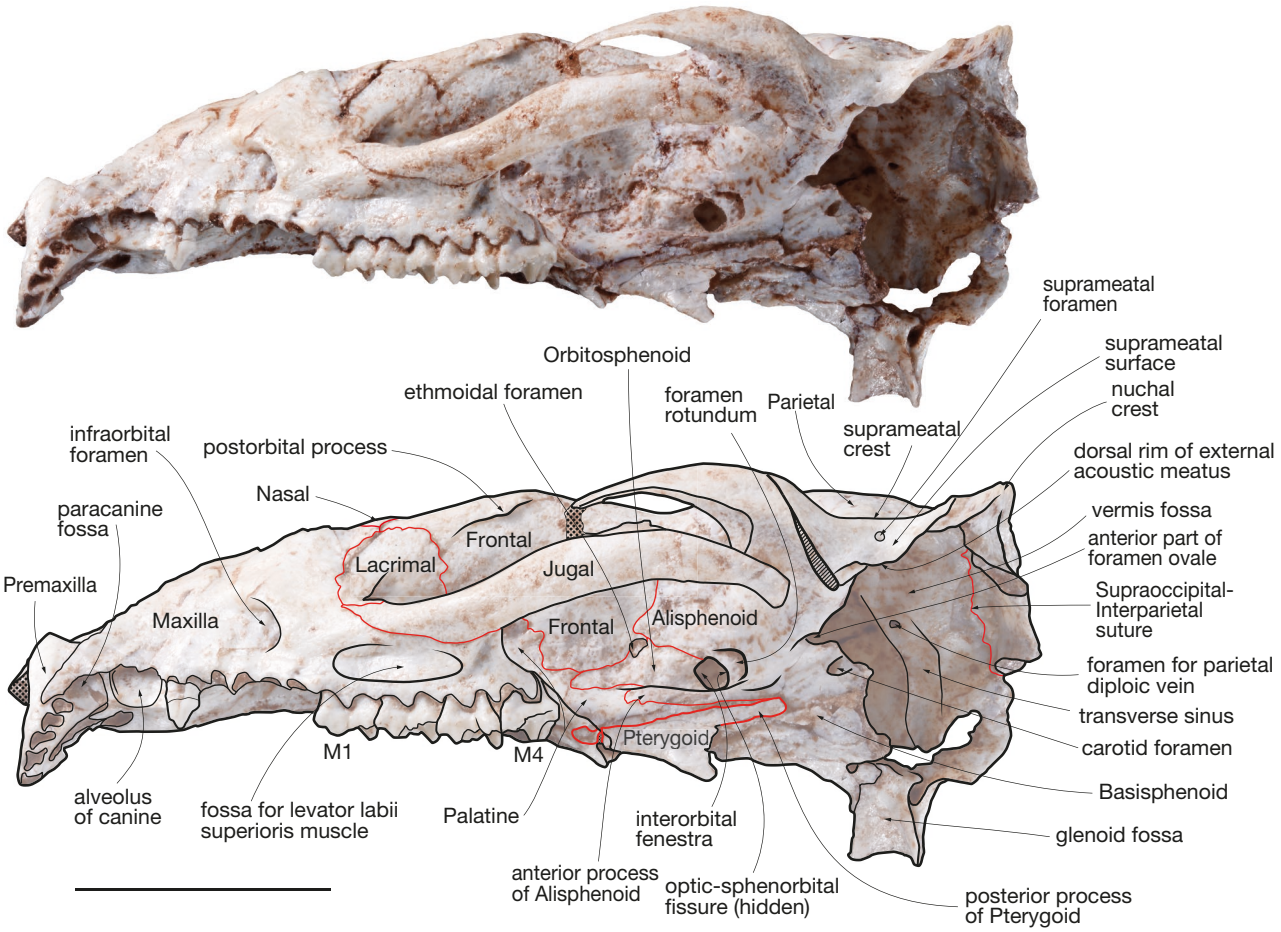

FIG. 27. — *Andinodelphys cochabambensis* (MHNC 13847): ventrolateral view of the left orbitotemporal fossa. Scale bar: 10 mm.

pterygoid. Slightly anterior to the foramen of the transverse canal sinus (see basisphenoid section below), it totally encloses a large, anteriorly opening foramen rotundum, which transmits the maxillary branch of the trigeminal nerve (V2). The lateral edge of the foramen is strongly convex laterally and presents a marked bulge on its lateral wall. Some scars and small fossae are observed around this bulge, and we interpret this area as the origin of the muscle *pterygoideus externus* as it is observed in a similar place in *Didelphis* (Hiiemae & Jenkins 1969). The dorsal edge of the foramen rotundum forms a sharp anterodorsally directed crest, which extends anteriorly and joins the dorsal edge of the optic-sphenorbital fissure (Fig. 24), (see below).

Between the foramen rotundum and the carotid foramen (see basisphenoid section below) is a lateral foramen for the transverse canal sinus (Figs 28-31). A transverse canal foramen is observable on both sides of the skull in MHNC 8308. In MHNC 8262 it is large on the right side but the condition is unclear on the left side and we suspect that it may have been obliterated by compression due to fossilisation. It is present but very small in MHNC 8370 and 13847, a possible consequence of the post-mortem distortion of the specimens. In the four specimens, the transverse canal foramina are located approximately halfway between the carotid foramen and rotundum foramen and slightly lateral to the former. According to Wible (2003) the transverse canal is ontogenetically entirely within the basisphenoid. However, the lateral foramina of the transverse canal are lateral to the posterior process of the pterygoid, which according to Wible (2003) covers the basisphenoid-alisphenoid boundary. Therefore, the lateral foramina of the transverse canal should pierce in the alisphenoid. In fact, in extant didelphids, if the transverse canal itself is obviously in the basisphenoid, its lateral foramina clearly appear to be in the alisphenoid and we tentatively interpret such a position in *Andinodelphys*.

The transverse canal foramen "transmits an extracranial vein or a pterygoid plexus that communicates with the cavernous sinus. In some species, this bilateral vein also communicates with its antimere" (Sánchez-Villagra & Wible 2002: 28). This vein is a major sinus of the external jugular vein (Archer 1976a). These authors have revised the endocranial configuration of the transverse canal vein, which, in some marsupials, perforates the basisphenoid transversely, thus creating an intramural connection between the two foramina. In extant didelphids, when present, this canal is parabolic, with its branches diverging posteriorly (e. g. *Didelphis, Marmosa, Metachirus, Thylamys*). In relation to this morphology the foramen for the transverse canal is posterolaterally oriented in didelphids. In dasyuroids,

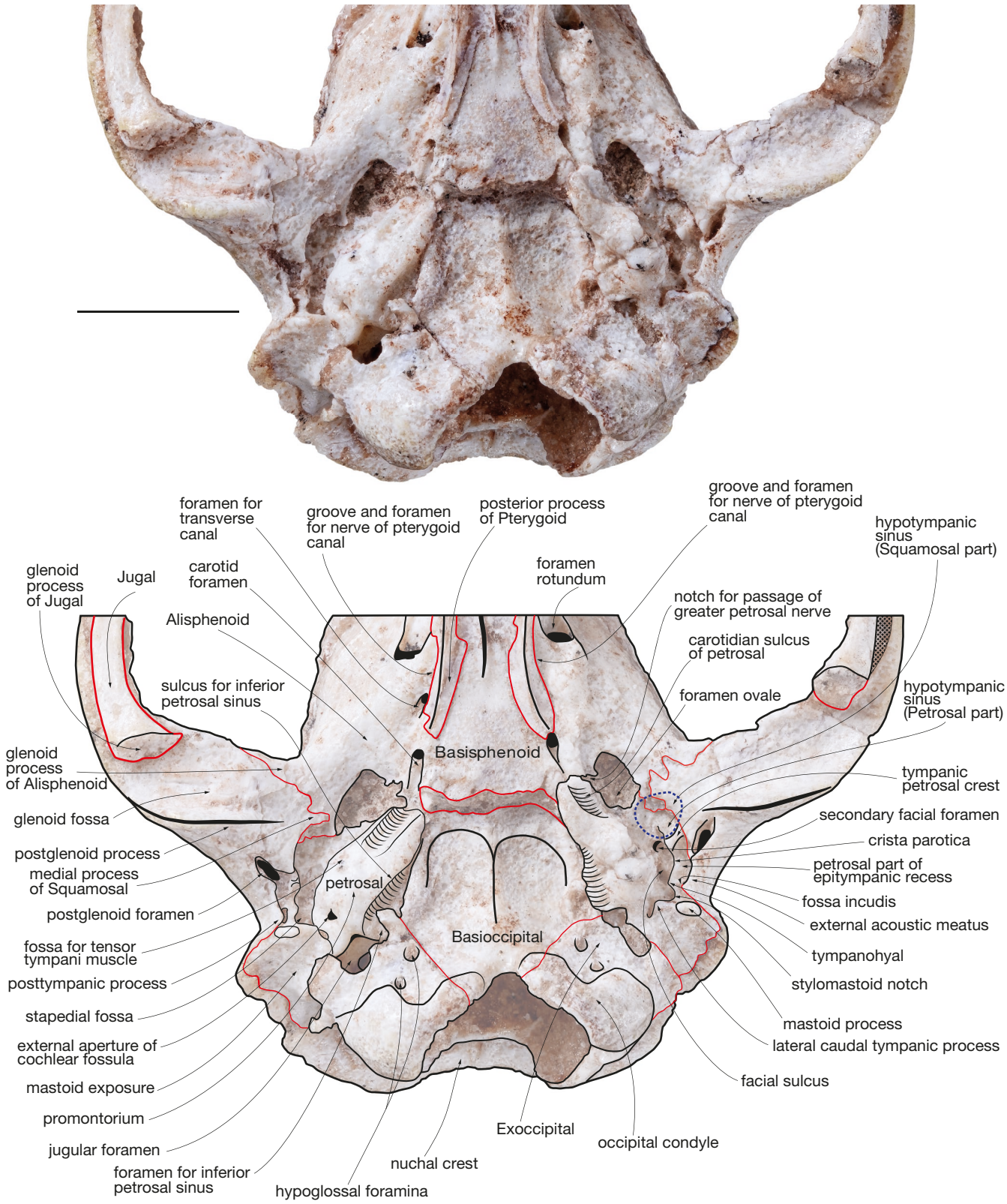

FIG. 28. — *Andinodelphys cochabambensis* (MHNC 8264): ventral view of the basicranium. Blue dotted line circle on the left side of the skull indicates the excavation of the dorsal part of the hypotympanic sinus in the basicranium. Scale bar: 5 mm.

(e. g. *Dasyurus, Sminthopsis, Sarcophilus, Thylacinus*) the canal is roughly transverse, almost straight, and the foramen opens laterally. In marsupials lacking an intramural connection, the vein of the transverse canal foramen either communicates with its antimere or directly connects independently to the cavernous sinus. In *Andinodelphys,* on the sections of the CTscan of

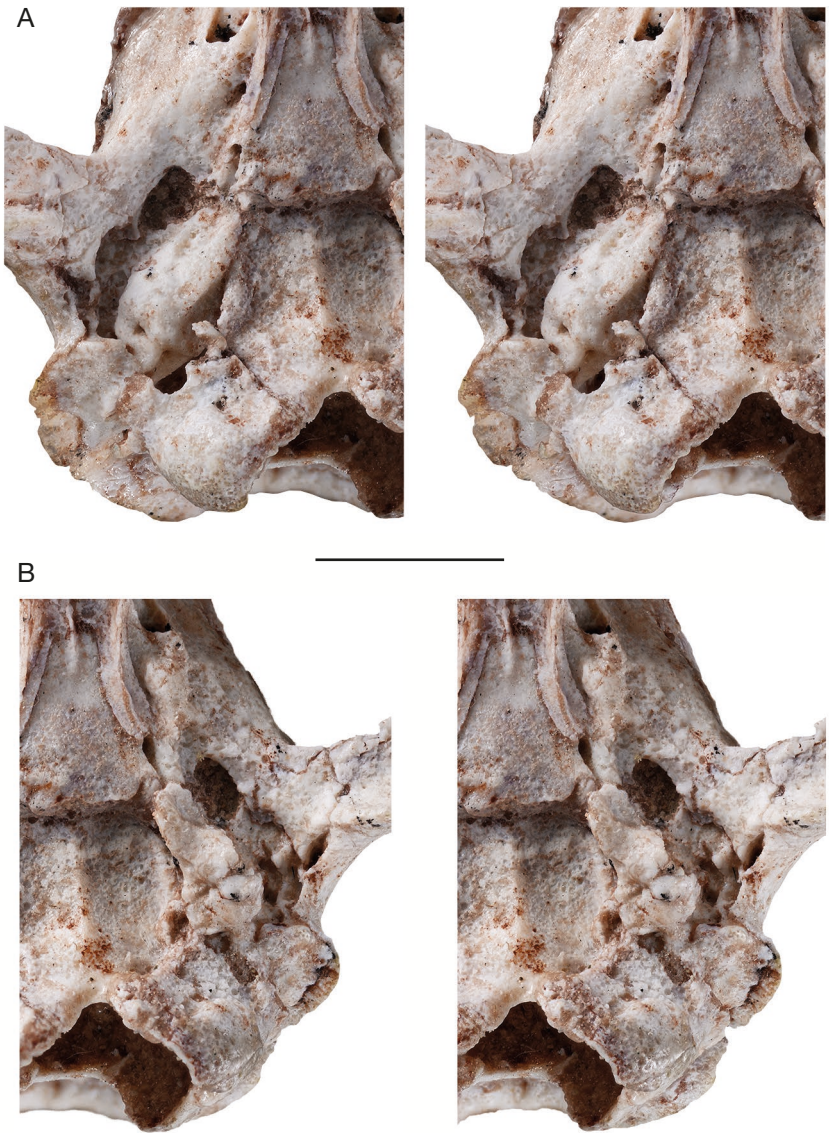

FIG. 29. — *Andinodelphys cochabambensis* (MHNC 8264): **A**, stereophotos of the right auditory region; **B**, stereophotos of the left auditory region. Scale bar: 5 mm.

MHNC 8264 (Fig. 32), an intramural canal pierces the basisphenoid from right to left foramina of the transverse canal. It is better observed on the right side of the skull since the left transverse canal has likely suffered some post-mortem compression. The foramina open posteriorly and the canal extends anteriorly, thus being parabolic as is observed in *Didelphis*. A different condition is observed on MHNC 8308. In this specimen, the foramen of the transverse canal opens within the braincase on the lateral wall of the internal sulcus for the internal carotid, on the lateral edges of the pituitary fossa. There is no intramural canal within the basisphenoid. This condition is observed in the CTscan sections (Fig. 33). An intramural connection between the transverse canal foramina is present in most, but not all, dasyurids since Sánchez-Villagra & Wible (2002: 30) observed that "in three specimens of *Dasyurus viverrinus* the foramen simply opens endocranially". Variation is also observed in *Thylacinus* (Archer 1976a). Therefore, the variation observed in *Andinodelphys* is also present in extant marsupials.

Anteromedial to the foramen rotundum, the alisphenoid has an elongated anterior process, which is anteroposteriorly subhorizontal and slightly sloping laterally. This process is a narrow and thin blade of bone, which extends anteriorly as far as the level of the hamular process of the pterygoid as observed on MHNC 8264. It does not reach the minor palatine foramen anteriorly but it is slightly anterior to the level of the ethmoidal foramen. A similar condition is observed in Recent didelphids. In its posterior part the anterior process overlies the part of the pterygoid that forms the lateral wall of the basipharyngeal groove. Because the anterior process of the alisphenoid is narrower than this wall, the pterygoid is visible on the dorsal and ventral edges of the process, as is clearly observed in *Monodelphis* (Wible 2003: fig. 4) (Figs 21-24). In its anterior region, the anterior process of the alisphenoid contacts the posterior blade of the palatine, which forms the lateral wall of the basipharyngeal groove. The alisphenoid forms the lateral wall of the optic-sphenorbital fissure. The

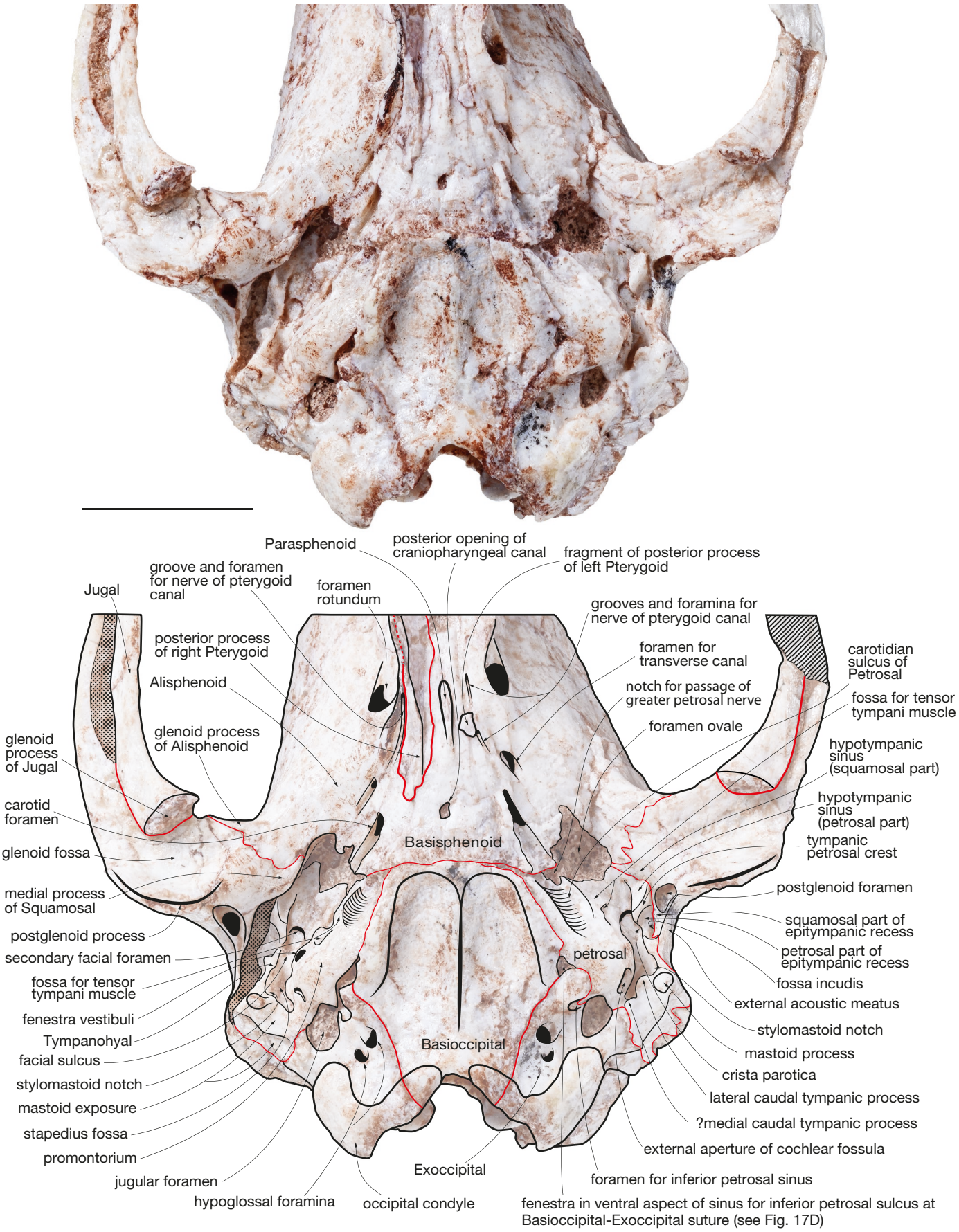

FIG. 30. — *Andinodelphys cochabambensis* (MHNC 8308): ventral view of the basicranium. Scale bar: 5 mm.

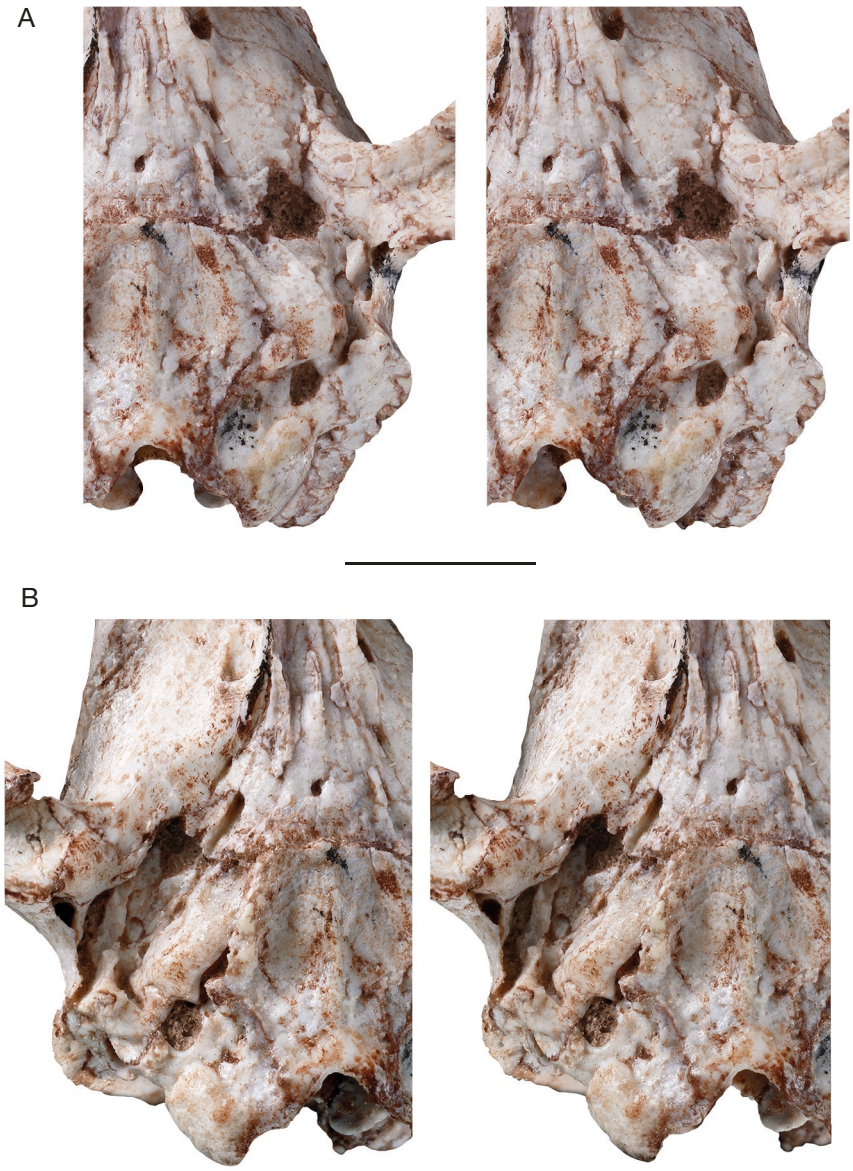

FIG. 31. — *Andinodelphys cochabambensis* (MHNC 8308): **A**, stereophotos of the right auditory region; **B**, stereophotos of the left auditory region. Scale bar: 5 mm.

ventrolateral edge of the optic-sphenorbital fissure is formed by the anterior process of the alisphenoid and its ventromedial edge is formed by the basisphenoid posteriorly and the presphenoid anteriorly. Its dorsal edge is also formed by a small anteriorly directed dorsal process of the alisphenoid, which contacts the orbitosphenoid and the frontal anteriorly, and reaches or almost reaches the ethmoid foramen.

On both sides of MHNC 8264, on the dorsal edge of the optic-sphenorbital fissure just medial to the dorsolateral crest of the groove extending anteriorly from the foramen rotundum, in the alisphenoid, is a small anteriorly-opening foramen (Fig. 34). This foramen is not observed in MHNC 8308, 8370, and 13847. It can be followed on the CTscan slices of MHNC 8264, and enters the anteroventral region of the brain cavity after a short intramural course in the alisphenoid lateral edge of the optic-sphenorbital fissure (Fig. 35). This foramen is probably not the anterior opening of the pterygoid canal, which, as observed by Wible (2003) in *Monodelphis*, is on the ventrolateral edge of the optic-sphenorbital fissure in the suture between the alisphenoid and the pterygoid. We have observed the anterior opening of the pterygoid canal in a similar position in *Didelphis* (SL and CM personal collections), *Marmosa* (MNHN-RH82), and *Caluromys* (MNHN uncatalogued). On a juvenile specimen of *Didelphis albiventris* (M3 and M4 still in crypt and P3 barely erupting), (CM personal collection), a similar foramen to that observed in MHNC 8264 is observed in a similar location (on the dorsal edge of the optic-sphenorbital fissure) but forming an incompletely closed groove (probably because of the young ontogenetic age of the specimen) rather than a proper foramen. This groove extends in the braincase on the dorsal aspect of the dorsal wall of the foramen rotundum, formed by the alisphenoid. We have not observed such a foramen in adult specimens of *Didelphis* or other didelphids (e.g. *Marmosa, Metachirus, Thylamys, Caluromys*). Such a foramen

has been observed by Archer (1976a) in *Dasyurus, Dasycercus*, and *Dasyuroides*, but this author regards the homology of this foramen as uncertain. Archer (1976a) did not observe the foramen either in *Marmosa*, but did not mention the condition in *Monodelphis, Caluromys* and *Metachirus*.

Orbitosphenoid. (Figs 21-24, 25, 27, 29)
As is typical in metatherians, the orbitosphenoid is not perforated by an optic foramen (Rougier *et al.* 1998; Wible 2003). Anteroventrally, the orbitosphenoid has a sub-horizontal suture with the palatine and is fused to the presphenoid posteroventrally. Anterodorsally, a long suture with the frontal extends obliquely as far as the ethmoidal foramen. The latter is ventrally directed and enclosed in the orbitosphenoid-frontal suture, with the orbitosphenoid forming its posteroventral edge and the frontal forming its anterodorsal edge. The alisphenoid is close to its posterodorsal edge but does not reach it (Fig. 24), thus resembling the condition observed in didelphids (except, for example, *Didelphis* and *Metachirus,* in which the alisphenoid overlaps the orbitosphenoid and frequently forms the lateral wall of the foramen). Between the ethmoidal foramen and the alisphenoid, the orbitosphenoid forms a small part of the lateral wall of the braincase. More ventrally, it forms the dorsal edge of the optic-sphenorbital fissure. The medial edge of the fissure is formed by the orbitosphenoid anteriorly, by the basisphenoid posteroventrally and by the presphenoid ventrally between the basisphenoid and the orbitosphenoids. Its dorsal and lateral edges are formed by the alisphenoid. Posteroventrally, at their junction with the presphenoid, the orbitosphenoids are fused in the sagittal plane and have a saddle-shaped posterior border. At this point is a large transverse vacuity in the base of the skull, which marks the confluence of the left and right optic-sphenorbital fissures. This vacuity is the interorbital fenestra, which was probably filled by a membrane during life, as is observed in many Recent didelphids (e.g., *Monodelphis, Marmosa, Caluromys, Metachirus*). A large interorbital fenestra is also present in *Pucadelphys*.

Basisphenoid and parasphenoid (Figs 18-21, 24, 26, 30)
The basisphenoid is a trapezoid bone, which is broadest posteriorly at its suture with the basioccipital. It narrows anteriorly toward the presphenoid. The anterior suture between the basisphenoid and the presphenoid is not observable in the basipharyngeal groove, which is totally roofed by the dorsomedial expansions of the pterygoids. However, on the medial wall of the optic-sphenorbital fissure, in the interorbital fenestra, the limit between the two bones is distinct. The length of the basisphenoid is approximately 60% the length between the posterior edge of the choanae and the basisphenoid-basioccipital suture. In other words, the anterior limit of the basisphenoid is approximately at the level of the posterior edge of the free vertical blade of the pterygoid. The posterior suture with the basioccipital is transverse and straight. It is located at the level of the foramen for the greater petrosal nerve and the postglenoid processes. On the ventral aspect of the basisphenoid is a median marked rod-shaped crest. This crest is present on the anterior region of the visible (i.e. not covered by the pterygoid) part of the basisphenoid but clearly extends anteriorly below the pterygoids as observed on MHNC 8264 and 8308 (Figs 18B; 19B). This structure is apparently absent in Recent didelphids but it is present in *Pucadelphys, Allqokirus,* and *Mayulestes*. It probably represents a remnant of the parasphenoid as observed by Wible *et al.* (2018) in several extant didelphids and in the microbiothere *Dromiciops*. In the posterior region of the basisphenoid of MHNC 8308, in the midline, is a small but distinct foramen, which could represent the posterior opening of the craniopharyngeal canal (Figs 19B; 30). When present, the craniopharyngeal canal houses a remnant of the pharyngeal diverticulum, from which the pars glandularis of the hypophysis develops (Wible 2008, 2011; Evans & de Lahunta 2013). It is commonly present in juveniles but generally obliterates in adults. On the posterolateral region of the basisphenoid is a large carotid foramen, which opens just posterior to the posterior end of the posterior process of the pterygoid. The foramen is circular and has a posteriorly concave ventral border. The carotid foramen extends posteriorly in a deep groove, which is just anterior to the carotid sulcus of the petrosal (see below). As stated by Wible (2003), but *contra* Marshall & Muizon (1995), the carotid is ontogenetically entirely within the basisphenoid.

Presphenoid (Figs 19, 20)
This bone is observed in the basipharyngeal groove of MHNC 8308, on which the ventromedial blades of the pterygoid roofing the groove are not fully preserved. It is a rod-shaped bone, which is tightly fused to the orbitosphenoids. It extends anteriorly into the nasal cavity. Posteriorly, the presphenoid contacts the basisphenoid in the midline of the skull and anteriorly, in the basipharyngeal groove, it contacts the underlying pterygoids and more anteriorly the palatines. In the orbitotemporal fossa, the presphenoid forms part of the ventromedial wall of the optic-sphenorbital fissure. It also forms the floor of the interorbital fenestra.

Squamosal (Figs 17-31)
The squamosal has a moderately developed squama on the posterolateral region of the braincase. It has a long dorsally convex suture with the parietal and interparietal dorsally. Posteriorly, the squamosal forms the lateral portion of the nuchal crest and has a suture with the pars mastoidea of the petrosal. This suture is visible in occipital view of the skull because the squamosal portion of the nuchal crest overhangs the occipital aspect of the petrosal (Fig. 25). The squamosal-petrosal suture runs ventrally on the occipital face of the skull and reaches the mastoid process ventrally.

Fig. 32. — CT-slices through the skull of MHNC 8264. The numbers for each illustrated slice refer to the position of the slice within the sequence of 1751 images (resolution binned images, voxel size = 0.02781 mm). Dorsal side of the skull toward the top of slices, right side of the skull toward the right. **A**, is the most posterior slice toward occiput (1359) and **H**, is the most anterior one, toward snout (1303). Scale bar: 5 mm.

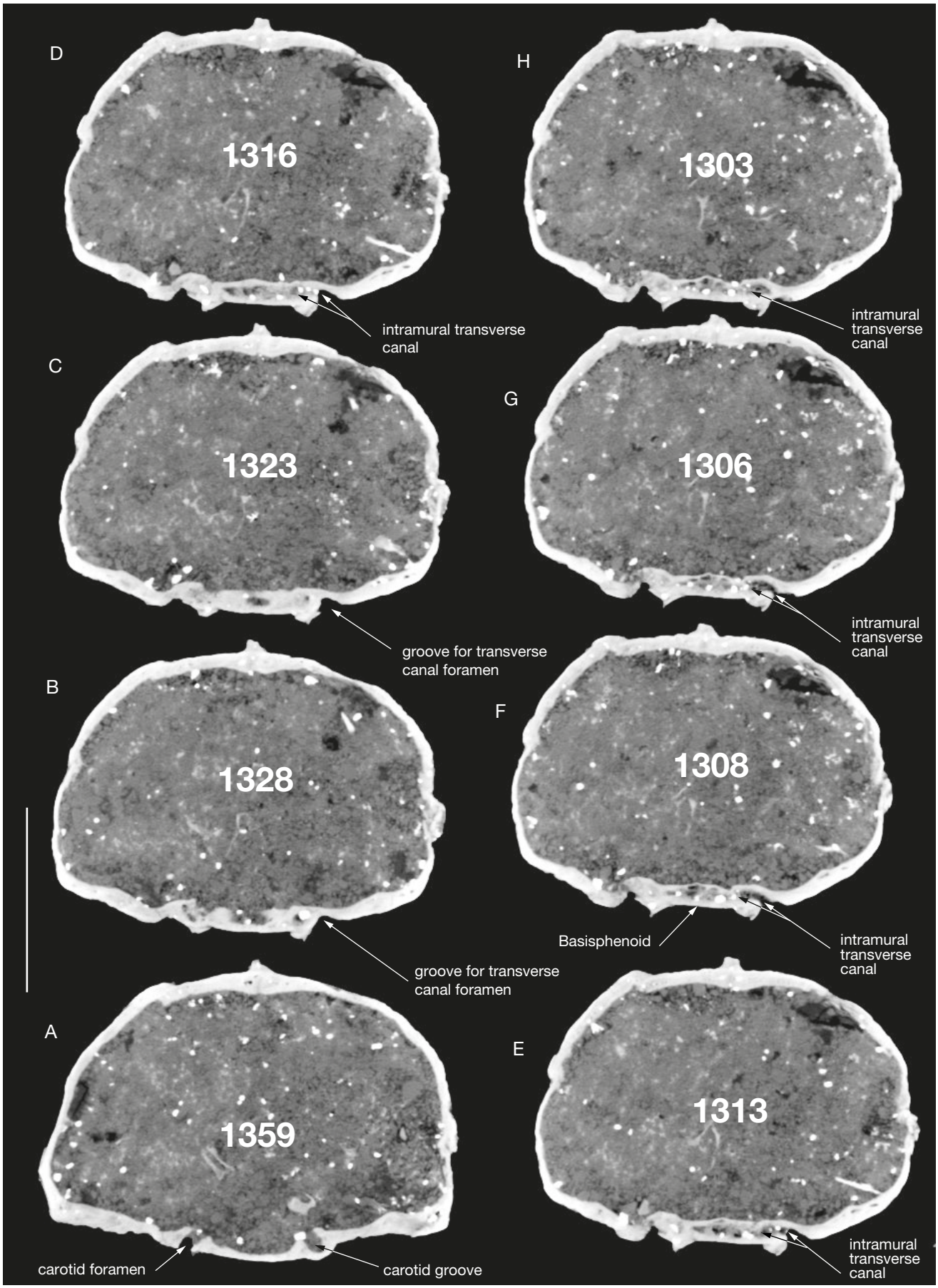
D
1316
intramural transverse canal
H
1303
intramural transverse canal
C
1323
groove for transverse canal foramen
G
1306
intramural transverse canal
B
1328
groove for transverse canal foramen
F
1308
Basisphenoid
intramural transverse canal
A
1359
carotid foramen
carotid groove
E
1313
intramural transverse canal

Anteriorly, on the roof of the braincase, the squamosal meets the alisphenoid at the level of the anterior edge of the posterior root of the zygoma and the suture turns ventrally at almost right angle. The squamosal-alisphenoid suture enters the dorsal face of the posterior zygomatic root in its anteromedial angle, where it delimitates a small glenoid process of the alisphenoid. On the anteromedial angle of the glenoid fossa the squamosal-alisphenoid suture runs medially towards the lateral edge of the foramen ovale. In this area, the relationships of the squamosal, alisphenoid and petrosal vary, but in all specimens the squamosal presents a medial process, which reaches or almost reaches the lateral rim of the foramen ovale. In MHNC 8308, this medial process of the squamosal is wedged between the alisphenoid anteriorly and the petrosal posteriorly (Fig. 30). It is triangular and its medial apex is pointed and forms a tiny portion of the lateral rim of the foramen ovale. In MHNC 8264, the medial process of the squamosal does not reach the lateral edge of the foramen ovale (Fig. 28). On this specimen, medial to the process, the rim of the foramen ovale is formed by a posterior extension of the alisphenoid, which wedges between the medial process of the squamosal anteriorly and the petrosal posteriorly. Both conditions are present in MHNC 8370. Apparently, on the left side of the skull the squamosal reaches the rim of the foramen ovale, while on the right side it does not and the alisphenoid forms the anterolateral rim of the foramen ovale (Fig. 26). The condition of MHNC 8308 is similar to that observed in *Pucadelphys* and that of MHNC 8264 resembles that of *Mayulestes*. The posteromedial edge of the medial process of the squamosal slopes posteromedially toward a small cupula. This shallow depression in the roof of the anterior region of the middle ear is posterolateral to the foramen ovale. It is formed posteromedially by the petrosal, anterolaterally by the medial process of the squamosal, and posterolaterally by the anteromedial face of the petrosal crest (see petrosal section below), which is distinctly concave (Fig. 28). The constitution of this depression is identical to that observed in *Mayulestes* (Muizon 1998) and forms what is regarded as an incipiently developed hypotympanic sinus (*sensu* Klaauw 1931: 19 and Archer 1976a: 227). The suture posterior to the medial process of the squamosal, is with the petrosal. It runs along the lateral border of the petrosal portion of the epitympanic recess and fossa incudis. In fact, the squamosal-petrosal suture passes within the epitympanic recess, which is divided into a medial petrosal portion (see petrosal section below) and a lateral squamosal portion. As is observed in MHNC 8308, in which this region is well-preserved, the two portions of the epitympanic recess are roughly similar in size and the medial wall of the squamosal in this region is slightly excavated. At the posterior end of the epitympanic recess, the squamosal also participates in the formation of the lateral part of the fossa incudis (see petrosal section below). The crest, which forms the ventral edge of the squamosal portion of the epitympanic recess, is the dorsal edge of the external acoustic meatus. Dorsal to it and on the lateral side of the squamosal is a subvertical area, which is ventral to the suprameatal crest (see below) and posterodorsal to the posterior face of the postglenoid process (Fig. 24). This area corresponds to the suprameatal surface of the squamosal (Novacek 1986). Posterior to the fossa incudis the squamosal laterally borders the crista parotica and the tympanohyal of the petrosal, and reaches the lateral edge of the mastoid process, from where it runs dorsally along the anterodorsal edge of the pars mastoidea of the petrosal and forms the ventrolateral portion of the nuchal crest (see above). Between the fossa incudis anteriorly and the lateral edge of the mastoid process, the ventral rim of the squamosal protrudes ventrally in a rounded to V-shaped (in lateral view) but flat (in ventral view) process, which extends the dorsal rim of the external acoustic meatus (Fig. 24). This process laterally borders the tympanohyal and is slightly anterior to the mastoid process. This structure corresponds to the posttympanic crest as defined by Wible (2003) and Wible *et al.* (2004). Lateral to the posttympanic crest and posteriorly bordering the suprameatal surface is the posttympanic process, which is weakly developed in *Andinodelphys*. In fact, the posttympanic process of *Andinodelphys* corresponds to the posterior edge of the suprameatal surface, which is slightly bent laterally at its contact with the pars mastoidea of the petrosal. In *Andinodelphys,* the distinction between posttympanic crest and process is subtle, a condition that is also present in *Pucadelphys* and *Mayulestes*. As a matter of fact, the posttympanic crest (sensu Wible 2003) of *Pucadelphys* and *Mayulestes* has been identified as posttympanic process by Marshall & Muizon (1995) and Muizon (1998) respectively.

Lateral to the medial process of the squamosal is the transversely elongated glenoid fossa for articulation of the dentary. The main axes of the two fossae are not exactly parallel and transverse. They are slightly oblique being oriented on an anterolateral-posteromedial axis. The glenoid fossa is approximately two times wider than long, and deeply concave. In lateral view, it has a section forming approximately a quarter of circle, the dorsal part of the fossa being sub-horizontal and the posterior wall being sub-vertical. The anterior edge of the cavity is roughly straight being distinctly oblique in dorsal view and oriented posteromedially-anterolaterally (especially in MHNC 8264 and 13847). The postglenoid process is wide and high. In posterior view, it is roughly semicircular and extends transversely for the whole width of the glenoid fossa. In posterior view, it is weakly asymmetrical, its ventralmost point being slightly shifted medially to the middle of the glenoid fossa. In MHNC 8308 the glenoid fossa and postglenoid process are slightly less expanded transversely than in the other three specimens. However, this condition could be the result of the post-mortem transverse compression, which affected this specimen. The preglenoid process of the jugal is small but distinct and located at the anterolateral angle of the glenoid fossa. On the posterolateral aspect of the postglenoid process is a small postzygomatic foramen (Fig. 25). According to Archer (1976a), in dasyurids, this foramen transmits a vein from the posterior root of the zygomatic arch to the postglenoid vein. This foramen is present in *Pucadelphys* but apparently absent in *Mayulestes*. Posterior to the medial edge of the postglenoid process is a large postglenoid foramen. This foramen transmits the sphenoparietal emissary vein (which externally becomes

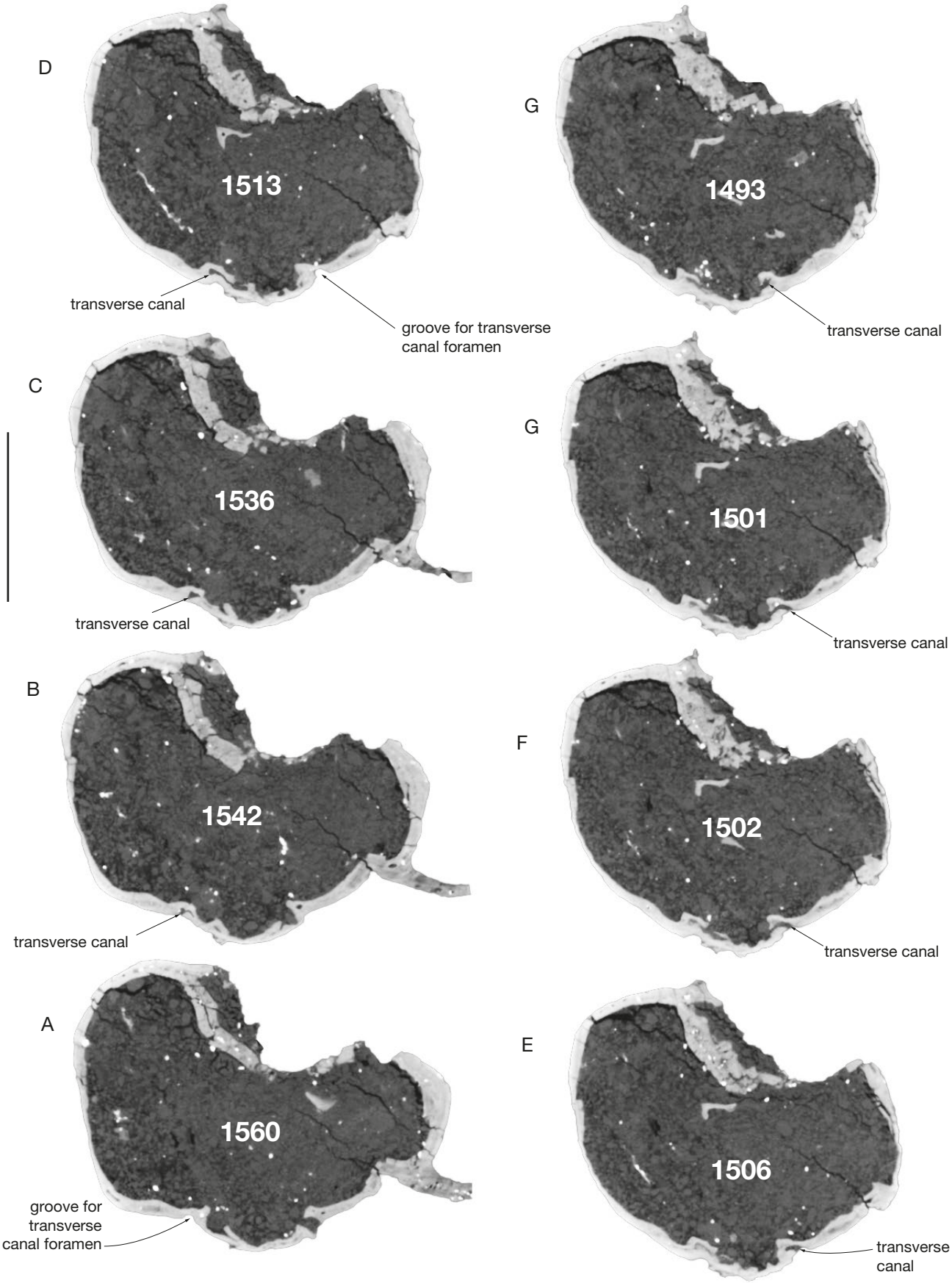

FIG. 33. — CT-slices through the skull of MHNC 8308. The numbers for each illustrated slice refer to the position of the slice within the sequence of 2069 images (resolution binned images, voxel size = 0.02543 mm). Dorsal side of the skull toward the top of slices, right side of the skull toward the left. **A**, is the most posterior slice, toward occiput (1560) and **H**, is the most anterior one, toward snout (1493). Scale bar: 5 mm.

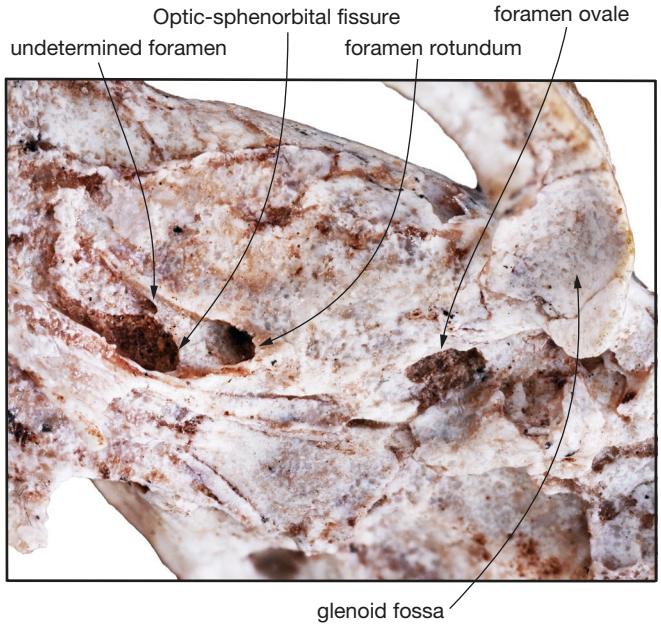

Fig. 34. — *Andinodelphys cochabambensis* (MHNC 8264): ventrolateral view of the left side of the skull showing the undetermined foramen described in text (p. 651) located on the dorsal edge of the optic-sphenorbital fissure.

the postglenoid vein) from the prootic sinus (Wible 1990), and the postglenoid artery (Archer 1976a; Wible 1987, 1990). The posteromedial side of the foramen forms the anterolateral edge of the epitympanic recess. From the postglenoid foramen, a deep groove excavates the ventromedial edge of the postglenoid process for the exit of the postglenoid vein. This groove fades ventrally but extends almost up to the ventral rim of the process. Externally the foramen is totally enclosed in the squamosal, while internally, the medial wall of the canal conveying the sphenoparietal emissary vein (or prootic sinus, more proximally) is formed by the lateral side of the petrosal, the medial wall being formed by the squamosal. On MHNC 13487, in which the petrosal and occipital bones are missing, the medial aspect of the squamosal is clearly exposed. On the roof of the braincase, a deep groove runs posterolaterally from the sagittal plane and descends towards the postglenoid foramen (Fig. 27). This groove transmitted the transverse sinus, which divides into three major vessels at the dorsal apex of the petrosal: the sigmoid sinus posteromedially, the superior sinus anteromedially and the prootic sinus anterolaterally. The prootic sinus becomes the sphenoparietal emissary vein after emitting the vein of the prootic canal within the petrosal (Wible 1990). The postglenoid foramen of *Andinodelphys* differs from that of *Pucadelphys,* in which it is not totally enclosed in the squamosal, even externally *contra* Marshall & Muizon (1995), a condition, which has been distinctly observed on 7 specimens.

The zygomatic process of the squamosal is narrow, slightly curved ventrally, and regularly tapers anteriorly. It is shorter than half of the total length of the orbitotemporal fossa (*c.* 40%), being proportionally shorter than in *Pucadelphys*. Its dorsal edge is slightly convex, while its ventral side is concave. The apex is very narrow. The dorsal edge of the process forms the most elevated point of the zygomatic arch. It extends posteriorly as the postzygomatic crest, which borders the posterior edge of the squamosal fossa. Further posteriorly, the crest reaches the posterolateral region of the braincase and forms, above the external acoustic meatus, a low and rounded posterodorsally oriented suprameatal crest (in fact, more a ridge than a crest), which connects to the nuchal crest posteriorly (Wible 2008) above the ventral limit of the latter (Figs 23, 24). Ventral to the suprameatal crest and dorsal to the dorsal rim of the external acoustic meatus is the suprameatal surface, which bears the small suprameatal foramen (Wible 2003) (Fig. 24). This foramen has been referred to as the subsquamosal foramen by Archer (1976a), Marshall & Muizon (1995), and Pavan & Voss (2016), but we follow here Wible (2003), Wible *et al.* (2004), and Muizon *et al.* (2018) because, according to these authors, the subsquamosal foramen is located above the suprameatal crest on the lateral wall of the braincase. The suprameatal foramen is defined as a medium-sized to small opening perforated in the suprameatal surface of the squamosal, below the suprameatal crest as is observed in *Andinodelphys*. It communicates with the postglenoid foramen and, in eutherians, conveys a branch of the ramus posterior of the stapedial artery into the substance of the squamosal (Wible 2008, 2011). In the xenarthran *Euphractus* and likely in *Zalambdalestes* and *Maelestes,* the suprameatal foramen may also transmit temporal rami from the ramus superior to the temporalis muscle (Wible 2003; Wible & Gaudin 2004; Wible *et al.* 2004, 2009). In *Didelphis*, the postglenoid artery (an offshoot of the external carotid artery) enters the skull via the postglenoid foramen and divides into a meningeal ramus, which extends dorsally within the braincase and a ramus temporalis, which exits the skull via the suprameatal foramen and supplies the temporalis muscle. (Wible 1987, 2003; Wible *et al.* 2004: 95). According to Archer (1976a: 223) the suprameatal

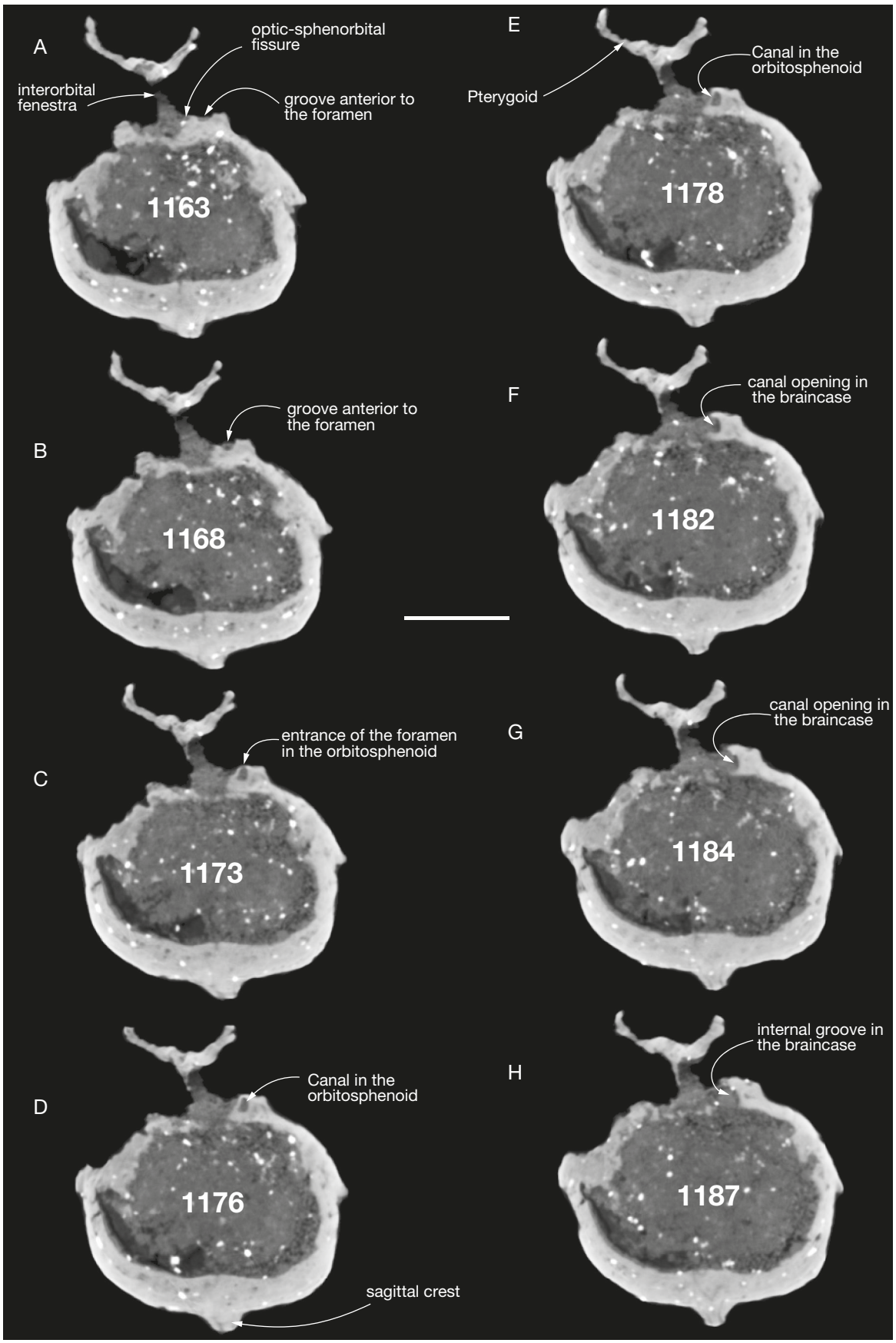

FIG. 35. — CT-slices through the skull of MHNC 8264. The numbers for each illustrated slice refer to the position of the slice within the sequence of 1751 images (resolution binned images, voxel size = 0.02781 mm). Occiput of the skull toward the slice 1178, left side of the skull toward the right; the skull is upside down, with pterygoids dorsally and sagittal crest ventrally. **A**, is the most anterior slice (1163) and **H**, is the most anterior one (1178). Scale bar: 3 mm.

foramen (his subsquamosal foramen) "carries postglenoid artery out onto parietal area of cranium from postglenoid foramen. Also carries vein from parietal area to postglenoid foramen". The suprameatal foramen of *Andinodelphys* varies in position, number and size in the four skulls available. In MHNC 8264 there is one single, medium-sized, and posteriorly located foramen on the right side, whereas there are two foramina on the left side, one large and posterior (just anterior to nuchal crest) and another small, slightly anterior to it. In MHNC 8308 a single medium-sized foramen is present, located in the anterior part of the suprameatal surface on both sides. In MHNC 8370 two foramina are present; one, large, in the posterior region of the surface and the other, medium-sized in the anterior half of the surface (observation of the two foramina is possible on the right side only). In MHNC 13847, two small foramina are observed on the left side (one anterior and one posterior), whereas two posteriorly located foramina are present on the right side, one ventral and small and the other dorsally placed (on the suprameatal crest) and medium-sized. The significant variation observed in *Andinodelphys* differs from the condition in most *Pucadelphys* specimens and in most Recent didelphids (e.g., *Didelphis, Monodelphis, Marmosa, Philander, Metachirus, Thylamys*), in which the suprameatal foramen is consistently single, distinctly larger than the large foramen in *Andinodelphys* and in a median to anterior location on the suprameatal surface. In *Andinodelphys,* the suprameatal foramen (foramina) is (are) located more posteriorly than in *Pucadelphys* and the Recent didelphids mentioned above. Interestingly, however, in two specimens of *Pucadelphys* (MHNC 8266 and 8379, two out of ten specimens in which this character can be observed), two foramina are present. One is anterior and has the large size and the anterior position of the suprameatal foramen of the didelphid genera mentioned above, and the other is small and posterior as is generally observed in *Andinodelphys*. Furthermore, variation also exists within Recent didelphids since a single, small and posteriorly located foramen is present in *Caluromys,* thus resembling the condition of *Andinodelphys*. A similar condition is observed in *Allqokirus*, while in *Mayulestes* a small foramen is present but anteriorly situated.

On the squama of the squamosal, just above the posterior root of the zygoma, is a small foramen; another smaller foramen is observed at the same dorsoventral level, slightly anterior to it. This condition is observed on MHNC 8264, 8308, and 13847. In MHNC 8370, observation of a foramen is uncertain due to the preservation of the specimen. This (these) foramen (foramina) is (are) likely to represent the subsquamosal foramen (foramina) (Figs 21, 23). They convey the temporal rami emitted by the arteria diploëtica magna (Wible *et al.* 2004) to the temporalis muscles. Subsquamosal foramina are absent in *Pucadelphys* (10 specimens), *Mayulestes* (one specimen) and *Allqokirus* (one specimen). They are either absent or tiny in didelphids. Wible (2003) observed subsquamosal foramina in most specimens of *Monodelphis* studied and in one specimen of *Didelphis*. We have not observed subsquamosal foramina on the squama of the squamosal of five specimens of *Didelphis* (out of six), five *Metachirus*, Seven *Caluromys*, four *Marmosa,* and two *Thylamys*.

Petrosal and auditory region (Figs 28-31, 36-39).
Although the petrosal of *Andinodelphys* has been described by Ladevèze & Muizon (2007), we consider useful to provide a further description of the auditory region of the skulls MHNC 8264 and 8308 in order to rectify some anatomical and nomenclatural errors of the description in Ladevèze & Muizon (2007). Furthermore, some newly discovered petrosals in the skeleton block (Fig. 3) belonging to the unprepared specimen MHNC 13933 and to MHNC 13847 (Figs 36-39) provide a useful complement to Ladevèze & Muizon (2007)'s description. The best-preserved auditory region of *Andinodelphys* is the left side of MHNC 8308 (Fig. 31A), which has suffered only a slight transversal compression. The right side of this specimen is also reasonably preserved, but the squamosal is slightly separated from the petrosal, and the petrosal is displaced dorsomedially against the basioccipital and, so, does not articulate correctly with the basisphenoid anteriorly, being slightly dorsal to it (Fig. 31B). On MHNC 8264, the lateral side of the left promontorium has been severely distorted in the region of the fenestra vestibuli by the articular condyle of the left dentary, but the lateral region of the tympanic cavity is still quite informative (Fig. 29B). On the right side of the specimen, in contrast, the promontorium is well-preserved but lateral part of the bone in the region of the epitympanic recess and fossa incudis is damaged (Fig. 29A). Therefore, the description below will essentially refer to the left side of MHNC 8308 but will be complemented, when necessary, with the well-preserved parts of the other auditory regions. In other respect, because the petrosal shares structures with most of its surrounding bone, for a better understanding of the whole auditory region, its description will refer to these structures as such and, therefore, will have to consider these other bones in spite of some redundancy with parts of the description above.

Tympanic view. (Figs 28-31; 36A) The petrosal of *Andinodelphys* is tightly articulated to the surrounding bones (squamosal, basisphenoid, basioccipital, exoccipital). No vacuity is observed in the auditory region except the large foramen ovale in the anterolateral region of the petrosal. This foramen is an oval-shaped to triangular vacuity limited posteriorly by the anterolateral region of the petrosal (see below) and anteriorly by the alisphenoid (see above). This vacuity presents on its anteromedial edge at the anteroposterior level of the basisphenoid-basioccipital suture, a small diverticulum (in fact an opened foramen), partly separated from the foramen ovale. This foramen is for the passage of the greater petrosal nerve (which exits the petrosal from the hiatus Fallopii on the dorsal face of the bone) on its way to the posterior opening of the pterygoid canal (Wible 2003). On the lateral side of the foramen ovale, the medial process of the squamosal may also provide a very small contribution to the foramen (see above).

The petrosal is composed of two major divisions, the pars cochlearis, which consists of the promontorium and the pars canalicularis consisting of the rest of the petrosal. The pars cochlearis houses the cochlear duct and saccule of the inner ear, and the pars canalicularis houses the semicircular

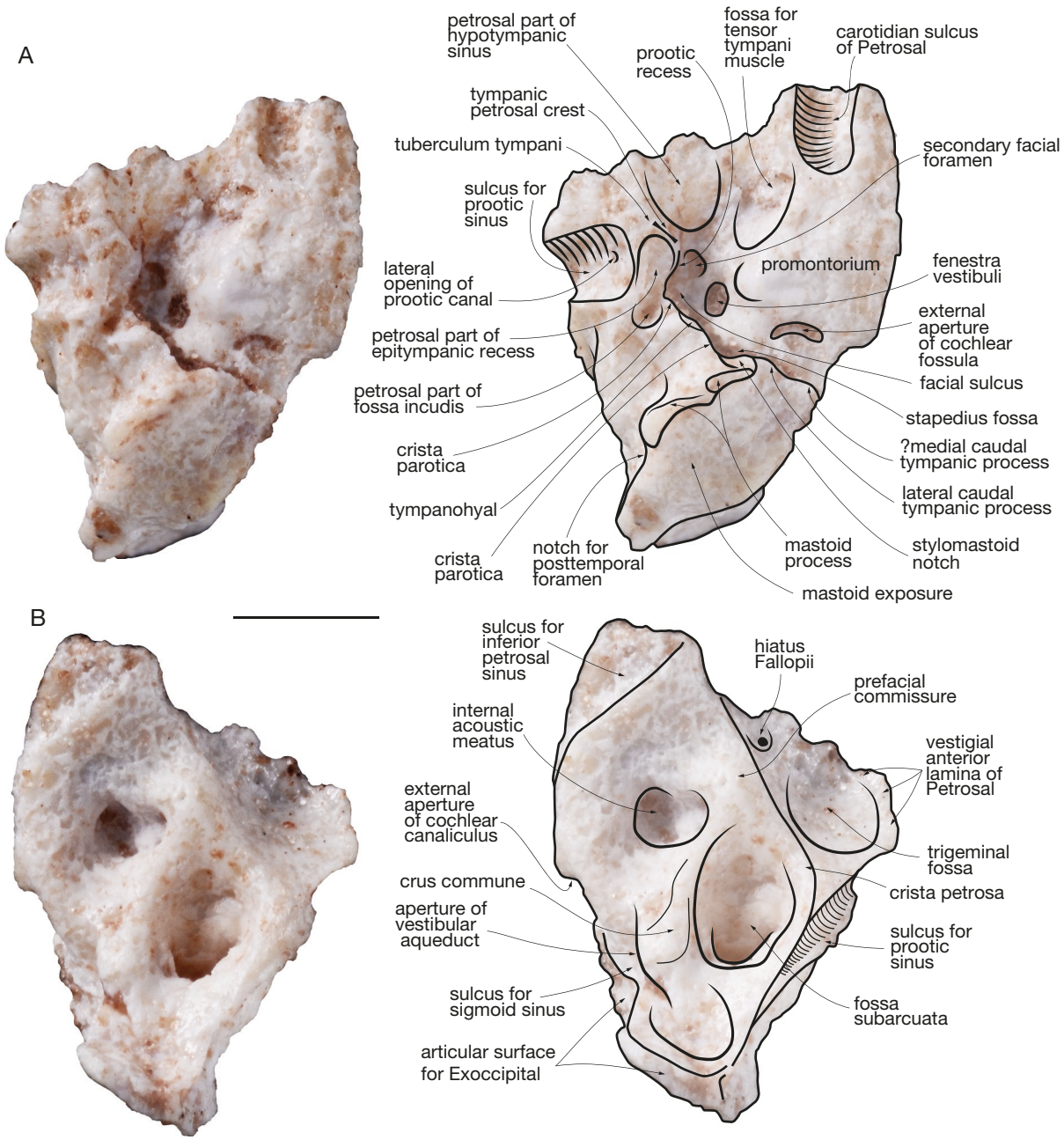

FIG. 36. — Right petrosal of *Andinodelphys cochabambensis* (MHNC 13933): **A**, tympanic view; **B**, cerebellar (dorsal) view. Scale bar: 2 mm.

canals and utricle. The pyriform promontorium is inflated posteriorly. It is oriented anteromedially-posterolaterally, and its ventral surface slopes anterolaterally. Its apex is excavated by a deep sulcus for the internal carotid artery on its way to the carotid foramen. This sulcus is roughly parallel to the petrosal-basioccipital suture. It extends anteriorly on the basisphenoid as the sulcus posterior to the carotid foramen (see above). This sulcus is present in *Pucadelphys, Allqokirus,* and *Mayulestes*. It is also present in several other sparassodonts (e.g., *Notogale*, *Sallacyon, Sipalocyon*, *Cladosictis, Prothylacinus, Borhyaena, Paraborhyaena, Arctodictis*). It is also present in several Petrosal types (Type I, II, III, and VI) from the early Eocene of Itaboraí (Ladevèze & Muizon 2010) and the so-called Gurlin Tsav Skull from the Late Cretaceous of Mongolia as scored by Rougier *et al.* (2015). It is apparently absent in all other metatherians. The promontorium fenestrae (fenestra vestibuli and external opening of the cochlear fossula), as preserved, are poorly developed. The fenestra vestibuli opens almost laterally. On the left side of MHNC 8308, it is at the anteroposterior level of the fossa incudis. It is roughly oval-shaped as preserved. However, this morphology may have been altered by the post-mortem distortion of the specimens, which makes inaccurate the measurement of the stapedial ratio (Ladevèze & Muizon 2007). The external opening of the cochlear fossula is posterolaterally oriented, facing the mastoid process. Its morphology has probably

also been altered by distortion. The promontorium does not present a well-developed rostral tympanic process in contrast to the condition observed in the Recent didelphids, but resembles *Pucadelphys* in this respect. However, as mentioned by Ladevèze & Muizon (2007) a distinct swelling is present ventral to the external opening of the cochlear fossula in the same place as the rostral process of Recent didelphids. It may represent an incipient development of a rostral process in *Andinodelphys*. A similar condition is observed in *Allqokirus* and *Mayulestes,* although more developed in this latter taxon. The portion of the petrosal lateral to the promontorium is a wide area extending from the posterior edge of the foramen ovale to the mastoid process. This region houses the hypotympanic sinus (*sensu* Klaauw 1931 and Archer 1976a), the facial nerve, the auditory ossicles, and the stapedial muscle. The anterior region of this area is as wide as the anterior aspect of the promontorium. Anteriorly, on the posterolateral edge of the foramen ovale, the hypotympanic sinus is a small cupula described above in the squamosal section (Fig. 28: blue dotted circle). It is roughly circular and composed of the petrosal posteromedially and the squamosal anterolaterally with a variable participation of the alisphenoid. A distinct hypotympanic sinus is absent in *Pucadelphys* but it is present in *Mayulestes* and *Allqokirus*.

The posterolateral edge of the hypotympanic sinus is formed by a robust but short, rounded ridge (Fig. 36A). This ridge is oblique being oriented anterolaterally-posteromedially. The anteromedial face of this ridge is strongly concave and forms part of the hypotympanic sinus. The posterolateral face is also concave and forms the anteromedial limit of the epitympanic recess (see below). The lateral extremity of the ridge is just medial to the postglenoid foramen and its medial extremity is lateral to the secondary facial foramen (see below) (Figs 28, 30). Following Archer (1976a), Muizon (1998) called a similar ridge in *Mayulestes* the petrosal crest. However, because this term could be confused with the crista petrosa a structure of the dorsal aspect of the petrosal (Fig. 36B), Ladevèze & Muizon (2010) proposed the term tympanic petrosal crest for this structure. A similar short and rounded tympanic petrosal crest is present in *Pucadelphys* and *Mayulestes*. It is also present, but much sharper, in most sparassodonts (e.g. *Notogale, Sipalocyon*), in didelphids, and in dasyurids. In Recent didelphids, the lateral extremity of the tympanic petrosal crest is greatly enlarged and forms a prominent spur-like process, the tuberculum tympani (Wible 2003), which projects ventrally and abuts against the medial edge of the postglenoid foramen. According to Toeplitz (1920), the tuberculum tympani could be regarded as homologous to the tegmen tympani of eutherians (see also Wible 2003), a statement that could perhaps be extended to the whole tympanic petrosal crest. In *Andinodelphys*, the lateral edge of the petrosal tympanic crest forms a small knob-like tuberculum tympani, which is barely more salient than the medial edge. A similar condition is observed in *Pucadelphys, Allqokirus,* and *Mayulestes*. In contrast, the tuberculum tympani is large and spur-like also in several other sparassodonts such as *Notogale* and *Sipalocyon* (Muizon *et al.* 2018: 369, supplementary data, files 6 and 7). It is noteworthy that the spur-like tympanohyal identified by Forasiepi *et al.* (2019: fig. 20A) in *Sipalocyon* is in fact the tuberculum tympani; the tympanohyal is located on the crista parotica, posteromedially to the fossa incudis, as in observed, for instance, in didelphids (Wible 1990, 2003) and *Allqokirus* (Muizon *et al.* 2018: fig. 24A); see also Fig. 36A. The medial edge of the tympanic petrosal crest of *Andinodelphys* is conspicuously ventral to the facial sulcus and is excavated by a deep recess, which is regarded here as probably homologous to the lateral trough of the non-therian mammals (Fig. 36A). This recess has been formally termed the prootic recess by Muizon *et al.* (2018: 406 and fig. 24A). In this trough is the tympanic aperture of the prootic canal (see below). A deep prootic recess is also present in *Pucadelphys* (Marshall & Muizon 1995), and *Allqokirus* (Muizon *et al.* 2018).

Bordering the posterior rim of the foramen ovale, between the carotid sulcus medially and the hypotympanic sinus laterally, is an elongated shallow fossa for the origin of the tensor tympani muscle. It is oriented roughly in an anteromedial-posterolateral direction. On the posterior border of this fossa is a marked pit, which is likely to be also part of the origin of the tensor tympani muscle. This pit is present on all the petrosals known and is therefore unlikely to be the result of distortion. As usual in therians, this fossa is on the lateral edge of the anterior region of the promontorium, but extends laterally on the ventral aspect of what we interpret as the vestigial anterior lamina of the petrosal.

In *Andinodelphys*, the anterior lamina of the petrosal is a blade-like anterior extension of the bone, which forms a significant part of the posteroventral lateral wall of the braincase (Figs 36B; 37A; 38). Part of the anterior lamina is appressed against the internal side of the squamosal, posterior to the alisphenoid. In non-therian mammals, the anterior lamina forms part of the lateral wall of the braincase between the alisphenoid anteriorly and the squamosal posteriorly. It encloses the foramen for the mandibular branch (V3) of the trigeminal nerve and in some cases the maxillary branch (V2) (see Wible [1990]; Hopson & Rougier [1993], and Rougier & Wible [2006] for a review). The anterior lamina greatly reduces in metatherians and eutherians (Wible 1990: 200) and disappears in most extant taxa; the mandibular branch of the trigeminal nerve exits the skull either between the alisphenoid and the petrosal (foramen ovale of metatherians) or the foramen is totally enclosed in the alisphenoid (eutherians). However, in basal metatherians and eutherians, a vestigial anterior lamina is still present although the pattern of exit of the V3 is that discussed above. This anterior lamina is partly ventral (i.e. the posterior rim of the foramen ovale) and partly lateral, this portion being covered by the squamosal laterally. In dorsal view of the petrosal both ventral and lateral parts of the anterior lamina are clearly visible (Ladevèze & Muizon 2007) and form a deep basin which houses the trigeminal ganglion, the trigeminal fossa (Muizon *et al.* 2018) (Fig. 38). It is noteworthy that the trigeminal ganglion is also housed in the medial face of the anterior lamina of non-therian mammals. The structure designated here and elsewhere (Muizon *et al.* 2018) as trigeminal fossa is the petrosal contribution to the cavum

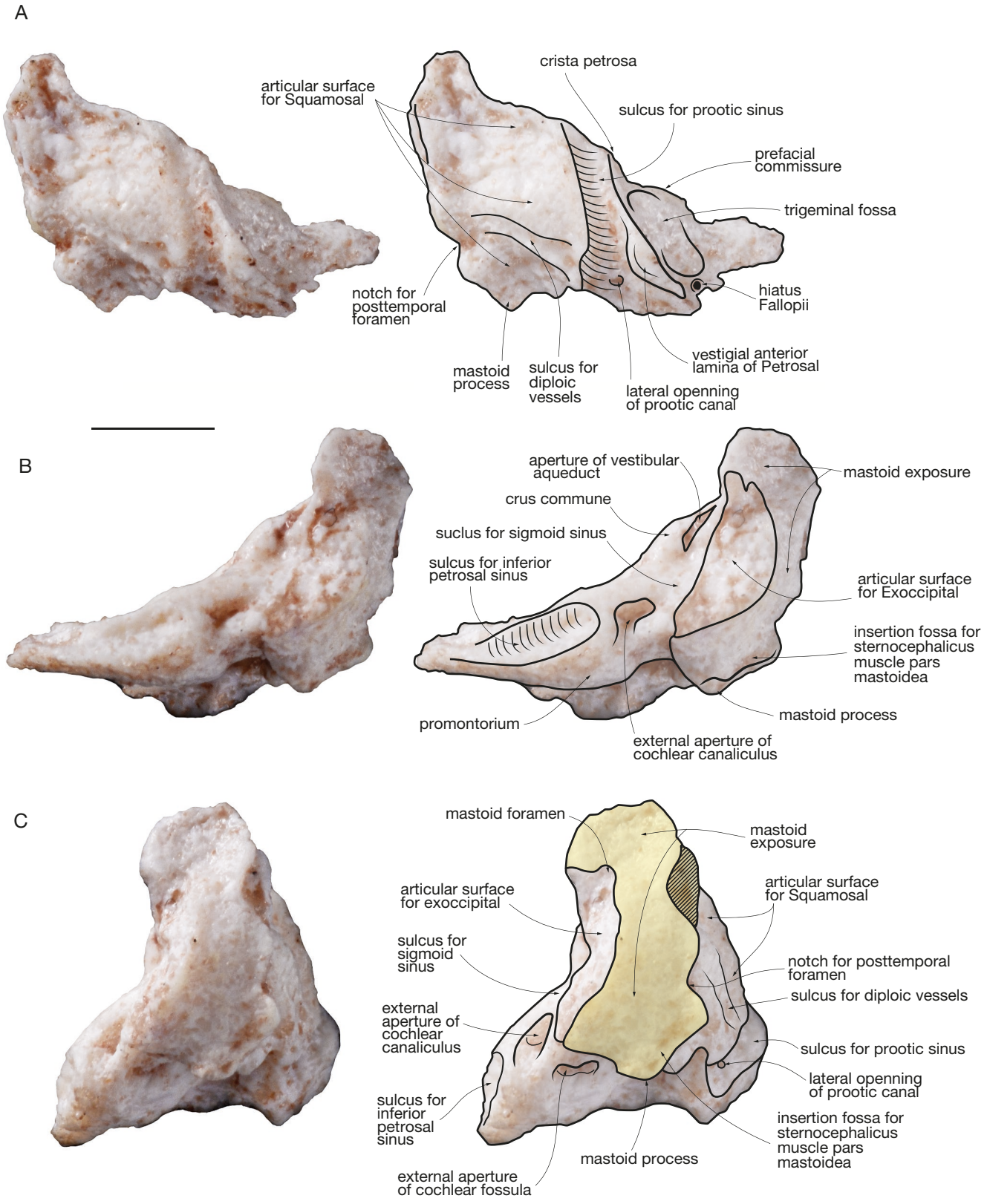

FIG. 37. — Right petrosal of *Andinodelphys cochabambensis* (MHNC 13933): **A**, squamosal view; **B**, medial view; **C**, occipital view. Yellow area indicates mastoid external exposure. Scale bar: 2 mm.

epiptericum (Wilson *et al.* 2016). A vestigial anterior lamina has been described in the metatherians *Pucadelphys* (Marshall & Muizon 1995), *Andinodelphys* (Ladevèze & Muizon 2007), and *Allqokirus* (Muizon *et al.* 2018), in some herpetotheriids (*Peratherium cuvieri*, *P. elegans* [very reduced], *Amphiperatherium minutum* [more expanded but in a juvenile individual],

see (Selva & Ladevèze 2017; Ladevèze *et al.* 2020). It has also been decribed in the eutherians *Alcidedorbignya* (Muizon *et al.* 2015), *Prokennalestes* (Wible *et al.* 2001), and in isolated "zhelestid" petrosals (Ekdale *et al.* 2004). This interpretation of the occurrence of a vestigial anterior lamina in metatherians confirms Wible's suggestions that "the anterior lamina … may not be totally absent in all marsupials" and that "a greatly reduced anterior lamina is a synapomorphy of marsupials and eutherians" (Wible 1990: 200 L and R). This vestigial anterior lamina of *Pucadelphys* and *Andinodelphys* is not exposed on the lateral wall of the braincase, as is the case, for instance, in *Vincelestes* (Hopson & Rougier 1993). In this genus, the anterior lamina separates the alisphenoid anteriorly and the squamosal posteriorly and the two bones have no contact. In therians, the anterior lamina has reduced and is overlapped laterally by the squamosal, which extends anteriorly, contacts the alisphenoid, and excludes internally the anterior lamina from the lateral wall of the braincase. A condition similar to that of *Pucadelphys* and *Andinodelphys* is also present in *Didelphodon* as observed on Supplementary fig. 8b of Wilson *et al.* (2016); see comment to character 168 in Appendix 3.

Rougier & Wible (2006: 277) have refuted the interpretation of a vestigial anterior lamina in *Pucadelphys*. In order to avoid duplication, we simply refer here to Marshall & Muizon (1995: 78-82) and Muizon *et al.* (2018: 408) for a discussion on the occurrence of an anterior lamina in *Pucadelphys* and *Allqokirus* respectively. Following these discussions, we persist in our interpretation of the structure described above, which houses the trigeminal ganglion in *Andinodelphys,* as a vestigial anterior lamina, and confirm our interpretation in *Pucadelphys* (Ladevèze & Muizon 2007) and *Allqokirus* (Muizon *et al.* 2018).

Posterior to the hypotympanic sinus and medial to the tympanic petrosal crest is the secondary facial foramen, which conveys the hyomandibular ramus of the facial nerve posteriorly. This foramen is distinctly anterolateral to the fenestra vestibuli. On the posterolateral edge of the tympanic petrosal crest is an elongated cavity located lateral to the fenestra vestibuli and separated from it by the facial sulcus. This cavity is the petrosal part of the epitympanic recess. It is bordered laterally by the squamosal, which forms its lateral half (see above), the petrosal-squamosal suture passing in the middle of the recess. On the posterior region of the epitympanic recess is a deep pit, the fossa incudis, which receives the crus breve of the incus. The epitympanic recess is the cavity, which receives the articulation between the incus and the malleus. Because the epitympanic recess is posterior to the ventral petrosal crest, it is also posterior to the prootic canal, which pierces the crest dorsally. This condition is present in *Pucadelphys, Mayulestes*, *Allqokirus*, and all Recent didelphids. Therefore, the depression designated by Wible (1990: fig. 2F and fig. 4C) as the epitympanic recess, which is anterior to the ventral petrosal crest cannot be this structure. As a matter of fact, it is too anterior to the fenestra vestibuli to possibly receive the malleus-incus articulation. As stated by Muizon (1998), it is the posterior periotic portion of the hypotympanic sinus. Furthermore, the ventrally directed trihedron identified by Wible as the lateral wall of the epitympanic recess (Wible 1990: fig. 4C, lw) is the lateral extremity of the ventral petrosal crest, which separates the epitympanic recess posteriorly from the hypotympanic sinus anteriorly. This trihedron corresponds to the tuberculum tympani, a term, which we retain here following Wible (2003). We prefer not to use the term "lateral wall of the epitympanic recess" because, strictly speaking, the lateral wall of the epitympanic recess, in early therians is formed by the squamosal. The epitympanic recess is a structure, which is carried by both the petrosal and the squamosal and what is generally called epitympanic recess on the petrosal is in fact the "petrosal part of the epitympanic recess". The same is true for the fossa incudis.

The medial edge of the epitympanic recess is a thin crest, which almost reaches the level of the facial sulcus dorsally: it is the crista parotica. In the posterior region of the epitympanic recess and medial to the fossa incudis, the crista parotica extends ventrally and slightly thickens. In this area, it contacts the posttympanic process of the squamosal and is fused to the tympanohyal. The tympanohyal is an ossification of Reichert's cartilage, which fuses to the petrosal at the crista parotica. This is why it is considered that the crista parotica also extends posterior to the tympanohyal (MacPhee 1981; Wible 2008, 2012). The portion of the crista parotica posterior to the tympanohyal is short and forms the lateral edge of the stylomastoid notch. The latter forms a saddle-shaped sulcus for the exit of the facial nerve from the middle ear on the anteromedial edge of the mastoid process. The latter is moderately developed but distinct and forms a small elongated knob at the ventral extremity of the nuchal crest in the posterior region of the external acoustic meatus.

On the medial wall of the stylomastoid notch and extending posteromedioventrally from the mastoid process is a conspicuous caudal tympanic process. It is a relatively thick ridge, markedly convex anteriorly, which projects anteromedially towards the external aperture of the cochlear fossula. This process has been interpreted by Muizon *et al.* (2015: fig. 36, 38) as homologous to the lateral caudal tympanic process of early eutherians. Medially the lateral caudal tympanic process bears a faint saddle-shaped notch with a tiny tubercle medial to this notch (Figs 30; 36A). This tubercle is limited medially by the petrosal-exoccipital suture and is facing (but not adjoined to) another small tubercle on the exoccipital. This medial tubercle of the petrosal of *Andinodelphys* is in the position of a medial caudal tympanic process (= "tympanic process" of Wible *et al.* 2004, 2009) as is observed in early eutherians (Muizon *et al.* 2015). This tubercle could tentatively be interpreted as a small medial caudal tympanic process. This process is present on the three skulls of *Andinodelphys* (although weakly developed on MHNC 8264) that preserve a petrosal and, apparently, on the isolated petrosal MHNC 8371. We have observed this process and notch is some Recent didelphids (e.g. *Didelphis, Philander, Marmosa*). It is noteworthy however that the position of this possible medial tympanic process is unusual since in eutherians it generally faces the lateral caudal tympanic process and tympanohyal; furthermore, according to MacPhee (1981:

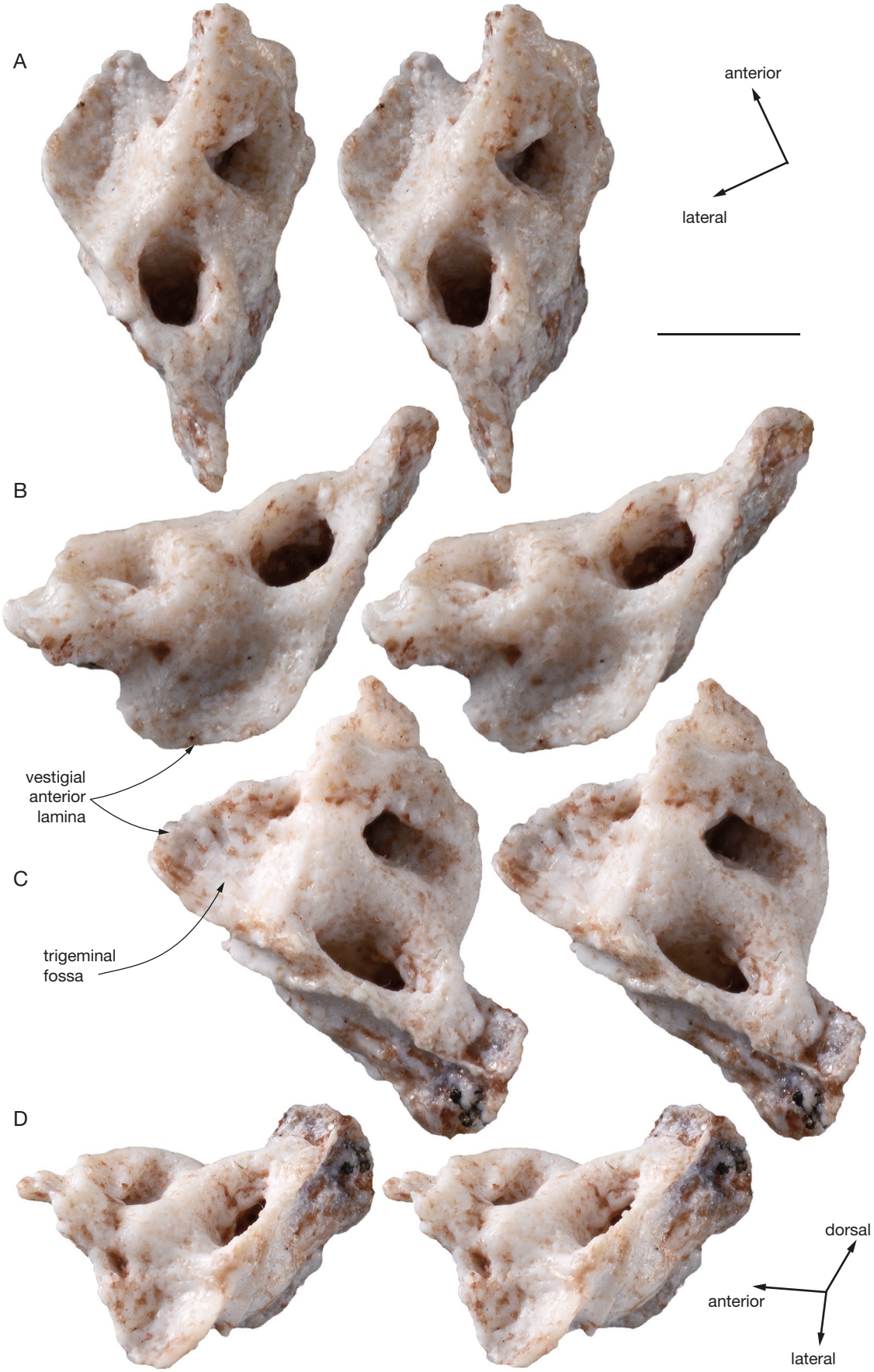

FIG. 38. — Cerebellar view (stereophotos) of the left petrosal of *Andinodelphys cochabambensis* showing the anterior lamina and the trigeminal fossa (= petrosal contribution to cavum epiptericum): **A**, MHNC 8370 in dorsal view; **B**, MHNC 8370 in dorsolateral view; **C**, MHNC 13847 in dorsal view; **D**, MHNC 13847 in dorsolateral view. For other anatomical features of the petrosal see figs 36 and 37. Scale bar: 2 mm.

17), the medial section of the caudal tympanic process arises from the the medial wall of the cochlear fossula, which may contradict our interpretation. Nevertheless, MacPhee's statement refers to eutherians and homologies with the condition in metatherians are not easy to establish. Be that as it may, this possible medial tympanic process forms the medial part of the caudal tympanic process and is clearly approximated to the medial wall of the cochlear fossula. The notch between the medial and lateral caudal tympanic processes has been interpreted by Muizon *et al.* (2015) as a possible passage for the posterior ramus of the stapedial artery in the pantodont *Alcidedorbignya inopinata*. This could not be the case of *Andinodelphys* because the stapedial artery is lost in adult marsupials and we hypothesize that it was also lost in the Bolivian genus. The notch between the medial and lateral caudal tympanic processes has also been regarded as a possible passage for the auricular branch of the vagus nerve (X) toward the facial nerve (VII). However, we have no indication on the condition of the passage of this nerve in Recent marsupials.

Dorsal and anterior to the caudal tympanic process is a deep fossa, which extends the facial sulcus posteromedially. It is the stapedius fossa for the origin of the stapedius muscle. The stapedius fossa is dorsal and posterolateral to the external aperture of the cochlear fossula. It strongly narrows medially and reaches a deep and elongated notch, through which it communicates with the jugular foramen (posterior lacerate foramen). This notch is the passage for the lateral head vein, which joins the inferior petrosal sinus to form the internal jugular vein (Ladevèze & Muizon 2007; Wible *et al.* 2009).

Occipital view. On the occiput, the petrosal presents a widely-exposed pars mastoidea (Figs 25; 37C). This exposure is dorsoventrally elongated and arched medially. It is wedged between the squamosal ventrolaterally, the interparietal dorsolaterally, the supraoccipital dorsally, and the exoccipital medially. A large slit-like posttemporal foramen is present at approximately mid-height of the lateral edge of the exposure. It is located in the suture between the squamosal and the pars mastoidea of the petrosal. This foramen is also present in *Pucadelphys* and in many extant didelphids but higher in the latter. The posttemporal foramen connects the vena and arteria diploëtica magna to the occipital vein and artery. The vena diploëtica magna is an offshoot of the sphenoparietal emissary vein, which supplies the occipital vein posteriorly. The arteria diploëtica magna is a branch of the occipital artery. In eutherians, it is connected to the ramus superior of the stapedial artery. Because this vessel is absent in adult marsupials, the arteria diploëtica magna is likely to be connected to the postglenoid artery (an offshoot of the external carotid artery) or (more likely) to the ramus temporalis (emitted by the postglenoid artery just dorsal to its entrance in the postglenoid foramen) before it exits the skull through the suprameatal foramen.

A single small mastoid foramen is present in the dorsal region of the mastoid exposure in the vicinity of the triple point petrosal-exoccipital-supraoccipital. In MHNC 8308 it is located in the middle of the dorsal region of the mastoid exposure, whereas in MHNC 8264, 13847, and 13933 it is located dorsally to or within the petrosal-exoccipital suture (Figs 25; 37C). On the ventrolateral angle of the mastoid exposure is the mastoid process, which extends dorsally along the petrosal-squamosal suture in a thick crest on the lateral edge of the exposure. The medial side of the exposure, on the petrosal-exoccipital suture, also forms an elevated crest, which abuts a similar crest on the exoccipital (Fig. 25). The salient ridge formed by the two bones is lateral to the dorsal occipital condyle and extends slightly dorsal to it. It is present in *Pucadelphys* and corresponds to what Marshall & Muizon (1995) designated the exoccipital process. No such elevated double crest is observed in the Recent didelphids. In *Mayulestes* and in *Allqokirus* the medial edge of the mastoid exposure of the petrosal presents a distinct elevated crest similar to the condition observed in *Andinodelphys* and *Pucadelphys*.

The posteromedial angle of the promontorium forms the anterior third of the edge of the jugular foramen. The foramen is large and distinctly more than three times larger than the external aperture of the cochlear fossula. On the medial edge of the promontorium is a deep anteroposterior sulcus for the inferior petrosal sinus (Ladevèze & Muizon 2007). This vessel merges posteriorly with the lateral head vein, which exits the facial sulcus medially reaching the lateral edge of the jugular foramen. The confluence of the two vessels forms the internal jugular vein, which exits the skull at the posteromedial angle of the petrosal.

Dorsal view. In dorsal view, the most conspicuous feature of the petrosal of *Andinodelphys* is the large trigeminal fossa which is excavated in the vestigial anterior lamina (see above). The trigeminal fossa is the petrosal contribution of the cavum epiptericum and receives during life, at least part of the trigeminal ganglion. On the specimens MHNC 8370 and 13847, the anterior lamina is completely preserved (Fig. 38), whereas on MHNC 13933, a small fragment of its anterolateral edge is missing (Fig. 36). A large trigeminal fossa is also present in *Didelphodon*, a structure designated as "petrosal contribution of the cavum epiptericum" by Wilson *et al.* (2016: supplementary figure 8). The presence of a large trigeminal fossa in *Didelphodon* suggest that a reduced anterior lamina was also present in this taxon (see comment on character 168 in character list below; Appendix 3). The rest of the anatomy of the cerebellar view of the petrosal of *Andinodelphys* has been abundantly described by Ladevèze & Muizon (2007) on the basis of MHNC 8370. The new petrosal of MHNC 13847 does not provide significant additional data, but is illustrated on Fig. 36B. We therefore refer to Ladevèze & Muizon (2007) for the description of the dorsal view of the petrosal.

Lateral view. The lateral view of the petrosal is covered by the squamosal and forms the petrosal-squamosal suture. In this area, a major characteristic is the presence of a large dorsoventrally oriented groove, the sulcus for the prootic sinus (Figs 37A; 39). It is located in the anterior region of the

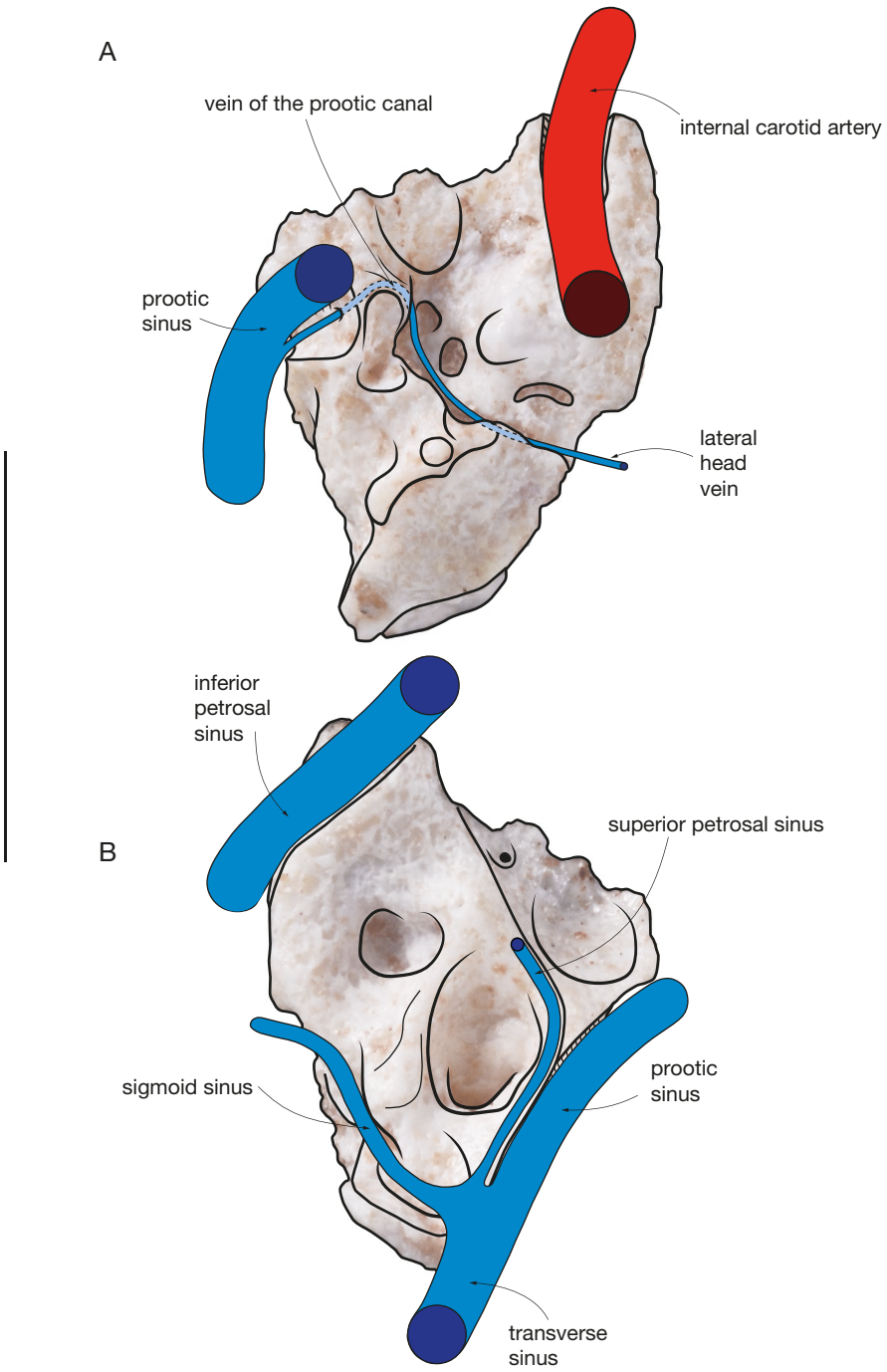

FIG. 39. — Reconstruction of the major vessels of the auditory region of *Andinodelphys cochabambensis*: **A**, tympanic view; **B**, cerebellar (dorsal) view. Scale bar: 5 mm.

suture, just posterior to the posterior edge of the trigeminal fossa. The sulcus is slightly concave posteriorly and widens ventrally. In its ventral end is a small foramen, which represents the lateral opening of the prootic canal, which runs in the substance of the petrosal above the petrosal tympanic crest and reaches the facial sulcus medially. The prootic canal conveys the prootic canal vein, which becomes the lateral head vein in the facial sulcus, and merge to the inferior petrosal sinus at the posteromedial angle of the petrosal. In the ventral part of the sulcus for the prootic sinus, on its posterior edge, at the level of the lateral foramen of the prootic canal, is a small notch from which a faint groove extends posteriorly. This groove is twice narrower than the prootic sulcus and slightly sinuous. It is subhorizontal and ends posteriorly at the level of the notch for the posttemporal foramen (Fig. 37A). This sulcus likely represents the passage of the diploic vessels, the arteria diploëtica magna and vena diploëtica magna, which respectively enter and exit the skull via the posttemporal foramen from the occipital artery and to the occipital vein respectively.

TABLE 5. — Measurements of various semicircular canals aspects of the bony labyrinth of *Andinodelphys cochabambensis* (MHNC 8370), as compared to selected metatherians. For each semicircular canal (**ASC**, **PSC**, **LSC**), height (**H**), width (**W**) and diameter (**D**) were measured, as well as the angles between each other. The inner ear height (**IEH**) was measured after Billet *et al.* (2013). The radius of curvature for each semicircular canal was calculated following Spoor *et al.* (2007).

Collection number		H ASC	W ASC	R ASC	H PSC	W PSC	R PSC	H LSC	W LSC	R LSC	IEH	mean R SC/IEH	H ASC/H PSC	H ASC/H LSC	H PSC/H LSC	Angle ASC/PSC	Angle ASC/LSC	Angle PSC/LSC	D ASC	D ASC/IEH	D PSC	D PSC/IEH	D LSC	D LSC/IEH
Andinodelphys cochabambensis	MHNC 8370	1.53	1.68	0.91	1.47	1.3	1.13	1.02	1.3	0.78	3.78	0.25	1.04	1.5	1.44	88	71	90	0.21	0.05	0.22	0.06	0.26	0.07
Pucadelphys andinus	MHNC 8266	1.5	1.68	0.8	1.29	1.47	0.69	1.06	1.2	0.57	3.21	0.21	1.16	1.42	1.22	101.95	97.75	83.94	0.15	0.05	0.21	0.07	0.17	0.05
Allqokirus australis	MHNC 8267	2.01	2.43	0.83	1.8	1.6	1.12	1.26	1.54	0.82	4.75	0.19	1.12	1.6	1.43	82.57	84.69	85.19	0.2	0.04	0.18	0.04	0.2	0.04
Amphiperatherium minutum	MNHN-GY-682	1.5	1.4	0.73	1.19	1.09	0.57	0.97	1.09	0.52	3.33	0.18	1.26	1.55	1.23	93.98	87.06	87.02	0.17	0.05	0.17	0.05	0.17	0.05
Peratherium elegans	PAR 39.22	2.14	1.91	1.01	1.48	1.72	0.80	0.95	1.68	0.66	3.86	0.21	1.45	2.25	1.56	112.11	89.04	90.49	–	–	–	–	–	–
Peratherium cuvieri	MNHN-GY-679	2.18	2.31	1.12	1.75	1.9	0.91	1.23	1.57	0.7	4.07	0.22	1.25	1.77	1.42	105.72	109.07	98.94	0.1	0.02	0.22	0.05	0.11	0.03
Herpetotherium cf. *fugax*	ZMB 50672	1.34	1.39	0.68	0.94	1.12	0.52	0.68	0.99	0.42	2.43	0.22	1.43	1.97	1.38	87	91.87	94	0.1	0.04	0.12	0.05	0.11	0.05
Didelphis marsupialis	MNHN RH61	2.94	3.02	1.49	2.4	2.48	1.22	1.56	1.74	0.83	5.32	0.22	1.23	1.88	1.54	98.96	80.29	94.41	0.19	0.04	0.21	0.04	0.24	0.05
Marmosa murina	MHNH. ZM.MO.2001.2239	1.9	1.86	0.94	1.2	1.26	0.62	0.88	1.1	0.5	3.59	0.19	1.58	2.16	1.36	98.7	83.59	94.43	0.21	0.06	0.18	0.05	0.21	0.06
Caluromys philander	MNHN. ZM.MO.1987.234	2.66	2.53	1.3	1.77	1.96	0.93	1.55	1.87	0.86	5.2	0.2	1.5	1.72	1.14	93	88.28	88.74	0.11	0.02	0.2	0.04	0.15	0.03
Dromiciops gliroides	IEEUACH 2162	1.83	2	0.96	1.35	1.28	0.66	0.95	1.27	0.56	4.02	0.18	1.36	1.93	1.42	113.35	81.41	94.7	0.12	0.03	0.15	0.04	0.14	0.03
Caenolestes fuliginosus	MNHN. ZM.MO.1982.2587	1.82	1.73	0.89	1.53	1.28	0.7	0.95	1.25	0.55	3.85	0.19	1.19	1.92	1.61	93.17	86.87	99.8	0.19	0.05	0.15	0.04	0.17	0.04
Perameles nasuta	MNHN.ZM.AC. A12417	3.06	2.91	1.49	2.21	2.27	1.12	1.67	2.02	0.92	6.15	0.19	1.38	1.83	1.32	93.96	84.79	90.7	0.19	0.03	0.23	0.04	0.24	0.04
Phascogale tapoatafa	MNHN. ZM.MO.2007.18	2.18	2.3	1.12	1.85	1.73	0.9	1.65	1.92	0.89	4.78	0.2	1.18	1.32	1.12	94.86	78.45	78.55	0.15	0.03	0.13	0.03	0.14	0.03

Bony labyrinth endocast. (Fig. 40). The bony labyrinth of the inner ear consists of a set of interconnected spaces within the petrosal bone. It contained in life the perilymph, in which the membranous labyrinth was suspended. The inferior part of the membranous labyrinth includes the cochlear duct, containing the spiral organ of hearing, and the saccule of the vestibule, housing receptors sensitive to linear motion. The superior part of the membranous labyrinth is involved in detecting rotational movement of the head. It includes the utricle of the vestibule, the semicircular ducts and ampullae, and the common crus between the anterior and posterior ducts. The bony semicircular and cochlear canals of the bony labyrinth are usually considered as closely following the path and shape of the inner membranous ducts (e.g., Blanks *et al.* 1975; Spoor 2003; David *et al.* 2010).

The general aspect of the bony labyrinth of *Andinodelphys* is quite similar to that reconstructed for *Pucadelphys* (Ladevèze *et al.* 2020), and the recently published sparassodont *Allqokirus* (Muizon *et al.* 2018).

The complete turns of the cochlea of the bony labyrinth of *Andinodelphys* are difficult to calculate because the segmentation of this part was difficult and the resulting 3D rendering is incomplete, but they were likely approaching those observed in *Pucadelphys* (approximately 1.8 turns).

The semicircular canals of the bony labyrinth of *Andinodelphys* are very similar in shape and diameter than those observed in *Pucadelphys* and *Allqokirus*. The anterior semicircular canal (PSC) has the widest area (explained by the radius of curvature), followed by the anterior semicircular canal (ASC°, and then the lateral (LSC) (Fig. 40; Table 5). The same is observed in *Allqokirus*, but in *Pucadelphys* the ASC exhibits the widest area. The LSC plan is perpendicular or approaching perpendicular to the plans of the two other canals (71° to ASC and 90° to PSC). The plans of the PSC and ASC also form a perpendicular angle (88°). Both these canals meet at the crus commune. The LSC and PSC meet at the second crus commune.

The vestibule, the central area of the bony labyrinth, is located between the cochlea anteriorly and the semicircular canals posteriorly. The vestibule of *Andinodelphys* is small and exhibits three ampullae located at the junction between it and the canals. The spherical and elliptical recesses of the vestibule are distinguished by a constriction of the vestibule lateral to the fenestra vestibuli: the swelling of the spherical recess (for the saccule) is visible in anterior view of the labyrinth and the elliptical recess (for the utricle and semicircular ducts) is bowed slightly medially to it (Fig. 40).

The anterior ampulla is dorsolateral to the vestibule and connects the ASC to the vestibule. The lateral ampulla is ventrolateral to the vestibule and connects the LSC to the vestibule. The posterior ampulla is ventromedial to the vestibule and connects the crus commune to the vestibule.

Basioccipital and exoccipital (Figs 25, 28-31)

The basioccipital is well preserved on MHNC 8308, while it is slightly sunk on MHNC 8264 relative to the presphenoid as a result of some post-mortem distortion. It is regularly hexagonal. Its anterior suture with the presphenoid is relatively straight and transverse. The anterolateral sutures with the petrosals are oblique, being oriented anteromedially-posterolaterally. The posterolateral sutures are almost symmetrical to the anterolateral and are for the exoccipitals. They extend form the posterior region of the medial edge of the promontorium to the ventrolateral edge of the foramen

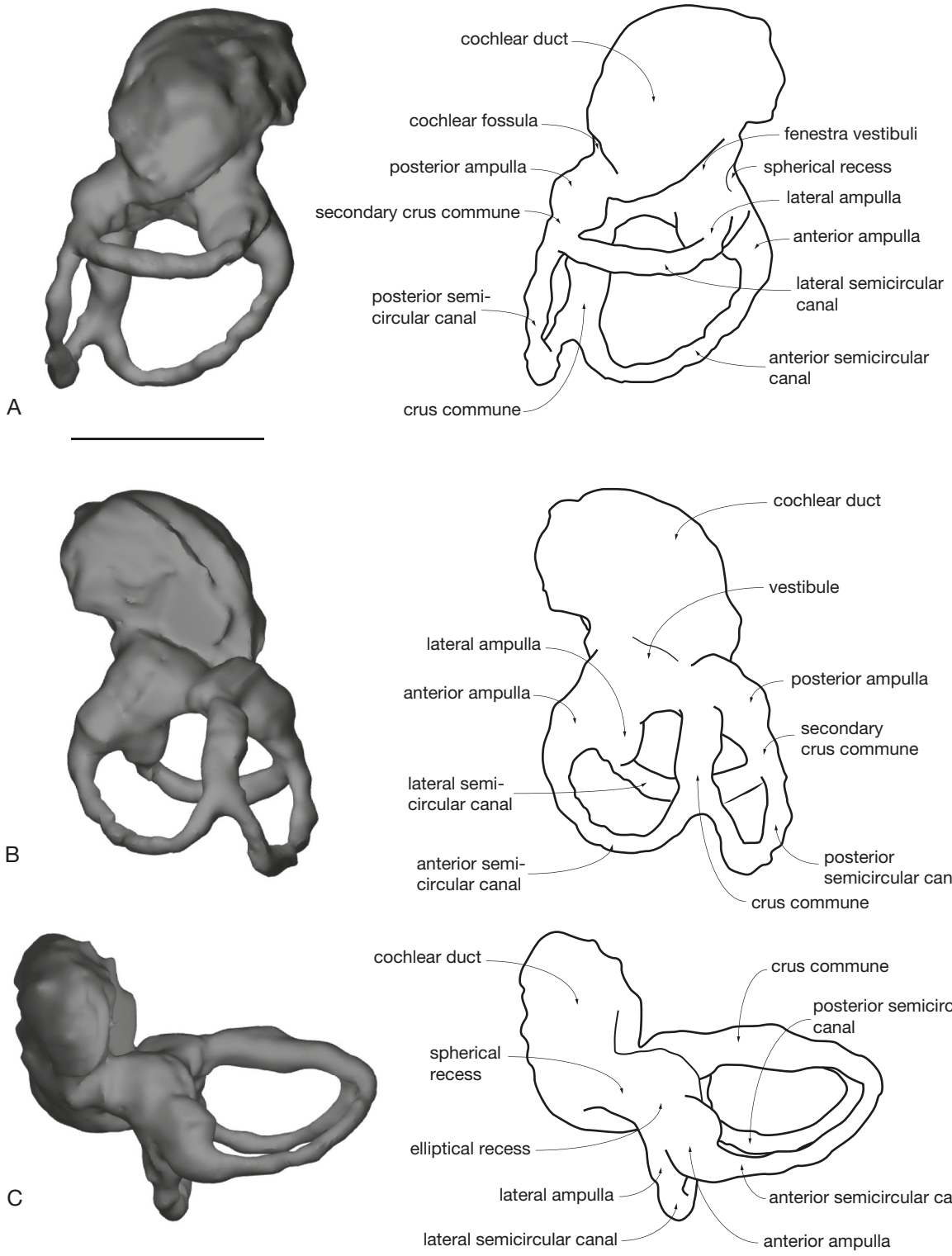

Fig. 40. — *Andinodelphys cochabambensis* (MHNC 8370), digital rendering of the left bony labyrinth of the inner ear: **A**, tympanic view; **B**, dorsal view and **C**, lateral view. Scale bar: 2 mm.

magnum, where they cross the ventral occipital condyles. The basioccipital-exoccipital sutures are distinct and the basioccipital is not fully fused to the exoccipital on MHNC 8308 and 8264. In contrast, on MHNC 8370 the suture is totally obliterated. The anterolateral edge of the basioccipital is closely appressed against the medial edge of the petrosal and closes the groove (on the petrosal) for the inferior petrosal sinus medially and ventrally. On MHNC 8370, on the dorsal face of the basioccipital, the groove for the inferior petrosal sinus is well-marked and slightly concave laterally (Fig. 17E).

The canal for the inferior petrosal sinus opens posteriorly at the level of the posterior edge of the promontorium, just anterior to the jugular foramen and is fully separated from it. The posterior opening of the canal, the foramen for the inferior petrosal sinus, is well posterior to the basioccipital-exoccipital suture and is formed dorsolaterally (*c.* one third) by the petrosal and ventromedially (*c.* two thirds) by the exoccipital. The jugular foramen is much larger than the foramen for the inferior petrosal sinus. It is limited anterolaterally by the posteromedial angle of the promontorium (*c.* one third) and posteromedially (*c.* two thirds) by the exoccipital. It is distinctly larger than the external aperture of the cochlear fossula. The jugular foramen transmits nerves IX, X, and XI and "occasionally conducts very small branch of sigmoid sinus of transverse venous system to internal jugular vein" (Archer 1976a: 221).

On MHNC 8308, at the lateral end of the left basioccipital-exoccipital suture is a triangular opening located at the basioccipital-exoccipital-petrosal triple point (Fig. 30). This fenestra opens dorsally in the canal for the inferior petrosal sinus. It is present on both sides of the specimen. It was probably present on the right side of MHNC 8264 but it is not observed on the left side because of the preservation of the specimen. It was probably present also in MHNC 8370, as distinct notches are observed on the anterolateral edges of the basioccipital of this specimen (Fig. 17D). A similar condition may be present in four specimens of *Pucadelphys* (MHNC 8377, 8378, 8379, 8380), but it is apparently absent in other specimens (MHNC 8266, 8376, 8381). We have not observed this foramen in other metatherians, fossil or extant. In *Andinodelphys* we hypothesize that it may have permitted exit of a branch of the inferior petrosal sinus. The latter would have had two branches exiting the skull, the posterior one forming the internal jugular vein with the sigmoid sinus, and the anterior one joining the vertebral vein. This possible interpretation is based on comparison with the condition in the dog (Evans & de Lahunta 2013).

The ventral surface of the basioccipital bears an elevated medial keel, which extends from the middle of the intercondylar fossa to the anterior suture with the basisphenoid. The lateral edge of the basioccipital bears a conspicuous cylindrical elevation, parallel to the medial edge of the petrosal, which corresponds to the floor of the canal of the inferior petrosal sinus. Between the median keel and the lateral elevation is a deep fossa for the rectus capitis muscle.

On the ventral side of the exoccipital posteromedial to the basioccipital-exoccipital suture, posterolateral to the jugular foramen and anteromedial to the dorsal occipital condyle, are two well-developed hypoglossal foramina. The posterior one is the smaller and is located close to the anteroventral edge of the dorsal occipital condyle. The anterior one is anterior to anteromedial to the other and is close to the basioccipital-exoccipital suture. It is one third (in MHNC 8264) to two times larger (in MHNC 8308) than the posterior one. In MHNC 8308 the anterior foramen is in fact a fossa, which receives two foramina a small anterior one and a larger posterior one. In MHNC 8370, three foramina are observed on the left side with one of them being placed very close to the medial edge of the jugular foramen. On the internal face of this exoccipital two foramina only are observed. The external condition of the right exoccipital of MHNC 8370 is very similar to that observed in some specimens of *Pucadelphys* (MHNC 8380). Therefore, some variation exists in the number of hypoglossal foramina. A similar variation is also observed in *Pucadelphys,* as three foramina are observed in MHNC 8266, 8377, and 8380, while two are present in MHNC 8379, 8381, and 8382. In *Didelphis virginiana* and *Monodelphis domestica* (Wible 2003: 175) "these foramina transmit parts of the hypoglossal nerve and accompanying arteries and veins with the arteries ultimately being branches of the vertebral artery". The hypoglossal foramina may also transmit branches of the sigmoid sinus to the internal jugular vein (Archer 1976a: fig. 2B).

The posterior edge of the basioccipital forms the ventral border of the foramen magnum. It presents a deep U-shaped intercondylar fossa, bordered laterally by the ventral occipital condyles. These condyles extend posterolaterally on the posteromedial edge of the exoccipitals, and are therefore crossed by the basioccipital-exoccipital suture. The ventral occipital condyles are elongated and oval-shaped. They are oriented anteromedially-posterolaterally, and form the ventral edge of the foramen magnum, being separated by the intercondylar fossa. Posterodorsolateral to the ventral exoccipital condyles are the large dorsal exoccipital condyles, which form the lateral edges of the foramen magnum. They contact the ventral condyles ventrally and extend dorsally onto the occiput. They are sub-circular to roughly quadrate in posterolateral view, being approximately as long as wide in contrast to *Pucadelphys*, in which they are distinctly ovoid and elongate. They project posteriorly forming the posteriormost point of the skull. They bear the atlantal articular surface. In lateral view the anterior edge of this surface is distinctly concave. Dorsal to the dorsal occipital condyles, no conspicuous dorsal atlantal facets are observed as described by Marshall & Muizon (1995) in *Pucadelphys*.

In posterior view, the exoccipital encloses the foramen magnum, being separated dorsally by a short notch of the supraoccipital and ventrally by the narrow intercondylar notch of the basioccipital (Fig. 25). The foramen magnum carries the vertebral arteries into the skull, all or part of the sigmoid sinus to the vertebral sinus and cranial nerves, which are likely the spinal roots of the accessory nerves (Archer 1976a; Wible 2003). The dorsal suture with the supraoccipital is distinctly observed on the three specimens, which preserve the exoccipital. It is smoothly convex dorsally and extends laterally to the dorsal region of the mastoid exposure of the petrosal, but not to its top. There, the suture is with the petrosal and turns regularly ventrally. The whole lateral edge of the exoccipital forms a roughly semi-circular suture from its intersection with the dorsal edge of the foramen magnum to the ventralmost point on the lateral edge of the jugular foramen. There, the paroccipital process of the exoccipital is poorly developed

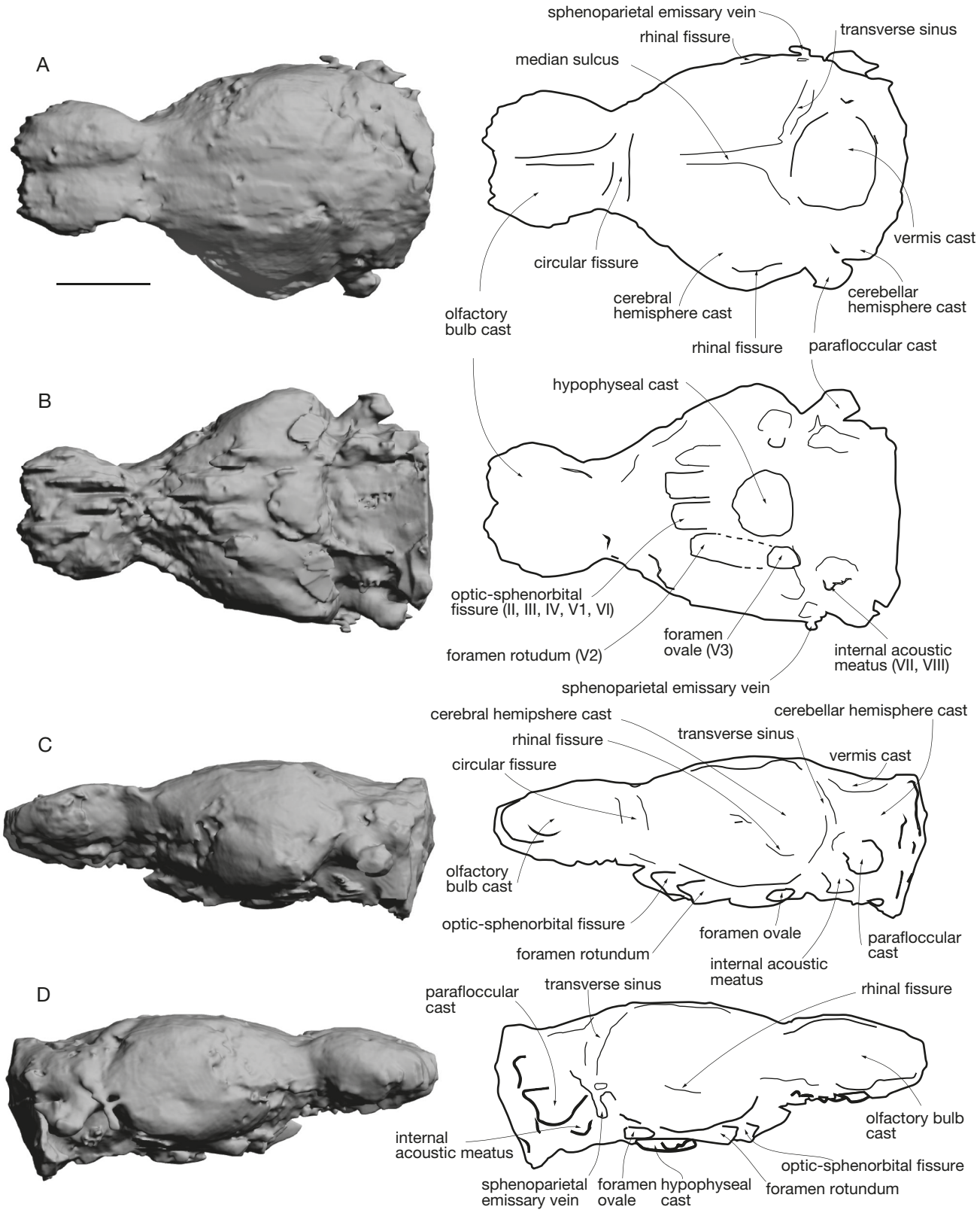

FIG. 41. — *Andinodelphys cochabambensis* (MHNC 8264): digital rendering of the cranial endocast; **A**, dorsal view; **B**, ventral view; **C**, left lateral view; **D**, right lateral view. Scale bar: 5 mm.

and forms a small knob on the posterolateral edge of the jugular foramen. Apparently, the petrosal does not bear a symmetrical tubercle appressed against the paroccipital process as is observed in *Pucadelphys*. As in this genus, the paroccipital process of *Andinodelphys* is separated from the dorsal occipital condyle by a distinct trough.

TABLE 6. — Endocast measurements for *Andinodelphys cochabambensis* (MHNC 8264) and Pucadelphys andinus (MHNC 8266).

	Andinodelphys cochabambensis	***Pucadelphys andinus***
Specimen number	MHNC 8264	MHNC 8266
Source	This study	This study and Macrini *et al.* (2007b)
Endocast flexure (°)	27	26
Endocast anteroposterior length (mm)	20.9	16.04
Endocast maximum width (mm)	12.3	9.32
Endocast maximim height (mm)	7.6	7.0
Cerebrum anteroposterior length (mm)	10.3	8.11
Cerebrum maximal width (mm)	12.3	9.06
Olfactory bulbs cast anteroposterior length (mm)	6.3	3.98
Olfactory bulbs cast maximum width (mm)	8.9	4.94
Olfactory bulbs cast maximum height (mm)	3.6	3.7
Cerebellum anteroposterior length (mm)	7.1	3.6
Cerebellum maximal width (mm)	12.1	6.6
Cerebellum maximal height (mm)	7.7	3.9
Hypophyseal fossa cast anteroposterior length (mm)	2.8	2.67
Hypophyseal fossa cast maximum width (mm)	3.1	2.95
Hypophyseal fossa cast maximum height (mm)	0.23	0.7
Total endocast volume (mm^3)	758.301	311.506
Olfactory bulb volume (mm^3)	91.61	36.41
Olfactory bulbs/endocast volume (%)	12%	11.7
Skull maximal length (mm)	48.9	32.28
Endocast length/skull length	43%	49%
Overall skull volume (mm^3)	2524.04	921,95
Endocast vol./Skull vol.	30%	34%

Supraoccipital (Fig. 25)

This bone occupies the central dorsal surface of the occiput between the nuchal crest dorsally and the exoccipitals ventrally. It forms the median region of the dorsal edge of the foramen magnum, where it is distinctly notched. Lateral to this notch, it has a dorsally convex suture with the exoccipital and laterally with the dorsal region of the mastoid exposure of the petrosal. Dorsally, it has a suture with the interparietal at the posterior base of the nuchal crest (the interparietal). The surface of the supraoccipital shield is smooth and no vertical ridge or crest is observed medially. Above the foramen magnum, medially the bone is flat and no bulge is observed as that present in *Monodelphis* for the vermis of the cerebellum (Wible 2003). A small foramen is present dorsomedially, between the supraoccipital and the interparietal, below the nuchal crest at its point of contact with the sagittal crest. A pair of small foramina is also present on the dorsolateral regions of the supraoccipital, as is observed in *Pucadelphys* (Marshall & Muizon 1995). These foramina are not clearly observed on MHNC 8370 and 13847, a condition which may be due to the distortion of the specimens.

Cranial endocast (Fig. 41)

Only one specimen (MHNC 8264) of our set of *Andinodelphys* skulls is well preserved enough to allow a poorly distorted digital reconstruction of the cranial endocast. Comparisons with Recent didelphids were possible thanks to published descriptions of metatherian brains (e.g., Owen 1837; Haight 1988; Macrini *et al.* 2007a). We also used the measurements of the proportions of endocranial casts of several Recent didelphids and australidelphian marsupials provided by Macrini *et al.* (2007b), (e.g., *Monodelphis domestica*, *Didelphis virginiana*, *Dasyurus hallucatus*, *Dromiciops gliroides*, *Vombatus ursinus*, *Phascolarctos cinereus*). Comparisons with fossil south american metatherians were limited to the description of the *Pucadelphys andinus* endocast (Macrini *et al.* 2007b).

The overall morphology of the cranial endocast of *Andinodelphys cochabambensis* (Fig. 41) is very similar to that of *Pucadelphys andinus* (Macrini *et al.* 2007b) and to the Recent didelphid marsupials *Monodelphis domestica* (Macrini *et al.* 2007a) and *Didelphis marsupialis* (Dom *et al.* 1970; Macrini *et al.* 2007a). It is elongate and narrow with large, spherical olfactory bulb casts on its anterior terminus (Fig. 41). In length, the braincase occupies almost half of the length of the skull, as it is the case in *Pucadelphys* (43 vs 49%). In lateral view, the endocast displays a flexure of 27° around the hypophyseal cast, which is very similar to the 26° flexure observed in *Pucadelphys* (Table 6). The width/length endocast aspect ratio is 0.59, the height/length ratio is 0.36, and the height/width ratio is 0.62. The endocast of the brain of *Andinodelphys* and *Pucadelphys* extend rather anteriorly, its anteriormost end reaching the orbit at the level of M3.

All the measurements and volumes are provided in Table 6 for *Andinodelphys* and *Pucadelphys*.

Olfactory bulbs. The olfactory bulb casts are elliptical and relatively large (Fig. 41), together composing about 12% of the total endocranial space. They are very similar to those of *Pucadelphys*, which represent 11.69% of the total endocranial space. The olfactory bulb casts of both *Andinodelphys* and *Pucadelphys* are relatively larger than those of the Recent marsupials for which this structure is published (see Macrini *et al.* 2007b for the compared taxa and measurements). However, they are quite similar in relative volume than those of *Didelphis virginiana* (approximately 11%). The olfactory bulb casts of both *Andinodelphys* and *Pucadelphys* are are much larger than in the other marsupials of comparison (*Monodelphis domestica*, *Dasyurus hallucatus*, *Dromiciops gliroides*, *Vombatus ursinus*, *Phascolarctos cinereus*) (Macrini *et al.* 2007b). The large relative size of the olfactory bulb casts in *Andinodelphys* and *Pucadelphys* suggests that these animals displayed a large endoturbinal area and an acute sense of olfaction, similar to that observed in Recent opossums (Rowe *et al.* 2005).

The olfactory bulb casts are separated from the rest of the endocranial cast by a well-developed circular fissure (*sensu* Loo 1930; Rowe 1996a, b; transverse fissure of Krause & Kielan-Jaworowska 1993), as in *Pucadelphys*. Such a deep and well-developed circular fissure is found in the extant marsupials considered here except for *Phascolarctos* (Macrini *et al.* 2007b).

On the ventral surface of the endocast, there is no trace of olfactory tracts from the bulbs to the telencephalon (Fig. 41).

Cerebrum and midbrain. Immediately posterior to the circular fissure, in dorsal view, are cast of the cerebral hemispheres. They are elongated and ovoid in shape. The surface of the cerebral hemispheres is smooth with no gyri and no sulci (= lissencephalic). The relatively small endocranial cavity of *Andinodelphys* suggests that the lissencephalic endocast had contained a lissencephalic brain because the latter was less likely to have been convoluted (see Edinger 1955; Tobias 1971; Holloway *et al.* 2004).

The two cerebral hemispheres are separated by the median or sagittal sinus, which is only slightly marked, as compared to the deep sinus observed on the endocast of *Pucadelphys* (Macrini *et al.* 2007b). In dorsal view, the two hemispheres are very similar to those of the endocast of *Pucadelphys*: they are triangular in shape and they do not expand much laterally, clearly less so than *Monodelphis*, in which they extend beyond the lateral extent of the paraflocular casts of the cerebellum. At their posterior end, the two cerebral hemispheres diverge from each other in the part anterior to the cast of the vermis. In lateral view (Fig. 41), the cerebral hemispheres are more elevated than the olfactory bulbs, and their ventral part is expanded in a piriform lobe, which does not protrude strongly ventrally.

The height/length aspect ratio of the cerebral hemisphere casts of *Andinodelphys* is 0.74, which is closer to the values obtained for *Monodelphis* (range 0.74-0.86) than that obtained for *Pucadelphys* (0.62). The width/length ratio of the cerebral hemisphere casts of *Andinodelphys* is 1.19, which is just between the ratios calculated for *Pucadelphys* (1.12) and *Monodelphis* (range 1.24-1.38; mean 1.29). The cerebral hemisphere cast length/total endocast length ratios are quite similar between *Andinodelphys* (0.49), *Pucadelphys* (0.51) and *Monodelphis* (range 0.42-0.50; mean 0.47).

The posterior portion of the rhinal fissure is visible on the lateral surface of the endocast, and is very similar to the rhinal fissure observed in *Didelphis virginiana* (Macrini *et al.* 2007a). However, a rhinal fissure is nowhere visible on the cerebral hemispheres of *Pucadelphys* (Macrini *et al.* 2007b). In *Monodelphis domestica*, the rhinal fissure is not visible on any of the endocasts, but it is clearly visible on dissected brains (Macrini *et al.* 2007a). The rhinal fissure marks the boundary between the isocortex (=neocortex) and the piriform lobe of the cerebrum (Jerison 1991).

Cerebellum. The midbrain of the endocast of *Andinodelphys* does not show dorsal exposure. It is the same in *Pucadelphys* and other marsupial endocasts used here as comparison. Lack of midbrain exposure in mammals can be explained by a cover by blood sinus, posterior expansion of the cerebral hemispheres, anterior expansion of the cerebellum, or any combination of these (Edinger 1964). It has been shown that the venous sinus system covers the midbrain in *Monodelphis*, *Didelphis*, *Dromiciops*, *Dasyurus*, and *Phascolarctos* (Macrini *et al.* 2007a), and the same can be assumed for *Andinodelphys*.

On the posterodorsal surface of the endocast, a large bulge, interpreted as the cast of the vermis of the cerebellum, covers the midbrain (Fig. 41). As in *Pucadelphys*, the vermis cast of *Andinodelphys* extends anterior to the casts of the paraflocculi. Cerebellar hemisphere casts are also visible on the endocast, but the imprints of the superior (dorsal) sagittal, transverse, and sigmoid sinuses are not visible. The paraflocular casts of the cerebellum are as prominent as those of the cerebellum of *Pucadelphys* and also *Didelphis*, *Monodelphis*, and *Phascolarctos*, but clearly less than those observed in *Dromiciops* and *Dasyurus* (Macrini *et al.* 2007a). The paired paraflocculi are a lateral extension of the cerebellum housed in the subarcuate fossa of the petrosal bone, and are involved with coordination, balance, and vestibular sensory acquisition.

At the ventro-central surface of the endocast of *Andinodelphys*, a conspicuous, circular, shallow hypophyseal cast contained in life the pituitary gland. It is very difficult to provide reliable measurements of the hypophyseal cast (especially its depth) but it is estimated as having a width/length aspect ratio of 1.11, as in *Pucadelphys*. Here, the hypophyseal fossa of *Andinodelphys* is quite small as compared to the values calculated for *Pucadelphys* (Macrini *et al.* 2007b), but its height may well be underestimated.

The pons and medulla oblongata are not visible on the ventral surface of *Andinodelphys*. They are not visible either on the endocasts of *Pucadelphys* and the extant marsupials of comparison. These structures may have been obscured by meninges of the brain and/ or blood sinuses.

Cranial nerves and blood vessels. Anterior to the hypophyseal cast are the paired casts of the canals that transmitted the maxillary branches of the trigeminal nerve (V2) (Fig. 41B). The paired canals for the V2 are more posterior and lateral to the hypophyseal cast in *Pucadelphys*. The right and left casts for the exit of the V2, the foramen rotundum, are widely separated from each other. The optic-sphenorbital fissure (optic-orbital foramen) is located anteromedial to the foramen rotundum and transmitted the cranial nerves II, III, IV, V1, VI, the ophthalmic artery, and a vein (Marshall & Muizon 1995). The right and left casts for the exit of these nerves in the endocast are close to each other but are not confluent. Posterolateral to the hypophyseal cast and anteromedial to the internal auditory meatus is the foramen ovale for the mandibular branch of the trigeminal nerve (V3). As in *Pucadelphys* and most metatherians (Wible 1990; Macrini *et al.* 2007b), the cavum epyptericum, the space at the level with the sphenoparietal fenestra which houses the trigeminal ganglion (V), is not confluent with the cavum supracochleare for the geniculate ganglion (VII). The cast of the internal auditory meatus for passage of cranial nerves VII and VIII is visible on the right side of the endocast.

On the dorsal and right lateral surface of the endocast (Fig. 41A, D), the pathway and ramification of the transverse sinus is well visible. The transverse sinus sulcus runs just between the cerebral hemisphere and the vermis and then divides into three branches: superior petrosal sinus, sigmoid sinus, and prootic sinus, the latter anastomoses with the sphenoparietal emissary vein, the cast of which is visible on the endocranial cast and exits the skull through the postglenoid foramen (Wible 1990, 2003).

Dentary (Figs 42, 43)

The corpus mandibularis is long and slender, and its anterior (symphyseal) extremity, tappers strongly dorsoventrally. In this respect, it clearly resembles, the condition observed in *Pucadelphys,* although slightly longer. The ventral margin of the dentary is slightly convex, and the deepest point of the bone is below m2-m3. It is less convex than in the extant didelphids *Didelphis* and *Caluromys*, in which the corpus is generally deeper, with the deepest point located more posteriorly, below m3-m4. The condition of *Andinodelphys* more resembles, in this respect, that of the extant *Metachirus, Monodelphis,* and *Marmosa*. The symphysis is unfused, and the development of salient crests and rugosities indicate a robust symphyseal ligament. Dorsal to the symphysis, between its dorsal border and the medial alveolar border of the canine, is a distinct anteroposteriorly elongated nutrient foramen (Figs 12B; 13B; 42B). Such a foramen is also present in *Pucadelphys, Mayulestes,* and *Allqokirus*, but slightly smaller and more anterior in these taxa. It is apparently absent in extant didelphids and most dasyuroids (except *Dasyurus* and *Pseudantechinus*). Furthermore, a conspicuous nutrient foramen is observed in the same position as in *Andinodelphys*, in *Deltatheridium, Lotheridium, Eodelphis, ?Protalphadon lulli* (Clemens 1966: fig. 58), and *Peratherium* spp. (MNHN.F.AU2370, QU8061.R, QU8062.R, QU8063.R, QU8214, QU13371). The symphysis extends posteriorly below the posterior root of p2, in contrast to the condition in *Pucadelphys*, *Mayulestes, Allqokirus, Deltatheridium*, and most extant didelphids, in which it does not extend further posteriorly than the anterior root of p2. In dasyuroids (e.g., *Dasyurus, Phascogale, Dasycercus, Sminthopsis, Sarcophilus*, and *Thylacinus*), the symphysis extends even more posteriorly than in *Andinodelphys*, as far as p3 or anterior root of m1.

The long axis of the symphysis lies at an angle of approximately 18° to the horizontal axis of the tooth row (the alveolar border) (Table 7). This condition is probably related to the length and anterior tapering of the rostrum of *Andinodelphys*. It contrasts with the shorter rostrum of *Pucadelphys* (*c.* 22.4° – not 40° as stated by Marshall & Muizon 1995) and especially of *Mayulestes* (29°) and *Allqokirus* (30°). Among extant didelphids, the condition of *Andinodelphys* resembles that of *Metachirus,* but differs from *Didelphis* and *Caluromys,* in which the symphysis is slightly less slanted.

There are three mental foramina. A small one below i3, a large one below p1, and another large one below m1 (usually below anterior root of m1). On the right mandible of MHNC 8308 there is another large foramen below p2. On the medial surface of the dentary, on the lower third of the mandibular body, is a wide and shallow groove, which extends from the anterior root of the angular process to almost the posterior angle of the mandibular symphysis. This structure represents the mylohyoid groove (Bensley 1902), which marks the course of a neurovascular bundle, which probably included the mylohyoid artery and nerve. In *Didelphis*, the mylohyoid groove receives, in its posterior part, below m3-4, and as far as the anterior root of the angular process, the mylohyoid muscle, which is involved in mastication and acts as an elevator of the tongue (Hiiemae & Jenkins 1969). Therefore, it is likely that the posterior part of the mylohyoid groove of *Andinodelphys* also received the insertion of the mylohyoid muscle. Posterior to the hypoconulid of m4 is a notable retromolar space, which is approximately 70% the length of m4.

On the ramus, the coronoid process is large but proportionally smaller than in *Didelphis,* shorter (proximodistally) than in *Caluromys,* and approaches the size observed in *Metachirus*. Its apex is wide and quadrate and extends posterodorsally. The dorsal half of the process is slightly (as compared to didelphids) recurved posteriorly, and the posterior edge of the coronoid process is short and markedly concave. The concave border resembles the condition generally observed in didelphids, but differs from the straight posterior border of the coronoid process in *Dasyurus*. The coronoid crest, which forms the anterior edge of the process is straight and thick, especially towards its base. Its ventral extremity extends on the lateral aspect of the body, but remains on its dorsal half and is posterior to the posterior root of m4. In this region, the coronoid crest is very salient laterally and may even be distinctly convex as in MHNC 8308. The masseteric fossa is remarkably deep, especially posteroventrally, in the region anteroventral to the condyloid process, and anteroventrally, posterior to the coronoid crest. In the posteroventral region of the masseteric fossa, the posterior shelf fossa is sub-horizontal and strongly projects laterally, being distinctly convex. The maximum lateral extension of this shelf is just ventral to the anteriormost point of the posterior edge of the coronoid process. The medial surface of the coronoid process is smooth and flat to slightly convex medially and bears no anterior crest.

In *Didelphis* (Turnbull 1970), the masseteric fossa receives the *temporalis (pars superficialis)* muscle in its dorsal and anterior region (on the coronoid crest); the rest of the fossa is occupied by the *zygomaticomandibularis* in its median region below the *temporalis* insertion and between the condyle and the anterior base of the coronoid process. The *masseter pars profunda* inserts in the ventral region of the masseteric fossa. The medial aspect of the coronoid process receives the insertion of the *temporalis pars profunda*. Muscle scars for the insertion of these muscles are difficult to observe in the six available specimens of mandibles of *Andinodelphys* (four individuals). However, given the similarity in the general morphology of the dentary of the two genera, we suspect that *Andinodelphys* had a pattern of the masticatory musculature similar to that of *Didelphis*.

Ventrally, the posterior crest of the coronoid process turns posteriorly and joins the articular condyle. In some specimens, the crest descends more ventral than the condyle before reaching it, as is observed in MHNC 8264, and form a distinct notch between the two processes (Fig. 42). This crest reaches the condylar process in its medial third and is approximately posterior to the m4 in the axis of the

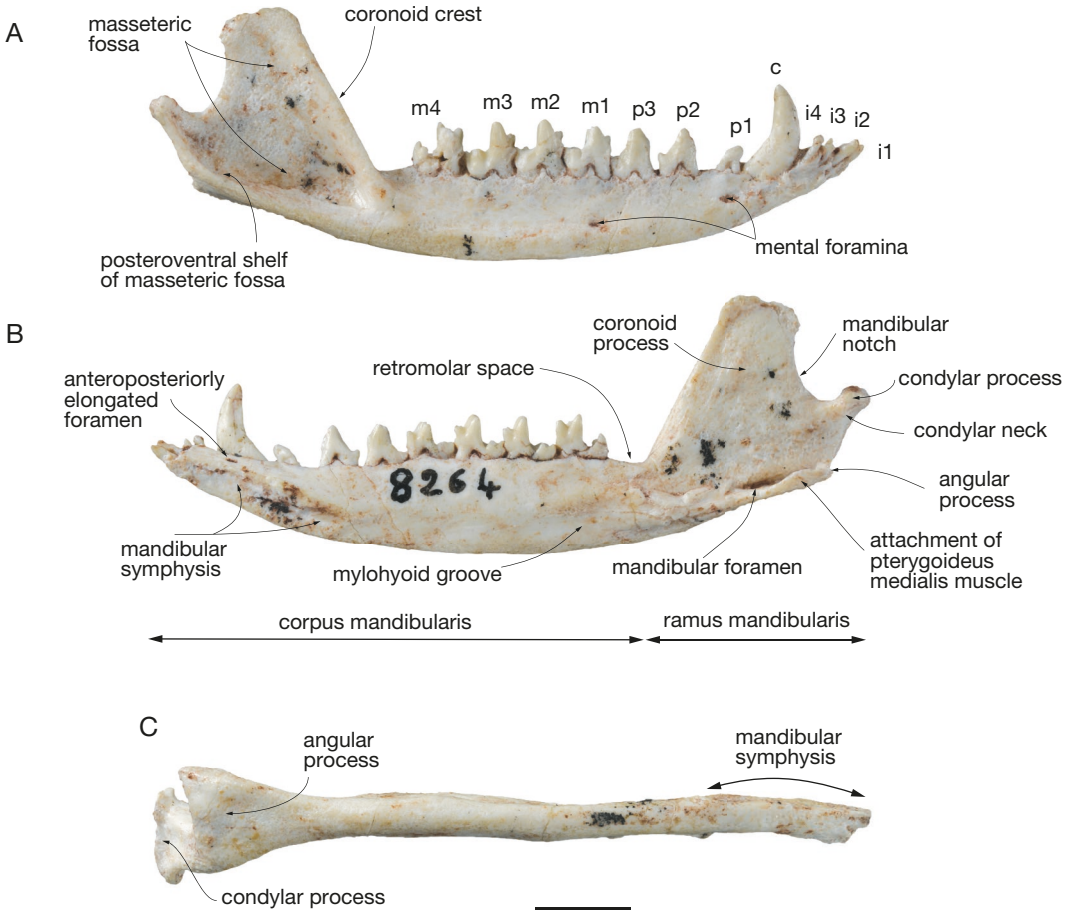

Fig. 42. — *Andinodelphys cochabambensis* (MHNC 8264): right dentary: **A**, lateral view; **B**, medial view; **C**, left dentary in ventral view. Scale bar: 5 mm.

Fig. 43. — *Andinodelphys cochabambensis* (MHNC 8308): left dentary: **A**, lateral view; **B**, medial view. Scale bar: 5 mm.

TABLE 7. — Comparative measurements of the symphyseal angle between the long axis of the symphysis and the horizontal axis of the tooth row in several fossil and extant metatherians.

Andinodelphys cochabambensis	MHNC	MHNC	MHNC	–	–	–	–	
specimens	8264	8308	8370					Mean
angle	17°	18°	19°	–	–	–	–	18°
Pucadelphys andinus	MHNC	MHNC	MHNC	MHNC	MHNC	MHNC	MHNC	
specimens	8266	8376	8377	8378	8380	8381	8382	Mean
angle	23°	23°	21°	22°	24°	24°	20°	22.4°
Mayulestes ferox MHNC 1249	29°	–	–	–	–	–	–	29°
Allqokirus australis MHNC 8267	30°	–	–	–	–	–	–	30°
Kokopellia juddi	OMNH	OMNH	–	–	–	–	–	
specimens	26361	34200						Mean
angle	21.5°	18.9°	–	–	–	–	–	20.2°
Protalphadon ?lulli UCMP 46882	18°	–	–	–	–	–	–	
Didelphis marsupialis	1932-3003	1900-581	2007-8	2007-7	–	–	–	
specimens								Mean
angle	23.5°	25.5°	27.3	26.4	–	–	–	25.7°
Monodelphis brevicaudata	MNHN-	MNHN-	MNHN-	–	–	–	–	
specimens	ZM-2004-317	ZM-MO-	ZM-MO-					
		2003-762	1967-330					Mean
angle	20.5°	22°	19°	–	–	–	–	20.5°
Metachirus nudicaudatus	CM uncat	RH81	MNHN-	–	MNHN-	–	–	
specimens			ZM-MO-		ZM-MO-			
			1985-1803		2001-1422			Mean
angle	18.5°	20.5°	17.5°	19.5°	18°	–	–	18.8°
Caluromys lanatus	MNHN-	MNHN-	MNHN-	MNHN-	–	–	–	
specimens	ZM-MO-	ZM-MO-	ZM-MO-	ZM-MO-				
	1992-2999	1929-651	1929-650	1929-652				Mean
angle	27°	27.5°	29.2°	32.2	–	–	–	29°
Dasyurus viverrinus	MNHN-ZM-	–	–	–	–	–	–	
specimen	AC-A.2627							
angle	28°	–	–	–	–	–	–	28°
Dasyurus maculatus	MNHN-	1865-32	–	–	–	–	–	
specimens	ZM-MO-							
	1994-2140							Mean
angle	39°	36°	–	–	–	–	–	37.5°

tooth row. Therefore, the lateral two thirds of the condyle are lateral to the tooth row and overhang the posteroventral region of the masseteric fossa. Only one third of the transverse length of the condyle is medial to the tooth row. The condyle is strongly elongated transversely and cylindrical. Its articular surface is posterodorsally oriented. In MHNC 8264 and 8306 its anteroposterior length is roughly constant, while in MHNC 8308 the condyle is transversely narrower and anteroposteriorly longer in its medial portion. The lateral part of the condyle is buttressed by the ascending posterior end of the posterior shelf of the masseteric fossa. On the posteromedial edge of the condylar process, just ventral to the point of junction between the coronoid and condylar processes, a robust ridge descends towards the posteromedial edge of the angular process. In lateral view, the articular surface of the condyle is located above the apex of the protoconid of m4, at a distance of approximately the height of the talonid of m4.

The angular process is shelf-like and inflected medially, as in most metatherians. It is triangular in ventral view and approximately twice as long as wide posteriorly. Its posterior edge is slightly concave and its medial angle is a short triangular process differing from the sharp, posteriorly-projecting spur-like process observed in didelphids and, to a greater extent, in dasyuroids. In *Didelphis*, the dorsal surface of the angular process receives the insertion of the internal pterygoid and its ventral aspect supports the superficial masseter (Hiiemae & Jenkins 1969). Sánchez-Villagra & Smith (1997) have established categories of the diversity of the angular process in marsupials based on the ratio of "angular process length to angular process shelf length". In *Andinodelphys* this ratio is 6.5/7.63 = 0.852 (MHNC 8308); 5.70 /6.39 = 0.892 (MHNC 8264); and 5.76/6.22 = 0.926 (MHNC 8370). The mean of the three specimens is *c.* 0.89, which places *Andinodelphys* in the "shelf-like" category (Ratio > 0.81). Slightly posterior to the point of departure of the angular process, on its lateral side, is a small mandibular foramen. It is circular to oval-shaped and extends posteriorly in a short sulcus on the lateral edge of the angular process, at its junction with the remaining part of the mandibular ramus. It is located ventral to the middle of the apex of the coronoid process.

COMPARISON AND DISCUSSION

In the following discussion, because *Andinodelphys* is morphologically very similar to *Pucadelphys,* concerning the characters that are identical in the two genera, we refer to discussion of *Pucadelphys* characters in Marshall & Muizon (1995), except when new discoveries, observations, or publications require further discussion on a given feature.

General cranial morphology

The general morphology of the skull of *Andinodelphys cochabambensis* is similar to that of *Pucadelphys andinus* from the same locality but significantly larger. The skull of *Andinodelphys* is approximately 35% longer (in absolute value) than that of *Pucadelphys* with a rostrum proportionally 24% longer. *Andinodelphys* approaches the size of *Mayulestes* and *Allqokirus* (although slightly smaller) and is among the largest known metatherian taxa of the Tiupampa fauna. Beside these size and skull proportion differences and a few cranial features discussed below, most of the cranial anatomy of *Andinodelphys* does not significantly depart from that of *Pucadelphys*. The comparative life reconstructions of *Andinodelphys* and *Pucadelphys* presented in Fig. 44 intent to bring to light overall resemblance existing between the two Tiupampan taxa.

Dental anatomy

The dental anatomy of *Andinodelphys* is also quite similar to that of *Pucadelphys*. Both genera have the same dental formula. In both genera, P3 is the highest tooth of the upper cheek tooth series, the protocone is massive and anteroposteriorly expanded, the centrocrista is slightly V-shaped, the stylar shelf is transversely narrower than half of the width of the molars (M1-3), the stylar cusps B and D are the largest of the stylar shelf, the metaconid is large, being conspicuously larger than the paraconid and barely smaller than the protoconid, and the paraconid and metaconid are adjoined at their bases. Dentally, except for its larger size, *Andinodelphys* differs from *Pucadelphys* in minor features such as the enlarged I1 and the smaller stylar cusp C. As in *Pucadelphys*, *Andinodelphys* differs from *Mayulestes* and *Allqokirus* in the following features: paracone and metacone well separated at their base (fused at their bases in the latter two); postmetacrista on upper molars (especially M3) not extended distolabially and not significantly more expanded than the mesiolabial angle of the tooth; angle between the paracone-metacone axis and the preparacrista on M4 not widely open and close to 90° (≥ to 130° in the latter two); metaconid on m3, twice as large in height and volume than the paraconid (subequal in size to smaller in the two latter), paraconid and metaconid adjoined at base (widely separated in the latter two); paracristid lacking a carnassial notch (conspicuous in the latter two); relatively straight labial edge of the protoconid in anterior view, (expanded labially at mid-height in the latter two).

Size and position of the I1

As is observed in didelphids, the I1 of *Andinodelphys* is larger and extends further ventrally than the other upper incisors, because a larger part of the root (as compared to other incisors) is external to the alveolus. Furthermore, I1 is separated from I2 by a small but distinct diastema, whereas the other incisors are not separated by diastemata. In anterior view, the crowns of the I1 converge one toward the other and are in contact medially, whereas their roots diverge dorsally. A similar condition is present in *Mayulestes*. In *Pucadelphys,* I1 is smaller than the other incisors and does not protrude ventrally more than the other incisors, as is observed in MHNC 8378, the only specimen that preserves all the upper incisors (Fig. 45). However, in this specimen the extra-alveolar portion of the root is proportionally larger than in the other incisors. Comparison with other fossil taxa is difficult because the premaxillae and incisors are almost never preserved. A similar condition, however, is present in *Didelphodon*, although in this taxon, both I1 "do not clearly angle each other or make contact with each other at their crown apices" (Wilson *et al.* 2016, supplementary notes: 56). Furthermore, in *Didelphodon* no diastema separates I1 and I2. As observed from the size and position of the upper incisors alveoli, the condition in the Gurlin Tsav skull resembles that of *Andinodelphys* in the larger size of the alveolus of I1 as compared to that of I2, but it differs in the probable absence of diastema. Apparently *Lotheridium*, a deltatheroidan from the Late Cretaceous of China, lacks an enlarged I1 (Bi *et al.* 2015). The I1 condition of *Andinodelphys* and didelphids is present in *Dromiciops* and in several dasyurids (e.g. *Barinya, Sminthopsis, Dasycercus, Phascogale*). In sparassodonts other than *Mayulestes* (in the latter the condition is similar to that of *Andinodelphys*) the I1 is not enlarged in the very few specimens preserving all the upper incisors (e.g., *Prothylacynus, Borhyaena, Cladosictis, Arctodictis*), as well as in thylacinids (e.g. *Thylacinus, Nimbacinus*). However, the condition in these taxa may be derived as possibly related to hypercarnivory.

Morphology of the M4.

As discussed in the description above, the M4 of *Andinodelphys* and *Pucadelphys* differs from that of *Mayulestes* and *Allqokirus* in the angle formed by the preparacrista and the centrocrista (or the paracone-metacone axis if the centrocrista is strongly V-shaped), which is close to *c.* 90°-100° in the former two genera and *c.* 130° in the latter two genera. The *Mayulestes* and *Allqokirus* condition is even more pronounced (approaching in some case 180°) in later sparassodonts, in which cristae can still be observed and have not been obliterated by the reduction of the M4 (Fig. 46). In sparassodonts, the opening of the angle is related to the labiolingual position of the metacone (more labial than in *Pucadelphys* and *Andinodelphys*) and to the length of the labial edge of the tooth (in the case of the M4 it is the posterolateral maxillary alveolar border), which on the M4 is not strictly speaking labial, but corresponds to the labial edge in anterior molars. Because of this lingual displacement of the metacone, the posterior edge of the protocone (i.e. from the posterolingual edge of the metacone to the lingual side of the protocone) is shortened, and is generally shorter than the labial edge of the tooth. The condition is reversed in *Andinodelphys* and

FIG. 44. — Life reconstructions of pucadelphyids: **A**, *Andinodelphys cochabambensis* (Charlène Letenneur); on the left is a complete animal (natural size) grasping on a branch and on the right, on the foreground, is a lateral view of the head (*c.* × 2).

Pucadelphys, in which the posterior edge of the protocone is longer than the labial edge of the tooth.

The condition of *Andinodelphys* and *Pucadelphys* (angle close to 90°) is present in *Mizquedelphys* and *Incadelphys* (MHNC 13917 and 13906 respectively, two undescribed specimens from Tiupampa under study by the authors) and in an isolated right M4 (DGM, uncat) from Itaboraí referred to *Itaboraidelphys* (Fig. 46C). It is also present in most extant didelphids (but

FIG. 44. — Life reconstructions of pucadelphyids: **B**, positioning of the silhouette of 3D digital rendering of the skull (MHNC 8264), on which the life reconstructions have been based; on the right is the head of the complete animal of fig. A and on the right is the head of the foregroung of fig. A (drawings of A and B are at the same scale); **C**, *Pucadelphys andinus* (Sophie Fernandez), scene of several individuals (natural size) on the ground. Scale bars: 1 cm.

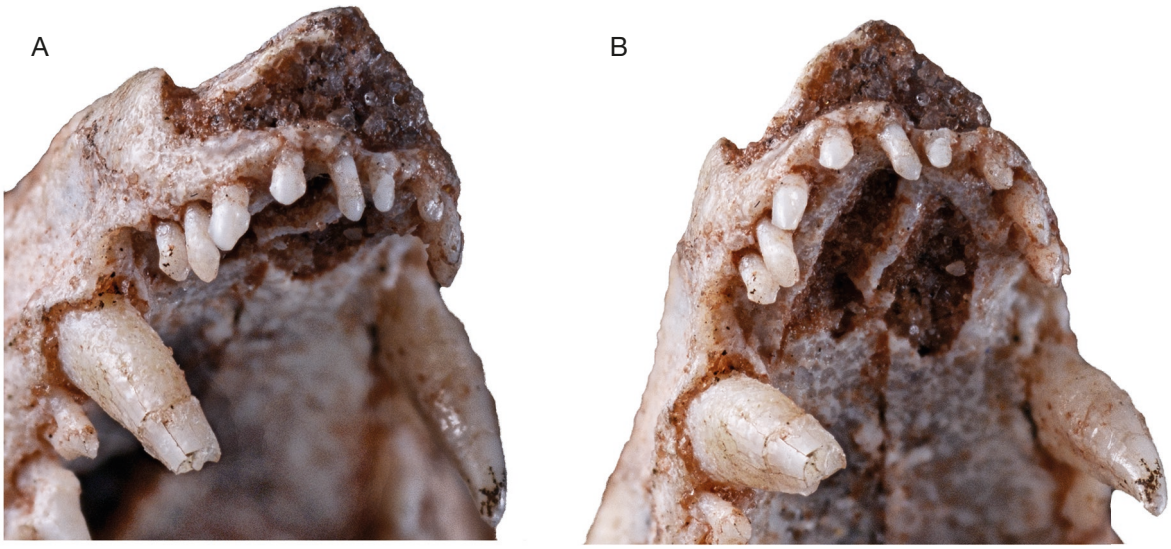

Fig. 45. — *Pucadelphys andinus* (MHNC 8378), upper incisors: **A**, anteroventrolateral view; **B**, anteroventral view. Scale bar: 5 mm.

absent in Gloriniinae and Caluromyinae), *Peradectes*, *Peratherium, Amphiperatherium* (Muizon 1992; Crochet 1980), and *Herpetotherium* (Horovitz *et al.* 2008; Korth & Cavin 2016; Korth 2018). We have observed a condition close to *Andinodelphys* and *Pucadelphys* in *Pappotherium, Holoclemensia* (Turnbull 1971; Fox 1975), *Aenigmadelphys* (OMNH 23475; Cifelli & Johanson 1994), *Turgidodon* (AMNH 77342, UCMP 32413, Cifelli 1990), and *Alphadon* (Lillegraven & McKenna 1986; Lillegraven 1969; Storer 1991). The condition in *Asiatherium* (with an angle of *c.* 110°) is intermediate between the right angle of *Andinodelphys* and the wide-open angle of Sparassodonts (Szalay & Trofimov 1996). However, it is noteworthy that some variation exists, in didelphids for instance, which may feature an angle significantly greater than 90°.

The condition of sparassodonts is present in the so-called Gurlin Tsav Skull (GTS), and the condition of the stagodontids *Didelphodon* and *Eodelphis* is close to that of *Mayulestes* and *Allqokirus,* although with a less open angle. In deltatheroidans, the condition varies since in *Lotheridium* the angle is almost 180° (Bi *et al.* 2015) whereas in *Deltatheroides* it is close to 90° (Rougier *et al.* 2004). Although the M4 of *Deltatheridium* is strongly reduced, it clearly presents the sparassodont condition (PSS-MAE 133). A wide-open angle is also present in pediomyids (Clemens 1966; Davis 2007).

In extant dasyurids and thylacinids, the angle is generally wide-open as in sparassodonts. However, this condition is not present in most fossil dasyurids and thylacinids, in which the angle is much less opened and approaches 90° as in *Andinodelphys* and *Pucadelphys* (e.g., Wroe 1996, 1999; Muirhead & Wroe 1998; Murray & Megirian 2006; Wroe & Musser 2001; Yates 2014). This record suggests that a wide-open angle of the centrocrista-preparacrista (or para-metacone axis – preparacrista) was independently acquired in sparassodonts and dasyuroids.

Therefore, the distribution of the character in metatherians suggests that: 1) the plesiomorphic condition is probably a small angle (close to 90°); and 2) the apomorphic state of a wide open-angle has evolved several times independently within metatherians.

The condition in Late Cretaceous eutherians varies. A wide-open angle is present in *Zalambdalestes, Maelestes, Kennalestes*, but an angle close to 90° is present in *Asioryctes*. Furthermore, the Palaeogene leptictids also feature a wide-open angle. However, noteworthy is the occurrence of an angle close to 90° on the last molar in the oldest eutherians, the Late Jurassic *Juramaia* (Luo *et al.* 2011), the Early Cretaceous eutherians *Ambolestes* (Bi *et al.* 2018), and *Prokennalestes* (Lopatin & Averianov 2017). Therefore, in the case of eutherians, the fossil record would also suggest that an angle close to 90° is the plesiomorphic condition.

Paraconid-metaconid relative arrangement on m3-m4

As described above, the paraconid and metaconid of *Andinodelphys* are adjoined at their base, as is observed in *Pucadelphys,* a condition more distinct on m3-m4 (Fig. 47). This condition differs from that in *Mayulestes* and *Allqokirus*, as well as in the other sparassodonts that retain a metaconid (i.e. *Patene, Nemolestes*). In these taxa, paraconid and metaconid are widely separated at their base. A similar condition is observed in *Deltatheridium* and *Sulestes*, but is absent in *Lotheridium*, which resembles pucadelphyids in this respect. Paraconid and metaconid adjoined at base are present, among others, in *Asiatherium*, *Aenigmadelphys* (OMNH 20531, 20612), stagodontids (e.g. *Eodelphis, Didelphodon*), some pediomyids (e.g. *Pediomys, Protolambda),* some species of *Alphadon* (e.g., *A. attaragos*), and *Itaboraidelphys* (Marshall & Muizon 1984; Szalay & Trofimov 1996; Cifelli 1990; Davis 2007; Scott & Fox 2015).

A separated paraconid and metaconid at base is also present in *Turgidodon, Peradectes, Peratherium, Herpetotherium*, *Dromiciops*, dasyurids, and in the fossil thylacinids (e.g., *Nimbacinus, Mutpuracinus*, *Badjcinus*). *Thylacinus* lacks a metaconid.

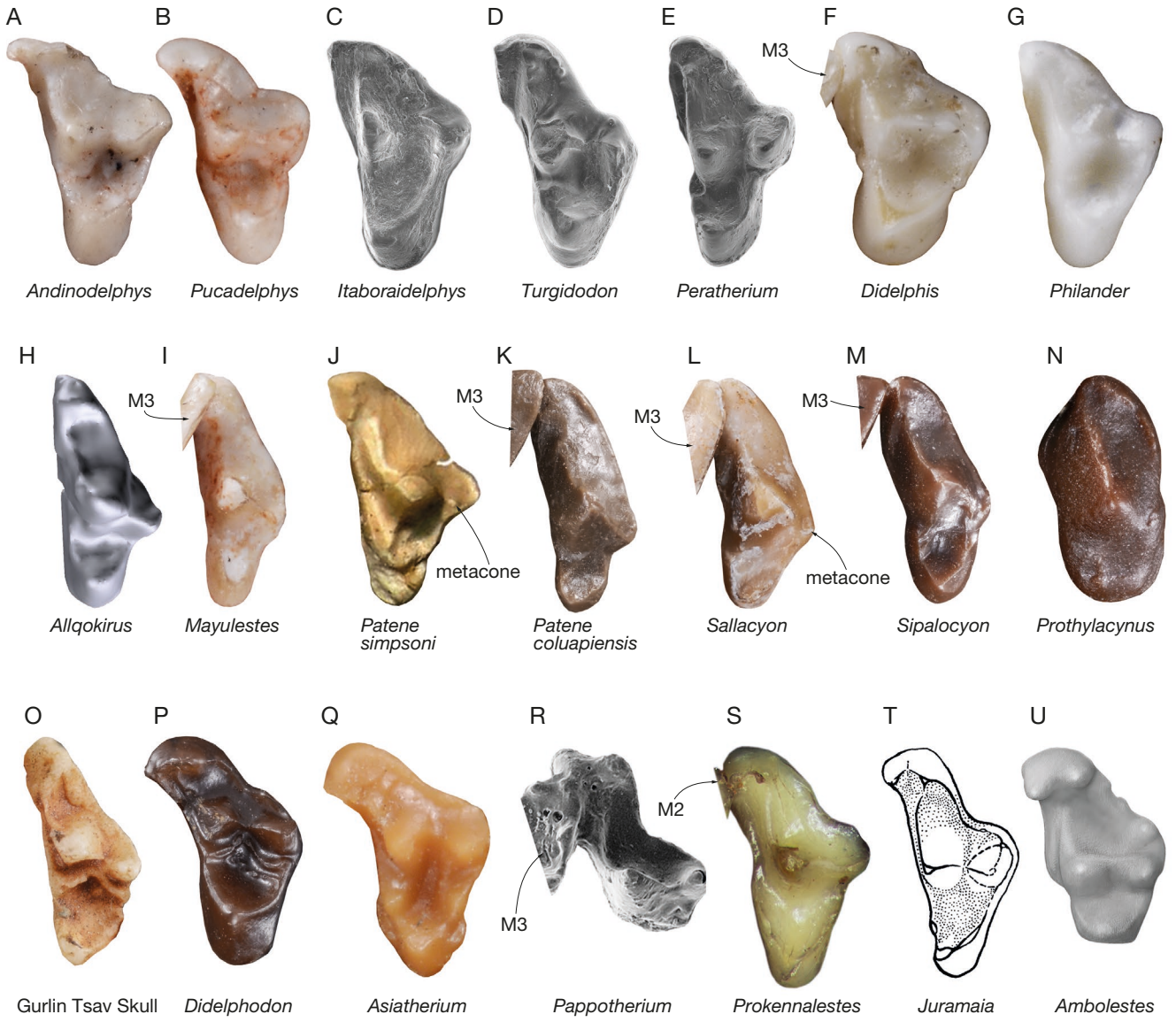

FIG. 46. — Occlusal view of the last upper molar of several metatherians (M4) and some early eutherians (M3): **A**, *Andinodelphys cochabambensis* (MHNC 8264); **B**, *Pucadelphys andinus* (MHNC 8266); **C**, *Itaboraidelphys camposi* (cast of DMG uncatalogued specimen, reversed), **D**, *Turgidodon rhaister* (cast of UCMP 52413, reversed); **E**, *Peratherium elegans* (cast of UM PFY 2001); **F**, *Didelphis albiventris* (MNHN RH 120); **G**, *Philander opossum* MNHN-ZM-MO-1998-2264; **H**, *Allqokirus australis* (MHNC 8267, reversed); **I**, *Mayulestes ferox* (MHNC 1249); **J**, *Patene simpsoni* (cast of MNRJ 1331-V, reversed); **K**, *P. coluapiensis* (cast of AMNH 28448, reversed); **L**, *Sallacyon hoffstetteri* (MNHN SAL 92); **M**, *Sipalocyon gracilis* (cast of MACN 692); **N**, *Prothylacynus patagonicus* (cast of MACN 707); **O**, Gurlin Tsav Skull (cast, reversed); **P**, *Didelphodon vorax* (cast of UCMP 48581); **Q**, *Asiatherium reshetovi* (cast of PIN 3907, reversed); **R**, *Pappotherium pattersoni* (SMP-SMU 61725) from Davis & Cifelli (2011: fig. 5 D1); **S**, *Prokennalestes minor* (PIN 3101/115) from Lopatin & Averianov (2017: pl. 3, fig. 4b, reversed); **T**, *Juramaia sinensis* (BMNH PM1343), from Luo *et al.* (2011: fig. 2g); **U**, *Ambolestes zhoui* (STM 33-5) from Bi *et al.* (2018: fig. 2a). Not to scale.

In extant didelphids the relationships of the para- and metaconid vary from one condition to the other (i. e. separated or adjoined), but it is never clear-cut and is generally somewhat intermediate. Similarly, in many taxa of early metatherians, the condition is not distinctly referable to any of the two character states and is also regarded as intermediate (e.g., *Adelodelphys, Simbadelphys, Kokopellia, Oklatheridium, Atokatheridium, Varalphadon, Protalphadon,* [Cifelli & Muizon 1997; Cifelli 2004; Davis & Cifelli 2011]). Given this distribution, the plesiomorphic condition of this character is difficult to determine; nevertheless, it clearly separates Pucadelphidae from early sparassodonts.

Carnassial notch on trigonid (Fig. 48)

Andinodelphys has no carnassial notch on the paracristid and a weak one on the protocristid. This condition is similar to that of *Pucadelphys*. A paracristid carnassial notch is also absent in *Itaboraidelphys*, which has been regarded as related to *Andinodelphys* (Marshall & Muizon 1988; Muizon *et al.* 2018, and see below). In contrast, well-developed carnassial notches are present on both cristids in *Mayulestes* and *Allqokirus*. In these taxa, the carnassial notch is more pronounced on the paracristid and extends as a deep groove or elongated fossa on the mesial flank of the trigonid. A similar condition is observed in *Patene*. In the other sparassodonts that have

lost the metaconid, there is no protocristid, but the paracristid is strongly developed and also features a deep paracristid carnassial notch (Fig. 48). Among marsupials, the paracristid carnassial notch is well developed in dasyuroids and weak in extant didelphids and *Dromiciops*. A conspicuous paracristid carnassial notch is also present in several stem metatherians, such as *Kokopellia, Asiatherium*, deltatheroidans, stagodontids, *Varalphadon, Turgidodon, Protalphadon, Alphadon*, pediomyids, *Peratherium, Herpetotherium*, and peradectids, although, in some cases, it is variably developed.

Therefore, the distribution of a paracristid carnassial notch among metatherians suggests that it likely represents a plesiomorphic condition. Here again, the distribution of the states of this character within the Tiupampa metatherian fauna separates Pucadelphyidae and sparassodonts.

Bony skull

Lacrimal

The lacrimal of *Andinodelphys* has a small facial process external to the orbit, which extends on the dorsal base of the rostrum. It is moderately expanded and does not form a large facial wing as observed, for instance, in cynodonts, morganucodonts (Kermack *et al.* 1981), deltatheroidans (Kielan-Jaworowska 1975b; Bi *et al.* 2015); the Gurlin Tsav skull (Szalay & Trofimov 1996) and sparassodonts (Muizon *et al.* 2018). The facial process of *Andinodelphys* is crescent-like, as is observed in *Pucadelphys* (contra Marshall & Muizon 1995) and extant didelphids, rather than wing-like. However, some variation is worth mentioning in *Pucadelphys* since one specimen (MHNC 8381) has a facial process significantly larger than in didelphids and other pucadelphyids, and approaches the wing morphology of deltatheroidans and sparassodonts. Be that as it may, *Andinodelphys* and *Pucadelphys* exhibit a derived condition within metatherians.

As in *Pucadelphys* and extant didelphids, the lacrimal of *Andinodelphys* has no contact with the nasal which is a derived character state. A broad lacrimal-nasal contact is a plesiomorphic condition within mammals and is present in multituberculates (Wible & Rougier 2000), *Morganucodon* (Kermack *et al.* 1981), *Vincelestes* (Bonaparte & Rougier 1987), deltatheroidans (Rougier *et al.* 1998; Bi *et al.* 2015), sparassodonts (Muizon 1999), and *Wynyardia* (Gregory 1920; Jones 1930). This characteristic is also commonly present as an individual variation in *Trichosurus* and *Phalanger* (Jones 1930) and given the fact that *Wynyardia bassiana* is apparently known by a single specimen, this condition may possible also represent an individual variation in this taxon. As in *Pucadelphys,* the condition of *Andinodelphys* is apomorphic within Metatheria.

Maxillopalatine vacuity

On the bony skull, one notable difference between *Andinodelphys* and *Pucadelphys* lies in the size of the major palatine foramen of the former, which is anteroposteriorly elongated and extends on the maxilla, forming a small maxillopalatine vacuity. However, this feature is not constant, since it is present in only three of the four skulls, on which it can be observed. On the fourth one (MHNC 8264), the major palatine foramen is large but not anteroposteriorly elongated; however, on this specimen a supplementary foramen perforates the maxilla anterior to the major palatine foramen (Fig. 18C). In the other three specimens, the anteroposterior enlargement of the major palatine foramen of *Andinodelphys* creates a small palatal vacuity in the maxilla. Palatal vacuities are absent in all the *Pucadelphys* skulls of our sample.

Palatal vacuities are present in the great majority of metatherians, in which they can perforate the palatine (palatine vacuities), and/or the maxillary (maxillary vacuities) or both (maxillopalatine vacuities). Palatal vacuities are absent in very few metatherian taxa. Among didelphids, they are totally missing in *Caluromys* and *Caluromysiops*, whereas they are present in all the other members of the family (Voss & Jansa 2009). They are poorly developed in *Marmosa* and *Micoureus*, in which they have the size observed in *Andinodelphys*. In *Didelphis* and *Philander,* maxillopalatine vacuities are large and are associated with more rounded posterior palatal (palatine) vacuities which pierce the palatine only. In other taxa, such as *Metachirus* and *Chironectes,* the maxillopalatine vacuities extend posteriorly and pierces a large part of the palatine.

Almost all Recent australidelphians have maxillopalatine vacuities. In dasyuroids, small anteroposteriorly elongate maxillopalatine vacuities are generally present in *Dasyurus*, but a double set of fenestrae is also present with greatly enlarged maxillopalatine fenestra in, for instance, *Phascogale, Sminthopsis, Dasyuroides, Pseudantechinus,* and *Thylacinus*. Maxillopalatine fenestrae are vestigial or absent, for instance, in *Myrmecobius* and *Notoryctes* (Marshall 1979a). In *Myrmecobius*, we have observed a small but distinct elongated maxillary vacuity anterior to the major palatine foramen in AMNH 155328, but in MNHN-ZM-AC-A2564 this foramen is absent. In *Notoryctes*, (MNHN-ZM-AC-1931-717, MNHN-ZM-1892.1243A, AMNH 202107), a palatal foramen is observed in the maxilla anterior to and similar in size to the major palatine foramen, a condition resembling that of *Andinodelphys* in MHNC 8264. Therefore, palatal vacuities in these two genera are reduced or vestigial in some individuals. They are absent in the petaurids *Dactylopsila* and *Petaurus.* In the latter, however, they are vestigial in some individuals, being present as anteroposteriorly enlarged major palatine foramina. Furthermore, it is noteworthy that intra- and interspecific variation exists in the size and number of the vacuities as observed, for instance, in *Planigale* (Archer 1976b) and *Sminthopsis* (Archer 1981).

Among fossil metatherians, palatal vacuities are present in most Late Cretaceous metatherian taxa in which they can be observed: *Eodelphis* (Fox 1981), *Didelphodon* (Wilson *et al.* 2016), *Pediomys* (Rougier *et al.* 1998, Luo *et al.* 2003, Forasiepi 2009), *Alphadon* (Rougier *et al.* 1998; Forasiepi 2009). They are large (*c.* 42% the palate length) in the ?deltatheroidan commonly referred to as the Gurlin Tsav skull from the Late Cretaceous of Mongolia (Szalay & Trofimov 1996). In *Asiatherium,* although Szalay & Trofimov (1996) regard the presence of maxillopalatal vacuities as uncertain, they have been coded as present in data matrices by Rougier *et al.* (1998), Luo *et al.* (2003), and Forasiepi

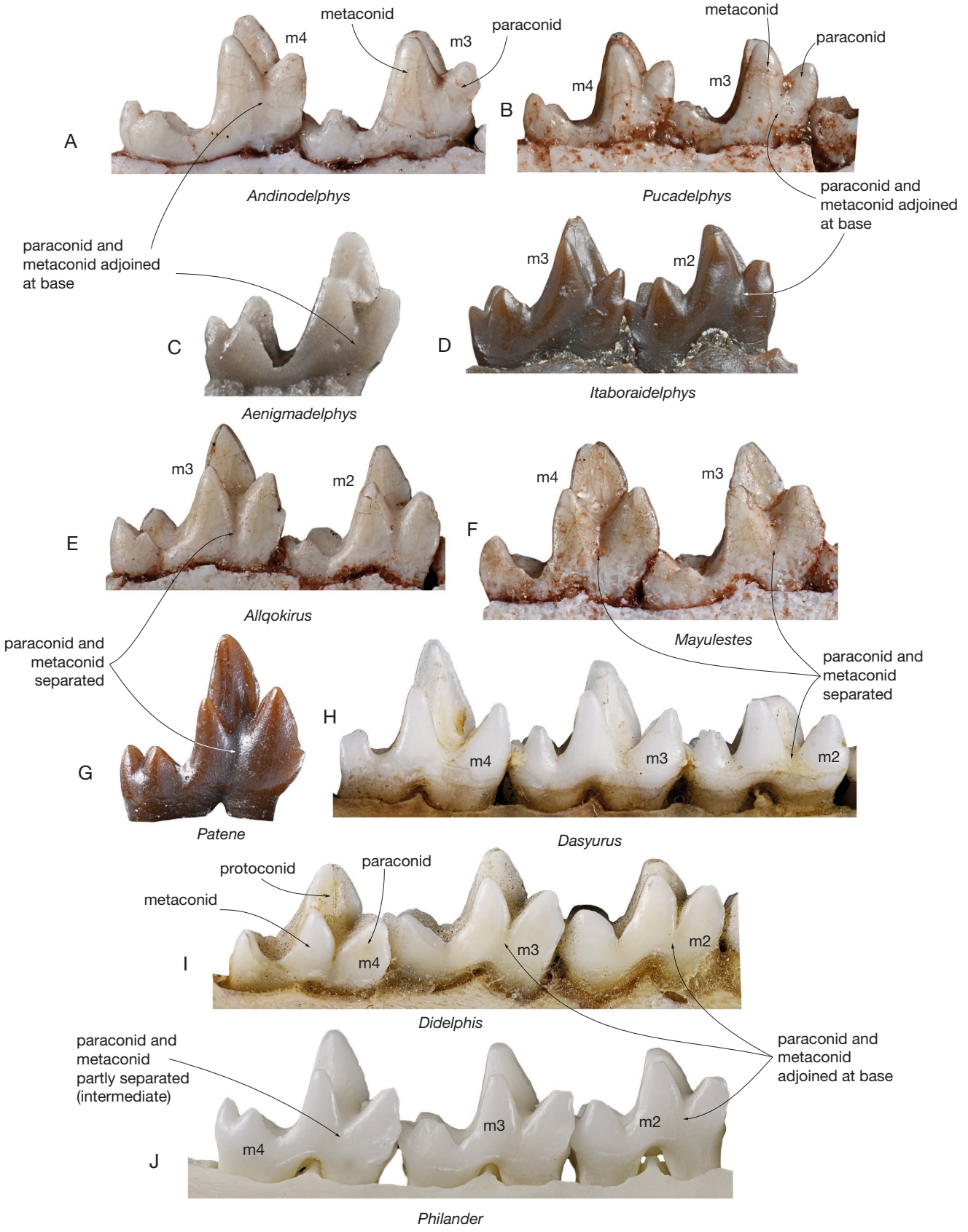

FIG. 47. — Medial view of the lower molars in several metatherian. **A**, *Andinodelphys cochabambensis* (m3-m4, MHNC 8264); **B**, *Pucadelphys andinus* (m2-m4 MHNC 8266, reversed); **C**, *Aenigmadelphys archeri* (m3, cast of OMNH 20531, reversed); **D**, *Itaboraidelphys camposi* (m2-3, cast of, DGM 804-M, reversed); **E**, *Allqokirus australis* (m2-m3, MHNC 8267); **F**, *Mayulestes ferox* (m3-m4, MHNC 1249, reversed); **G**, *Patene simpsoni* (m3 cast of DGM 798-M); **H**, *Dasyurus hallucatus* (m2-m4, MNHN-ZM-AC-1871-284); **I**, *Didelphis albiventris* (m2-m4, MNHN-RH 161); **J**, *Philander opossum* (m2-m4, MNHN-ZM-MO-1998-2264). Not to scale.

(2009). Palatal vacuities are absent in the deltatheroidans *Deltatheridium* and *Lotheridium* (in the latter, absence is definitive on the palatine, but probable only on the maxilla), (Bi *et al.* 2015). They are present in *Herpetotherium* (Sánchez-Villagra *et al.* 2007; Horovitz *et al.* 2008), but the condition in *Peradectes, Mimoperadectes*, and *Peratherium* is unknown. Within the Tiupampa metatherian fauna, they are absent in *Pucadelphys, Mayulestes, Allqokirus*, *Szalinia*, and *Mizquedelphys*. They are present (with the variation described above) in *Andinodelphys* and, when present, they are small. Small slot-like maxillopalatine fenestrae are present in *Sparassocynus*, a carnivorous didelphoid from the Plio-Pleistocene of Argentina (Beck & Taglioretti 2019) and they appear to have been probably also present, but small, in *Epidolops* (Beck 2017). They are absent in sparassodonts, which have been regarded as the sister group of the Pucadelphyidae by Muizon *et al.* (2018).

The absence of maxillopalatal fenestrae in *Pucadelphys* has been regarded by Muizon (1992) and Marshall & Muizon (1995) as a plesiomorphic feature. This interpretation was based on the fact that ontogenetic studies (Parker 1886: 260) have shown that the palatal plates of the maxillae and palatines of the marsupial skull are solid in early stages of development and become fenestrated in later stages by bone resorption (see also Marshall 1979a; Marshall & Muizon 1995). Interestingly, observations in *Dromiciops* confirm Parker's studies. In this taxon, the maxillopalatine vacuities are very large in adults but they are barely more developed than the major palatine foramina in a juvenile skull, as figured by Giannini *et al.* (2004: fig. 2). Similar observations have been made on skulls of juvenile and adult *Lutreolina* and *Didelphis* (Flores *et al.* 2003).

Palatal vacuities are not common in non-metatherian mammals. They are present only in some multituberculates, and in some eutherians (e.g., rabbits, some rodents, macroscelidans, hedgehogs), (Marshall 1979a and references therein). It is therefore tempting to follow Marshall (1979a) in considering that a solid palate is likely to be the plesiomorphic condition among therians and that palatal vacuities were independently acquired in several lineages of multituberculates and eutherians as well as in metatherians.

However, the distribution of this character in Late Cretaceous metatherians, would suggests that the presence of maxillopalatine vacuities may rather be the plesiomorphic character state for metatherians. Furthermore, their absence in a few taxa of didelphids and dasyurids while they are present in most others would confirm this interpretation being an indication that they probably disappeared in some lineages of these families. Be that as it may, considering the great variability of the presence (and absence) and number of palatal fenestrae observed in the metatherian fossil record as early as the Late Cretaceous in North America and Asia, it is likely that this this feature had a complex evolution within metatherians with multiple disappearances and/or appearances.

Given the diverse distribution of palatal vacuities within Metatheria, their absence in some taxa and clades may be interpreted as a derived condition, which independently occurred in several lineages probably by paedomorphic retention of the unperforated condition of the palate in later developmental stages. In this study, we therefore rather favour the hypothesis that the lack of maxillopalatine vacuities in Pucadelphyda might be a synapomorphous loss, the condition of *Andinodelphys* rather indicating a vestigial condition than an incipient development.

Transverse canal

Andinodelphys possesses a transverse canal (Figs 28, 30, 32, 33). This structure has been recorded as absent in *Pucadelphys* by Marshall & Muizon (1995), a statement based on the observation of one specimen only (the three other specimens described by these authors are either not fully prepared or not well preserved enough to allow observation). In the large sample of *Pucadelphys* skulls reported by Ladevèze *et al.* (2011), six skulls are well preserved enough to undoubtedly allow observation of this region and, among them, two specimens clearly present a small transverse canal (MHNC 8377 and 8380). Therefore, this character is clearly polymorphic in *Pucadelphys*.

A transverse canal is variably present in mammals. It is absent in monotremes (Luo *et al.* 2007), *Morganucodon* (Kermack *et al.* 1981), Megazostrodon (Gow 1986; Luo *et al.* 2007), *Haldanodon* (Lillagraven & Krusat 1991), *Gobiconodon* (Luo *et al.* 2003), and *Repenomanus* (Hu *et al.* 2005). It is absent in most multituberculates (Kielan-Jaworowska *et al.* 1986) but present in *Kyroptobaatar* (Wible & Rougier 2000). It is absent in the symmetrodont *Zhangheotherium* (Hu *et al.* 1997) and in the zatherian *Vincelestes* (Hopson & Rougier 1993). A transverse canal is generally absent in eutherians but it has been observed in *Solenodon, Dasypus*, *Rattus, Nandinia, Genetta, and Felis* (Wible & Gaudin 2004; Wible 2012; O'Leary *et al.* 2013; Wible & Spaulding 2013).

In contrast, a transverse canal is present in most metatherians: *Asiatherium, Andinodelphys, Mizquedelphys* (undescribed specimen MHNC 13917), some specimens of *Pucadelphys*, some sparassodonts (e.g., *Sipalocyon, Notogale, Prothylacynus, Lycopsis* – Forasiepi 2009), (but see Archer 1976a who regards the transverse canal of sparassodonts – when present – as not clearly homologous with the transverse canal of didelphids), most didelphids, *Mimoperadectes*, *Peratherium*, caenolestids, most dasyurids, thylacinids, microbitheres, peramelemorphians, macropodoids, acrobatids, petaurids, phascolarctids and vombatids (Sánchez-Villagra & Wible 2002; Horovitz *et al.* 2009). However, some extinct metatherians lack a transverse canal such as the Gurlin Tsav skull (personal observation), some specimens of *Pucadelphys* (Marshall & Muizon 1995), and most sparassodonts (Muizon *et al.* 2018). Among the latter, the canal is absent for example in early taxa such as *Mayulestes, Allqokirus, and Callistoe*, but also in Neogene taxa such as *Borhyaena, Arctodictis, Australohyaena, Hondadelphis*, and *Thylacosmilus*. The transverse canal is exceptionally absent in some didelphids (e.g., *Caluromys*) and some dasyurids (e.g., *Planigale*) (Archer 1976a). The condition in *Deltatheridium* and *Didelphodon* is unknown (Forasiepi 2009; Wilson *et al.* 2016) and uncertain in *Epidolops* (Beck 2017).

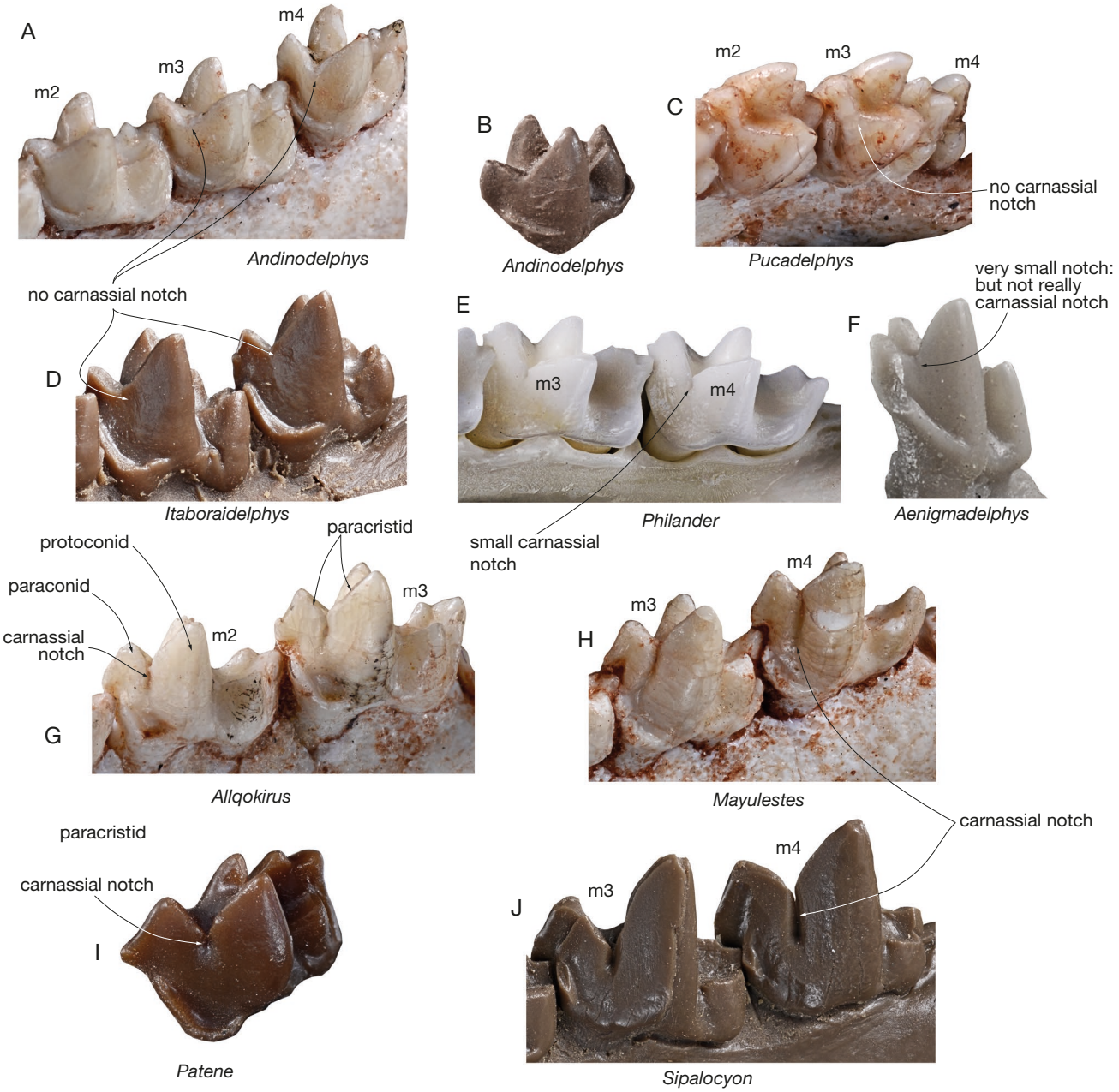

FIG. 48. — Mesiolabial view of posterior lower molars in several metatherians. **A**, *Andinodelphys cochabambensis* (m2-m4, MHNC 8306, reversed); **B**, *Andinodelphys cochabambensis* (m4, cast of MHNC 8307); **C**, *Pucadelphys andinus* (m2-m3, MHNC 8384); **D**, *Itaboraidelphys camposi* (m3-m4, cast of DGM 817-M, reversed); **E**, *Philander opossum* (m3-m4, MNHN-ZM-MO-1998-2264) *Aenigmadelphys archeri* (m3, cast of OMNH 20531, reversed); **F**, *Allqokirus australis* (M2-m3, MHNC 8267); **G**, *Mayulestes ferox* (m2-m3, MHNC 1249, reversed), **H**, *Patene simpsoni* (m3, cast of DGM 798-M); **I**, *Sipalocyon gracilis* (m3-m4, cast of YPM-PU 15375, reversed). Not to scale.

Therefore, it appears that a transverse canal is generally absent in non-metatherian mammals (with some exceptions, cited above), whereas its presence is the most common state in metatherians. We therefore follow Marshall & Muizon (1995), who stated that the absence of a transverse canal is probably the plesiomorphic state for mammals. Because of the distribution of this character among metatherians, we also agree with these authors that this structure is likely to have evolved multiple times within metatherians. The distribution of this character among Pucadelphyda (Pucadelphyidae + Sparassodonta) would lend support to this interpretation.

Tympanic process of alisphenoid

A characteristic feature of most metatherians is the presence of large posteriorly projected wing of the alisphenoid, which borders part of the middle ear anteriorly and/or ventrally. This tympanic process of the alisphenoid forms an alisphenoid bulla, which is present, but more or less developed, in all extant marsupials (except in some vombatids [*Vombatus* and *Lasiorhinus*] and some acrobatids [*Acrobates* and *Distoechurus*]) and in many fossil taxa. *Andinodelphys* lacks a tympanic process of the alisphenoid, a condition observed in all the other Tiupampa metatherians for which this part of the

skull is known (i.e. *Pucadelphys, Mizquedelphys, Mayulestes*, and *Allqokirus*).

Marshall & Muizon (1995) and Muizon (1994, 1998) regarded this condition as plesiomorphic in *Pucadelphys* and *Mayulestes* respectively. However, a tympanic process of the alisphenoid has been observed in several Cretaceous metatherians. It is present in *Asiatherium* and in the Gurlin Tsav skull (Szalay & Trofimov 1996), and in *Didelphodon* (Wilson *et al.* 2016). The fact that it is present in several Late Cretaceous taxa in which it can be observed, would suggest that a tympanic process of the alisphenoid is the plesiomorphic condition for metatherians. A tympanic process of the alisphenoid has also been observed in the early Eocene metatherians, *Peratherium cuvieri* (Selva & Ladevèze 2017), *Herpetotherium* and *Mimoperadectes* (Horovitz *et al.* [2009]; but see Jansa *et al.* [2014] for a different interpretation), but it is absent in the Tiupampa taxa mentioned above. It is absent in most sparassodonts (including the early Palaeocene *Mayulestes* and *Allqokirus* and the early Eocene *Callistoe*) except in hathliacynids (e.g., *Notogale*, *Sipalocyon, Cladosictis*) and thylacosmilids, in which it probably represents a derived condition (reversal?) (Marshall & Muizon 1995). This feature is also apparently absent in the early Eocene *Epidolops* (Beck 2017) and in the Late Cretaceous *Deltatheridium* (Forasiepi 2009: 143; personal communication of G. Rougier to A. Forasiepi); condition in *Lotheridium* is unclear because of the poor preservation of the alisphenoid in the holotype of *L. mengi* (ZMNH M9032), (Bi personal communication to CM). Therefore, the distribution of this character in early metatherians is variable and diverse, suggesting that it may have appeared and disappeared several times during early metatherian evolution. Therefore, it is difficult to know if the absence of a tympanic process of the alisphenoid in the Tiupampa metatherians is apomorphic or plesiomorphic within metatherians. However, it likely represents a plesiomorphic condition within Pucadelphyda (Pucadelphyidae + Sparassodonta), since the five Tiupampa pucadelphydans for which the basicranium is known lack a tympanic process of the alisphenoid.

Hypotympanic sinus

Andinodelphys features a small circular cavity in the roof of the middle ear, located between the foramen ovale anteromedially and the tympanic petrosal crest posterolaterally (Fig. 28). This depression excavates the petrosal posteromedially and the squamosal and alisphenoid anterolaterally. As pointed out by Beck (2017: 391), this structure, houses the dorsal part of the hypotympanic sinus (*contra* Ladevèze & Muizon 2007), an interpretatation that we follow here. In *Andinodelphys*, it is similar to that observed in *Mayulestes*. It is absent in *Pucadelphys*. Auditory sinuses are common in extant therians. They are air cavities (other than the epitympanic recess) within or between bones of the middle ear. Within metatherians, the most common sinuses are the hypotympanic and epitympanic sinuses. The former is located anterior to the epitympanic recess, anterolateral to the petrosal and medial to the glenoid fossa. In most extant taxa, it excavates the alisphenoid only, most of it being housed in the tympanic process of the alisphenoid, which project ventrally below the tympanum. Therefore, most of the sinus is actually ventral to the tympanum and, hence, hypotympanic. However, the dorsal part of the sinus excavates the roof of the middle ear cavity, which is slightly dorsal to the tympanum. In *Andinodelphys* and *Mayulestes*, which lack a tympanic process of the alisphenoid, the small cavity in the roof of the middle ear is the bony materialization of the hypotympanic sinus, which represent the part of the sinus located above the tympanum. The remaining part of the sinus is likely to have extended ventrally below the tympanum during life being limited ventrally by the fibrous membrane of the tympanic cavity (in the absence of any kind of bony tympanic bulla) (MacPhee 1981). To conclude, although what is referred to, here, (in *Andinodelphys* and *Mayulestes*) as the hypotympanic sinus is actually dorsal to the tympanum it corresponds to part of a sinus that was during life mainly ventral to the tympanum: the hypotympanic sinus (see Beck & Taglioretti [2019] for discussion on the position of the hypotympanic sinus relative to the tympanum). In taxa that lack a tympanic process of the alisphenoid, the hypotympanic sinus is excavated mostly in the petrosal and squamosal, with, in some taxa (e.g., *Mayulestes*), a small participation of the alisphenoid between them. The epitympanic sinus is located posterolaterally to the epitympanic recess and excavates the squamosal and/or the pars mastoidea of the petrosal. Because this sinus extends mostly dorsally, it is generally almost totally dorsal to the tympanum, thus epitympanic. Such a sinus is absent in *Andinodelphys*. The fossa erroneously identified by Muizon (1999) as the mastoid epitympanic sinus in the posterior region of the petrosal of *Notogale*, is in fact the stapedial fossa.

Auditory sinuses in general are absent in *Morganucodon* (Kermack *et al.* 1981); *Gobiconodon, Sinoconodon* (Crompton & Sun 1985; Crompton & Luo 1993), *Repenomanus* (Hu *et al.* 2005), monotremes (Watson 1916), *Vincelestes* (Rougier *et al.* 1992), Late Cretaceous eutherians (*Asioryctes, Barunlestes, Kennalestes, Zalambdalestes, Maelestes*; Kielan-Jaworowska 1981, 1984; Kielan-Jaworowska & Trofimov 1980; Wible *et al.* 2004; Wible *et al.* 2009) and generalized extant eutherians (Van Kampen 1905; Novacek 1977). A hypotympanic sinus occurs in the great majority of extinct and extant metatherians except *Deltatheridium* (Rougier *et al.* 1998) *Pucadelphys* (Marshall & Muizon 1995), and *Mizquedelphys* (MHNC 13917). Condition in *Lotheridium* is unknown (Bi *et al.* 2015). In regard of the distribution, the absence of auditory sinuses likely represents the plesiomorphic condition for mammals. Therefore, *Andinodelphys* is more derived than *Pucadelphys* in this respect.

Inferior petrosal sinus and foramen

As mentioned above a conspicuous foramen is observed at the junction of the basioccipital, exoccipital and petrosal (Fig. 30). This foramen opens the canal for the inferior

petrosal sinus ventrally, anterior to its posterior end. This foramen may have conveyed a branch of the inferior petrosal sinus which may have joined the vertebral vein. A similar condition may have been present in some specimens of *Pucadelphys*, although it cannot be ascertained because of the preservation of the specimens. The condition in *Mayulestes* and *Allqokirus* is unknown. The condition of *Andinodelphys* appears to be unique among metatherian (apart from a possible presence in *Pucadelphys*).

The other characters discussed by Marshall & Muizon (1995: 64-82) are identical in *Pucadelphys* and *Andinodelphys* and will not be further discussed here. They are: number of incisors, structure of lower incisors, number of molar and premolars, inflected angular process of the dentary, mylohyoid groove, labial mandibular foramen, orbit large and confluent with temporal fossa, nasal-lacrimal contact, alisphenoid-parietal contact, preglenoid process of the jugal, foramen ovale, subsquamosal foramen (= suprameatal foramen, in this paper), Orientation of ectotympanic and tympanic membrane, pars mastoidea contribution to occiput, mastoid and paroccipital process, shape of fenestra vestibuli and stapedial footplate, stapedial artery, course of internal carotid artery, sulcus for facial nerve, anterior lamina of petrosal.

Characters of dentition of *Andinodelphys* are very similar to those of *Pucadelphys* except the size and relative position of the I1

Specific comparison with Itaboraidelphys and phylogenetic analysis

Marshall & Muizon (1988) and Muizon (1992) have regarded the molars of *Andinodelphys cochabambensis* as representing an adequate dental structural ancestor for *Itaboraidelphys camposi* from the late Palaeocene-early Eocene of Itaboraí (Brazil). However, *Andinodelphys* differs from *Itaboraidelphys* in its smaller size (25% smaller in linear tooth dimensions), more gracile molars with sharper crests and cusps and deeper basins, upper molars with a less V-shaped centrocrista, paracone and metacone with a distinct vertical ridge on their labial edges, p2 distinctly smaller than p3 (subequal in size to p2 slightly larger than p3 in *Itaboraidelphys*) lower molars with a higher trigonid and smaller entoconid, and trigonid of m3 slightly wider than talonid (slightly narrower in *Itaboraidelphys*). *Andinodelphys* and *Itaboraidelphys* share the same large size of stylar cusps B and D, with a small stylar cusp C, the latter being twinned in some specimens, the posterior edge of the protocone distolingually expanded, which displaces its apex anteriorly, the paracone conspicuously smaller than the metacone, the angle para-metacone axis-preparacrista on M4 close to 90°, and the adjoined paraconid and metaconid. In spite of the small differences mentioned above, which are likely to represent plesiomorphic conditions in *Andinodelphys*, the latter compares best with *Itaboraidelphys* among the metatherian taxa of the Itaboraí fauna.

Ladevèze & Muizon (2010) have performed a parsimony analysis including several isolated petrosals from the late Palaeocene-early Eocene of Itaboraí. This analysis resulted in a sister group relationship of Type II petrosals (MNRJ 6728-V and MNRJ 6729-V) with pucadelphyids (*Pucadelphys* and *Andinodelphys*). In order to test this relationship, Muizon *et al.* (2018: 422-423) compared the area of the promontorium relative to the molar size in *Andinodelphys* and *Itaboraidelphys.* Assuming that the promontorium area relative to the length of the molars was similar in both taxa these authors calculated an estimation of the promontorium area in *Itaboraidelphys* on the basis of the upper and lower molar proportions. The two calculated estimated values (12.1 mm^2 and 12.9 mm^2) felt seemed perfectly within the range of the promontorium area measured on the two Type II petrosals (11.1 mm^2 and 13.96 mm^2). Their result provided a mean promontorium area of *Andinodelphys* (9.42 mm^2) 24,8% smaller than in *Itaboraidelphys* (12.53 mm^2), a difference that matches the size difference evaluated by Marshall & Muizon (1988) between the teeth of *Andinodelphys* and *Itaboraidelphys,* the former being approximately 25% smaller than the latter. Consequently, Muizon *et al.* (2018) concluded that, on the basis of both dental and petrosal anatomy, the Type II petrosals of Itaboraí could plausibly be referred to *Itaboraidelphys.* As a consequence, in the parsimony analysis below we tentatively referred dental remains of *Itaboraidelphys camposi* and Type II petrosals to the same taxon (contra Beck [2017], who referred the Type II petrosal to *Epidolops*, a hypothesis that has been challenged by Muizon *et al.* [2018]). The phylogenetic analysis presented here uses the data matrix of Muizon *et al.* (2018). However, after re-examination of casts, specimens, and literature we changed the scorings of some characters for some taxa. These changes are mentioned in the character list below (Appendix 3). Furthermore, in order to complement the data on deltatheroidans we added two Asiatic taxa of this group of metatherians (*Sulestes* and *Lotheridium*) and three North American ones (*Atokatheridium, Oklatheridium,* and *Nanocuris*). Scoring of these taxa in our matrix is respectively based on the descriptions, illustrations, and scorings of Averianov *et al.* (2010) and Bi *et al.* (2015) on the one hand and Kielan-Jaworowska & Cifelli (2001), Fox *et al.* (2007), Davis *et al.* (2008), Wilson & Riedel (2010), Davis & Cifelli (2011) on the other hand. Because of the condition of the stylar shelf of upper molars and postglenoid foramen in *Lotheridium,* we added a fifth state to character 35 (4, width of stylar shelf reduced labial to metacone on penultimate molar) and a third state to character 177 (2, postglenoid foramen located anterior to postglenoid process). Three other characters of *Lotheridium* were coded thanks to personal communication of Bi to one of us (CM); they are characters 71, 185, and 210. Four other in-group taxa (*Alphadon-Turgidodon-Protalphadon*, *Varalphadon, Pediomys,* and the so-called Gurlin Tsav skull (GTS) figured by Szalay & Trofimov 1996) were also added. Furthermore, we added three supplementary out-group taxa: *Vincelestes, Zalambdalestes*, and *Leptictis*.

RESULTS OF THE PHYLOGENETIC ANALYSES

We have performed three sets of parsimony analyses, each set including one analysis with unweighted characters and one analysis with implied weighting (Goloboff k = 3). The first set of analyses takes into account the whole of our character list (364). Then, given the possible bias related to dental characters (e.g. related to hypercarnivory), which are well known to be strongly homoplastic (e.g. Muizon & Lange-Badré 1997; Ladevèze *et al.* 2011; Sansom *et al.* 2017; Solé & Ladevèze 2017), we have performed a second set of analyses excluding all dental characters and, consequently, excluding the taxa known by teeth only or teeth and partial jaws. The third set of analyses was performed with the exclusion of some dental characters only, which are regarded more specifically related to hypercarnivory (see p. 695), in the light of the preceding analyses.

Results of the first analyses with all characters

The analysis of this significantly modified matrix (as a consequence of the additional taxa and changes mentioned above and in the character list and scorings; 364 characters and 51 taxa) with PAUP* resulted in 6 shortest trees (L = 1577, CI = 0.305, RI = 0.667). As seen in the strict consensus tree (L = 1584, CI = 0.306, RI = 0.665) (Fig. 49A) the relationships of *Itaboraidelphys* are the same as those retrieved by Ladevèze & Muizon (2010). *Itaboraidelphys* is the sister group of the clade *Pucadelphys* + *Andinodelphys* and, as such, is included here in Pucadelphyidae.

The relationships of Stagodontidae and Deltatheroida resulting from this analysis are different from those retrieved by Muizon *et al.* (2018). The Gurlin Tsav Skull (GTS) forms a clade with Stagodontidae (*Eodelphis* and *Didelphodon*) and this clade is sister-group to Sparassodonta. Deltatheroida and Pucadelphyidae are successive sister groups to this (Stagodontidae-GTS + Sparassodonta) clade. This result significantly differs from that of Muizon *et al.* (2018), in which the deltatheroidans and stagodontids were early diverging groups in the metatherian clade. The present result also differs from most other studies, in which deltatheroidans are almost always in a basal position in the Metatheria tree (e. g. Averianov *et al.* 2010; Rougier *et al.* 2015; Bi *et al.* 2015; Forasiepi *et al.* 2015; Wilson *et al.* 2016; Beck 2017). Moreover, stagodontids, although generally less basal than deltatheroidans, are, in these analyses, generally retrieved closer to North American metatherians than to sparassodont, with one exception however (Engleman & Croft 2014), in which they were also the sister group of sparassodonts. As mentioned by these authors, although stagodontids have been regarded as closely related to sparassodonts by Marshall *et al.* (1990), this interpretation has been seriously questioned by Fox & Naylor (1995), but also by Muizon & Lange-Badré (1997), and Muizon (1999) because it is based almost exclusively on heavily homoplastic dental characters related to hypercarnivory. This statement may also apply in the case of this analysis. Therefore, this statement essentially concerns the dental synapomorphies (non-ambiguous and ambiguous) supporting 1) the clade (deltatheroidans (GTS, stagodontids) sparassodonts)): 33(1), 48(1), 57(1), 70(0), 71(0), 80(1), 84(2), 85(2), 43(0), 47(0), 50(0), 95(1), 96(0); and 2) those supporting the clade ((GTS, stagodontids) sparassodonts): 6(1), 12(1), 23(0), 24(0), 30(1), 38(1), 46 (2), 50(0), 55(1), 64(1), 72(1).

In order to overcome this bias, we have performed a new analysis with downweighted homoplastic characters with Goloboff constant value = 3. The use of higher Goloboff constant values (as recommended by Goloboff *et al.* 2017) retrieved consensus trees almost identical to the strict consensus and did not downwheight homoplastic characters, which justifies the selection of a low value of the Goloboff constant (3) in the present study. In the single tree obtained (CI = 0.303, RI = 0.6637; Fig. 49B), stagodontids are placed in a more basal position, similar to that retrieved in the tree provided by Muizon *et al.* (2018: fig. 29B) after an analysis with downweighted homoplastic characters. However, the GTS and deltatheroidans remain closely related, basal to sparassodonts. The change in the position of the stagodontids in our new tree likely reveals the elevated degree of homoplasy of the characters (mostly dental) that placed them in a sister group relationship to the sparassodonts, and therefore the weakness of this topology. The position of GTS, which is now a direct sister-group of sparassodonts, approaches the results of Rougier *et al.* (2015) and Wilson *et al.* (2016: fig. 3), and the position of the deltatheroidans as the sister-group of the GTS + sparassodonts is not so discrepant with that retrieved by these authors, in which deltatheroidans are only one node more basal to their clade including GTS + pucadelphydans (i.e. the first diverging clade of Marsupialiaformes) (see below p. 693). The analyses of Rougier *et al.* (2015) and Wilson *et al.* (2016) also resulted in a position of the stagodontids more closely nested within North American taxa but not in a basal position in the tree as in Forasiepi *et al.* (2015) and Muizon *et al.* (2018). Furthermore, it is noteworthy that the topologies obtained here and those retrieved by Rougier *et al.* (2015) and Wilson *et al.* (2016) resulted from different character lists (although most of characters of these authors are included in our list) and in the fact that two ingroup Operational Taxonomic Units (OTU) are considered by these authors at family level (borhyaenoids, and dasyurids) in contrast to ours, what may explain the slight differences in our results concerning the deltatheroidans and GTS + pucadelphydans relationships. In our new analysis, the clade Pucadelphyda is retained, but according to this topology, should now include deltatheroidans and the GTS. In this context, our discussion below will focus on the new tree obtained with downweighted homoplastic characters (Fig. 49B).

Another interesting result is the position of *Varalphadon*, a North American genus that has been regarded as a sparassodont by Carneiro (2018). Although the position of *Varalphadon* as a sister group of *Pediomys* could perhaps be argued, it confirms Muizon *et al.* (2018: 430)'s conclusions that this taxon is very probably not closely related to sparassodonts.

Below we provide the unambiguous synapomorphies of the following clades resulting from the implied weighted analy-

sis (Fig. 46B): 1) Pucadelphyda (as retrieved in the present result), 2) Deltatheroidans + GTS + sparassodonts, 3) GTS + sparassodonts, and 4) Pucadelphyidae. We also provide the ambiguous synapomorphies with delayed (Deltran) and accelerated (Acctran) optimisations. The strict synapomorphies are in bold. Only the unambiguous synapomorphies are fully detailed. For the ambiguous synapomorphies we only indicate the subsequent reversals and convergences.

1) Pucadelphyda as in Fig. 49B (= clade pucadelphyids, deltatheroidans, GTS, sparassodonts)

Unambiguous synapomorphies of the clade pucadelphyids, deltatheroidans, GTS, sparassodonts

20 (1). First upper and lower premolars oblique relative to tooth row [reversal in (*Deltatheridium*, *Deltatheroides*), and sparassodonts excluding (*Patene* (*Mayulestes*, *Allqokirus*))];
104 (2). Angled ventral margin of the dentary behind last molar continuous to condyle (reversal in borhyaenoids without *Lycopsis*; straight in deltatheroidans);
145 (0). Flaring of maxillary cheek posterior to infraorbital foramen present (reversal in *Sulestes*, *Hondadelphys*, *Lycopsis*);
147 (2). Fossa for the levator labii muscle in the anterior end of the jugal, present mainly in the maxilla;
161 (0). Posterior process of pterygoid, which covers the alisphenoid-basisphenoid suture, present (convergent with *Thylacinus*);
183 (1). Hypotympanic sinus formed by squamosal, alisphenoid and petrosal [absent in *Pucadelphys*, and (*Sulestes* (*Deltatheridium*, *Deltatheroides*))];
185 (1). Medial process of the squamosal, which extends into the middle ear and forms part of the roof of the tympanic cavity, present.
205 (1). Cavum epiptericum floored by petrosal and alisphenoid [reversal in sparassodonts without (*Patene* (*Mayulestes*, *Allqokirus*)); convergent with stagodontids];
260 (1). Foramen on dorsal arch of last lumbar vertebra, present (reversal in borhyaenids; convergent with dasyuromorphs);
282 (1). Extension of the deltoid crest reaches distal half of the humerus (convergent with didelphids);
287 (1). Lateral extension of capitulum, present and straight with a flat shelf and/or a salient crest [convergent with *Thylacinus* and (*Didelphis*, *Metachirus*)];
331 (1). Astragalus, dorso-distal tuber of the head, present;
353 (0). Spatial relationship between navicular and entocuneiform: entocuneiform distal to navicular (convergent with dasyuromorphs).

Fourteen ambiguous synapomorphies (Acctran, fast) may also support this clade

150 (0). Palatal vacuities absent (reversal in GTS);
156 (1). Morphology of the postpalatine torus foramen, wide-open groove (the section is approximately half a circle or less) (reversal in *Andinodelphys*; convergent with dasyuromorphians);
175 (0). Proportions of the postglenoid process, higher than wide and roughly parabolic (very low and wider than high in (GTS, Sparassodonta); convergent with didelphids and *Sminthopsis*);
181 (0). Transverse canal absent [reversal in *Andinodelphys* and (*Notogale* ((*Sipalocyon*, *Cladosictis*), borhyaenoids))];
210 (1). Deep groove for internal carotid artery excavated in medial side of promontorium apex ventrally present (reversal in deltatheroidans);
213 (0). Rostral tympanic process of petrosal, absent or low ridge or smooth tubercle (tall ridge reaching apex of promontorium in (*Notogale* ((*Sipalocyon*, *Cladosictis*), borhyaenoids)) but restricted to posterior half of promontorium in borhyaenoids];
262 (1). Ventral median keel on anterior lumbar vertebrae present (reversal in *Prothylacinus*; convergent with *Metachirus*, *Dromiciops*, and *Thylacinus*);
272 (1). Infraspinous/supraspinous fossa width at the level of the neck, supraspinous fossa narrower (reversal in *Sipalocyon* and in ((*Borhyaena*, *Arctodictis*) (*Australohyaena* (*Thylacosmilus* (*Callistoe*, *Paraborhyaena*)))); convergent with *Dromiciops*];
283 (1). Distal end of deltoid crest, forming a distinct angle or process [reversal in sparassodonts without (*Patene* (*Mayulestes*, *Allqokirus*)); convergent with (*Didelphis*, *Metachirus*), *Dromiciops*, and *Dasyurus*];
303 (2). Iliac and gluteus fossae: gluteus fossa larger (convergent with *Metachirus* and dasyuromorphians);
315 (1). Tibia straight [reversal in (*Patene* (*Mayulestes*, *Allqokirus*)) and *Thylacosmilus*; convergent with *Thylacinus*];
323 (0). Astragalus, astragalonavicular facet extends onto ventromedial side of head, absent [reversal in sparassodonts without (*Patene* (*Mayulestes*, *Allqokirus*))];
354 (1). Angle between navicular and distal metatarsal facets of ectocuneiform, parallel to the distal facet [reversal in ((*Borhyaena*, *Arctodictis*) (*Australohyaena* (*Thylacosmilus* (*Callistoe*, *Paraborhyaena*)))), convergent with dasyuromorphians except *Thylacinus*];
360 (1). Mt III thickness relative to that of Mt I, Mt III thinner than Mt I (convergent with dasyuromorphians).

Six ambiguous synapomorphies (Deltran, slow) may also support the clade Pucadelphyda

223 (0). Hiatus Fallopii on dorsal (cerebellar) face of petrosal [reversal in sparassodonts without (*Patene* (*Mayulestes*, *Allqokirus*)) and *Hondadelphys*; convergent with *Herpetotherium*];
248 (1). Shape of the cranial facets of atlas: dorsal third of the facet much more concave than the ventral two thirds and strongly inflected medially (reversal in *Prothylacynus*, borhyaenids; convergent with didelphids, *Dasyurus*, *Thylacinus*);

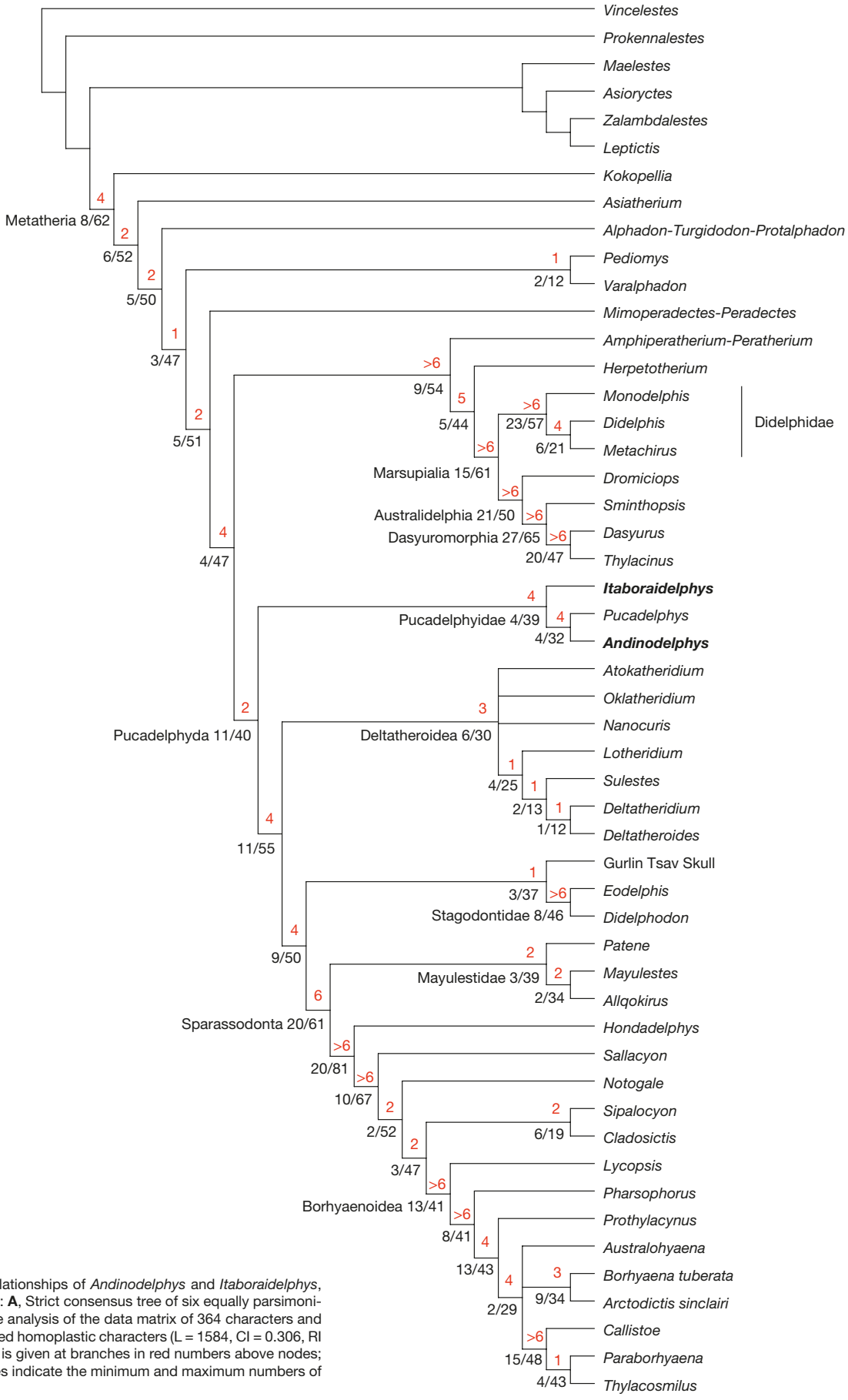

FIG. 49. — Phylogenetic relationships of *Andinodelphys* and *Itaboraidelphys*, among other metatherians: **A**, Strict consensus tree of six equally parsimonious trees resulting from the analysis of the data matrix of 364 characters and 51 taxa with equally weighted homoplastic characters (L = 1584, CI = 0.306, RI = 0.665); the Bremer index is given at branches in red numbers above nodes; black numbers below nodes indicate the minimum and maximum numbers of synapomorphies.

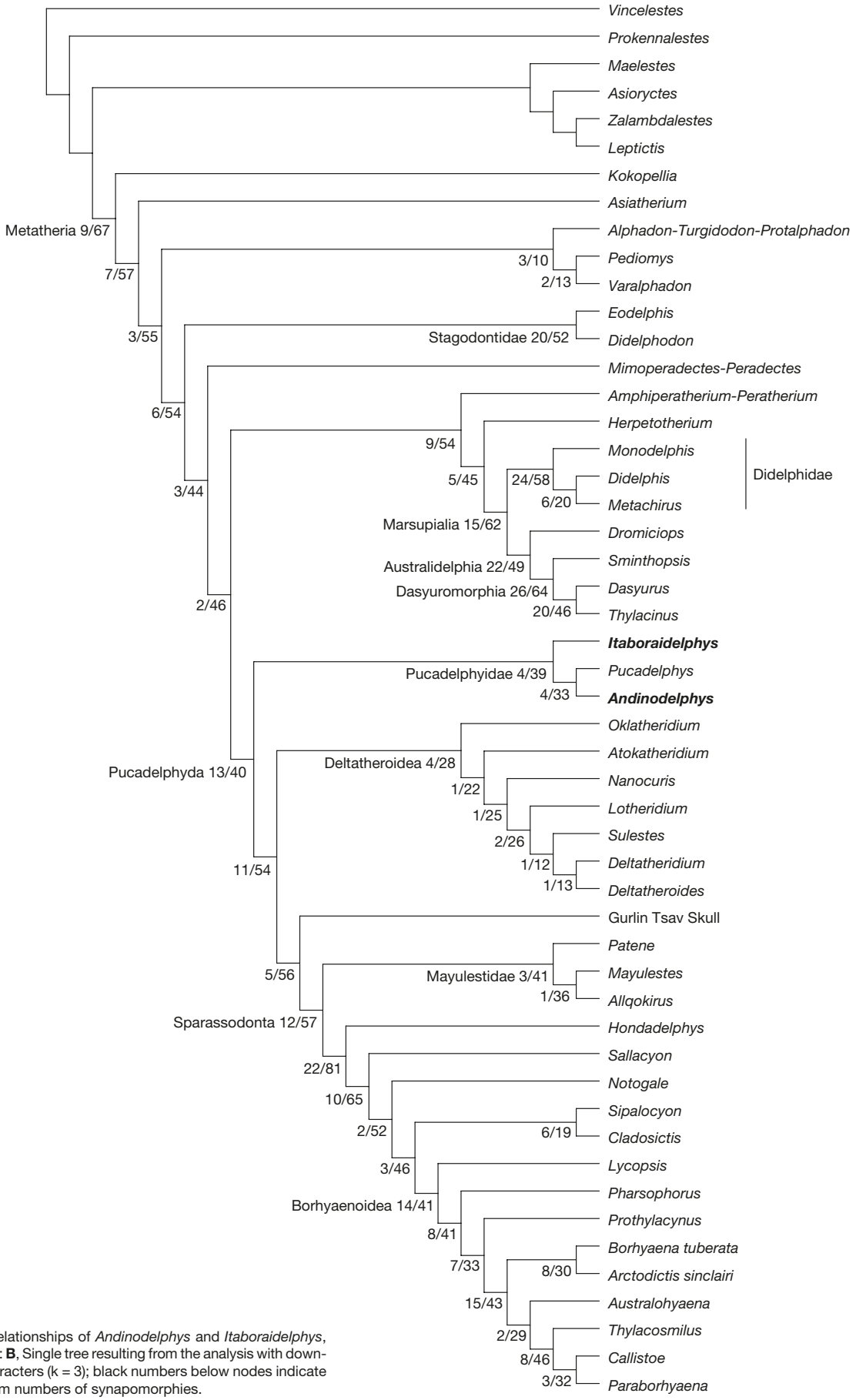

FIG. 49. — Phylogenetic relationships of *Andinodelphys* and *Itaboraidelphys*, among other metatherians: **B**, Single tree resulting from the analysis with down-weighted homoplastic characters (k = 3); black numbers below nodes indicate the minimum and maximum numbers of synapomorphies.

262 (1). Ventral median keel on anterior lumbar vertebrae, present (reversal in *Prothylacynus*; convergent with *Metachirus*, *Dromiciops*, and *Thylacinus*);
272 (1). Infraspinous/supraspinous fossa width at the level of the neck: supraspinous fossa narrower (reversal in *Sipalocyon*, *Arctodictis*, *Callistoe*; convergent with *Dromiciops*);
303 (2). Iliac and gluteus fossae: gluteus fossa larger;
360 (1). Mt III thickness relative to that of Mt I: Mt III thinner than Mt I (convergent with dasyuromorphs).

2) Clade Deltatheroida + GTS + Sparassodonta
Unambiguous synapomorphies supporting the clade Deltatheroida + GTS + Sparassodonta:
33 (1). Size of molars (upper and lower) increases posteriorly: marked [convergent with (*Dasyurus*, *Thylacinus*)];
48 (1). Metacone and paracone adjoined at base (on, at least, half of their height) (adjoined on most of their height; apices of cusps only are separated in borhyaenoids but *Lycopsis*; convergent with *Thylacinus*);
57 (1). Protocone size (on penultimate or antepenultimate molar): small and anteroposteriorly narrow (reversal in *Hondadelphys*, absent or very small in borhyaenoids but *Lycopsis*; convergent with *Thylacinus*);
70 (0). Trigonid vs talonid width (on penultimate or antepenultimate molar): wider than talonid (reversal in *Nanocuris*; convergent with *Andinodelphys*);
71 (0). Protoconid labial expansion; the labial edge of the protoconid at mid-height is strongly convex, protruding labially and overhangs the base of the crown: present (reversal in *Lotheridium*);
80 (1). Paraconid elongated with anterior projection of the paraconid keel (ridge) mostly in the ventral half of the cusp: present [reversal in *Lotheridium*, (*Callistoe*, *Paraborhyaena*); convergent with *Thylacinus*];
84 (2). Height of metaconid vs paraconid (on penultimate molar): lower [subequal in (*Patene* (*Mayulestes*, *Allqokirus*)); convergent with stagodontids];
85 (2). Volume of the metaconid vs paraconid (on penultimate molar), in occlusal and lingual views: smaller [convergent with (*Dasyurus*, *Thylacinus*), and stagodontids];
139 (0). Naso-lacrimal contact, present (reversal in *Thylacosmilus*);
149 (2). Number of palatal pits independently of their size: two between ultimate, penultimate and antepenultimate molars [two pits between first, antepenultimate, and penultimate molars in Deltatheriidae-but reversal in *Deltatheroides*, one pit in borhyaenids; convergent with (*Dasyurus*, *Thylacinus*)].

Thirty-one ambiguous synapomorphies (Acctran, fast) may also support the clade Deltatheroida + GTS + Sparassodonta
1 (1). Number of upper incisors: four [reversal in (*Patene* (*Mayulestes*, *Allqokirus*)); convergent with dasyuromorphians];
2 (1). Size of extra-alveolar portion of root of I1 as long as on other incisors and as long as crown [reversal in (*Patene* (*Mayulestes*, *Allqokirus*)); convergent with Australidelphia];
3 (0). Implantation of the first upper incisors in anterior view: incisors parallel [reversal in (*Patene* (*Mayulestes*, *Allqokirus*))];
10 (1). Number of lower incisors: three (reversal in Mayulestidae, *Hondadelphys*; convergent with dasyuromorphians and stagodontids);
43 (0). Stylar cusp C, absent or tiny (convergent with Australidelphia);
47 (0). Shape of paracone and metacone: conical (convergent with *Thylacinus*);
50 (0). Centrocrista, straight (convergent with *Dromiciops*, *Thylacinus*);
95 (1). Shape of entoconid: transversely compressed (convergent with didelphids and dasyuromorphians);
96 (0). Relative height of entoconid: lower than hypoconid [reversal in *Patene*, *Hondadelphys*, (*Sipalocyon*, *Cladosictis*); convergent with *Herpetotherium*, *Thylacinus*, and stagodontids];
106 (1). Anteroventral edge of mandibular symphysis: less slanting, forming an angle > 25° (reversal in *Nanocuris*; convergent with *Thylacinus*, and stagodontids);
118 (0). Condyle vertical position vs tooth row: approximately at the same level or slightly below [reversal in (*Patene* (*Mayulestes*, *Allqokirus*)), *Sipalocyon*; convergent with *Thylacinus*];
120 (0). Length of the rostrum: less than (or equal to) ⅓ total length of the skull (reversal in sparassodonts; convergent with *Dromiciops*, *Dasyurus*, *Thylacinus*);
141 (0). Lacrimal tubercle: present, knob-like (reversal in *Allqokirus*; convergent with *Herpetotherium*);
154 (0). Posterior palatine spine: weak or absent and posterior edge of the palate concave posteriorly;
159 (0). Anteroposterior position of the sphenopalatine foramen relatively to the molars: above penultimate or antepenultimate molar [reversal in ((*Borhyaena*, *Arctodictis*) (*Australohyaena* (*Thylacosmilus* (*Callistoe*, *Paraborhyaena*)))); convergent with *Monodelphis* and (*Dasyurus*, *Thylacinus*)];
228 (2). Tuberculum tympani: expanded in a sharp anteroventrally directed process (triangular in lateral view) [reversal in (*Patene* (*Mayulestes*, *Allqokirus*)); convergent with (*Herpetotherium*, Marsupialia)];
251 (1). Axis, posterior extension of the neural process: distinctly longer than anterior extension [convergent with (*Dasyurus*, *Thylacinus*)];
252 (1). Ventral sagittal crest of axis: distinctly concave because of the development of a robust ventral process posteriorly (convergent with dasyuromorphians);
256 (1). C6 spinous process: lamina [convergent with (*Didelphis*, *Metachirus*), and (*Dasyurus*, *Thylacinus*)];
258 (2). First thoracic vertebra with a (relative to other vertebrae) tall spinous process: T3;

273 (1). Scapular notch: between 90 and 130° (convergent with *Metachirus*, and dasyuromorphians);
274 (1). Clavicle: absent;
293 (0). Shape of articular facet for the humerus on the radius: anteroposteriorly compressed (convergent with *Sminthopsis*, and *Asiatherium*);
301 (1). Length of the iliac neck: short, less than 15% the total pelvis length;
304 (1). Epipubic bones: absent (convergent with *Thylacinus*);
306 (1). Torsion between proximal and distal epiphyses of femur: absent [reversal in *Lycopsis*, and (*Australohyaena* (*Thylacosmilus* (*Callistoe*, *Paraborhyaena*))); convergent with didelphids];
310 (1). Ossified patella: present (convergent with *Amphiperatherium-Peratherium*); (personal observation of SL in *Peratherium cuvieri*, MNHN.F.GY679A);
320 (0). Anteroposterior length of the of the medial malleolus of the tibia at base relative to the greatest anteroposterior length of the distal epiphysis (as seen in distal view): subequal (convergent with *Sminthopsis*);
327 (1). Astragalus, medial extent of sustentacular facet: reaches the medial edge of the neck (reversal in Borhyaenoidea);
329 (1). Astragalus, width of astragalar neck: neck narrower or as wide as head;
334 (1). Calcaneus, longest dimension of ectal facet: anteroposterior.

One ambiguous synapomorphies (Deltran, slow) may also support the Deltatheroida + GTS + Sparassodonta clade
178 (2). Suprameatal foramen: at the same level or above postzygomatic crest (reversal in Mayulestidae, *Callistoe*; convergent with *Dromiciops*, *Sminthopsis*).

3) Clade GTS + Sparassodonta
Unambiguous synapomorphies of the GTS + Sparassodonta clade:
38 (1). Postmetacrista (on antepenultimate or penultimate molar): distinctly longer than preparacrista [convergent with *Deltatheridium*, *Nanocuris*, didelphids, (*Dasyurus*, *Thylacinus*), *Amphiperatherium-Peratherium*, stagodontids, (*Pediomys*, *Varalphadon*)];
54 (0). Conules wing-like cristae: present [convergent with (*Dasyurus*, *Thylacinus*)];
167 (1). Foramina for temporal rami: absent [reversal in *Mayulestes*, *Notogale*, (*Thylacosmilus* (*Callistoe*, *Paraborhyaena*)); convergent with (herpetoriids, Marsupialia), and stagodontids];
170 (0). Sagittal crest: extending to frontals (convergent with *Didelphis*);
175 (2). Proportions of the postglenoid process: very low and wider than high.

Twenty-two ambiguous synapomorphies may also support the clade GTS + Sparassodonta (Acctran, fast):
6 (1). Size of I3 vs I2: I3=I2 [reversal in (*Patene* (*Mayulestes*, *Allqokirus*)), in (*Thylacosmilus* (*Callistoe*, *Paraborhyaena*))); convergent with Australidelphia and stagodontids];
12 (1). Lower incisors procumbent: absent [convergent with (*Dasyurus*, *Thylacinus*), and *Didelphodon*];
23 (0). Diastema posterior to first upper premolar: absent [reversal in sparassodonts excluding (*Patene* (*Mayulestes*, *Allqokirus*)) but diastema lost in borhyaenoids excluding *Lycopsis* and reacquired in *Prothylacinus*];
24 (0). Diastema posterior to first lower premolar: absent (reversal in sparassodonts excluding (*Patene* (*Mayulestes*, *Allqokirus*)) and *Hondadelphys* but diastema lost in borhyaenoids without *Lycopsis*; convergent with *Sulestes*);
45 (0). Stylar cusp E: present and distinct [reversal in sparassodonts excluding (*Patene* (*Mayulestes*, *Allqokirus*)); convergent with pucadelphyids and *Alphadon-Turgidodon-Protalphadon*];
55 (1). Conules labiolingual position (on penultimate or antepenultimate molar): closer to para/metacone [reversal in sparassodonts excluding (*Patene* (*Mayulestes*, *Allqokirus*)); convergent with stagodontids];
64 (1). Size of ultimate lower molar: larger in height and/or length than penultimate molar [convergent with (*Dasyurus*, *Thylacinus*), and stagodontids];
66 (0). Lingual opening of trigonid basin on penultimate molar when possible: wide open: angle between protocristid (or postprotocristid when metaconid is lost) and paracristid more than 45° (convergent with *Nanocuris* and *Thylacinus*);
67 (1). Trigonid basin floor: sloping lingually;
68 (2). Trigonid proportions: longer than wide;
72 (1). Trigonid vs talonid length (on penultimate or antepenultimate molar): longer than talonid [convergent with (*Sulestes* (*Deltatheridium*, *Deltatheroides*)), (*Dasyurus*, *Thylacinus*), and stagodontids];
82 (1). Height of protoconid (Hpo) relative to length of ultimate or penultimate lower molar (Lm): Hpo/Lm > 0.9 [reversal in *Hondadelphys*; convergent with (*Deltatheridium*, *Deltatheroides*), and *Dasyurus*];
89 (1). Relative lengths of para- and protocristid: paracristid > protocristid (convergent with (*Nanocuris* (*Lotheridium* (*Sulestes* (*Deltatheridium*, *Deltatheroides*)))), and (herpetotheriids, Marsupialia)];
93 (1). Hypoconulid of last molar: taller than other talonid cusps [convergent with (*Pucadelphys*, *Andinodelphys*), and *Sminthopsis*];
102 (1). Postcingulid on last molar: absent [reversal in *Australohyaena*; convergent with (*Deltatheridium*, *Deltatheroides*), and (herpetotheriids, Marsupialia)];
103 (1). Depth/length of the dentary below molars: intermediate (between 1,5 and 2) (convergent with *Didelphodon*);
130 (1). Dorsoventral position of the medial palatal process of the premaxilla: with posterior end shifted dorsally, forming an incisive fossa (reversal in *Sipalocyon*, *Thylacosmilus*; convergent with dasyuromorphians);
160 (1). Development of pterygoids: well developed and expanded on medial side but no midline contact (reversal in *Mayulestes*, *Arctodictis*);

221 (1). Diameter of stapedius fossa: distinctly less than twice the size of that of the fenestra vestibuli (=small and shallow) [convergent with (*Herpetotherium*, Marsupialia) and stagodontids];
234 (1). Posttemporal sulcus on squamosal surface of petrosal: absent [reversal in *Sipalocyon*; convergent with (herpetotheriids, Marsupialia)].

Four ambiguous synapomorphies may also support the GTS + Sparassodonta clade (Deltran, slow):
159 (0). Anteroposterior position of the sphenopalatine foramen relative to the molars: above penultimate or antepenultimate molar [reversal in ((*Borhyaena*, *Arctodictis*) (*Australohyaena* (*Thylacosmilus* (*Callistoe*, *Paraborhyaena*)))); convergent with *Monodelphis* and *Thylacinus*];
181 (0). Transverse canal: absent [reversal in (*Notogale* ((*Sipalocyon*, *Cladosictis*), borhyaenoids)), but lost in ((*Borhyaena*, *Arctodictis*) (*Australohyaena* (*Thylacosmilus* (*Callistoe*, *Paraborhyaena*)))); convergent with *Pucadelphys*];
210 (1). Deep groove for internal carotid artery excavated in medial side of promontorium apex ventrally: present (convergent with pucadelphyids);
228 (1). Tuberculum tympani: moderately developed (lateral end of tympanic petrosal crest larger than medial one) (reversal in *Mayulestes*).

4) Pucadelphyidae
Unambiguous synapomorphies supporting Pucadelphyidae:
41 (1). Stylar cusp B subequal to or approaching the size of the paracone (convergent with GTS and stagodontids);
57 (3). Protocone size (on penultimate or antepenultimate molar), expanded posteriorly with posterolingual projection (convergent with Marsupialia);
85 (0). Metaconid larger than paraconid (on penultimate molar), in occlusal and lingual views;
214 (1). Tensor tympani fossa: distinct elongated fossa at anterolateral edge of promontorium (convergent with sparassodonts and *Thylacinus*).

Fifteen ambiguous synapomorphies (Acctran, fast) may also support the Pucadelphyidae
137 (2). Postorbital process: conspicuous protruding process [convergent with *Lotheridium*, sparassodonts (excluding *Patene* (*Mayulestes*, *Allqokirus*)), *Didelphis*, *Mimoperadectes-Peradectes*];
148 (0). Facial process of the lacrimal, large triangular and pointed anteriorly (convergent with GTS);
178 (1). Suprameatal foramen below postzygomatic crest [convergent with (*Patene* (*Mayulestes*, *Allqokirus*)), *Callistoe*, didelphids, (*Dasyurus*, *Thylacinus*)];
182 (0). Tympanic process of the alisphenoid, absent [convergent with (*Patene* (*Mayulestes*, *Allqokirus*)) and borhyaenoids];
193 (0). Secondary foramen ovale totally enclosed in the alisphenoid, absent [convergent with (*Patene* (*Mayulestes*, *Allqokirus*)), ((*Borhyaena*, *Arctodictis*) (*Australohyaena* (*Thylacosmilus* (*Callistoe*, *Paraborhyaena*)))), *Monodelphis*, *Dromiciops*, and *Dasyurus*];
228 (0). Tuberculum tympani: Absent (medial and lateral ends of tympanic petrosal crest equally developed) (convergent with *Mayulestes*);
245 (0). Ventral foramen at the base of the transverse process of the atlas, absent (convergent with dasyuromorphians);
263 (1). Mammillary processes (metapophyses) in third lumbar vertebra anterior to the last lumbar, present (convergent with dasyuromorphs);
296 (0). Distolateral process of scaphoid, absent;
311 (1). Parafibula, absent (convergent with didelphids);
314 (1). Proximal dimensions of tibia, subequal mesdiolaterally than anteroposteriorly (convergent with dasyuromorphs);
325 (1). Astragalus, visibility of medial plantar tuberosity of the astragalus in dorsal view, visible [convergent with Marsupialia, (*Callistoe, Paraborhyaena*), and *Eodelphis*];
350 (1). Ventral curvature of the tuber calcis, absent (convergent with *Sipalocyon*, and Marsupialia);
357 (1). Proximal ends of metatarsal II and III, Mt II extends more proximally than Mt III (convergent with dasyuromorphs);
363 (1). Ungual phalange, cleft [convergent with (*Borhyaena*, *Arctodictis*)].

Five ambiguous synapomorphies (Deltran, slow) may also support Pucadelphyidae (Deltran, slow)
43 (1). Stylar cusp C present [convergent with (herpetotheriids, Marsupialia), and *Alphadon-Turgidodon-Protalphadon*];
47 (1). Shape of paracone and metacone, triangular (flat labial face) [convergent with (herpetotheriids, Marsupialia)];
50 (1). Centrocrista V-shaped [convergent with (herpetotheriids, Marsupialia)];
95 (0). Entoconid conical (convergent with *Dromiciops*, and *Amphiperatherium-Peratherium*);
210 (1). Deep groove for internal carotid artery excavated in medial side of promontorium apex ventrally: absent [convergent with (GTS, sparassodonts)].

Discussion on the first set of analyses
The close relationships of deltatheroidans with sparassodonts, retrieved in this analysis (Fig. 49B, analysis with implied weighting), is not a true novelty, since Marshall & Kielan-Jaworowska (1992) proposed a phylogeny of metatherians, in which the deltatheroidans are the sister-group to all the other metatherians (i.e. the clade "c" on their figure 4 grouping Borhyaenoidea, Stagodontidae, and other Marsupialia). This result is similar to that of Wilson *et al.* (2016: fig. 3), in which the clade grouping deltatheroidans and *Pappotherium* is the sister-group of the Marsupialiaformes, the latter corresponding to the clade "f" of Marshall & Kielan-Jaworowska

(1992: fig. 4). Given the taxa taken into account by Marshall & Kielan-Jaworowska (1992), their hand-generated tree is almost identical to that of Wilson *et al.* (2016) retrieved with TNT.

However, the result retrieved here (Fig. 49B) differs from all other hypotheses in placing the deltatheroidans as a sister-group of a GTS + Sparassodonta clade. This new position of the deltatheroidans has been induced by the inclusion of new taxa in the original matrix of Muizon *et al.* (2018) such as *Itaboraidelphys* and several taxa of Asiatic and North American deltatheroidans. In contrast, the addition of the Operational Taxonomic Unit (OTU), *Alphadon-Turgidodon-Protalphadon* and *Pediomys* likely had little effect on the topology of our strict consensus tree. The difference between our tree and that of Wilson *et al.* (2016) probably results from our character list, which, following Forasiepi *et al.* (2015), is "sparassodont oriented" (with 17 sparassodont taxa and characters more representative of the order), whereas Wilson *et al.* (2016), following Rougier *et al.* (2015), treated the order as a single OTU, "borhyaenids". This choice probably created a bias in their analysis at the level of the relationships of various taxa or clades close to the sparassodonts. Be that as it may, the close relationships of deltatheroidans (retrieved by Wilson *et al.* 2016) with a clade placing the GTS as a sister group of the sparassodonts and Pucadelphyidae – i.e. their clade (GTS (borhyaenoids (*Mayulestes* (*Jaskhadelphys* (*Andinodelphys Pucadelphys*))))) – is not so far from an alternative grouping in which deltatheroidans would be included in the Pucadelphyda, as it is the case in our analysis (see above p. 686). In other words, the group including deltatheroidans and GTS + pucadelphydans retrieved by Wilson *et al.* (2016) is only paraphyletic, not polyphyletic and given the numerous biases (character definition, scoring, missing data, functional complexes and associated characters, homoplasies…) of phylogenetic analyses, in some cases, one single modification in character scoring or addition of a new character may induce displacement of loss of one node, a modification which may turn paraphyly into monophyly.

The new position of the deltatheroidans, and the direct sister-group relationship of the GTS (from the Late Cretaceous of Mongolia) and the South American sparassodonts brings strong support to Forasiepi (2009)'s hypothesis that sparassodonts may have their origin in the Late Cretaceous. Furthermore, the Laurasian nature of the deltatheroidans (Asia and North America) and GTS (Mongolia), implies that the Pucadelphyidae and Sparassodonta appeared either in Asia or in North America and migrated separately to South America. Although perfectly possible, this alternative is clearly less parsimonious than a single southward migration of a common ancestor of the clade Pucadelphyidae + Sparassodonta (= Pucadelphyda) and a South American radiation of the Pucadelphyda as proposed previously by Muizon *et al.* (2018). If the palaeobiogeographical scenario resulting from this analysis is correct (although less parsimonious), then Pucadelphyidae and Sparassodonta were very probably present in North America at least during the Late Cretaceous. So far, none of them have been recognized yet in this subcontinent. An intent of identifying sparassodonts in North America has been proposed by Carneiro (2018), who described *Varalphadon janetae* from the early Late Cretaceous of Utah and suggested that the genus *Varalphadon* could be included in the order. However, and unfortunately, because neither *V. janetae,* nor the other species of *Varalphadon* (*V. creber, V. wahweapensis*) exhibit any of the sparassodont dental features (the three species are known by dental remains only), this hypothesis was regarded as doubtful by Muizon *et al.* (2018: 430). As discussed above, our present analysis confirms this interpretation.

It is noteworthy, however, that deltatheroidans are present in North America. *Deltatheroides* is possibly present in the Late Cretaceous of Alberta (Fox 1974), and several taxa referred to deltatheroidans have been recently recorded in North America, such as *Atokatheridium*, *Oklatheridium*, and *Nanocuris* (Kielan-Jaworowska & Cifelli 2001; Fox *et al.* 2007; Davis *et al.* 2008; Wilson & Riedel 2010). They are represented by fragmentary and scarce dental remains and have been included in our data matrix in spite of their incompleteness. However, they present characters shared by deltatheroidans and sparassodonts such as the reduced metaconid, the labially expanded (strongly convex at mid-height) protoconid, the para- and metaconid widely separated and not adjoined at base, the paracone and metacone adjoined at base, and the well-developed postmetacrista. Nevertheless, because of the available material (teeth only), no cranial characters are taken into account to support their inclusion within the deltatheroidans or their non-inclusion within the sparassodonts. Therefore, given the poor data available for these taxa, it is perfectly conceivable that, if some more complete specimens were discovered (especially including some cranial remains), they may very well prove to be referable to sparassodonts rather than deltatheroidans. In the case of *Nanocuris*, the reduction of the last lower molar (Wilson & Riedel 2010: fig. 2) is shared with deltatheroidans but not with sparassodonts, which would preclude this taxon from being included in sparassodonts, but *Atokatheridium* and *Oklatheridium*, which feature dental characters shared by deltatheroidans and sparassodonts are potential candidate for being regarded as North American early derived sparassodonts. As a matter of fact, the basal position of these two genera in the deltatheroidan clade of our tree, could be an indication that they may not be so distant from the sparassodonts. The position of the GTS, placed between deltatheroidans and sparassodonts, is also significant. This remarkably preserved skull is probably one of the best-preserved therian skull ever discovered in the Late Cretaceous and, even though, still remains to be thoroughly described. Therefore, a better knowledge of the anatomy of this specimen may either confirm its sister-group relationship with the sparassodonts or may result in a capture of its branch by the deltatheroidans. In this context, we are reluctant to take a formal decision on the taxonomic position of the GTS although its upper molars morphology certainly better fits that of sparassodonts than that of deltatheroidans. Nevertheless, it is noteworthy that the sister group relationship of the GTS with stagodontids retrieved in the strict consensus tree (although poorly supported here) is that recovered by Rougier *et al.* (1998 and 2004).

The search for Pucadelphyidae (or pucadelphyid relatives) in North America is not simple, but a potential candidate exists in the Campanian genus *Aenigmadelphys*. *A. archeri* is known by isolated upper (M1, M2, M3, and M4) and lower (m3 and m4) molars from the Kaiparowits Formation of Utah (Cifelli & Johanson 1994). Although it exhibits more primitive dental features than the Tiupampa Pucadelphyidae, *Aenigmadelphys* matches relatively well a possible pucadelphyid ancestral morphotype. It is clearly smaller than *Pucadelphys* and *Andinodelphys* but approaches the size (although still slightly smaller) of *Mizquedelphys*. In general shape, the teeth of *Aenigmadelphys* are more gracile than the robust teeth of *Pucadelphys* and *Andinodelphys*, but approach the slenderness of those of *Mizquedelphys*. The upper molars differ from pucadelphyids in having a paracone larger than the metacone (it is smaller in pucadelphyids), a mesiodistally shorter protocone, and a slightly deeper ectoflexus. The upper molars resemble each other in the stylar cusp C absent or small (although more developed in pucadelphyids) and the generally well-developed stylar cusps B and D, the former being always larger than the latter. They also resemble each other in their slightly V-shaped centrocrista (a feature slightly more pronounced, however, in pucadelphyids) and in the lingually placed conules (i.e. in occlusal, view placed closer to the apex of the protocone than to those of the paracone and metacone). On the lower molars (referred specimens OMNH 20531, 20612, Cifelli 1990: fig. 2H-M, see Kielan-Jaworowska *et al.* 2004: 454L), the major difference between *Aenigmadelphys* and pucadelphyids is the smaller size difference between the paraconid and the metaconid, in the former than in than in the latter (i.e. the paraconid is much smaller relative to the metaconid in pucadelphyids than in *Aenigmadelphys*). This possible relationship will be analized in a work in progress by the authors on the partial skull of *Incadelphys* (MHNC 13906) mentioned above.

Results of second set of analyses excluding dental characters

As mentioned above, because several clades considered in this study include highly carnivorous taxa (sparassodont, stagodontids, deltatheroidans, and dasyuroids) it is possible that the results of our analyses with all characters may be partly forced by the dental characters related to this ecology, which are well known to be highly homoplastic (e.g., Muizon & Lange-Badré 1997; Ladevèze *et al.* 2011; Sansom *et al.* 2017; Solé & Ladevèze 2017). For instance, some of the synapomorphies shared by deltatheroidans, GTS, and sparassodonts are actually dental convergences with stagodontids. These are linked to carnivorous adaptations: metaconid lower than paraconid [84 (2)], metaconid smaller in volume than paraconid [85 (2)]. Likewise, the GTS shares dental features with sparassodonts, which are convergences with stagodontids: postmetacrista distinctly longer than preparacrista [38 (1)], ultimate lower molar larger in height and/or length than penultimate molar [64 (1)], trigonid longer than talonid [72 (1)].

Furthermore, studies of Sansom *et al.* (2017: 819) have shown that "dental morphology is found to convey a phylogenetic signal that is different to that derived from osteology and is comparatively less consistent with molecular data". These authors concluded that dental data alone are generally found to be less likely to reconstruct phylogenetic relationships accurately given their incongruence with osteological and molecular characters.

In our present case, we suspect that dental characters conveyed a misleading phylogenetical signal in our first set of analyses (combining dental and osteological characters). It is however difficult to securely evaluate all those that are clearly related to hypercarnivory, because dental characters are diverse and many of them probably interrelated. Therefore, in a second set of analyses, we decided, in a first step, to remove all our dental characters (1-102), retaining only the dentary, cranial, and postcranial characters, and thus not following recommendation by Sansom *et al.* (2017: 819) (but see below our third set of analyses). Consequently, we also had to remove all the taxa known by teeth only or teeth with incomplete dentaries (i.e. *Kokopellia, Deltatheroides, Atokatheridium, Oklatheridium, Nanocuris, "Alphadon-Turgidodon-Protalphadon", Varalphadon*, and *Patene*).

A heuristic analysis of the 262 remaining characters and the 37 ingroup taxa resulted in 2181 equally parsimonious trees with the following indices: L = 999, CI = 0.331, RI = 0.645 and a strict consensus tree (Fig. 50A) with the following indices: L = 1131, CI = 0.293, RI = 0.575. This tree is poorly resolved, but two major clades are preserved, the sparassodonts and the clade (*Amphiperatherium-Peratherium* (*Herpetotherium*, Marsupialia)). These two clades have unresolved relationships with the other ingroup taxa.

In order to obtained a better resolution of our tree we performed another analysis with downweighted homoplastic characters (Goloboff k = 3). The consensus tree (CI = 0.331, RI = 0.644) of the nine equally parsimonious trees obtained is provided in Fig. 50B. The clade Pucadelphyda *sensu* Muizon *et al.* (2018) is retrieved, and *Deltatheridium* and *Asiatherium* are basal within Metatheria. The stagodontids *(Didelphodon + Eodelphis)* are sister group of *Pediomys*, and this clade is part of a larger clade including the marsupials, *Mimoperadectes, Amphiperatherium-Peratherium*, and *Herpetotherium*. Interesting novelty (as compared to the first analyses) is the presence of the GTS as a sister group of the Pucadelphyda (not of the sparassodonts as in the first analysis of Fig. 49B). A clade comprising *Lotheridium* and *Sulestes* is separate from *Deltatheridium* (i.e. not included in deltatheroidans) and is the sister group of the GTS + Pucadelphyda clade. However, we suspect that the polyphyly of deltatheroidans, retrieved in this analysis, could be an artefact because most of the deltatheroidan synapomorphies are dental, and therefore not taken into account here. As in the previous analyses with the complete character set, *Itaboraidelphys* is included in Pucadelphyidae, although its relationships with *Andinodelphys* and *Pucadelphys* are unresolved. Hathliacynidae is monophyletic, whereas it was paraphyletic in the previous analyses with all characters.

In spite of the splitting of deltatheroidans (probably an artefact), which represents a small incongruence with most earlier phylogenies, this analysis sheds light on the results of the first analyses. The position of Stagodontidae retrieved in the second analyses (Fig. 50A, B) indicates that its position in the consensus of the first set of analyses (Fig. 49A), as a sister group (with the GTS) of the sparassodonts, was controlled by dental (molar) characters (38, 46, 54, 55, 64, 72) probably (or possibly) related to hypercarnivory, which are well known to be highly homoplastic. Similarly, deltatheroidans (*Deltatheridium* on the one hand and *Lotheridium-Sulestes* on the other) and the GTS, which are now successive sister groups of Pucadelphyda were, in the first set of analyses, retrieved placed between the Pucadelphyidae and Sparassodonta (thus splitting Pucadelphyda *sensu* Muizon *et al.* 2018) (Fig. 49A). This topology was also induced by dental (molar) characters (33, 39, 47, 48, 50, 57, 70, 71, 80, 84, 85, 95, 97), which are also probably or possibly related to hypercarnivory. Here (Fig. 50B), the position of the stagodontids and that of the GTS and deltatheroidans are supported by cranial, dentary, and postcranial characters only. It is noteworthy that the branching of the GTS, as the sister group of Pucadelphyda, is congruent with that retrieved by Wilson *et al.* (2016).

Below we provide the unambiguous synapomorphies of the following clades resulting from the second analysis (without dental characters, implied weighting, Fig. 50B): 1) GTS + Pucadelphyda, and 2) Pucadelphyda (as retrieved in this second analysis), We also provide the ambiguous synapomorphies with both Acctran and Deltran optimisations. The strict synapomorphies are in bold. Only the unambiguous synapomorphies are fully detailed. For the ambiguous synapomorphies we only indicate the subsequent reversals and convergences.

Unambiguous synapomorphies supporting the GTS + Pucadelphyda clade:

210 (1). Deep groove for internal carotid artery excavated in medial side of promontorium apex ventrally: present.

Three ambiguous synapomorphies (Acctran, fast) also support the GTS + Pucadelphyda clade

104 (2). Ventral margin of the dentary behind last molar continuous to condyle, straight;

148 (0). Anterior medial and lateral palatal processes of the maxilla approximately of the same size (reversal in sparassodonts);

170 (0). Sagittal crest extending to frontals [reversal in pucadelphyids; convergent with (*Pediomys*, stagodontids), and *Didelphis*).

One ambiguous synapomorphy (Deltran, slow) also supports the GTS + Pucadelphyda clade:

135 (0). Naso-frontal suture, acute W- or V-shaped [reversal in sparassodonts without *Allqokirus* and *Mayulestes*; convergent with ((*Pediomys*, stagodontids), (herpetotheriids, Marsupialia))].

Unambiguous synapomorphies supporting Pucadelphyda:

120 (1). Length of the rostrum between ⅓ and ½ total length of the skull [reversal in borhyaenoids but reversed back in *Lycospis* and (*Callistoe* (*Paraborhyaena*, *Thylacosmilus*)); convergent with (herpetotheriids, Marsupialia)];

178 (2). Suprameatal foramen at the same level or above postzygomatic crest [reversal in sparassodonts without *Allqokirus* and *Mayulestes*, but reverse in *Callistoe*; convergent with didelphids, and (*Dasyurus*, *Thylacinus*)];

182 (0). Tympanic process of the alisphenoid, absent [reversal in (*Hondadelphys* (*Sallacyon* (*Notogale*, *Sipalocton*, *Cladosictis*)))];

193 (0). Secondary foramen ovale totally enclosed in the alisphenoid, absent [reversal in sparassodonts without *Allqokirus* and *Mayulestes*, but reversed back in ((*Borhyaena*, *Arctodictis*), (*Australohyaena* (*Callistoe* (*Paraborhyaena*, *Thylacosmilus*)))); convergent with *Monodelphis*, *Dromiciops*, and *Dasyurus*];

214 (1). Tensor tympani fossa distinct elongated at anterolateral edge of promontorium (convergent with *Thylacinus*).

No ambiguous synapomorphy (Acctran, fast) supports Pucadelphyda but fifteen ambiguous synapomorphies (Deltran, slow) may also support Pucadelphyda:

104 (2). Ventral margin of the dentary behind last molar continuous to condyle, straight [reversal in ((*Borhyaena*, *Arctodictis*), (*Australohyaena* (*Callistoe* (*Paraborhyaena*, *Thylacosmilus*))))];

155 (1). Size of foramen or groove in lateral edge of postpalatine torus, present and small (less than half the diameter of the minor palatine foramen or groove) [convergent with ((*Pediomys*, stagodontids), (herpetotheriids, Marsupialia))];

161 (0). Posterior process of pterygoids, which covers the alisphenoid-basisphenoid suture: present (convergent with *Thylacinus*);

198 (1). Size of jugular foramen relative to fenestra cochleae: at least three times larger (convergent with *Herpetotherium*, *Didelphis*, and dasyuromorphs);

248 (1). Shape of the cranial facets of atlas: dorsal third of the facet much more concave than the ventral two thirds and strongly inflected medially [reversal in (*Borhyaena*, *Arctodictis*), *Prothylacinus*; convergent with didelphids and (*Dasyurus*, *Thylacinus*)];

260 (1). Foramen on dorsal arch of last lumbar vertebra, present [reversal in *Arctodictis*; convergent with (*Dasyurus*, *Thylacinus*)];

262 (1). Ventral median keel on anterior lumbar vertebrae, present (reversal in *Prothylacinus*; convergent with *Metachirus*, *Dromiciops*, *Thylacinus*);

272 (1). Infraspinous/supraspinous fossa width at the level of the neck: supraspinous fossa narrower reversal in *Sipalocyon*, *Arctodictis*, *Callistoe*; convergent with *Dromiciops*);

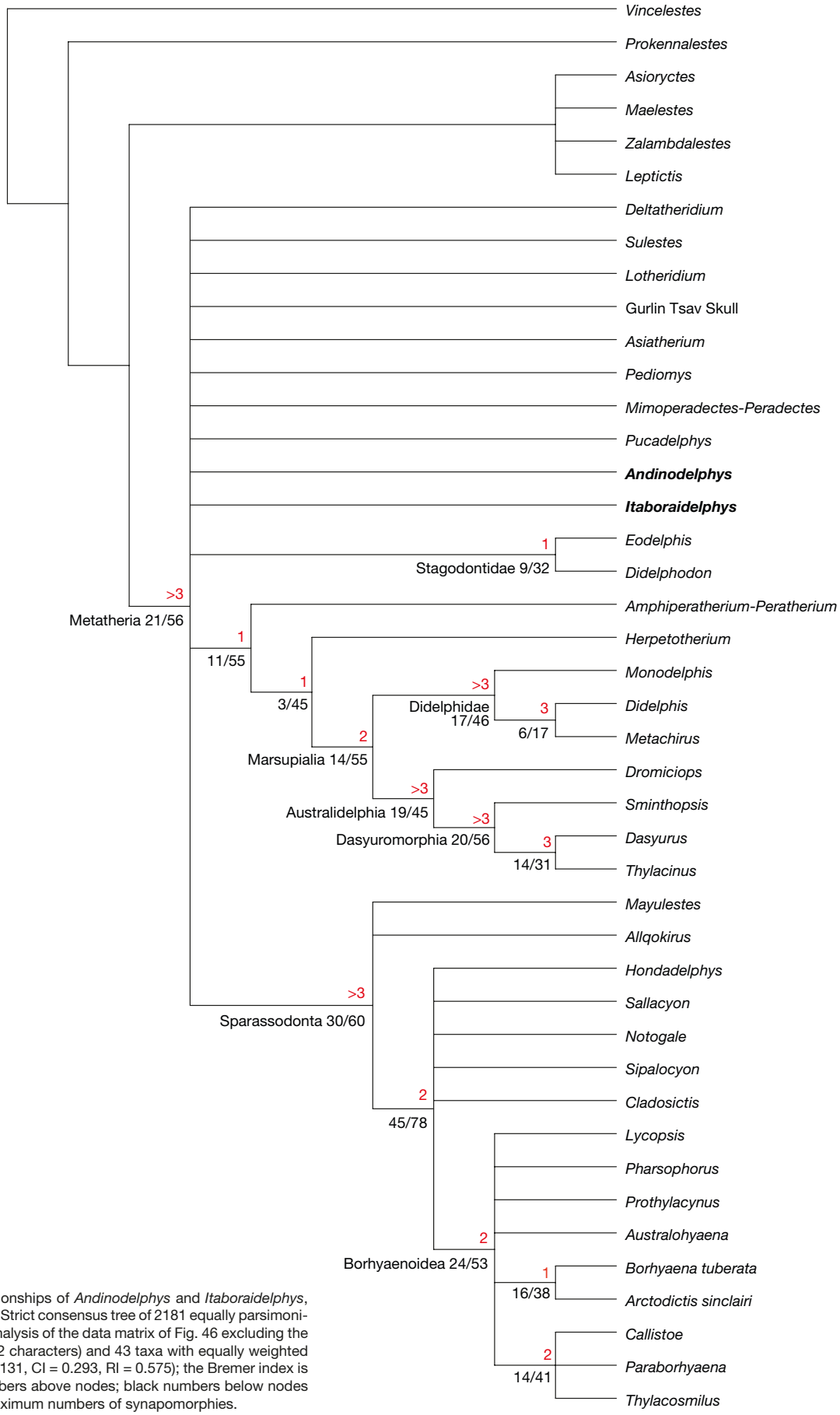

FIG. 50. — Phylogenetic relationships of *Andinodelphys* and *Itaboraidelphys*, among other metatherians: **A**, Strict consensus tree of 2181 equally parsimonious trees resulting from the analysis of the data matrix of Fig. 46 excluding the 102 dental characters (i.e. 262 characters) and 43 taxa with equally weighted homoplastic characters (L = 1131, CI = 0.293, RI = 0.575); the Bremer index is given at branches in red numbers above nodes; black numbers below nodes indicate the minimum and maximum numbers of synapomorphies.

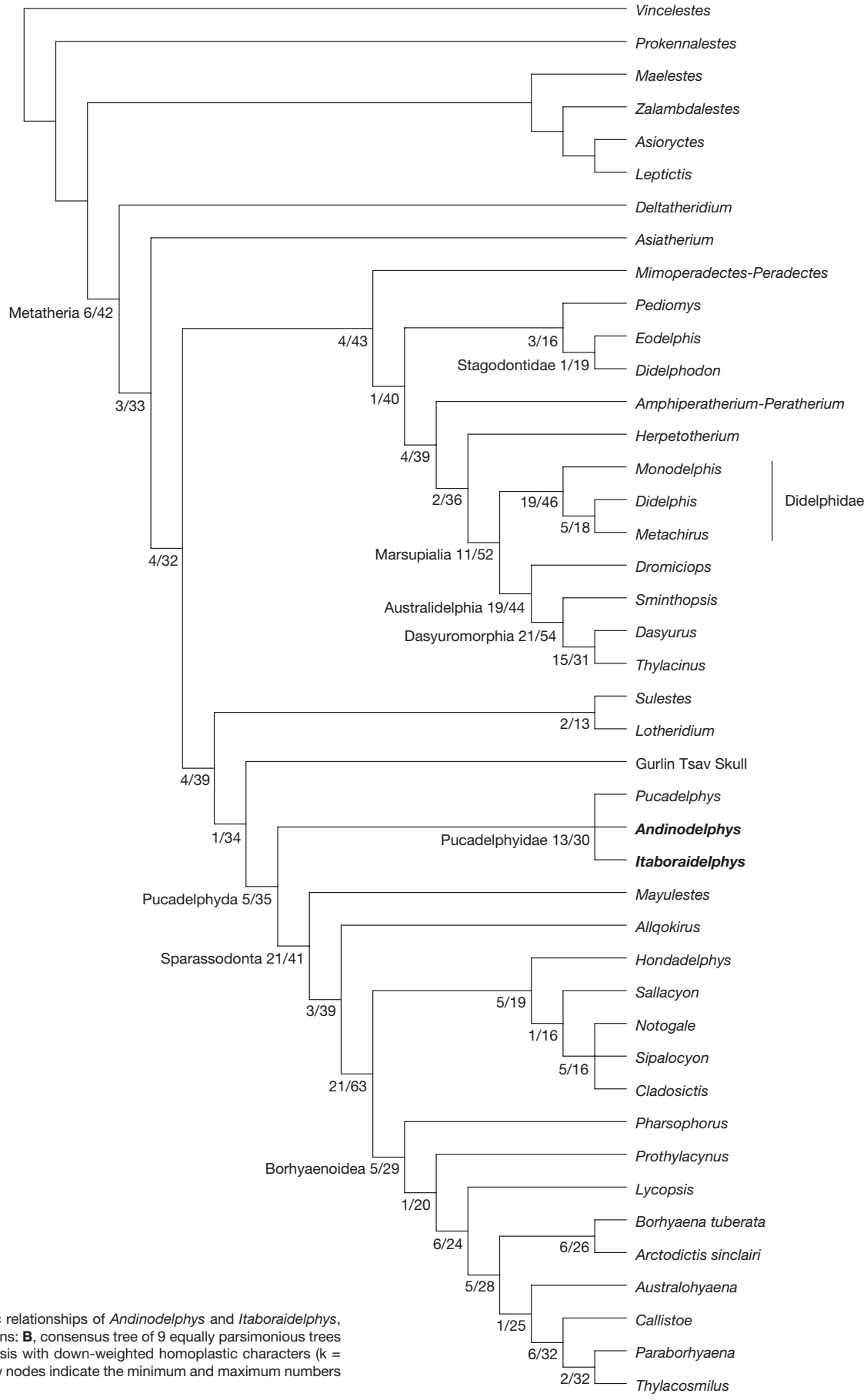

FIG. 50. — Phylogenetic relationships of *Andinodelphys* and *Itaboraidelphys*, among other metatherians: **B**, consensus tree of 9 equally parsimonious trees resulting from the analysis with down-weighted homoplastic characters (k = 3); black numbers below nodes indicate the minimum and maximum numbers of synapomorphies.

282 (1). Extension of the deltoid crest: reaches distal half of the humerus (convergent with didelphids);
287 (1). Lateral extension of capitulum, present: straight with a flat shelf and/or a salient crest [convergent with (*Didelphis*, *Metachirus*) and *Thylacinus*];
303 (2). Iliac and gluteus fossae: gluteus fossa larger;
331 (1). Astragalus: dorso-distal tuber of the head, present;
353 (0). Spatial relationship between navicular and entocuneiform: entocuneiform distal to navicular (convergent with dasyuromorphs);
360 (1). Mt III thickness relative to that of Mt I: Mt III thinner than Mt I (convergent with dasyuromorphians).

Discussion on the second set of analyses

The present topology resulting from the analysis of dentary, cranial and postcranial characters only (Fig. 50B) sustains monophyly of the South American metatherian carnivorous radiation (Pucadelphyda) suggested by Muizon *et al.* (2018) and concur with the close relationships of the Pucadelphyda with the GTS retrieved by Wilson *et al.* (2016). Given the great overall similarity existing between the Tiupampa pucadelphyids and mayulestids, this hypothesis appears more likely than the surprising result obtained with the full set of characters (Fig. 49B). It suggests that the pucadelphydans may have had their origin in a GTS-like or *Lotheridium*-like metatherian ancestral group in the Late Cretaceous of Asia and/or North America (although as yet unknown in North America) with no close relationships with *Deltatheridium* (as well as, possibly, *Deltatheroides*). In contrast to the analysis with the whole set of characters, this analysis is, therefore, biogeographically more parsimonious, since a single southward migration of an ancestral pucadelphydan is possible with a local radiation in South America.

Results of the third analyses excluding some dental characters

The second set of analyses has resolved some surprising results found in the first set of analyses but supported polyphyly of Deltatheroida, which contradicts all previous studies (e.g. Rougier *et al.* 1998, 2004, 2015; Luo *et al.* 2003; Williamson *et al.* 2014; Bi *et al.* 2015; Wilson *et al.* 2016). As mentioned above, this result is a probable artefact related to the lack of dental characters, considering that deltatheroidans are essentially defined by dental characters (see above).

Therefore, in order to minimize the impact of a drastic exclusion of all the dental characters, we have performed a third set of analyses excluding only the dental characters mentioned above (p. 695) that support the close relationships of stagodontids, deltatheroidans and sparassodonts and which are possibly or probably related to hypercarnivory. Because dental carnivorous adaptations of metatherians are generally focused on molars, we excluded only the 19 molars characters supporting these close relationships (i.e. 33, 38, 39, 46, 47, 48, 50, 54, 55, 57, 64, 70, 71, 72, 80, 84, 85, 95, 97). As in the second set of analyses, we have excluded the taxa (or OTU) represented solely (or essentially solely) by dental remains, i.e. *Atokatheridium, Oklatheridium, Deltatheroides, Nanocuris, Kokopellia, Varalphadon,* and *Alphadon-Turgidodon-Protalphadon*. However, we have retained *Patene*, which is known, besides teeth, by a complete dentary (*P. coloradensis*). A heuristic analysis of the 345 remaining characters and the 38 ingroup taxa resulted in 12 equally parsimonious trees with the following indices: L = 1436, CI = 0.316, RI = 0.649 and a strict consensus tree (Fig. 51A) with the following indices: L = 1525, CI = 0.298, RI = 0.618. This tree is still poorly resolved but retains the clades (*Amphiperatherium-Peratherium* (*Herpetotherium*, Marsupialia)) and Sparassodonta. Furthermore, deltatheroidans are monophyletic.

The analysis with downweighted homoplastic characters (Goloboff k = 3) resulted in one single tree (CI = 0.315, RI = 0.647), in which the pucadelphydans are monophyletic (Fig. 51B). In this hypothesis, deltatheroidans are placed in a paraphyletic stem assemblage of the clade Metatheria. *Lotheridium* is sister group to a clade that comprises Pucadelphyda (*sensu* Muizon *et al.* 2018) and a clade including Marsupialia and their stem fossil relatives. In the latter, peradectids are sister group of a clade including stagodontids and (*Pediomys*, *Asiatherium*). This clade is the sister group of (herpetotheriids, Marsupialia), this assemblage being closely related to the GTS. The main differences with the preceding analysis are the basal position of the deltatheroidans (even if paraphyletic) and the position of the GTS, sister group of a clade of Laurasiatian taxa, with no close relationships with the South American clade Pucadelphyda.

Below we provide the unambiguous synapomorphies of the following clade Pucadelphyda resulting from the implied weighting analysis (Fig. 51B). We also provide the ambiguous synapomorphies with accelerated (Acctran) and delayed (Deltran) optimisations. The strict synapomorphies are in bold. Only the unambiguous synapomorphies are fully detailed. For the ambiguous synapomorphies we only indicate the subsequent reversals and convergences.

Unambiguous synapomorphies supporting the Pucadelphyda in this analysis:

104 (2). Ventral margin of the dentary behind last molar continuous to condyle, straight [reversal in borhyaenoids excluding Lycopsis; convergent with Didelphodon and Australidelphia];
120 (1). Length of the rostrum between ⅓ and ½ total length of the skull [reversal in borhyaenoids excluding Lycopsis, but then reversed back in (Thylacosmilus (Callistoe, Paraborhyaena)); convergent with (herpetotheriids, Marsupialia)];
161 (0). Posterior process of pterygoids, which covers the alisphenoid-basisphenoid suture: present (convergent with Thylacinus);
198 (1). Size of jugular foramen relative to fenestra cochleae: at least three times larger (convergent with Herpetotherium, Didelphis, and dasyuromorphs);
214 (1). Tensor tympani fossa distinct elongated at anterolateral edge of promontorium ((convergent with Thylacinus and didelphids);

260 (1). Foramen on dorsal arch of last lumbar vertebra, present [reversal in (Callistoe, Paraborhyaena); convergent with dasyuromorphs];
262 (1). Ventral median keel on anterior lumbar vertebrae, present (reversal in Prothylacinus; convergent with Metachirus, Dromiciops, and Thylacinus);
272 (1). Supraspinous fossa narrower than infraspinatus fossa at the level of the scapular neck [reversal in Sipalocyon and ((Borhyaena, Arctodictis), (Australohyaena (Thylacosmilus (Callistoe, Paraborhyaena)))); convergent with Dromiciops];
282 (1). Extension of the deltoid crest: reaches distal half of the humerus (convergent with didelphids);
287 (1). Lateral extension of capitulum, present: straight with a flat shelf and/or a salient crest [convergent with (Didelphis, Metachirus) and Thylacinus];
303 (2). Iliac and gluteal fossae: gluteal fossa larger (convergent with Metachirus and dasyuromorphians);
331 (1). Astragalus: dorso-distal tuber of the head, present;
353 (0). Spatial relationship between navicular and entocuneiform: entocuneiform distal to navicular (convergent with dasyuromorphs);
360 (1). Mt III thickness relative to that of Mt I: Mt III thinner than Mt I (convergent with dasyuromorphs).

Ten ambiguous synapomorphies (Acctran, fast) may also support the Pucadelphyda in this analysis:

1 (0). Number of upper incisors, five [reversal in Sparassodonta excluding Mayulestidae; convergent with (herpetotheriids, Marsupialia)];
3 (1). I1s roots diverging dorsally [reversal in Sparassodonta excluding Mayulestidae; convergent with (herpetotheriids, Marsupialia)];
154 (1). Posterior palatine spine, absent and posterior edge of the palate straight [reversal in Mayulestidae; convergent with (herpetotheriids, Marsupialia)];
156 (1). Morphology of the postpalatine torus foramen, wide-open groove (the section is approximately half a circle or less) (reversal in Andinodelphys; convergent with dasyuromorphs);
178 (1). Suprameatal foramen, below postzygomatic crest [reversal in Sparassodonta excluding Mayulestidae; convergent with didelphids and (Dasyurus, Thylacinus)];
283 (1). Distal end of deltoid crest, forming a distinct angle or process [reversal in Sparassodonta excluding Mayulestidae; convergent with Dromiciops, Dasyurus, and (Didelphis, Metachirus)];
315 (1). Tibia shape, straight (reversal in Mayulestidae; convergent with Thylacinus);
331 (1). Astragalus: dorso-distal tuber of the head, present;
353 (0). Entocuneiform distal to navicular (convergent with dasyuromorphs);
354 (1). Navicular facet of ectocuneiform parallel to the distal metatarsal facet [reversal in ((Borhyaena, Arctodictis), (Australohyaena (Thylacosmilus (Callistoe, Paraborhyaena))))];

Four ambiguous synapomorphies (Deltran, slow) may also support Pucadelphyda in this analysis:

155 (1). Size of foramen or groove in lateral edge of postpalatine torus, present and small (less than half the diameter of the minor palatine foramen or groove) [convergent with ((peradectids (((Asiatherium, Pediomys), stagodontids)), (herpetotheriids, Marsupialia)))];
210 (1). Deep groove for internal carotid artery excavated in medial side of promontorium apex ventrally, present (convergent with GTS)
248 (1). Shape of the cranial facets of atlas: dorsal third of the facet much more concave than the ventral two thirds and strongly inflected medially [reversal in Prothylacinus, and (Borhyaena, Arctodictis); convergent with didelphids and (Thylacinus, Dasyurus)];
300 (1). Tuberosity for the rectus femoris muscle, protuberance (convergent with dasyuromorphs);

Discussion on the third set of analyses

The result of the third set of analyses (implied weighting analysis – Figs 51B; 52) is favoured here. They concord with those of Rangel *et al.* (2019) as far as the Tiupampian taxa are concerned. *Andinodelphys* and *Pucadelphys* are sister taxa and both are included in a clade (Pucadelphyidae) that is sister to Sparassodonta. *Mayulestes* and *Allqokirus* are the earliest known sparassodonts. The relationships within the sparassodonts retrieved by Rangel *et al.* (2019) is very similar to those of Muizon *et al.* (2018) and to those obtained in this paper. Several minor discrepancies still remain however. The Itaboraian genus *Itaboraidelphys* is included by Rangel *et al.* (2019) in Notometatheria, as the sister taxon of *Didelphopsis,* both taxa forming the sister group of Herpetotheriidae. Our analyses place *Itaboraidelphys* within Pucadelphyidae as the sister taxon to the clade (*Andinodelphys, Pucadelphys*). In fact, this difference is obviously related to our hypothesis to refer the two Type II Itaboraí petrosals to *Itaboraidelphys* (following Muizon *et al.* [2018]), what Rangel *et al.* (2019) did not. Another difference is in the non-recognition of the taxon Mayulestidae *sensu* Muizon *et al.* (2018) that is including *Allqokirus, Mayulestes,* and *Patene.* However, it is noteworthy that Rangel *et al.* (2019) retrieved a paraphyletic Mayulestidae, which, in our point of view, is not drastically different from a monophyletic family. In fact, given the elevated number of dental characters of their data matrix and the total absence of cranial characters for *Patene*, it is possible that, if relevant cranial remains of *Patene* (or a closely related taxon) are discovered, given the phylogenetic closeness of the three genera, they could very well provide essential data in favour of a monophyletic Mayulestidae *sensu* Muizon *et al.* (2018). Furthermore, surprisingly, Rangel *et al.* (2019) restricted the family Mayulestidae to the genus *Mayulestes*, instead of retaining a paraphyletic "Mayulestidae" including the three genera as defined by Muizon *et al.* (2018), whereas they retained a paraphyletic family "Hathliacynidae" (represented in

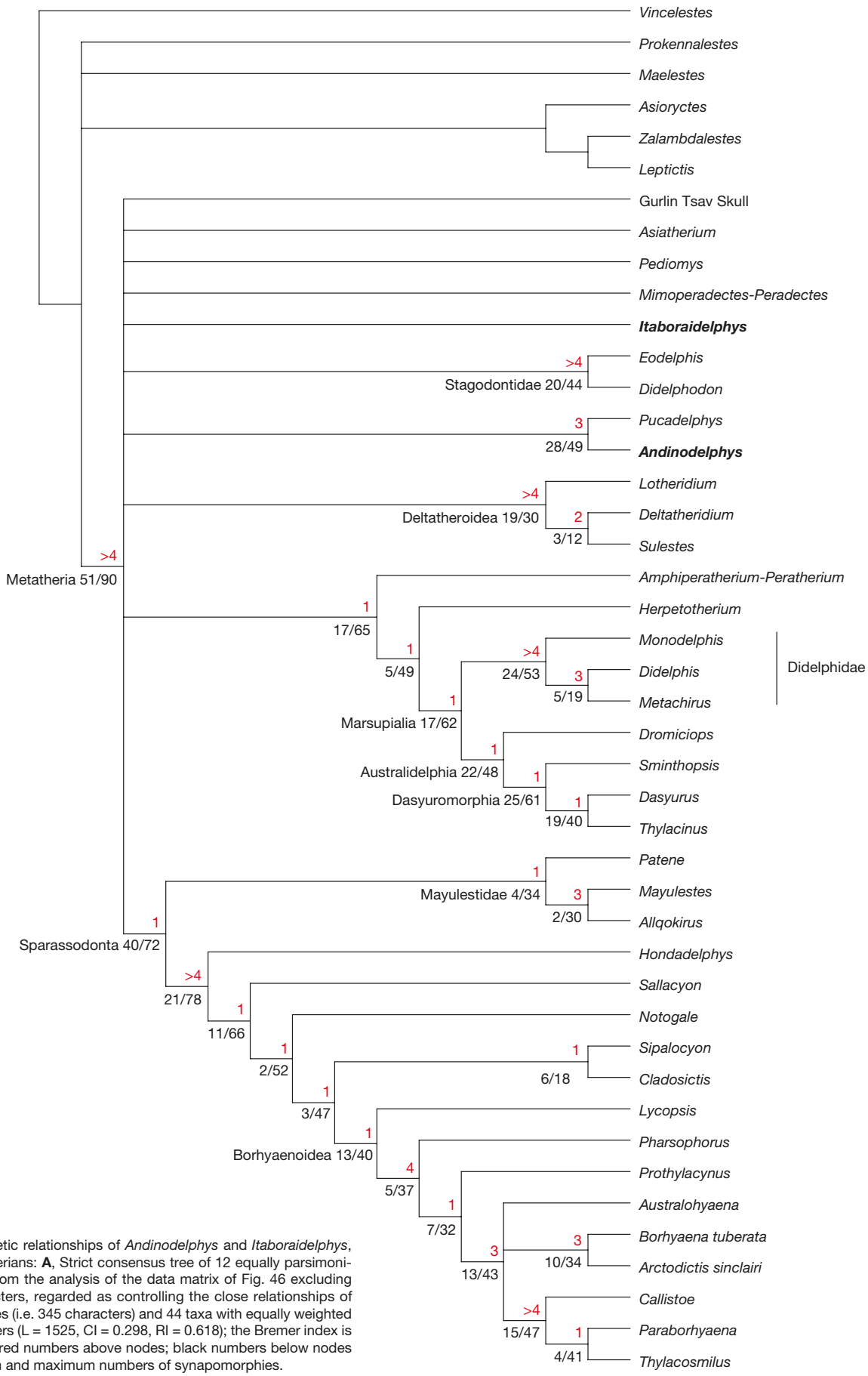

FIG. 51. — Phylogenetic relationships of *Andinodelphys* and *Itaboraidelphys*, among other metatherians: **A**, Strict consensus tree of 12 equally parsimonious trees resulting from the analysis of the data matrix of Fig. 46 excluding the 19 dental characters, regarded as controlling the close relationships of the carnivorous clades (i.e. 345 characters) and 44 taxa with equally weighted homoplastic characters (L = 1525, CI = 0.298, RI = 0.618); the Bremer index is given at branches in red numbers above nodes; black numbers below nodes indicate the minimum and maximum numbers of synapomorphies.

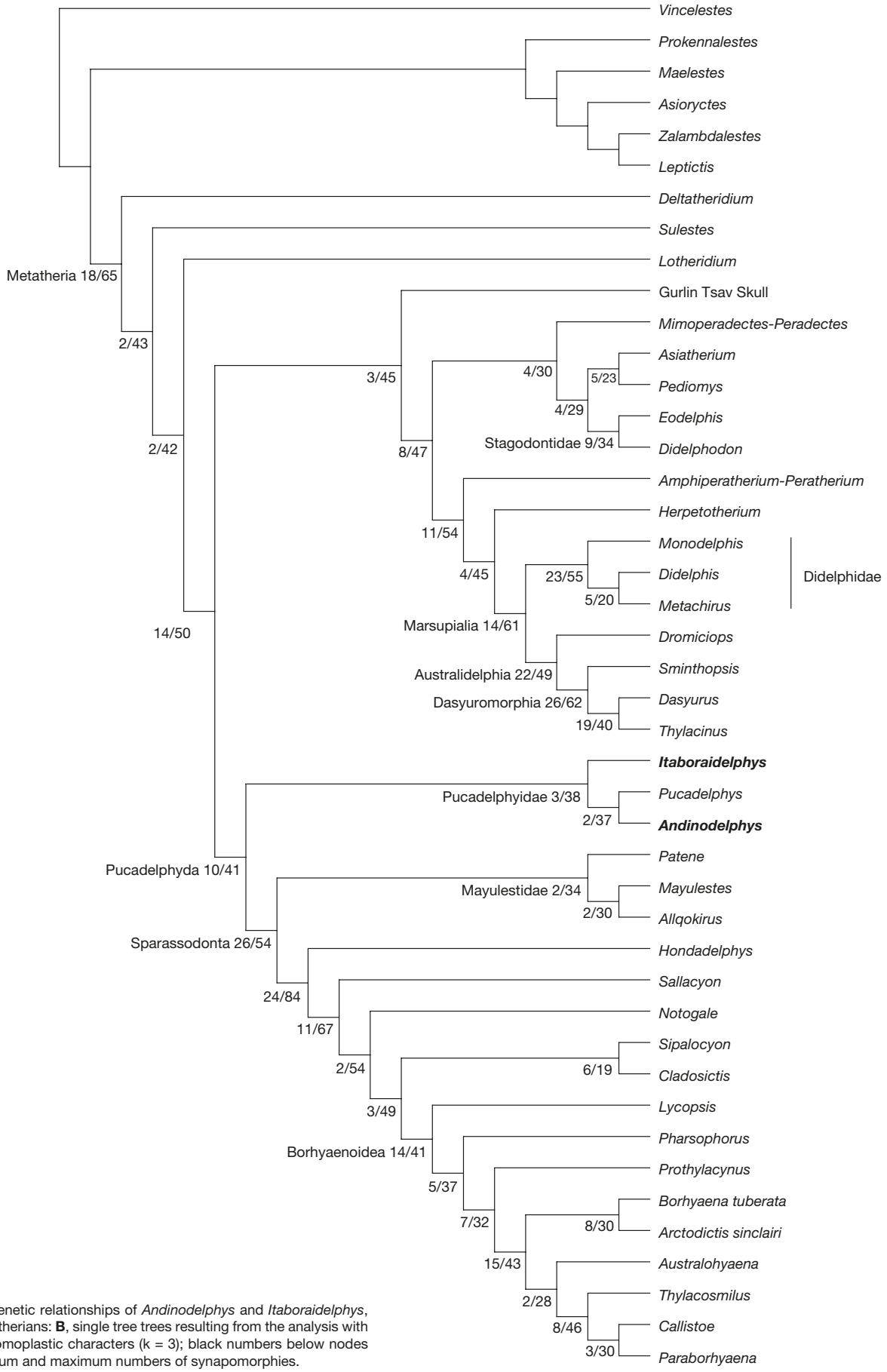

FIG. 51. — Phylogenetic relationships of *Andinodelphys* and *Itaboraidelphys*, among other metatherians: **B**, single tree trees resulting from the analysis with down-weighted homoplastic characters (k = 3); black numbers below nodes indicate the minimum and maximum numbers of synapomorphies.

their matrix by the genera *Sipalocyon, Notogale, Acyon,* and *Cladosictis*). Because *Hathliacynus* is a junior synonym of *Cladosictis* (Marshall 1981), following the treatment of the Mayulestidae by Rangel *et al.* (2019) and according to their result, the family Hathlyacynidae should be restricted to the clade (*Acyon, Cladosictis*), which they retrieved in their fig. 12. Be that as it may, it is noteworthy that the paraphyly of "Hathliacynidae" is another similarity of our analysis to that of Rangel *et al.* (2019).

The superorder Pucadelphyda was erected by Muizon *et al.* (2018) to include Pucadelphyidae and Sparassodonta, but it is noteworthy that the only non-sparassodont taxa they included in the superorder are *Pucadelphys* and *Andinodelphys*. The analysis performed by Rangel *et al.* (2019) also included in the Pucadelphyda a clade comprising two other Tiupampian taxa (*Jaskhadelphys* and *Szalinia*) as well as *Minusculodelphys* (from Itaboraí) and *Kiruwamaq* (from Santa Rosa, Peru). *Jaskhadelphys* and *Szalinia,* which were not included in Muizon *et al.* (2018)'s analysis, since it was essentially focussed on sparassodonts, will be considered in a work in progress by the authors on a skull of *Mizquedelphys* and a partial skull of *Incadelphys*. Furthermore, Rangel *et al.* (2019: 286) also included in the Pucadelphyda, the Tiupampian genera *Mizquedelphys, Tiulordia*, and *Incadelphys* (not included in their analysis). Muizon *et al.* (2018) have included *Mizquedelphys* in Pucadelphyidae, and, therefore, in Pucadelphyda; *Tiulordia* and *Incadelphys* were regarded by these authors as "Ameridelphia" *incertae sedis* together with *Jaskhadelphys* and *Szalinia*. Pending further discoveries and studies based on osteological remains (and/or more complete dental remains), we can provisionally accept the hypothesis of Rangel *et al.* (2019) to include these four genera within the Pucadelphyda. It is noteworthy, however, that the consensus tree of Rangel *et al.* (2019: fig. 12) indicates a Bremer value of 3 for the clade (Pucadelphyidae, Sparassodonta), whereas it is only of 1 for their Pucadelphyda. This means that their clade Pucadelphyda ((*Szalinia,* Jaskhadelphydae), (Pucadelphyidae, Sparassodonta)) is not strongly supported and, because *Jaskhadelphys minutus*, the only known jaskhadelphyid species is very incompletely known, (two upper molars only), the discovery of some new character or better preserved specimens, could easily significantly modify their topology concerning the (*Szalinia*, Jaskhadelphyidae) clade. To conclude, we consider, nevertheless, that the decision of Rangel *et al.* (2019) to include in the Pucadelphyda nine out of the twelve metatherian genera recorded at Tiupampa as well as *Kiruwamaq* (one single isolated ?M3) and *Minusculodelphis* (dental remains only) is to be taken with caution concerning the taxa represented by dental remains only (or almost exclusively).

Another interesting concordant result with Rangel *et al.* (2019), obtained in our first set of analyses (analysis with all characters and implied weighting Fig. 49B), is the position of *Varalphadon*, which, as evidenced by Muizon *et al.* (2018), has no close relationships with the Sparassodonta.

CONCLUSIONS

Two hypotheses are here advanced as regard to the palaeobiogeographic history of the Sparassodonta. In a first scenario, based on a complete set of morphological characters, sparassodonts probably originated outside South America and not as an endemic carnivorous radiation including pucadelphyids and sparassodonts, as suggested by Muizon *et al.* (2018). In this hypothesis (resulting from the first set of analyses), sparassodonts may have originated from basal taxa of the still poorly known North American deltatheroidan radiation (e.g. *Atokatheridium* or *Oklatheridium*), but are unlikely to have been related to the Cenomanian North American genus *Varalphadon* as shown by the result of this analysis (Fig. 49).

An alternate scenario, resulting from the second and third sets of analyses, the former excluding all dental characters, and the latter excluding selected dental characters possibly or probably related to hypercarnivory, supported the monophyly of Pucadelphyda (Pucadelphyidae and Sparassodonta) and therefore advocates for a common biogeographic and phylogenetic origin of the two pucadelphydan clades. If an independent southward migration of pucadelphyids and sparassodonts is required by the first analysis (which renders the evolutionary history of the Pucadelphyda more complex but still quite possible) it is unlikely, unnecessary, and more parsimonious, as far as palaeobiogeography is concerned, in the case of the second and third ones.

This result also raises the problem of the North American origin of the Pucadelphyda in the case of a single southward dispersal of this clade. As discussed above (p. 694), great dental similarities exist between pucadelphyids and the late Campanian (Judithian) North American genus *Aenigmadelphys*. Striking similarities also exist between this latter taxon and the Tiupampian *Incadelphys, Jaskhadelphys,* and *Szalinia,* which would lend support to Rangel *et al.*'s (2019) hypothesis for their inclusion in the Pucadelphyda. Such a similarity is especially true for *Incadelphys* and *Mizquedelphys*, for which the teeth of the partial skulls mentioned in this study are so similar to the teeth *Aenigmadelphys* that, if found in North America, they could easily have been referred to a species of this genus. Nevertheless, further study is needed to address this problem in detail. Be that as it may, it is therefore possible that *Aenigmadelphys* could represent an ancestral North American morphotype for the South American pucadelphydan radiation.

Furthermore, as exposed by Goin *et al.* (2016), the great diversity of the Tiupampa mammalian fauna and its early Palaeocene age, as well as the absence of therians in the diverse and slightly older Campanian fauna of Los Alamitos (Argentina), strongly supports the independent southward migration of several groups of metatherians and eutherians, which already encompassed a radiation in North America and further diversified or became extinct in South America (e.g., Muizon & Cifelli 2000; Case *et al.* 2005, Muizon *et al.* 2015; Clemens 2017). As far as metatherians are concerned, this hypothesis is well established in the case of the Polydolopimorphia which are present in the Late Cretaceous of North

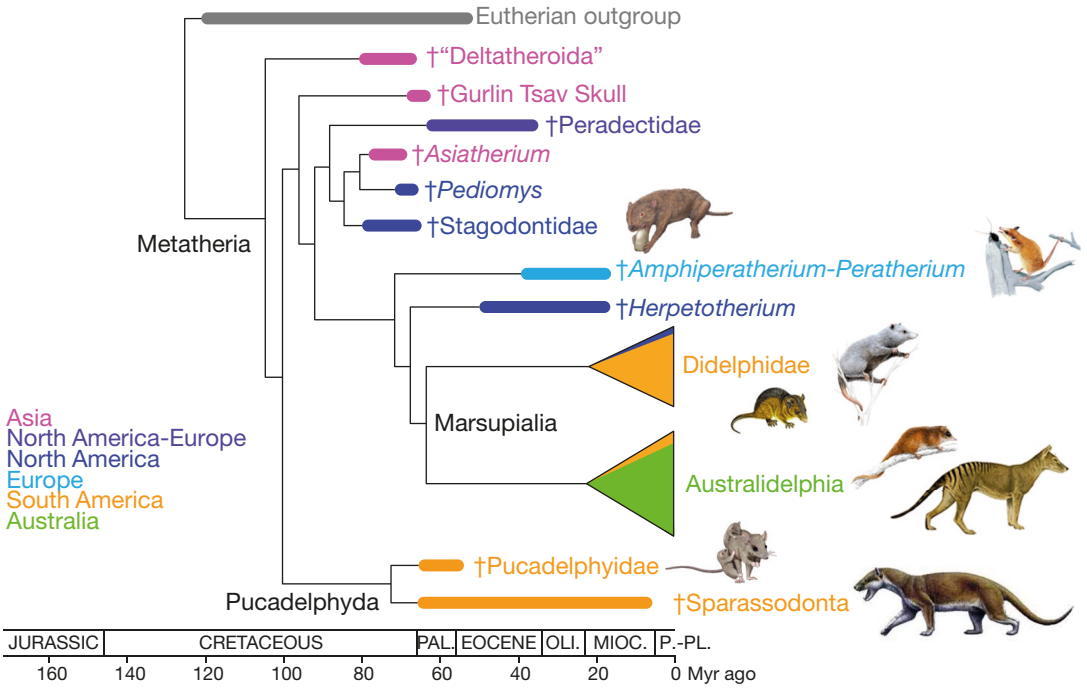

FIG. 52. — Time-calibrated phylogenetic relationships (favoured here) of the taxa of Metatheria included in the third set of analyses with implied weighting (k = 3). Abbreviations: **PAL.**, Palaeocene; **OLI.**, Oligocene; **MIOC.**, Miocene; **P.-PL.**, Pliocene-Pleistocene.

America. (*Glasbius,* [see Williamson *et al.* 2012, 2014, who placed *Glasbius* and *Roberthoffstertteria* in the same clade, but see Wilson *et al.* 2016, who suggested instead convergent dental evolution and Davis 2007, who included *Glasbius* in the Pediomyoidea], *Ectocentrocristus*, and *Hatchitherium* [Case *et al.* 2005]) and at Tiupampa (*Roberthoffstetteria*; Goin *et al.* 2003) as well as in the slightly older Grenier Farm locality of Argentina (*Cocatherium*; Goin *et al.* 2006). Furthermore, Peradectia occur in the early Palaeocene (Puercan3) of North America (*Peradectes*; Clemens 2006; Williamson *et al.* 2012) and, slightly later, at Tiupampa (*Peradectes*; Muizon 1992), and, even later, in the early Eocene beds of Laguna Umayo, Peru (Crochet 1980). Similarly, pantodonts and mioclaenids are known in North America prior those found at Tiupampa (Clemens 2017; Lofgren *et al.* 2004). Therefore, most of the mammal groups known at Tiupampa very likely dispersed from North America during the latest Cretaceous or the earliest Palaeocene (Puercan). Finally, the Tiupampan microbiotherian *Khasia* (Muizon 1992) has been referred (on the basis of dental remains only) to the North American Late Cretaceous pediomyids (Woodburne *et al.* 2014a; Goin *et al.* 2016; Carneiro *et al.* 2018). Although we do not endorse this interpretation (see above and Muizon *et al.* in press), it may simply reveal an indication of close relationships of the two families as suggested by Muizon (1992) and probably advocates for an origin of microbiotherians within pediomyids (or pediomyoids). Because we consider that pediomyoids are absent in South America (*contra* Carneiro *et al.* 2018; see below, Appendix 1) and because microbiotherians are unknown in North America, geographical origin of the latter (i.e. of australidelphians) could have taken place either in North or South America. Furthermore, stagodontids have been tentatively identified at Itaboraí with the referral of the genus *Eobrasilia* to this family of North American carnivorous metatherians by Carneiro & Oliveira (2017a). However, it has also been suggested that the resemblance of the poorly known genus *Eobrasilia* with North American stagodontids may simply reflect convergent evolution of durophagous craniodental features (Eldridge *et al.* 2019: 815).

As shown by Carneiro *et al.* (2018) and others (e.g., Case *et al.* 2005; Forasiepi 2009; Goin *et al.* 2016; Carneiro & Oliveira 2017a, b), the South American Palaeocene therian mammal fauna is not the result of a single radiation but instead that of multiple southward migrations of elements of North American lineages, which diversified or went extinct in South America. This major dispersal event, the First American Biotic Interchange or FABI (Goin *et al.* 2012; Carneiro *et al.* 2018), likely occurred during the latest Cretaceous, probably via the Aves Ridge, an island chain related to the volcanic activity of the Caribbean and Central America (Pindell & Kennan 2009). As stated by Goin *et al.* (2012), at the end of the Cretaceous, an intermittent land connection existed between the Americas, which permitted faunal dispersal. In the absence of a continuous land connection, the therian dispersals between the Americas (so far only recorded from North to South America) may have been possible through "island hopping". In any case, the strong regression and sea level drop that characterises the Late Cretaceous likely permitted multiple therian dispersal event. Nevertheless, although some of them are now well established, understanding of these events is still very poor and highly speculative because of the scarcity of solid fossil record other than dental in the

Late Cretaceous of North America and in the early Palaeocene of South America. Establishing phylogenetic affinities based almost exclusively on dental remains (in some cases fragmentary) is extremely questionable since dental characters have been shown to be strongly homoplastic and subject to major individual variation (e.g., Muizon & Lange-Badré 1997; Ladevèze *et al.* 2011; Sansom *et al.* 2017; Solé & Ladevèze 2017). In fact, given the poorness of the fossil record, the discovery of well-preserved therian cranial remains in the Late Cretaceous of North America may drastically modify (or corroborate) the current hypotheses on the evolutionary histories of South American Palaeogene metatherians and eutherians. A similar major migratory event occurred much later between the Americas in the late Cenozoic-early Pleistocene (the GABI or Great American Biotic Interchange) and was also characterised by multiple individual migrations of different groups (Stehli & Webb 1985). However, study of the GABI is much easier than in the case of the FABI since, in the late Cenozoic, the fossil record is much better in terms of abundance and completeness and, since the groups have encompassed a long evolutionary history, they are therefore more easily recognizable.

Acknowledgements
The locality of Tiupampa was discovered in 1982 during a field expedition funded by National Geographic Society (grant N°2467/82). The specimens described in this paper were discovered in 1996 during a field season at Tiupampa funded by the Institut Français d'Études Andines and the CNRS. Fossil collecting was carried out under the auspices of research agreements between the Fundación para las Ciencias (Bolivia) and the Muséum national d'Histoire naturelle (France). The specimens are the property of the MHNC and have been provided on loan to the MNHN for curation and study. Field expedition has benefited of logistical support from the IRD (Institut de Recherche pour le Développement) in Bolivia. We thank our Bolivian colleagues (Ricardo Céspedes-Paz, Ramiro Suárez-Sorruco, Mario Suárez-Riglos) for their collaboration and logistic support during the field season. Special thanks are due to Céline Bens, Aurélie Verguin, Géraldine Véron, and Christine Lefèvre, (MNHN), who provided access to MNHN specimens under their care. Warm thanks to Guillermo Rougier who provided casts of *Deltatheridium pretribuberculare* (specimens PSS MAE 132 and 133), to Richard Cifelli for generously providing hundreds of casts of North American Cretaceous metatherians, to William Clemens who provided excellent photographs (taken by David Strauss) of the holotypes of *Lycopsis longirostris* and *Hondadelphys fieldsi* and a cast of the holotype of *Crustulus fontanus*, to Steve Wroe for providing stl files of the skulls of *Thylacinus cynocephalus* and *Nimbacinus dicksoni.* Special thanks also to Gregory Wilson for providing access to the CT data of the skulls of *Didelphodon vorax* NDGS 431 and UW BM 94084. This work has benefited from fruitful discussions with Shundong Bi (who provided unpublished data on *Lotheridium*), Guillaume Billet, Richard Cifelli, Brian Davis, and Javier Gelfo. Special thanks are due to the reviewers, Robin Beck and Gregory Wilson, whose invaluable comments significantly improved the manuscript. Photographs were made by Philippe Loubry and Lilian Cazes. CT scanning of the specimens was performed by Miguel Garcia at the AST-RX technical platform of scientific access to RX tomography (UMS 2700 "Acquisition et Analyse de Données pour l'Histoire Naturelle"), CNRS-MNHN, Paris) Data processing was undertaken by Florent Goussard and Nathalie Poulet at the 3D imaging facilities Lab of the UMR 7207 CR2P (MNHN CNRS SU). The artistic reconstructions depicting the past life of *Andinodelphys* and *Pucadelphys* in Tiupampa were realised respectively by Charlene Letenneur and Sophie Fernandez (CR2P). Lastly, our warmest thanks to Emmanuel Côtez for his extremely careful edition of the manuscript. The MNHN gives access to the collections in the framework of the RECOLNAT national Research Infrastructure.

REFERENCES

Andreis R. R. 1977. — Geología del área de Cañadón Hondo, Depto. Escalante, provincia del Chubut, República Argentina. *Revista del Museo de La Plata, Obra del Centenario, Geología* 4: 77-102.

Archer M. 1976a. — The basicranial region of marsupicarnivores (Marsupialia), interrelationships of carnivorous marsupials, and affinities of the insectivorous marsupial peramelids. *Zoological Journal of the Linnean Society* 59: 217-322. https://doi.org/10.1111/j.1096-3642.1976.tb01016.x

Archer M. 1976b. — Revision of the marsupial genus *Planigale* Throughton (Dasyuridae). *Memoirs of the Queensland Museum* 17 (3): 341-365. https://www.biodiversitylibrary.org/page/48804334

Archer M. 1981. — Results of the Archbold expeditions NO. 104. Systematic revision of the marsupial dasyurid genus *Sminthopsis* Thomas. *Bulletin of the American Museum of Natural History* 168 (2): 65-223. http://hdl.handle.net/2246/1050

Argot C. 2003. — Postcranial functional adaptations in the South American Miocene borhyaenoids (Mammalia, Metatheria): Cladosictis, Pseudonotictis, and Sipalocyon. *Alcheringa: An Australasian Journal of Palaeontology* 27: 303-356. https://doi.org/10.1080/03115510308619110

Averianov A. O., Archibald J. D. & E. G. Ekdale 2010. — New material of the Late Cretaceous deltatheroidans mammal *Sulestes* from Uzbekistan and phylogenetic reassessment of the metatherian-eutherian dichotomy. *Journal of Systematic Paleontology* 8 (3): 301-330. https://doi.org/10.1080/14772011003603499

Babot M. J., Powell J. E. & Muizon C. de 2002. — *Callistoe vincei*, a new Proborhyaenidae (Borhyaenoidea, Metatheria, Mammalia) from the early Eocene of Argentina. *Geobios* 35: 615-629. https://doi.org/10.1016/S0016-6995(02)00073-6

Babot J., García-López D., Deraco V., Herrera C. M. & del Papa C. 2017. — Mamíferos paleógenos del subtrópico de Argentina: síntesis de estudios estratigráficos, cronológicos y taxonómicos, *in* Muruaga C. M. & Grosse P. (eds), *Ciencias de la Tierra y Recursos Naturales del NOA*. Relatorio del XX Congreso Geológico Argentino, San Miguel de Tucumán: 730-753.

Bauzá N., Gelfo J. N., & López G. M. 2019. — Early steps in the radiation of notoungulate mammals in southern South America: A new henricosborniid from the Eocene of Patagonia. *Acta Palaeontologica Polonica* 64 (3): 597-207. https://doi.org/10.4202/app.00565.2018

Beck R. M. 2017. — The skull of *Epidolops ameghinoi* from the early Eocene Itaboraí fauna, Southern Brazil, and the affinities of the extinct marsupialiform order Polydolopimorphia. *Journal of Mammalian Evolution* 24 (4) 373-414. https://doi.org/10.1007/s10914-016-9357-6.

BECK R. M. & TAGLIORETTI M. L. 2019. — A nearly complete juvenile skull of the marsupial *Sparassocynus derivatus* from the Pliocene of Argentina, the affinities of "sparassocynids", and the diversification of opossums (Marsupialia; Didelphimorphia; Didelphidae). *Journal of Mammalian Evolution*. https://doi.org/10.1007/s10914-019-09471-y

BENSLEY B. A. 1902. — On the identification of the Meckelian and mylohyoid grooves in the jaws of Mesozoic and Recent mammals. *University of Toronto Studies, Biological Series* 3: 75-82. https://doi.org/10.5962/bhl.title.66541

BI S., JIN X., LI S. & DU T. 2015. — A new Cretaceous metatherian mammal from Henan, China. *PeerJ* 3: e896. https://doi.org/10.7717/peerj.896.

BI S., ZHENG X., WANG X., CIGNETTI N.E., YANG S. & WIBLE J. R. 2018. — An Early Cretaceous eutherian and the placental-marsupial dichotomy. *Nature* 558: 390-395. https://doi.org/10.1038/s41586-018-0210-3

BILLET G., GERMAIN D., RUF I., MUIZON C. DE & HAUTIER L. 2013. — The inner ear of *Megatherium* and the evolution of the vestibular system in sloths. *Journal of Anatomy* 223: 557-567. https://doi.org/10.1111/joa.12114

BLANKS R. H. I., CURTHOYS I. S. & MARKHAM C. H. 1975. — Planar relationships of the semicircular canals in man. *Acta of Oto-Laryngology* 80: 185-296. https://doi.org/10.3109/00016487509121318

BONAPARTE J. & MORALES J. 1997. — Un primitivo Notonychopidae (Litopterna) del Paleoceno Inferior de Punta Peligro, Chubut, Argentina. *Estudios Geológicos* 53: 183-186.

BONAPARTE J. & ROUGIER G. 1987. — Mamíferos del Cretácico Inferior de Patagonia, *in IV Congreso Latinoamericano de Paleontología*. Santa Cruz, Bolivia 1: 343-359.

BONAPARTE J. J., VAN VALEN L. M., & KRAMARZ A. 1993. — La fauna local de Punta Peligro, Paleoceno Inferior, de la provincia de Chubut, Patagonia, Argentina. *Evolutionary Monographs* 14: 1-21.

BRANNICK A. L., WILSON G. P., VARRICCHIO D. J. & EKDALE E. G. 2016. — Nestled among dinosaur eggs: new *Alphadon* specimens from Egg Mountain and their implications for metatherian evolution [abstract], *in* the Society of Vertebrate Paleontology 76th Annual Meeting; 2016, Oct 26-29; Salt Lake City, UT. http://vertpaleo.org/PDFS/2016/SVP-2016-Program-Book-v10-with-covers.aspx (last consultation on 9/12/2020).

BREMER K. 1988. — The limits of amino acid sequence data in angiosperm phylogenetic reconstruction. *Evolution* 42 (4) 795-803. https://doi.org/10.2307/2408870

BUTLER P. M. 1956. — The skull of *Ictops* and the classification of Insectivora. *Proceedings of the Zoological Society of London* 126: 453-481. https://doi.org/10.1111/j.1096-3642.1956.tb00449.x

CABRERA A. 1927. — Datos para el conocimiento de los dasyuroideos fósiles argentinos. *Revista del Museo de la Plata* 30: 271-315.

CALLE A. Z., HORTON B. K., LIMACHI R., STOCKLI D. F., UZEDA-ORELLANA G. V., ANDERSON R. B. & LONG, S. P. 2018. — Cenozoic provenance and depositional record of the Subandean foreland basin during growth of the central Andean fold-thrust belt, southern Bolivia, *in* ZAMORA VALCARCE G., MCCLAY & K., RAMOS V. A. (eds), *Petroleum Basins and Hydrocarbon Potential of the Andes of Peru and Bolivia*. American Association of Petroleum Geologists, Memoir 117: 483-530. https://doi.org/10.1306/13622132M1173777

CARNEIRO L. M. & OLIVEIRA E. V. 2017a. — Systematic affinities of the extinct metatherian *Eobrasilia coutoi* Simpson, 1947, a South American early Eocene Stagodontidae: implications for "Eobrasiliinae". *Revista Brasileira de Paleontologia* 20: 355-372. https://doi.org/10.4072/rbp.2017.3.07

CARNEIRO L. M. & OLIVEIRA E. V. 2017b. — The Eocene South American metatherian *Zeusdelphys complicatus* is not a protodidelphid but a hatcheriform: paleobiogeographic implications. *Acta Palaeontologica Polonica* 62: 497-207. https://doi.org/10.4202/app.00351.2017

CARNEIRO L. M. 2018. — A new species of *Varalphadon* (Mammalia, Metatheria, Sparassodonta) from the upper Cenomanian of southern Utah, North America: Phylogenetic and biogeographic insights. *Cretaceous Research* 84: 88-96. https://doi.org/10.1016/j.cretres.2017.11.004

CARNEIRO L. M., OLIVEIRA E. V. & GOIN F. J. 2018. — *Australopediomys marshalli* gen. et sp. nov., a new pediomyoidea (Mammalia, Metatheria) from the Paleogene of Brazil: Paleobiogeographic implications. *Revista Brasileira de Paleontologia* 21 (2): 120-131. https://doi.org/10.4072/rbp.2018.2.03

CASE J. A., GOIN F. J. & WOODBURNE M. O. 2005. — "South American" marsupials from the Late Cretaceous of North America and the origin of marsupial cohorts. *Journal of Mammalian Evolution* 12: 461-494. https://doi.org/10.1007/s10914-005-7329-3

CHEMISQUY M. A. 2015. — Peramorphic males and extreme sexual dimorphism in *Monodelphis dimidiata* (Didelphidae). *Zoomorphology* 134: 587-599. https://doi.org/10.1007/s00435-015-0274-7

CHORNOGUBSKY L. & GOIN F. J. 2015. — A review of the molar morphology and phylogenetic affinities of Sillustania quechuense (Metatheria, Polydolopimorphia, Sillustaniidae) from the early Paleocene of Laguna Umayo, South eastern Peru. *Journal of Vertebrate Paleontology* 35 (6): e983238. https://doi.org/10.1080/02724634.2015.983238

CIFELLI R. L. 1990. — Cretaceous mammals of Southern Utah. I. Marsupials from the Kaiparowits Formation (Judithian). *Journal of Vertebrate Paleontology* 10 (3): 295-319. https://doi.org/10.1080/02724634.1990.10011816

CIFELLI R. L. 1993. — Early Cretaceous mammal from North America, and the evolution of marsupial dental characters. *Proceedings of the National Academy of Sciences USA* 90: 9413-9416. https://doi.org/10.1073/pnas.90.20.9413

CIFELLI R. L. 2004. — Marsupial mammals from the Albian–Cenomanian (Early-Late Cretaceous) boundary, Utah. *Bulletin of the American Museum of Natural History* 285: 62-79. https://doi.org/cpgs94

CIFELLI R. L. & JOHANSON Z. 1994. — New mammal from the upper Cretaceous of Utah. *Journal of Vertebrate Paleontology* 14 (2): 292-295. https://doi.org/10.1080/02724634.1994.10011558

CIFELLI R. L. & MUIZON C. DE 1997. — Dentition and jaw of *Kokopellia juddi*, a primitive marsupial or near-marsupial from the Medial Cretaceous of Utah. *Journal of Mammalian Evolution* 4 (4): 241-258. https://doi.org/10.1023/A:1027394430433

CIFELLI R. L. & MUIZON C. DE 1998. — Marsupial mammal from the upper Cretaceous North Horn Formation, central Utah. *Journal of Paleontology* 72 (3): 532-537. https://doi.org/10.1017/S0022336000024306

CLARK C. T. & SMITH K. K. 1993. — Cranial osteogenesis in *Monodelphis domestica* (Didelphidae) and *Macropus eugenii* (Macropodidae). *Journal of Morphology* 215:119-249. https://doi.org/10.1002/jmor.1052150203

CLEMENS W. A. 1966. — Fossil mammals from the type Lance Formation, Wyoming. Part II. Marsupialia. *University of California Publications in Geological Sciences* 62: 1-122.

CLEMENS W. A. 1968. — A mandible of *Didelphodon vorax* (Marsupialia, Mammalia). *Contribution in Science* 133: 1-11. https://www.biodiversitylibrary.org/page/52117669

CLEMENS W. A. 2006. — Early Paleocene (Puercan) peradectid marsupials from northeastern Montana, North American Western Interior. *Palaeontographica, Abteilung A* 277: 19-31.

CLEMENS W. A. 2017. — A pantodont (Mammalia) from the latest Puercan North American Land Mammal age (earliest Paleocene) of the Western interior, USA. *Historical Biology* 30 (1-2): 183-188. https://doi.org/10.1080/08912963.2016.1276178

CLYDE W. C., WILF P., IGLESIAS A., SLINGERLAND R. L., BARNUM T., BIJL P. K., BRALOWER T. J., BRINKHUIS H., COMER E. E., HUBER B. T., IBAÑEZ-MEJIA M., JICHA B. R., KRAUSE J. M., SCHUETH J. D., SINGER B. S., RAIGEMBORN M. S., SCHMITZ M. D., SLUIJS A., ZAMALOA M. C. 2014. — New age constraints

for the Salamanca Formation and lower Río Chico Group in the western San Jorge Basin, Patagonia, Argentina: Implications for Cretaceous-Paleogene extinction recovery and land mammal age correlations. *Geological Society of America Bulletin* 126 (3-4): 289-306. https://doi.org/10.1130/B30915.1

Croft D. A., Gelfo J. N., & López G. M. 2020. — Splendid innovation: the extinct South American native ungulates. *Annual Review of Earth and Planetary Sciences* 48: 259-290. https://doi.org/10.1146/annurev-earth-072619-060126

Crochet J. Y. 1980. — *Les marsupiaux du Tertiaire d'Europe*. Éditions de la Fondation Singer Polignac, Paris. 279 p. https://gallica.bnf.fr/ark:/12148/bpt6k3326526p

Crochet J.-Y. & Sigé B. 1996. — Un marsupial ancien (transition Crétacé – Tertiaire) à denture évoluée en Amérique du Sud (Chulpas, Formation Umayo, Pérou). *Neues Jahrbuch für Geologie und Paläontologie*, *Monatshefte* 1996 (10): 622-634. https://doi.org/10.1127/njgpm/1996/1996/622

Crompton A. W. & Sun A.-L. 1985. — Cranial structure and relationships of the Liassic mammal *Sinoconodon*. *Zoological Journal of the Linnean Society* 85: 99-119. https://doi.org/10.1111/j.1096-3642.1985.tb01500.x

Crompton A. W. & Luo Z. 1993. — Relationships of early mammals. *Sinoconodon*, *Morganucodon oehleri*, and *Dinnetherium*, *in* Szalay F. S., Novacek M. J. & McKenna M. C. (eds), *Mammal Phylogeny. Vol. 1: Mesozoic Differentiation, Multituberculates, Monotremes Early Therians and Marsupials*. Springer-Verlag, New York: 30-44. https://doi.org/10.1007/978-1-4613-9249-1_4

Dalrymple G. B. 1979. — Critical tables for conversion of K-Ar ages from old to new constants. *Geology* 7: 558-260. https://doi.org/dbcc9m

David R., Droulez J., Allain R., Berthoz A., Janvier P. & Bennequin D. 2010. — Motion from the past. A new method to infer vestibular capacities of extinct species. *Compte Rendus Palevol* 9: 397-410. https://doi.org/10.1016/j.crpv.2010.07.012

Davis B. M. 2007. — A revision of "pediomyid" marsupials from the Late Cretaceous of North America. *Acta Palaeontologica Polonica* 52: 217-256.

Davis B. M. & Cifelli R. L. 2011. — Reappraisal of the tribosphenidan mammals from the Trinity Group (Aptian-Albian) of Texas and Oklahoma. *Acta Palaeontologica Polonica* 56 (3): 441-462. https://doi.org/10.4202/app.2011.0037

Davis B. M., Cifelli R. L. & Kielan-Jaworowska Z. 2008. — Earliest evidence of Deltatheroida (Mammalia: Metatheria) from the Early Cretaceous of North America, *in* Sargis E. J. & Dagosto M. (eds), *Mammalian Evolutionary Morphology, a tribute to Frederick Szalay*. Springer Verlag, New York: 3-24. https://doi.org/10.1007/978-1-4020-6997-0_1

DeCelles P. & Horton B. K. 2003. — Early to Middle Tertiary foreland development and the history of Andean crustal shortening in Bolivia. *Geological Society of America Bulletin* 115: 58-27. https://doi.org/b6mh8k

Demouy S., Paquette J. L., Saint Blanquat M. de, Benoit M., Belousova E. A., O'Reilly S. Y., García F., Tejada L. C., Gallegos R. & Sempere T. 2012. — Spatial and temporal evolution of Liassic to Paleocene arc activity in southern Peru unraveled by zircon U-Pb and Hf in-situ data on plutonic rocks. *Lithos* 155: 183-200. https://doi.org/10.1016/j.lithos.2012.09.001

Dom R., Fisher B. L., & Martin G. F. 1970. — The venous system of the head and neck of the opossum (*Didelphis virginiana*). *Journal of Morphology* 132 (4): 487-496. https://doi.org/10.1002/jmor.1051320408

Duchêne D. A., Bragg J. G., Duchêne S., Neaves L. E., Potter S., Moritz C., Johnson R. N., Ho S. Y. W., & Eldridge M. D. B. 2018. — Analysis of phylogenomic tree space resolves relationships among marsupial families. *Systematic Biology* 67 (3): 400-412. https://doi.org/10.1093/sysbio/syx076

Eaton J. G. 1993. — Therian mammals of the Cenomanian (Late Cretaceous) Dakota Formation, southwestern Utah. *Journal of Vertebrate Paleontology* 13: 105-224. https://doi.org/10.1080/02724634.1993.10011491

Eberle J. J., Clemens W. A., McCarthy P. J., Fiorillo A. R., Erickson G. R. & Drukenmiller P. S. 2019. — Northermemost record of the Metatheria: a new Late Cretaceous pediomyid from the North slope of Alaska. *Journal of Systematic Palaeontology* 17 (21): 1805-1824. https://doi.org/10.1080/14772019.2018.1560369

Edinger T. 1964. — Midbrain exposure and overlap in mammals. *American Zoologist* 4: 5-19. https://doi.org/10.1093/icb/4.1.5

Edinger T. 1955. — Hearing and smell in cetacean history. *Monatsschrift für Psychiatrie und Neurologie* 129: 37-58. https://doi.org/10.1159/000139733

Ekdale E. G., Archibald D. J. & Averianov A. O. 2004. — Petrosal bones of placental mammals from the Late Cretaceous of Uzbekistan. *Acta Palaeontologica Polonica* 49 (1): 161-176.

Eldridge M. D. B., Beck R. M., Croft D. A., Travouillon K. J. & Fox B. J. 2019. — An emerging consensus in the evolution, phylogeny, and systematics of marsupials and their fossil relatives (Metatherian). *Journal of Mammalogy* 100 (3): 802-837. https://doi.org/10.1093/jmammal/gyz018

Engelman R. K. & Croft D. A. 2014. — A new species of small-bodied sparassodont (Mammalia: Metatheria) from the Middle Miocene locality of Quebrada Honda, Bolivia. *Journal of Vertebrate Paleontology* 34: 672-688. https://doi.org/10.1080/02724634.2013.827118

Evans H. E. & de Lahunta A. 2013. — *Miller's Anatomy of the Dog*. Saunders, St Louis, 850 p.

Flores D. A., Giannini N. P. & Abdala F. A. 2003. — Cranial ontogeny of *Lutreolina crassicaudata* (Didelphidae): a comparison with *Didelphis albiventris*. *Acta Theriologica* 48 (1): 1-2. https://doi.org/10.1007/BF03194261

Flynn A. G., Davis A. J., Williamson T. E., Heizler M., Fenley IV W., Leslie C., Secord R., Brusatte S. L., & Peppe D. J. 2020. — Early Eocene Magnetostratigraphy and revised biostratigraphy of the Ojo Alamo Sandstone and lower Nacimiento Formation, San Juan Basin, New Mexico, USA. *Geological Society of America Bulletin*. https://doi.org/10.1130/B35481.1

Forasiepi A. M. 2009. — Osteology of *Arctodictis sinclairi* (Mammalia, Metatheria, Sparassodonta) and phylogeny of Cenozoic metatherian carnivores from South America. *Monografías del Museo Argentino de Ciencias Naturales* 6: 1-174.

Forasiepi A. M., Babot M. J & Zimicz N. 2015. — *Australohyaena antiqua* (Mammalia, Metatheria, Sparassodonta), a large predator from the late Oligocene of Patagonia. *Journal of Systematic Palaeontology* 13 (6): 503-525. Published online June 2014. https://doi.org/10.1080/14772019.2014.926403

Forasiepi A. M., Macphee R. D. E. & Hernández del Pino S. 2019. — Caudal Cranium of *Thylacosmilus atrox* (Mammalia, Metatheria, Sparassodonta), a South American Predaceous Sabertooth. *Bulletin of the American Museum of Natural History* 2019 (433): 1-66. https://doi.org/10.1206/0003-0090.433.1.1

Fox R. C. 1971. — Marsupial mammals from the early Campanian Milk River Formation, Alberta, Canada. *Zoological Journal of the Linnean Society* 50: 147-164.

Fox R. C. 1974. — *Deltatheroides*-like mammals from the Upper Cretaceous of North America. *Nature* 249: 392. https://doi.org/10.1038/249392a0

Fox R. C. 1975. — Molar structure and function in the Early Cretaceous mammal *Pappotherium*: evolutionary implications for Mesozoic Theria. *Canadian Journal of Earth Sciences* 12 (3): 412-442. https://doi.org/10.1139/e75-037

Fox R. C. 1981. — Mammals from the Upper Cretaceous Oldman Formation, Alberta. V *Eodelphis* Matthew, and the evolution of the Stagodontidae. *Canadian Journal of Earth Sciences* 18 (2): 350-365. https://doi.org/10.1139/e81-027

FOX R. C. 1983. — Notes on the North American Tertiary marsupials *Herpetotherium* and *Peradectes*. *Canadian Journal of Earth Sciences* 20 (10): 1565-1578. https://doi.org/10.1139/e83-146

FOX R. C. 1987. — Palaeontology and the early evolution of marsupials, *in* ARCHER M. (ed.), *Possums and Opossums: Studies in Evolution*. Surrey Beatty & Sons Pty Ltd and the Royal Zoological Society of New South Wales, Sydney: 161-169.

FOX R. C. & NAYLOR B. G. 1986. — A new species of *Didelphodon* Marsh (Marsupialia) from the Upper Cretaceous of Alberta, Canada: paleobiology and phylogeny. *Neues Jahrbuch für Geologie und Paläontologie* 172 (3): 357-380.

FOX R. C. & NAYLOR B. G. 1995. — The relationships of the Stagodontidae, primitive North American Late Cretaceous mammals, *in* SUN A. & WANG Y. (eds), *Sixth Symposium on Mesozoic Terrestrial Ecosystems and Biota*. China Ocean Press, Beijing: 247-250.

FOX R. C. & NAYLOR B. G. 2006. — Stagodontid marsupials from the Late Cretaceous of Canada and their systematic and functional implications. *Acta Palaeontologica Polonica* 51 (1) 13-36.

FOX R. C., SCOTT C. S. & BRYANT H. N. 2007. — A new, unusual therian mammal from the Upper Cretaceous of Saskatchewan, Canada. *Cretaceous Research* 28: 821-229. https://doi.org/10.1016/j.cretres.2006.12.005

GABBERT S. L. 1998. — Basicranial anatomy of *Herpetotherium* (Marsupialia: Didelphimorphia) from the Eocene of Wyoming. *American Museum Novitates* 3235: 1-13. http://hdl.handle.net/2246/3244

GAYET M., MARSHALL L. G. & SEMPERE T. 1992. — The Mesozoic and Paleocene Vertebrates of Bolivia and their stratigraphic context: a review, *in* SUAREZ-SORUCO R. (ed.), *Fósiles y Facies de Bolivia*. Vol. 1. *Vertebrados*. *Revista Técnica de Yacimientos Petrolíferos Fiscales de Bolivia* 12 (3-4): 393-434.

GEISLER J. H. 2001. — New morphological evidence for the phylogeny of Artiodactyla, Cetacea, and Mesonychidae. *American Museum Novitates* 3344: 1-53. http://hdl.handle.net/2246/2897

GELFO J. N. 2007. — The "condylarth" *Raulvaccia peligrensis* (Mammalia: Didolodontidae) from the Paleocene of Patagonia, Argentina. *Journal of Vertebrate Paleontology* 27 (3): 651-660. https://doi.org/fg25pj

GELFO J. N., ORTIZ-JAUREGUIZAR E. & ROUGIER G. W. 2007. — New remains and species of the "Condylarth" genus *Escribania* from the Paleocene of Patagonia, Argentina. *Earth and Environmental Science Transactions of the Royal Society of Edinburgh* 98: 127-138. https://doi.org/10.1017/S1755691007006081

GELFO J., GOIN F., WOODBURNE M. O. & MUIZON C. DE 2009. — Biochronological relationships of South American Paleogene mammalian faunas. *Palaeontology* 52: 251-269. https://doi.org/10.1111/j.1475-4983.2008.00835.x

GELFO J., GOIN F., BAUZÁ N. & REGUERO M. 2019. — The fossil record of Antarctic land mammals: commented review and hypotheses for future research. *Advances in Polar Studies* 30 (3): 274-292. https://doi.org/10.13679/j.advps.2019.0021

GHEERBRANT E. 1992. — Les mammifères paléocènes du bassin d'Ouarzazate (Maroc), I. Introduction générale et Palaeoryctidae. *Palaeontographica* (A) 224: 67-132.

GIANNINI N. P., ABDALA F. & FLORES D. A. 2004. — Comparative ontogeny of the skull in *Dromiciops gliroides* (Marsupialia: Microbiotheriidae). *American Museum Novitates* 3460: 1-17. https://doi.org/fg33mg

GOIN F. J. & PASCUAL R. 1987. — News on the biology and taxonomy of the marsupials Thylacosmilidae (late Tertiary of Argentina). *Anales de la Academia Nacional de Ciencias Exactas y Naturales, Buenos Aires* 39: 219-246.

GOIN F. J., PALMA R. M., PASCUAL R. & POWELL J. E. 1986. — Persistencia de un primitivo Borhyanenidae (Mammalia, Marsupialia) en el Eoceno temprano de Salta (FM. Lumbrera, Argentina). Aspectos geologicos y paleoambientales relacionados. *Ameghiniana* 23 (1-2) 47-56.

GOIN F., CANDELA A. & LOPEZ G. 1998. — Middle Eocene marsupials from Antofagasta de la Sierra Northwestern Argentina. *Geobios* 31 (1): 75-85. https://doi.org/10.1016/S0016-6995(98)80098-3

GOIN F. J., CASE J. A., WOODBURNE M. O., VIZCAÍNO S. F. & REGUERO M. A. 1999. — New discoveries of "opossum-like" marsupials from Antarctica (Seymour Island, Medial Eocene). *Journal of Mammalian Evolution* 6: 335-365. https://doi.org/10.1023/A:1027357927460

GOIN F., CANDELA A. & MUIZON C. DE 2003. — The affinities of *Roberthoffstetteria nationalgeographica* (Marsupialia) and the origin of the polydolopine molar pattern. *Journal of Vertebrate Paleontology* 23: 869-876. https://doi.org/10.1671/2383-11

GOIN F. J., PASCUAL R., TEJEDOR M., GELFO J. N., WOODBURNE M., CASE J., REGUERO M., BOND M., CIONE A., UDRIZAR SAUTHIER D., BALARINO L., SCASSO R., MEDINA F. A. & UBALDÓN M. C. 2006. — The earliest Tertiary therian mammal from South America. *Journal of Vertebrate Paleontology* 26 (2): 505-510. https://doi.org/crwn2q

GOIN F. J., GELFO N. F., CHORNOGUBSKY L., WOODBURNE M. O. & MARTIN T. 2012. — Origins, radiations, and distribution of South American mammals: from greenhouse to icehouse worlds, *in* PATTERSON B. D. & COSTA L. P. (eds), *Bones, Clones, and Biomes: An 80-Million Year History of Recent Neotropical Mammals*. University of Chicago Press, Chicago: 20-50. https://doi.org/10.7208/chicago/9780226649214.003.0003

GOIN F. J., WOODBURNE M. O., ZIMICZ A. N., MARTIN G. M. & CHORNOGUBSKY L. 2016. — *A Brief History of South American Metatherians. Evolutionary Contexts and Intercontinental Dispersals*. Springer, Dordrecht, 237 p. https://10.1007/978-94-017-7420-8

GOIN F. J., VIEYTES E. C., GELFO J. N., CHORNOGUBSKY L., ZIMICZ A. N. & REGUERO M. A. 2018. — New metatherian mammal from the Early Eocene of Antarctica. *Journal of Mammalian Evolution*. Pp. 1-20. https://doi.org/10.1007/s10914-018-9449-6

GOLOBOFF P. A., TORRES A. & ARIAS S. 2017. — Weighted parsimony outperforms other methods of phylogenetic inference under models appropriate for morphology. *Cladistics* 34: 407-437. https://doi.org/10.1111/cla.12205

GOW C. E. 1986. — A new skull of *Megazostrodon* (Mammalia, Triconodonta) from the Elliot Formation (Lower Jurassic) of Southern Africa. *Palaeontologia Africana* 26 (2): 13-23. http://hdl.handle.net/10539/16138

GRADSTEIN F. M., OGG J. G., SCHMITZ M. D., & OGG G. M. 2012. — *The Geologic Time Scale 2012*. Elsevier, Oxford 1144 p.

GREGORY W. K. 1920. — Studies in comparative myology and osteology; NIV. A review of the evolution of the lacrymal bone of vertebrates with special references to that of mammals. *Bulletin of the American Museum of Natural History* 42 (2): 95-263. http://hdl.handle.net/2246/1227

GREGORY W. K. & SIMPSON G. G. 1926. — Cretaceous mammal skulls from Mongolia. *American Museum Novitates* 225: 1-20. http://hdl.handle.net/2246/3193

HAIGHT J. R. 1988. — Marsupials, Nervous System, *in* IRWIN L. N. (ed.), *Comparative Neuroscience and Neurobiology*. Birkhäuser, Boston, Massachusetts: 63-68. https://doi.org/10.1007/978-1-4899-6776-3_28

HALLIDAY T. J. D., UPCHURCH P. & GOSWAMI A. 2017. — Resolving the relationships of Paleocene placental mammals. *Biological Reviews* 92: 521-550. https://doi.org/10.1111/brv.12242

HERSHKOVITZ P. 1982. — The staggered marsupial lower third incisor (i3). *Geobios, Mémoire Spécial* 6: 191-200.

HERSHKOVITZ P. 1995. — The staggered marsupial third lower incisor: hallmark of Cohort Didelphimorphia, and description of a new genus and species with staggered i3 from the Albian (Lower Cretaceous) of Texas. *Bonner zoologische Beiträge* 45: 153-169.

HIIEMAE K. & JENKINS F. A. 1969. — The anatomy and internal architecture of the muscles of mastication in *Didelphis marsupialis*. *Postilla* 140: 1-49. https://www.biodiversitylibrary.org/page/10598728

HOLLOWAY R. L., BROADFIELD D. C. & YUAN M. S. 2004. — *The Human Fossil Record.* Volume 3. *Brain Endocasts; the Paleoneurological Evidence.* New York: Wiley-Liss, 315 p. https://doi.org/10.1002/0471663573

HOPSON J. A. & ROUGIER G. W. 1993. — Braincase structure in the oldest skull of a therian mammal: implications for mammalian systematic and cranial evolution. *American Journal of Science* 293: 268-299. https://doi.org/10.2475/ajs.293.A.268

HOROVITZ I. & SÁNCHEZ-VILLAGRA M. R. 2003. — A morphological analysis of marsupial mammal higher-level phylogenetic relationships. *Cladistics* 19: 181-212. https://doi.org/10.1111/j.1096-0031.2003.tb00363.x

HOROVITZ I., LADEVÈZE S., ARGOT C., MACRINI T. E., MARTIN T., HOOKER J. J., KURZ C., MUIZON C. DE & SÁNCHEZ-VILLAGRA M. R. 2008. — The anatomy of *Herpetotherium* cf. *fugax* Cope 1873, a metatherian from the Oligocene of North America. *Palaeontographica* 284 (4-6): 109-141. https://doi.org/10.1127/pala/284/2008/109

HOROVITZ I., MARTIN T., BLOCH J., LADEVÈZE S., KURZ C. & SÁNCHEZ-VILLAGRA M. R. 2009. — Cranial anatomy of the earliest marsupials and the origin of opossums. *PlosOne* 4 (12): 1-9. https://doi.org/10.1371/journal.pone.0008278

HORTON B. K., HAMPTON B. A. & WAANDERS G. 2001. — Paleogene synorogenic sedimentation in the Altiplano plateau and implications for initial mountain building in the central Andes: *Geological Society of America Bulletin* 113: 1387-2400. https://doi.org/b9vmx6

HU Y., WANG Y., LUO Z.-X. & LI C. 1997. — A new symmetrodont mammal from China and its implications for mammalian evolution. *Nature* 390: 137-142. https://doi.org/10.1038/36505

HU Y., MENG J. & LI C. 2005. — Large Mesozoic mammals fed on young dinosaurs. *Nature* 433: 149-152. https://doi.org/10.1038/nature03102

IGLESIAS A., WILF P., JOHNSON K. R., ZAMUNER A. B., CÚNEO N. R., MATHEOS S. D. & SINGER B. S. 2007. — A Paleocene lowland macroflora from Patagonia reveals significantly greater richness than North American analogs. *Geology* 35: 947-950. https://doi.org/10.1130/G23889A.1

JANSA S. A., BARKER F. K. & VOSS R. S. 2014. — The early diversification history of didelphid marsupials: a window into South America's "splendid Isolation". *Evolution* 68 (3): 684-695. https://doi.org/10.1111/evo. 12290

JERISON H. J. 1991. — Fossil brains and the evolution of the neocortex, *in* FINLAY B. L., INNOCENTI G. & SCHEICH H. (eds), *The Neocortex: Ontogeny and Phylogeny.* NATO Advanced Science Institutes Series A: Life Sciences. Vol. 200, Plenum Press, New York, New York: 5-29. https://doi.org/10.1007/978-1-4899-0652-6_2

JERNVALL J. 1995. — Mammalian molar cusp pattern: developmental mechanisms of diversity. *Acta Zoologica Fennica* 198:1-61.

JOHANSON Z. 1996. — New marsupial from the Fort Union Formation, Swain Quarry, Wyoming. *Journal of Paleontology* 70 (6): 1023-1031. https://doi.org/10.1017/S0022336000038725

JONES W. F. 1930. — A re-examination of the skeletal characters of *Wynyardia bassiana*, an extinct Tasmanian marsupial. *Papers and Proceedings of the Royal Society of Tasmania* 1930: 96-115.

JOUVE S., MUIZON C. DE, CÉSPEDES-PAZ R., SOSSA-SORRUCO V. & KNOLL S. 2020. — The longirostrine crocodyliforms from Bolivia and their evolutionthrough the Cretaceous-Palaeogene boundary. *Zoological Journal of the Linnean Society*: zlaa081. https://doi.org/10.1093/zoolinnean/zlaa081

KERMACK K. A., MUSSETT F. & RIGNEY H. W. 1981. — The skull of *Morganucodon*. *Zoological Journal of the Linnean Society* 71: 1-158. https://doi.org/10.1111/j.1096-3642.1981.tb01127.x

KIELAN-JAWOROWSKA Z. 1969. — Preliminary data on the Upper Cretaceous eutherian mammals from Bayn Dzack, Gobi Desert. *Palaeontologia Polonica* 19: 171-191.

KIELAN-JAWOROWSKA Z. 1975a. — Preliminary description of two new eutherian genera from the Late Cretaceous of Mongolia. *Palaeontologia Polonica* 33: 5-16.

KIELAN-JAWOROWSKA Z. 1975b. — Evolution of the therian mammals in the Late Cretaceous of Asia. Part I. Deltatheridiidae. *Palaeontologia Polonica* 33: 103-132.

KIELAN-JAWOROWSKA Z. 1977. — Evolution of the therian mammals in the Late Cretaceous of Asia. Part II. Postcranial skeleton in *Kennalestes* and *Asioryctes*. *Palaeontologia Polonica* 37: 65-83.

KIELAN-JAWOROWSKA Z. 1981. — Evolution of the therian mammals in the Late Cretaceous of Asia. Part IV. Skull structure of *Kennalestes* and *Asioryctes*. *Palaeontologia Polonica* 42: 157-174.

KIELAN-JAWOROWSKA Z. 1984. — Evolution of the therian mammals in the Late Cretaceous of Asia. Part V. Skull structure in Zalambdalestidae. *Palaeontologia Polonica* 46: 107-117.

KIELAN-JAWOROWSKA Z. & CIFELLI R. L. 2001. — Primitive boreosphenidan mammal (?Deltatheroida) from the Early Cretaceous of Oklahoma. *Acta Palaeontologica Polonica* 46: 377-291.

KIELAN-JAWOROWSKA Z. & DASHZEVEG D. 1989. — Eutherian mammals from the Early Cretaceous of Mongolia. *Zoologica Scripta* 18: 347-355. https://doi.org/10.1111/j.1463-6409.1989.tb00460.x

KIELAN-JAWOROWSKA Z. & NESSOV L. A. 1990. — On the metatherian nature of the Deltatheroida, a sister group of the Marsupialia. *Lethaia* 23: 1-10. https://doi.org/10.1111/j.1502-3931.1990.tb01776.x

KIELAN-JAWOROWSKA Z. & TROFIMOV B. A. 1980. — Cranial morphology of the Cretaceous eutherian mammal *Barunlestes*. *Acta Palaeontologica Polonica* 25:167-185.

KIELAN-JAWOROWSKA Z., PRESLEY R. & POPLIN C. 1986. — The cranial vascular system in taeniolabidoid multituberculate mammals. *Philosophical Transactions of the Royal Society B* 313: 525-602. https://doi.org/10.1098/rstb.1986.0055

KIELAN-JAWOROWSKA Z., CIFELLI R. L. & LUO Z.-X. 2004. — *Mammals from the Age of Dinosaurs. Origins, Evolution, and Structure*. Columbia University Press, New York: 1-630. https://doi.org/10.7312/kiel11918

KLAAUW J. C. VAN DER 1931. — The auditory bulla in some fossil mammals with a general introduction to this region of the skull. *Bulletin of the American Museum of Natural History* 62: 1-352. http://hdl.handle.net/2246/353

KORTH W. W. 2018. — Review of the marsupials (Mammalia: Metatheria) from the late Paleogene (Chadronian–Arikareean: late Eocene–late Oligocene) of North America. *Paläontologische Zeitschrift* 92 (3) 499- 523. https://doi.org/10.1007/s12542-017-0396-y

KORTH W. W. & CAVIN J. 2016. — New material of the marsupial (Mammalia, Metatheria) *Herpetotherium merriami* (Stock and Furlong, 1922) from the John Day Formation, late Oligocene, Oregon, USA. *Journal of Paleontology* 90 (6): 1225-2232. https://doi.org/10.1017/jpa.2016.117

KRAUSE D. W. & KIELAN-JAWOROWSKA Z. 1993. — The endocranial cast and encephalization quotient of *Ptilodus* (Multituberculata, Mammalia). *Palaeovertebrata* 22: 99-212.

KUHN H.-J. & ZELLER U. 1987. — The cavum epiptericum in monotremes and therian mammals, *in* KUHN H.-J. & ZELLER U. (eds), *Morphogenesis of the Mammalian Skull*. Verlag Paul Parey, Hamburg: 51-70.

LADEVÈZE S. 2004. — Metatherian petrosals from the late Paleocene of Itaboraí, Brazil, and their phylogenetic implications. *Journal of Vertebrate Paleontology* 24 (1): 202-213. https://doi.org/10.1671/16

LADEVÈZE S. & MUIZON C. DE 2007. — The auditory region of early Palaeocene Pucadelphydae (Mammalia, Metatheria) from Tiupampa with phylogenetic implications. *Palaeontology* 50 (5): 1123-1154. https://doi.org/10.1111/j.1475-4983.2007.00703.x

LADEVÈZE S. & MUIZON C. DE 2010. — Evidence of early evolution of Australidelphia (Metatheria Mammalia) in South America: phylogenetic relationships of the metatherians from the Late Palaeocene of Itaboraí (Brazil) based on teeth and petrosal bones. *Zoological Journal of the Linnean Society* 159 (2): 746-784. https://doi.org/10.1111/j.1096-3642.2009.00577.x

LADEVÈZE S., MUIZON C. DE, BECK R, GERMAIN D. & CÉSPEDES-PAZ R. 2011. — Earliest evidence of mammalian social behaviour in the basal Tertiary of Bolivia. *Nature* 474: 83-86. https://doi.org/10.1038/nature09987

LADEVÈZE S., SMITH R. & SMITH T. 2012. — Reassessment of the morphology and taxonomic status of the earliest herpetotheriid marsupials of Europe. *Journal of Mammalian Evolution* 19: 249-261. https://doi.org/10.1007/s10914-012-9195-0

LADEVÈZE S., SELVA C. & MUIZON C. DE 2020. — What are "opossum-like" fossils? The phylogeny of herpetotheriid and peradectids metatherians, based on new features from the petrosal anatomy. *Journal of Systematic Palaeontology* 18 (17): 1463-1479, https://doi.org/10.1080/14772019.2020.1772387

LESLIE C., PEPPE D., WILLIAMSON T., BILARDELLO D., HEITZLER M., SECORD R., & LEGGETT T. 2018. — High-resolution magnetostratigraphy of the upper Nacimiento Formation, San Juan Basin, New Mexico, USA: implications for basin evolution and mammalian turnover. *American Journal of Science* 318: 300-334. https://doi.org/10.2475/03.2018.02

LILLEGRAVEN J. A. 1969. — Latest Cretaceous mammals of upper part of Edmonton Formation of Alberta, Canada, and review of marsupial-placental dichotomy in mammalian evolution. *The University of Kansas Paleontological Contributions,* article 50 (Vertebrata 12): 1-122. http://hdl.handle.net/1808/3825

LILLAGRAVEN J. A. & KRUSAT G. 1991. — Cranio-mandibular anatomy of *Haldanodon exspectatus* (Docodonta, Mammalia) from the late Jurassic of Portugal and its implications on the evolution of mammalian characters. *Contribution to Geology, University of Wyoming* 28: 39-138.

LILLEGRAVEN J. A. & MCKENNA M. C. 1986. — Fossil mammals from the "Mesaverde" Formation (Late Cretaceous, Judithian) of the Bighorn and Wind River Basins, Wyoming, with definitions of Late Cretaceous North American Land-mammal "ages". *American Museum Novitates* 2840: 1-68. http://hdl.handle.net/2246/3575

LOFGREN D. L., LILLEGRAVEN J. A. CLEMENS W. A. GINGERICH P. D. AND WILLIAMSON T. E. 2004. — Paleocene Biochronology: The Puercan through Clarkforkian Land Mammal Ages, *in* WOODBURNE M. O. (ed.), *Late Cretaceous and Cenozoic Mammals of North America. Biostratigraphy and Geochronology*. Columbia University Press, New York: 43-105. https://doi.org/10.7312/wood13040-005

LOO Y. T. 1930. — The forebrain of the opossum, *Didelphis virginiana*. Part I. Gross anatomy. *Journal of Comparative Neurology* 51: 13-64. https://doi.org/10.1002/cne.900510103

LOPATIN A. V. & AVERIANOV A. O. 2017. — The stem placental mammal *Prokennalestes* from the Early Cretaceous of Mongolia *Paleontological Journal* 51 (12): 1293-1374. https://doi.org/10.1134/S0031030117120048

LUO Z.-X., JI Q., WIBLE J. R. & YUAN C.-X. 2003. — An Early Cretaceous tribosphenic mammal and metatherian evolution. *Science* 302: 1934-1940. https://doi.org/10.1126/science.1090718

LUO Z.-X., CHEN P., LI G. & CHEN M. 2007. — A new eutriconodont mammal and evolutionary development in early mammals. *Nature* 446: 288-293. https://doi.org/10.1038/nature05627

LUO Z.-X., YUAN C.-X., MENG Q.-J. & JI Q. 2011. — A Jurassic eutherian mammal and divergence of marsupials and placentals. *Nature* 476: 442-445. https://doi.org/10.1038/nature10291

MACRINI T. E., ROWE T. & VANDEBERG J. L. 2007a. — Cranial endocasts from a growth series of *Monodelphis domestica* (Didelphidae, Marsupialia): a study of individual and ontogenetic variation. *Journal of morphology* 268 (10): 844-865. https://doi.org/10.1002/jmor.10556

MACRINI T. E., MUIZON C. DE, CIFELLI R. L. & ROWE T. 2007b. — Digital cranial endocast of *Pucadelphys andinus*, a Paleocene metatherian. *Journal of Vertebrate Paleontology* 27 (1): 99-107. https://doi.org/c5c959

MACPHEE R. D. 1981. — Auditory regions of primates and eutherian insectivores: Morphology, ontogeny, and character analysis. *Contribution in Primatology* 18:1-282.

MARSHALL L. G. 1976. — New didelphine marsupials from the La Venta fauna (Miocene) of Colombia, South America. *Journal of Paleontology* 50 (3): 402-418. https://www.jstor.org/stable/1303521

MARSHALL L. G. 1977. — A new species of *Lycopsis* (Borhyaenidae: Marsupialia) from the La Venta fauna (late Miocene) of Colombia, South America. *Journal of Paleontology* 51 (3): 633-642. https://www.jstor.org/stable/1303691

MARSHALL L. G. 1979a. — Evolution of metatherian and eutherian (mammalian) characters: a review based on cladistics methodology. *Zoological Journal of the Linnean Society* 66: 369-410. https://doi.org/10.1111/j.1096-3642.1979.tb01914.x

MARSHALL L. G. 1979b. — Review of the Prothylacininae, an extinct subfamily of South American "dog-like" marsupials. *Fieldiana Geology, new series* 3: 1-50. https://www.biodiversitylibrary.org/page/2842762

MARSHALL L. G. 1981. — Review of the Hathlyacyninae, an extinct subfamily of South American "dog-like" marsupials. *Fieldiana Geology, new series* 7: 1-120. https://doi.org/10.5962/bhl.title.3520

MARSHALL L. G. 1987. — Systematics of Itaboraian (middle Paleocene) age 'opossum-like' marsupials from the limestone quarry at Sao José de Itaborai, Brasil, *in* ARCHER M. (ed.), *Possums and Oppossums: Studies in Evolution*. Vol. 1. Surrey Beatty & Sons Pty Limited and The Royal Zoological Society of New South Wales, Sydney: 91-160.

MARSHALL L. G. & KIELAN-JAWOROWSKA Z. 1992. — Relationships of the dog-like marsupials, deltatheroidans and early tribosphenic mammals. *Lethaia* 25: 361-374. https://doi.org/10.1111/j.1502-3931.1992.tb01639.x

MARSHALL L. G. & MUIZON C. DE 1984. — Un nouveau Marsupial didelphidé (*Itaboraidelphys camposi* nov. gen. nov. sp.) du Paléocène moyen (Itaboraïen) de Sao José de Itaboraí (Brésil). *Comptes Rendus hebdomadaires des Séances de l'Académie des Sciences*, Paris, sér. II, 299 (18): 1297-1300.

MARSHALL L. G. & MUIZON C. DE 1988. — The dawn of the age of mammals in South America. *National Geographic Research* 4 (1): 23-55.

MARSHALL L. G. & MUIZON C. DE 1995. — Part II: The skull, *in* MUIZON C. DE (ed.), Pucadelphys andinus *(Marsupialia, Mammalia) from the early Paleocene of Bolivia*. Muséum national d'Histoire naturelle, Paris: 21-90 (Mémoires du Muséum national d'Histoire naturelle; 165).

MARSHALL L. G., BUTLER R. F., DRAKE R. E. & CURTIS D. H. 1981. — Calibration of the beginning of the Age of Mammals in Patagonia. *Science* 212: 43-45. https://doi.org/10.1126/science.212.4490.43

MARSHALL L.G., MUIZON C. DE & SIGÉ B. 1983. — Late Cretaceous mammals (Marsupialia) from Bolivia. *Geobios* 16 (6): 739-745. https://doi.org/10.1016/S0016-6995(83)80090-4

MARSHALL L. G., MUIZON C. DE, GAYET M., LAVENU A. & SIGÉ B. 1985. — The "Rosetta Stone" for mammalian evolution in South America. *National Geographic Research* 1: 274-288.

MARSHALL L. G., CASE J. A. & WOODBURNE M. O. 1990. — Phylogenetic relationships of the families of marsupials, *in* GENOWAYS H. H. (ed.), *Current Mammalogy*. Plenum Press, New York: 433-505.

MARSHALL L. G., MUIZON C. DE & SIGOGNEAU-RUSSELL D. 1995. — Part I: The locality of Tiupampa: age, taphonomy and mammalian fauna, *in* MUIZON C. DE (ed.), Pucadelphys andinus *(Marsupialia, Mammalia) from the early Paleocene of Bolivia*. Muséum national d'Histoire naturelle, Paris: 11-20 (Mémoires du Muséum national d'Histoire naturelle; 165).

MARSHALL L. G., SEMPERE T. & BUTLER R. F. 1997. — Chronostratigraphy of the mammal-bearing Palaeocene of South America. *Journal of South American Earth Sciences* 10: 49-70. https://doi.org/10.1016/S0895-9811(97)00005-9

MARKWICK P. J. 1998. — Fossil crocodilians as indicators of Late Cretaceous and Cenozoic climates: implications for using palaeontological data in reconstructing palaeoclimate. *Palaeogeography Palaeoclimatology, Palaeoecology* 137: 205-271. https://doi.org/10.1016/S0031-0182(97)00108-9

MATTHEW W. D. 1916. — A marsupial from the Belly River Cretaceous. *Bulletin of the American Museum of Natural History* 35: 477-500. http://hdl.handle.net/2246/1386

MITCHELL K. J., PRATT R. C., WATSON L. N., GIBB G. C., LLAMAS B., KASPER M., EDSON J., HOPWOOD B., MALE D., AMSTRONG K. N., MEYER M., HOFREITER M., AUSTIN J., DONNELLAN M. S., LEE M. S. Y., PHILLIPS M. J. & COOPER A. 2014. — Molecular phylogeny, biogeography, and habitat preference evolution of marsupials. *Molecular Biology and Evolution* 31: 2322-2330. https://doi.org/10.1093/molbev/msu176

MUIRHEAD J. & WROE S. 1998. — A new genus and species, *Badjcinus turnbulli* (Thylacinidae: Marsupialia), from the late Oligocene of Riversleigh, Northern Australia, and an investigation of thylacinid phylogeny. *Journal of Vertebrate Paleontology* 18 (3): 612-626. https://doi.org/10.1080/02724634.1998.10011088

MUIZON C. DE 1992. — La fauna de mamíferos de Tiupampa (Paleoceno inferior, Formación Santa Lucía), Bolivia, *in* SUAREZ-SORUCO R. (ed.), *Fósiles y facies de Bolivia*. Vol. I. *Vertebrados. Revista Técnica de Yacimientos Petrolíferos y Fiscales de Bolivia* 12 (3-4): 575-624, December 1991, Santa Cruz, Bolivia.

MUIZON C. DE 1994. — A new carnivorous marsupial from the Palaeocene of Bolivia and the problem of marsupial monophyly. *Nature* 370: 208-211. https://doi.org/10.1038/370208a0

MUIZON C. DE 1998. — *Mayulestes ferox*, a borhyaenoid (Metatheria, Mammalia) from the early Palaeocene of Bolivia. Phylogenetic and paleobiologic implications. *Geodiversitas* 20: 19-142.

MUIZON C. DE 1999. — Marsupial skulls from the Deseadan (late Oligocene) of Bolivia and phylogenetic analysis of the Borhyaenoidea (Marsupialia, Mammalia). *Geobios* 32 (3): 483-509. https://doi.org/10.1016/S0016-6995(99)80022-9

MUIZON C. DE & ARGOT C. 2003. — Comparative anatomy of the didelphimorph marsupials from the early Palaeocene of Bolivia (*Pucadelphys*, *Andinodelphys*, and *Mayulestes*). Palaeobiologic implications, *in* JONES M., DICKMAN C. & ARCHER M. (eds), *Predators with Pouches: the Biology of Carnivorous Marsupials*. Surrey Beatty & Sons, Sydney: 42-63.

MUIZON C. DE & CIFELLI R. L. 2000. — The "condylarths" (archaic Ungulata, Mammalia) from the early Palaeocene of Tiupampa (Bolivia): implications on the origin of the South American ungulates. *Geodiversitas* 22 (1): 47-150.

MUIZON C. DE & LANGE-BADRÉ B. 1997. — Carnivorous dental adaptations in marsupials and placentals and phylogenetical reconstruction. *Lethaia* 30: 351-366. https://doi.org/10.1111/j.1502-3931.1997.tb00481.x

MUIZON C. DE & MARSHALL L. G. 1992. — *Alcidedorbignya inopinata* (Mammalia: Pantodonta) from the early Paleocene of Bolivia: Phylogenetic and Paleobiogeographic implications. *Journal of Paleontology* 66 (3): 499-520. https://doi.org/10.1017/S002233600003403X

MUIZON C. DE, GAYET M., LAVENU A., MARSHALL L.G., SIGÉ B. & VILLARROEL C. 1983. — Late Cretaceous vertebrates including mammals from Bolivia. Geobios 16 (6): 747-753. https://doi.org/10.1016/S0016-6995(83)80091-6

MUIZON C. DE, MARSHALL L. G. & SIGÉ B. 1984. — The mammal fauna from the El Molino Formation (Late Cretaceous, Maestrichtian) at Tiupampa South Central Bolivia. *Bulletin du Muséum national d'Histoire naturelle, 4ème série, Section C, Sciences de la terre, paléontologie, géologie, minéralogie* 6 (4): 327-351. https://www.biodiversitylibrary.org/page/55710289

MUIZON C. DE, CIFELLI R. L. & CÉSPEDES-PAZ R. 1997. — The origin of the dog-like borhyaenoid marsupials of South America. *Nature* 389: 486-489. https://doi.org/10.1038/39029

MUIZON C. DE, CIFELLI R. L. & BERGQVIST L. 1998. — Eutherian tarsals from the early Paleocene of Bolivia. *Journal of Vertebrate Paleontology* 18 (3): 655-663. https://doi.org/10.1080/02724634.1998.10011092

MUIZON C. DE, BILLET G., ARGOT C., LADEVÈZE S. & GOUSSARD F. 2015. — *Alcidedorbignya inopinata,* a basal pantodont (Eutheria, Mammalia) from the early Palaeocene of Bolivia: anatomy, phylogeny, and palaeobiology. *Geodiversitas* 37 (4): 397-634. https://doi.org/10.5252/g2015n4a1

MUIZON C. DE, LADEVÈZE S., SELVA C., VIGNAUD R. & GOUSSARD F. 2018 – *Allqokirus australis* (Sparassodonta, Metatheria) from the early Palaeocene of Tiupampa (Bolivia) and the rise of the metatherian carnivorous radiation in South America. *Geodiversitas* 40 (16): 363-459. https://doi.org/10.5252/geodiversitas2018v40a16

MUIZON C. DE, BILLET G. & LADEVÈZE S. 2019. — New remains of kollpaniine "condylarths" (Panameriungulata) from the early Palaeocene of Bolivia shed light on hypocone origins and molar proportions among ungulate-like placentals. *Geodiversitas*. 41 (25): 841-874. https://doi.org/10.5252/geodiversitas2019v41a25. http://geodiversitas.com/41/25

MURRAY P. F. & MEGIRIAN D. 2006. — Cranial morphology of the Miocene thylacinid *Mutpuracinus.archibaldi* (Thylacinidae, Marsupialia) and relationships within the Dasyuromorphia, Alcheringa: An Australasian *Journal of Palaeontology* 30: 229-276. https://doi.org/10.1080/03115510609506865

MYERS T. J. 2001. — Marsupial body mass prediction. *Australian Journal of Zoology* 49: 99 -118. https://doi.org/10.1071/ZO01009

NESSLINGER C. L. 1956. — Ossification centers and skeletal development in the postnatal Virginia opossum. *Journal of Mammalogy*, 37: 382-294. https://doi.org/10.2307/1376739

NILSSON M. A., CHURAKOV G., SOMMER M., VAN TRAN N., ZEMANN A., BROSIUS J., SCHMITZ J. 2010. — Tracking marsupial evolution using archaic genomic retroposon insertions. *PLoS Biology* 8:e1000436. https://doi.org/10.1371/journal.pbio.1000436

NIXON K. 2008. — WinClada, version 1.00. 08. Computer program published by the author, Ithaca, New York, United States.

NOVACEK M. J. 1977. — Aspects of the problem of variation, origin, and evolution of the eutherian auditory bulla. *Mammal Review* 7: 131-149. https://doi.org/10.1111/j.1365-2907.1977.tb00366.x

NOVACEK M. J. 1986. — The skull of leptictid insectivorans and the higher-level classification of eutherian mammals. *Bulletin of the American Museum of Natural History* 183 (1): 1-112. http://hdl.handle.net/2246/1628

NOMINA ANATOMICA VETERINARIA (NAV) 2005. — 5th edition. Editorial Committee, Hannover, Columbia, Ghent, Sapporo, 1-166.

OLIVEIRA E. V. & GOIN F. J. 2012. — Marsupiais do Início do Paleógeno no Brasil: Diversidade e afinidades, *in* CÁCERES N. C. (ed.), *Os marsupiais do Brasil: biologia, ecologia e conservação.* UFMS, Campo Grande: 275-307,

OLIVEIRA E. V., ZIMICZ N. & GOIN F. J. 2016. — Taxonomy, affinities, and paleobiology of the tiny metatherian mammal *Minusculodelphis*, from the early Eocene of South America. *The Science of Nature* 103: 6: 1-11. https://doi.org/10.1007/s00114-015-1331-2

O'LEARY M. A., BLOCH J. I., FLYNN J. J., GAUDIN T. J., GIALLOMBARDO A., GIANNINI N. P., GOLDBERG S. L., KRAATZ B. P., LUO Z .-X., MENG J., NI X., NOVACEK M. J., PERINI F. A., RANDALL Z. J., ROUGIER G. W., SARGIS E. J., SILCOX M. T., SIMM ONS N. B., SPAULDING M., VELAZCO P. M., WEKSLER M., WIBLE J. R. & CIRRANELLO A. L. 2013. — The placental mammal ancestor and the post-K-Pg radiation of placentals. *Science* 339: 662-667. https://doi.org/10.1126/science.1229237

ORTIZ-JAUREGUIZAR E. & PASCUAL R. 2011. — The tectonic setting of the Caribbean region and the K/T turnover of the South American land-mammal fauna. *Boletín Geológico y Minero* 122: 333-344. http://hdl.handle.net/11336/98171

ORTIZ-JAUREGUIZAR E., CLADERA G. & GIALLOMBARDO A. 1999. — Relaciones de similitud entre las faunas del lapso Cretácico superior-Paleoceno superior en América del Sur. *Temas Geológicos Mineros* 26: 280-283.

OWEN R. 1837. — On the structure of the brain in marsupial animals. *Philosophical Transactions of the Royal Society of London* 127: 87-92. https://www.biodiversitylibrary.org/page/52046207

PARKER W. K. 1886. — On the structure and development of the skull in the Mammalia. *Philosophical Transactions of the Royal Society of London* 176: 1-275. https://www.biodiversitylibrary.org/page/55201970

PASCUAL R. 1980. — Nuevos y singulares tipos ecológicos de marsupiales extinguidos de América del Sur (Paleoceno tardío o Eoceno temprano) del Noroeste argentino. *Actas II Congreso Argentino Paleontología y Bioestratigrafía y I Congreso Latinoamericano Paleontología* 2: 151-173, Buenos Aires.

PASCUAL R. 1981. — Adiciones al conocimiento de *Bonapartherium hinakusijum* (Marsupialia, Bonapartheriidae) del Eoceno temprano del Noroeste argentino. *Anais II Congreso Latinoamericano de Paleontología* 2: 507-520, Porto Alegre.

PASCUAL R. & ORTIZ-JAUREGUIZAR E. 2007. — The Gondwanan and South American episodes: two major and unrelated moments in the history of the South American mammals. *Journal of Mammalian Evolution* 14: 75-137. https://doi.org/10.1007/s10914-007-9039-5

PATTERSON B. 1965. — The auditory region of the borhyaenid marsupial Cladosictis. *Breviora* 217: 1-9. https://www.biodiversitylibrary.org/page/4312642

PAULA COUTO C. DE 1952a. — Fossil mammals from the beginning of the Cenozoic in Brazil. Marsupialia: Polydolopidae and Borhyaenidae. *American Museum Novitates* 1559: 1-27. http://hdl.handle.net/2246/2386

PAULA COUTO C. DE 1952b. — Fossil mammals from the beginning of the Cenozoic in Brazil. Marsupialia: Didelphidae. *American Museum Novitates* 1567: 1-26. http://hdl.handle.net/2246/2389

PAVAN S. E. & VOSS R. S. 2016. — A revised subgeneric classificationof short-tailed opossum (Didelphidae: *Monodelphis*). *American Museum Novitates* 3868: 1-44. https://doi.org/10.1206/3868.1

PETTER G. & HOFFSTETTER R. 1983. — Les marsupiaux du Déséadien (Oligocène supérieur) de Salla (Bolivie). *Annales de Paléontologie* 69 (3): 175-234.

PINE R. H., DALBY P. L., & MASTSON J. O. 1985. — Ecology, postnatal development, morphometrics, and taxonomic status of the short-tailed opossum *Monodelphis dimidiata*, an apparently semelparous annual marsupial. *Annals of the Carnegie Museum* 54: 195-231. https://www.biodiversitylibrary.org/page/52403409

PINDELL J. L. & KENNAN L. J. G. 2009. — Kinematic evolution of the Gulf of Mexico, the Caribbean, and Northern South America in the mantle reference frame: an update, *in* JAMES K., LORENTE M. A. & PINDELL J. (eds), The Origin and Evolution of the Caribbean Plate. *Geological Society of London, Special publication* 328: 1-60. https://doi.org/10.1144/SP328.1

PORZECANSKI A. L. & CRACRAFT J. 2005. — Cladistic analysis of distributions and endemism (CADE): using raw distributions of birds to unravel the biogeography of the South American aridlands. *Journal of Biogeography* 32: 261-275. https://doi.org/10.1111/j.1365-2699.2004.01138.x

RAK A. J., MCQUARRIE N., EHLERS & T. A. 2017. — Kinematics, exhumation, and sedimentation of the north central Andes (Bolivia): An integrated thermochronometer and thermokinematic modeling approach. *Tectonics* 36 (11): 2524-2554. https://doi.org/10.1002/2016TC004440

RANGEL C. C., CARNEIRO L. M., BERGQVIST L. P., OLIVERIA E. V., GOIN F. J. & BABOT M. J. 2019. — Diversity, affinities, and adaptations of the basal sparassodont *Patene* Simpson, 1935 (Mammalia, Metatheria). *Ameghiniana* 56 (4): https://doi.org/10.5710/AMGH.06.05.2019.3222

REGUERO M. A., GELFO J. N., LOPEZ G. M., BOND M., ABELLO A., SANTILLANA S. N. & MARENSI S. A. 2014. — Final Gondwana breakup: The Paleogene South American native ungulates and the demise of the South America-Antarctica land connection. *Global and Planetary Changes* 123, part B: 400-413. https://doi.org/10.1016/j.gloplacha.2014.07.016

REIG O. A. & SIMPSON G. G. 1972. — *Sparassocynus* (Marsupialia Didelphidae), a peculiar mammal from the late Cenozoic from Argentina. *Journal of Zoology* 167: 511-539. https://doi.org/10.1111/j.1469-7998.1972.tb01742.x

RIGGS E. S. 1934. — A new marsupial saber-tooth from the Pliocene of Argentina and its relationships to other South American predacious marsupials. *Transactions of the American Philosophical Society* N.S. 24 (1): 1-32.

ROSE K. D. 1999. — Postcranial skeleton of Eocene Leptictidae (Mammalia) and its implications for behavior and relationships. *Journal of Vertebrate Paleontology* 19: 355-372. https://doi.org/10.1080/02724634.1999.10011147

ROSE K. D. 2006. — The postcranial skeleton of early Oligocene *Leptictis* (Mammalia: Leptictida), with a preliminary comparison to *Leptictidium* from the middle Eocene of Messel. *Palaeontographica* (A) 278: 37-56. https://doi.org/10.1127/pala/278/2006/37

ROSE K. D. 2010. — New marsupial from the early Eocene of Virginia. *Journal of Paleontology* 84: 561-565. https://doi.org/10.1666/09-140.1

ROSEN B. R. 1988. — From fossils to earth history: applied historical biogeography, *in* MYERS A. A. & GILLER P. S. (eds), *Analytical Biogeography: an Integrated Approach to the Study of Animal and Plant Distributions*. Chapman and Hall, London: 437-481. https://doi.org/10.1007/978-94-009-1199-4_17

ROUGIER G. W. & WIBLE J. R. 2006. — Major changes in the mammalian ear region and basicranium, *in* CARRANO M. T., GAUDIN T. J., BLOB R. W. & WIBLE J. R. (eds), *Amniote Paleobiology: Perspective on the Evolution of Mammals, Birds, and Reptiles*. University of Chicago Press, Chicago: 269-311.

ROUGIER G. W., WIBLE J. R. & HOPSON J. 1992. — Reconstruction of the cranial vessels in the Early Cretaceous mammal Vincelestes neuquenianus: implications for the evolution of the mammalian cranial vascular system. *Journal of Vertebrate Paleontology* 12 (2): 188-216. https://doi.org/10.1080/02724634.1992.10011449

ROUGIER G. W., WIBLE J. R. & NOVACEK M. J. 1998. — Implications of *Deltatheridium* specimens for early marsupial history. *Nature* 396: 459-463. https://doi.org/10.1038/24856

ROUGIER G. W., WIBLE J. R. & NOVACEK M. J. 2004. — New specimens of *Deltatheroides cretacicus* (Metatheria, Deltatheroida) from the Late Cretaceous of Mongolia. *Bulletin of the Carnegie Museum of Natural History* 36: 245-266. https://doi.org/cgbprc

ROUGIER G. W., DAVIS B. M. & NOVACEK M. J. 2015. — A deltatheroidan mammal from the upper Cretaceous Baynshiree Formation, eastern Mongolia. *Cretaceous Research* 52:167-177. https://doi.org/10.1016/j.cretres.2014.09.009

ROWE T. 1996a. — Brain heterochrony and the evolution of the mammalian middle ear, *in* GHISELIN M. & PINNA G. (eds), *New Perspectives on the History of Life*. *Memoir* 20. California Academy of Sciences, San Francisco: 71-95.

ROWE T. 1996b. — Coevolution of the mammalian middle ear and neocortex. *Science* 273: 651-654. https://doi.org/10.1126/science.273.5275.651

ROWE T. B., EITING T. P., MACRINI T. E. & KETCHAM R. A. 2005. — Organisation of the olfactory and respiratory skeleton in the nose of the Gray short-tailed opossum *Monodelphis domestica*. *Journal of Mammalian Evolution* 12: 303-336. https://doi.org/10.1007/s10914-005-5731-5

SANSOM R. S., WILLS M. A. & WILLIAMS T. 2017. — Dental data perform relatively poorly in reconstructing mammal phylogenies: morphological partitions evaluated with molecular benchmarks. *Systematic Biology* 66 (5): 813-822. https://doi.org/10.1093/sysbio/syw116

SÁNCHEZ-VILLAGRA M. R. & SMITH K. K. 1997. — Diversity and evolution of the marsupial mandibular angular process. *Journal of Mammalian Evolution* 4: 119-144. https://doi.org/10.1023/A:1027318213347

SÁNCHEZ-VILLAGRA M. R. & WIBLE J. R. 2002. — Patterns of evolutionary transformation in the petrosal bone and some basicranial features in marsupial mammals, with special reference to didelphids. *Journal of Zoological Systematic and Evolutionary Research* 40: 26-45. https://doi.org/10.1046/j.1439-0469.2002.00173.x

Sánchez-Villagra M. R., Ladevèze S., Horovitz I., Argot C., Hooker J. J., Macrini T. E., Martin T., Moore-Fay S., Muizon C. de, Schmelzle T, & Asher R. J. 2007. — Exceptionally preserved North American Paleogene metatherians and new inferences about their evolutionary relationships and lifestyle. *Biology Letters* 3 (3): 318-322. https://doi.org/10.1098/rsbl.2007.0090

Scott C. S. & Fox R. C. 2015. — Review of the Stagodontidae (Mammalia, Marsupialia) from the Judithian (Late Cretaceous) Belly River Group of southeastern Alberta, Canada. *Canadian Journal of Earth Sciences* 52: 682-695. https://doi.org/10.1139/cjes-2014-0170

Segall W. 1970. — Morphological parallelisms of the bulla and auditory ossicles in some insectivores and marsupials. *Fieldiana Zoology* 51: 169-205. https://doi.org/10.5962/bhl.title.2899

Selva C. & Ladevèze S. 2017. — Computed microtomography investigation of the skull of Cuvier's famous 'opossum' (Marsupialiformes, Herpetotheriidae) from the Eocene of Montmartre. *Zoological Journal of the Linnean Society* 180 (3): 672-693. https://doi.org/10.1111/zoj.12495

Sempere T., Butler R. L. & Marshall L. G. 1997. — Stratigraphy and chronology of the Upper Cretaceous-Lower Paleogene strata in Bolivia and northwest Argentina. *Geological Society of America, Bulletin* 109 (6): 709-727. https://doi.org/czzndb

Sigogneau-Russell D., Dashzeveg D. & Russell D. E. 1992. — Further data on *Prokennalestes* (Mammalia, Eutheria *inc. sed.*) from the Early Cretaceous of Mongolia. *Zoologica Scripta* 21: 205-209. https://doi.org/10.1111/j.1463-6409.1992.tb00322.x

Sinclair W. J. 1906. — Mammalia of the Santa Cruz Beds: Marsupialia. *Reports of the Princeton University expeditions to Patagonia* 4 (3): 333-460. https://www.biodiversitylibrary.org/page/51838575

Solé F. & Ladevèze S. 2017. — Evolution of the hypercarnivorous dentition in mammals (Metatheria, Eutheria) and its bearing on the development of tribosphenic molars. *Evolution and Development* 12 (2): 56-68. https://doi.org/10.1111/ede.12219

Somoza R., Cladera G. & Archangelsky S. 1995. — Una nueva tafoflora paleocena de Chubut, Patagonia. Su edad y ambiente de depositación. *VI Congreso Argentino de Paleontología y Bioestratigrafía*, *Actas*: 265-269.

Spoor F. 2003. — The semicircular canal system and locomotor behaviour, with special reference to hominin evolution. *Courier-Forschungsinstitut Senckenberg* 243: 93-104.

Spoor F., Garland T., Krovitz G., Ryan T. M., Silcox M. T. & Walker A. 2007. — The primate semicircular canal system and locomotion. *Proceedings of the National Academy of Sciences* 104 (26): 10808-10812. https://doi.org/10.1073/pnas.0704250104

Sprain C. J., Renne P. R., Wilson G. P. & Clemens W. A. 2015. — High-resolution chronostratigraphy of the terrestrial Cretaceous-Paleogene transition and recovery interval in the Hell Creek region, Montana. *Geological Society of America Bulletin* 127 (3-4): 393-409. https://doi.org/10.1130/B31076.1

Sprain C. J., Renne P. R., Clemens W. A. & Wilson G. P. 2018. — Calibration of C29r: new high-precision geochronologic and paleomagnetic constraints from the Hell Creek region, Montana. https://doi.org/10.1130/B31890.1

Springer M. S., Burk-Herrick A., Meredith R., Eizirik E., Teeling E., O'Brien S. J. & Murphy W. J. 2007. — The adequacy of morphology for reconstructing the early history of placental mammals. *Systematic Biology* 56 (4): 673-684 https://doi.org/10.1080/10635150701491149

Stehli F. G. & Webb S. D. (eds) 1985. — *The Great American Biotic Interchange*. Plenum Press, New York: 1-532.

Storer J. E. 1991. — The mammals of the Gryde local fauna, Frenchman Formation (Maastrichtian: Lancian), Saskatchewan. *Journal of Vertebrate Paleontology* 11 (3): 350-369. https://doi.org/10.1080/02724634.1991.10011403

Swofford D. L. 2002. — *PAUP*: Phylogenetic analysis using parsimony (and other methods), version 4.0b1.0*. Sunderland, Massachusetts: Sinauer.

Szalay F. S. & Trofimov B. A. 1996. — The Mongolian Late Cretaceous *Asiatherium*, and the early phylogeny and paleobiogeography of Metatheria. *Journal of Vertebrate Paleontology* 16 (3) 474-509. https://www.jstor.org/stable/4523738

Thewissen J. G. M. 1989. — Mammalian frontal diploic vein and the human foramen caecum. *The Anatomical Record* 223: 242-244. https://doi.org/10.1002/ar.1092230217

Tobias P. V. 1971. — *The Brain in Hominid Evolution*. Columbia University Press, New York, 170 p. https://doi.org/10.5962/bhl.title.15880

Toeplitz C. 1920. — Bau und Entwicklung des Knorpelschädels von *Didelphis marsupialis*. *Zoologica* 27: 1-24.

Turnbull W. D. 1970. — Mammalian masticatory apparatus. *Fieldiana: Geology* 18 (2): 149-356. https://doi.org/10.5962/bhl.title.5442

Turnbull W. D. 1971. — The trinity therians: their bearing on evolution in marsupials and other therians, *in* Dahlberg A. A. (ed.), *Dental Morphology and Evolution*. University of Chicago Press, Chicago: 151-179.

Turnbull W. D. & Segall W. 1984. — The ear region of the marsupial sabretooth, *Thylacosmilus*: influence of the sabretooth lifestyle upon it, and convergence with placental sabertooths. *Journal of Morphology* 181: 239-270. https://doi.org/10.1002/jmor.1051810302

Vandenbergh N., Hilgen F. J. & Speijer R. 2012. — The Paleogene period, *in* Gradstein F. M., Ogg J. G., Schmitz M. D. & Ogg G. M. (eds), *The Geologic Time Scale 2012*. Elsevier, Oxford: 855-921. https://doi.org/10.1016/B978-0-444-59425-9.00028-7

Van Kampen P. N. 1905. — Die Tympanalegend des Säugetierschädels. *Morphologische Jahrbuch* 34: 321-722.

Voss R. S. & Jansa S. A. 2009. — Phylogenetic relationships and classification of didelphid marsupials, an extant radiation of New World metatherian mammals. *Bulletin of the American Museum of Natural History* 322: 1-177. https://doi.org/10.1206/322.1

Watson M. S. 1916. — The monotreme skull: a contribution to mammalian morphogenesis. *Philosophical Transactions of the Royal Society B* 207: 335-347. https://doi.org/10.1098/rstb.1916.0007

Wible J. R. 1987. — The eutherian stapedial artery: character analysis and implications for superordinal relationships. *Zoological Journal of the Linnean Society* 91: 107-135. https://doi.org/10.1111/j.1096-3642.1987.tb01725.x

Wible J. R. 1990. — Petrosals of Late Cretaceous marsupials from North America, and a cladistic analysis of the petrosal in therian mammals. *Journal of Vertebrate Paleontology* 10 (2): 183-205. https://doi.org/10.1080/02724634.1990.10011807

Wible J. R. 1993. — Cranial circulation and relationships of the colugo Cynocephalus (Dermoptera, Mammalia). *American Museum Novitates* 3072: 1-27. http://hdl.handle.net/2246/4969

Wible J. R. 2003. — On the cranial osteology of the short-tailed opossum *Monodelphis brevicaudata* (Marsupialia, Didelphidae). *Annals of the Carnegie Museum* 72 (3): 1-66. https://www.biodiversitylibrary.org/page/52469617

Wible J. R. 2008. — On the cranial osteology of the Hispaniolan solenodon, *Solenodon paradoxus*, Brandt, 1833 (Mammalia, Lipotyphla, Solenodontidae). *Annals of the Carnegie Museum* 77 (3): 321-402. https://doi.org/10.2992/0097-4463-77.3.321

Wible J. R. 2009. — The ear region of the pen-tailed treeshrew, *Ptilocercus lowii* Gray 1848 (Placentalia, Scandentia, Ptilocercidae). *Journal of Mammalian Evolution* 16 (3): 199-234. https://doi.org/10.1007/s10914-009-9116-z

Wible J. R. 2010. — Petrosal anatomy of the nine-banded armadillo *Dasypus novemcinctus* Linnaeus, 1758 (Mammalia, Xenarthra, Dasypodidae). *Annals of the Carnegie Museum* 79 (1): 1-28. https://doi.org/10.2992/007.079.0101

Wible J. R. 2011. — On the treeshrew skull (Mammalia, Placentalia, Scandentia). *Annals of the Carnegie Museum* 79 (3): 149-230. https://doi.org/10.2992/007.079.0301

WIBLE J. R. 2012. — The ear region of the aardvark, *Orycteropus afer* (Pallas, 1766) (Mammalia, Placentalia, Tubulidentata). *Annals of the Carnegie Museum* 80 (2): 115-146. https://doi.org/10.2992/007.080.0202

WIBLE J. R. & GAUDIN T. J. 2004. — On the cranial osteology of the yellow armadillo *Euphractus sexcinctus* (Dasypodidae, Xenarthra, Placentalia). *Annals of Carnegie Museum* 73: 117-196. https://www.biodiversitylibrary.org/page/52457341

WIBLE J. R. & HOPSON J. A. 1993. — Basicranial evidence for early mammal phylogeny, *in* SZALAY F. S., NOVACEK M. J. & MCKENNA M. C. (eds), *Mammal Phylogeny: Mesozoic Differentiation, Multituberculates, Monotremes, Early Therians, and Marsupials*. Springer-Verlag, New York: 45-62. https://doi.org/10.1007/978-1-4613-9249-1_5

WIBLE J. R. & HOPSON J. A. 1995. — Homologies of the prootic canal in mammals and nonmammalian cynodonts. *Journal of Vertebrate Paleontology* 15: 331-356. https://doi.org/10.1080/02724634.1995.10011233

WIBLE J. R. & ROUGIER G. W. 2000. — Cranial anatomy of *Kryptobaatar dashzevegi* (Mammalia, Multituberculata), and its bearing on the evolution of mammalian characrters. *Bulletin of the American Museum of Natural History* 247: 1-124. https://doi.org/dkpqq3

WIBLE J. R. & SPAULDING M. 2013. — On the cranial osteology of the African palm civet, *Nandinia binotata* (Gray, 1830) (Mammalia, Carnivora, Feliformia). *Annals of the Carnegie Museum of Natural History* 82 (1): 1-114. https://doi.org/10.2992/007.082.0101

WIBLE J. R., ROUGIER G. W., NOVACEK M. J. & MCKENNA M. C. 2001. — Earliest eutherian ear region: a petrosal of *Prokennalestes* from the Early Cretaceous of Mongolia. *American Museum Novitates* 3322: 1-44. https://doi.org/ckv3s3

WIBLE J. R., NOVACEK M. J. & ROUGIER G. W. 2004. — New data on the skull and dentition in the Mongolian Cretaceous eutherian mammal *Zalambdalestes*. *Bulletin of the American Museum of Natural History* 281: 1-144. https://doi.org/c4wpk4

WIBLE J. R., ROUGIER G. W., NOVACEK M. J. & ASHER R. J. 2009. — The eutherian mammal *Maelestes gobiensis* from the Late Cretaceous of Mongolia and the phylogeny of Cretaceous Eutheria. *Bulletin of the American Museum of Natural History* 327: 1-123. https://doi.org/10.1206/623.1

WIBLE J. R., SHELLEY S. L. & ROUGIER G. W. 2018. — The mammalian parasphenoid: its occurrence in marsupials. *Annals of the Carnegie Museum* 85 (2): 113-164. https://doi.org/10.2992/007.085.0202

WILLIAMSON L. A. & CARR T. D. 2007. — Bomburia and Ellipsodon (Mammalia: Mioclaenidae) from the early Paleocene of New Mexico. *Journal of Paleontology* 81 (5): 966-985. https://doi.org/10.1666/pleo05-116.1

WILLIAMSON T. E., BRUSATTE S. L., CARR T. D., WEIL A. & STANDHARDT B. R. 2012. — The phylogeny and evolution of Cretaceous-Palaeogene metatherians: cladistic analysis and description of new early Palaeocene specimens from the Nacimiento formation, New Mexico. *Journal of Systematic Palaeontology* 10 (4): 625-651. https://doi.org/10.1080/14772019.2011.631592

WILLIAMSON T. E., BRUSATTE S. L. & WILSON G. P. 2014. — The origin and early evolution of metatherian mammals: the Cretaceous record. *Zookeys* 465: 1-76. https://doi.org/10.3897/zookeys.465.8178

WILSON G. P. & RIEDEL J. A. 2010. — New specimen reveals deltatheroidan affinities of the North American Late Cretaceous mammal *Nanocuris*. *Journal of Vertebrate Paleontology* 30 (3): 872-884. https://doi.org/10.1080/02724631003762948

WILSON G. P., EKDALE E. G., HOGANSON J. W., CALEDE J. J. & VANDER LINDEN A. 2016. — A large carnivorous mammal from the Late Cretaceous and the North American origin of marsupials. *Nature Communications* 7: 13734. https://doi.org/10.1038/ncomms13734

WOODBURNE M. O., GOIN F. J., BOND M., CARLINI A. A., GELFO J. N., LOPEZ G. M. IGLESIAS A. & ZIMICZ A. N. 2014a. — Paleogene land mammal faunas of South America; a response to global climatic changes and indigenous floral diversity. *Journal of Mammalian Evolution* 21: 1-73 https://doi.org/10.1007/s10914-012-9222-1

WOODBURNE M. O., GOIN F. J., RAIGEMBORN M. S., HEIZLER M., GELFO J. N. & OLIVEIRA E. V. 2014b. — Revised timing of the South American Early Paleogene land mammal ages. *Journal of South American Earth Sciences* 54: 109-219. https://doi.org/10.1016/j.jsames.2014.05.003

WROE S. 1996. — *Muribacinus gadiyuli*, (Thylacinidae: Marsupialia), a very plesiomorphic thylacinid from the Miocene of Riversleigh, Northwestern Queensland, and the problem of paraphyly for the dasyuridae (Marsupialia). *Journal of Vertebrate Paleontology* 70 (6): 1032-144. https://doi.org/10.1017/S0022336000038737

WROE S. 1999. — The geologically oldest dasyurid, from the Miocene of Riversleigh, North-West Queensland. *Palaeontology* 42 (3): 501-527. https://doi.org/10.1111/1475-4983.00082

WROE S. & MUSSER A. 2001. — The skull of *Nimbacinus dicksoni* (Thylacinidae: Marsupialia). *Australian Journal of Zoology* 49: 487-514. https://doi.org/10.1071/ZO00032

WROE S., EBACH M., SHANE A., MUIZON C. DE & MUIRHEAD J. 2000. — Cladistic analysis of dasyuromorphian (Marsupialia) phylogeny using cranial and dental characters. *Journal of Mammalogy* 81: 1008-1024. https://doi.org/df6t89

YATES A. M. 2014. — New craniodental remains of *Thylacinus potens* (Dasyuromorphia: Thylacinidae), a carnivorous marsupial from the late Miocene Alcoota Local Fauna of central Australia. *PeerJ* 2: e547; https://doi.org/10.7717/peerj.547

ZIMICZ A. N., FERNÁNDEZ M., BOND M., CHORNOGUBSKY L., ARNAL M., CÁRDENAS M., & FERNICOLA J. C. 2020. — *Archaeogaia macachaae* gen. et sp. nov., one of the oldest Notoungulata Roth, 1903 from the early-middle Paleocene Mealla Formation (Central Andes, Argentina) with insights into the Paleocene-Eocene south American biochronology. *Journal of South American Earth Sciences*: 102772. https://doi.org/10.1016/j.jsames.2020.102772

Submitted on 25 November 2019;
accepted on 31 March 2020;
published on 31 December 2020.

Appendix 1. — Comments on the affinities of *Australopediomys marshalli* from the early Eocene of Brazil.

Paula couto (1952b) described a mandible fragment (with p2-m1) from the Palaeocene (now regarded as early Eocene – Woodburne *et al.* 2014a, b; Goin *et al.* 2016; Carneiro *et al.* 2018; Rangel *et al.* 2019) of Itaboraí (Brazil), which he referred to a new genus and species of Didelphidae, *Mondelphopsis travassosi*. Marshall (1987) referred to the holotype of *M. travassosi* a partial mandible (with m1-4) and maxilla (with M2-4) and referred the species to the Microbiotheriidae. Recently, Carneiro *et al.* (2018) retrieved the maxilla from the hypodigm of *M. travassosi* and referred it to a new genus and species of Pediomyoidea, *Australopediomys marshalli*. This interpretation could indicate that representatives of this superfamily were present in South America and, therefore, could have been present at Tiupampa and possibly gave rise to Microbiotherians (likely closely related to Pediomyioidea) in South America. However, the holotype of *A. marshalli*, (the maxilla with M2-4) bears little similarities with pediomyoids and we do not endorse the interpretation of Carneiro *et al.* (2018). *Australopediomys* differs from pediomyoids in the eight following characters: 1) paracone much smaller in high and volume than metacone (sub-equal in pediomyoids – personal observation); 2) labial edge of paracone distinctly less convex than on metacone on M3 and flat on M2 and M4 with labial edge of metacone convex (in pediomyoids paracone is sub-conical with labial edge much more convex than on metacone [Davis 2007]); 3) para- and metacingulum absent; (always present in pediomyoids – personal observation); 4) internal conular cristae lacking (always present in pediomyoids [Davis 2007]); 5) anterior stylar shelf sub-equal in width to posterior on M3 and only slightly narrower on M2; (in pediomyoids, anterior stylar shelf is absent [Davis 2007] or, if present on M3 it is extremely narrow – personal observation); 6) stylar cusp B largest cusp of molars (generally absent to small in pediomyoids; when present, it is smaller than St C – personal observation); 7) stylar cusp D small (generally large in pediomyoids – personal observation); 8) ectoflexus relatively deep (as in *Kokopellia* and alphadontid species) on M3-4 and symmetrical (anteroposteriorly) on M3; (generally shallow to absent in pediomyoids [Davis 2007], although, in some cases, it can approach the condition of *Australopediomys* [personal observation]).

Nevertheless, similarities exist between *Australopediomys* and pediomyoids, as previously evidenced by Carneiro *et al.* (2018). We have observed the five following features: 1) straight centrocrista (plesiomorphic condition); 2) basal posterior projection of the protocone (a feature present in several other groups of metatherians not closely related to pediomyoids: e.g., pucadelphyids, herpetotheriids, didelphids, dasyurids); 3) thickening of the protocristae ("conuloids" of Carneiro *et al.* 2018); however, this feature is variably present in other taxa with crushing adaptation – but not all of them: e.g., *Dakotadens*, *Turgidodon* (Carneiro *et al.* 2018). Noteworthy, this feature shows notable intra- and interspecific variation among pediomyoids and is even absent in some species (e.g., *Protolambda hatcheri*); 4) preparacrista contacts stylar cusp A (not stylar cusp B, which is the plesiomorphic pattern): this feature is absent in the pediomyoids, *Aquiladelphis* and *Iqualadelphis* (in which the preparacrista contact StB [Davis 2007]), but present in pediomyids, which do not have a stylar cusp B. As a matter of fact, this condition is also present in microbiotheres, which are lacking a stylar cusp B either; furthermore, this character is present in other taxa with a well-developed StB such as *Albertatherium* (Fox 1971, 1987); 5) angle between preparacrista and centrocrista of M4 wide open (greater than 90° and close to 130°, personal observation, see discussion above p. 675-678); however, it is worth noting that this feature is present in many other groups of metatherians especially, for example, in those showing carnivorous adaptations (e.g., stagodontids and sparassodonts). Therefore, we consider that *Australopediomys* is not a pediomyoid and that this superfamily is absent so far in South America. We however acknowledge that microbiotheres bear strong similarities with pediomyids (see above p. 703), which may indicate close phylogenetic affinities (an assertion that should be tested with parsimony analyses). Consequently, because microbiotheres have not been recovered so far in North America their geographic origin is unknown.

APPENDIX 2. — Additional illustrations of the premolars and molars of the holotype of *Mayulestes ferox*. Figures 53 to 58.

FIG. 53. — *Mayulestes ferox* Holotype MHNC 1249. Stereophotos of the left upper premolars and molars in occulsal view. Scale bar: 5 mm.

Appendix 2. — Continuation.

Fig. 54. — *Mayulestes ferox* Holotype MHNC 1249. Stereophotos of the right upper premolars and molars in occulsal view. Scale bar: 5 mm.

Appendix 2. — Continuation.

Fig. 55. — *Mayulestes ferox* Holotype MHNC 1249. **A**, right upper premolars and molars in ventrolabial view; **B**, left upper premolars and molars in labial view. Scale bar: 5 mm.

Appendix 2. — Continuation.

Fig. 56. — *Mayulestes ferox* Holotype MHNC 1249. Stereophotos of the right lower premolars and molars in occulsal view. Scale bar: 5 mm.

Appendix 2. — Continuation.

Fig. 57. — *Mayulestes ferox* Holotype MHNC 1249. Stereophotos of the left lower p3 and molars in occulsal view. Scale bar: 5 mm.

Appendix 2. — Continuation.

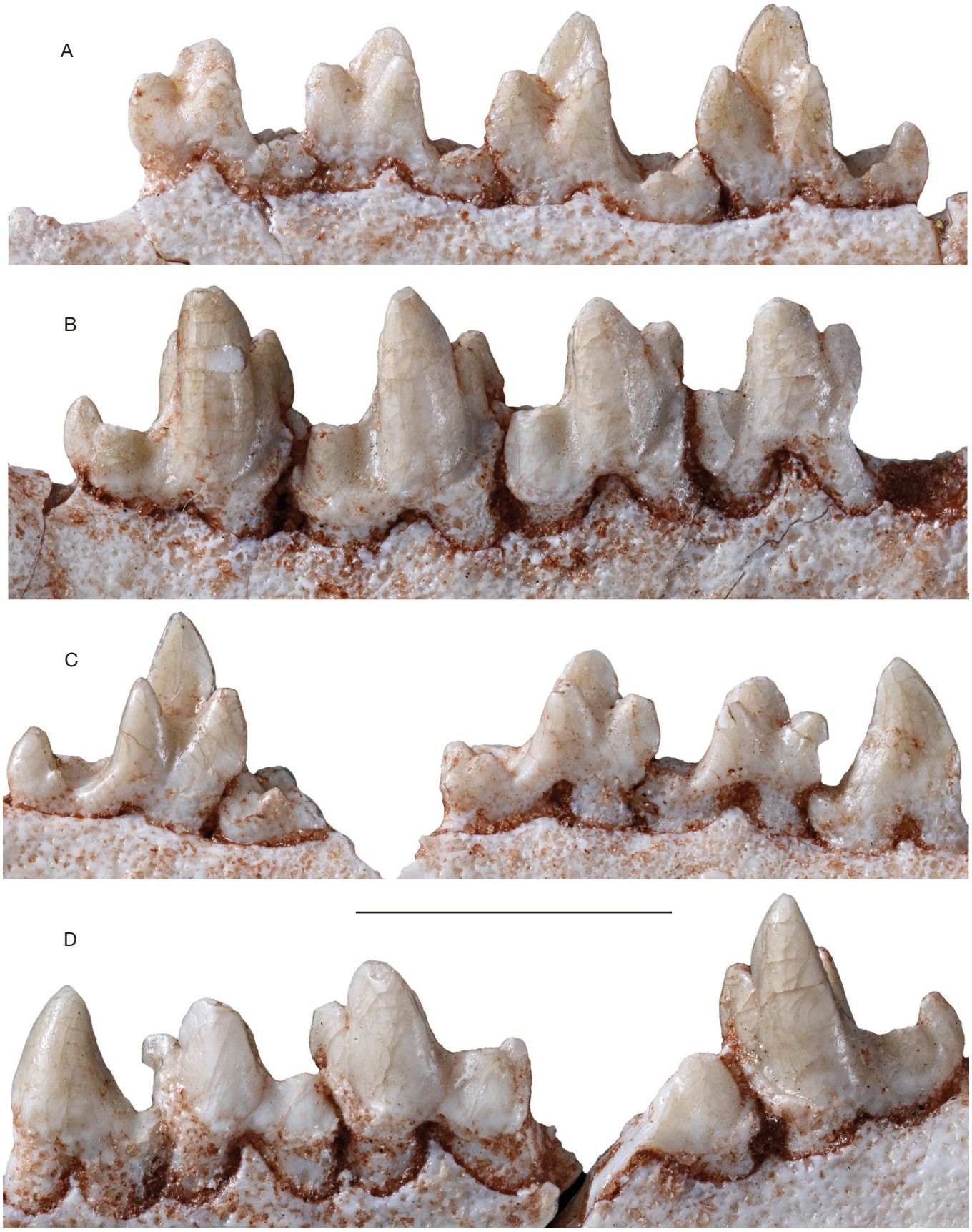

Fig. 58. — *Mayulestes ferox* Holotype MHNC 1249. **A**, right lower molars in lingual view; **B**, right lower molars in labial view; **C**, left p3 and lower molars in lingual view; **D**, left p3 and lower molars in labial view. Scale bar: 5 mm.

APPENDIX 3. — CHARACTER LIST: This character list is that of Muizon *et al.* (2018) indicating the changes in some scorings and characters definitions as compared to the earlier version of this matrix provided by those authors. The data matrix and character list of Muizon *et al.* (2018: 439-455) has been established mainly on the basis of that of Forasiepi *et al.* (2015) which was significantly modified with scoring changes and modification and addition of characters. Therefore, this character list is significantly different from that of Forasiepi *et al.* (2015) that was used as a starting point. When a character is identical to that of Forasiepi *et al.* (2015), it bears the number of Forasiepi *et al.*'s list as follows: (F000). When the character states have been modified or when some rewording has been necessary, it is indicated as follows: (F000, modified). We refer to Forasiepi *et al.* (2015) and to Forasiepi (2009) for the credit on the original mention of these characters. Scoring changes (from Forasiepi *et al.* 2015) mentioned in Muizon *et al.* (2018) are not reproduced here.

Dental characters 1 to 102
Mandibular characters 103 to118
Cranial characters: 119 to 242
Post-cranial characters: 243 to 364

Dental characters

1. **Number of upper incisors (F108):** five (0); four (1); three (2); two or less (3). Changes in scorings of Muizon *et al.* (2018): *Deltatheridium*: ? > 1. **Ordered.**

Comment: in sparassodonts and dasyuromorphians with four incisors, it is probable that the I5 has been lost (Forasiepi 2009; Hershkovitz 1995). Sparassodonts with three upper incisors probably also lost the I1 (see Forasiepi 2009: 149, 150 and references therein for a discussion on the homologies of metatherian upper incisors).

2. **Size of extra-alveolar portion of root of I1 (F109, modified):** longer than on others incisors and longer than crown; (the length of the extra-alveolar root is greater than that of the crown) (0); as long as on other incisors and as long as crown (1).

Comment: This character corresponds in part to the character formulated by several authors as "size (or shape) of first upper incisor" (Muizon et al. *1997; Rougier* et al. *1998; Wroe* et al. *2000; Luo* et al. *2003.). However, we consider that this formulation is imprecise and often erroneous in stating that the I1 is enlarged. In fact, in most cases the crown of I1 is not significantly larger than that of the other incisors, but in some cases, it is only slightly longer. The most characteristic feature is the length of the extra-alveolar portion of the root which is notably long. The sparassodonts with three incisors are scored inapplicable because the I1 is assumed to be missing (see character 1).*

3. **Implantation of the first upper incisors in anterior view**: incisors parallel (0); roots diverging dorsally (1).
4. **Diastema between 11 and I2**: Absent (0); Present (1).
5. **Size of I4 vs I3 (F110):** I4 subequal to smaller than I3 (0); I4 larger (1).
6. **Size of I3 vs I2:** I3>I2 (0); I3=I2 (1); I3<I2 (2). **Ordered.**
7. **Size of I5 vs I4 (F111):** I5 subequal to or larger than I4 (0); I5 smaller than I4 (1); I5 lost (2). **Ordered.**
8. **Shape of upper incisors:** peg-shaped (0); spatulate (1).
9. **Upper incisor arcade (F112 modified):** parabolic (0); slightly convex anteriorly (1); transverse (2); not an arcade, compressed transversely with incisors telescoped (3). **Ordered.**
10. **Number of lower incisors (F113):** four (0); three (1); less than three (2). Changes in scorings of Muizon *et al.* (2018): *Deltatheridium, Deltatheroides*: ? > 1. **Ordered.**
11. **Staggered i3 (F114):** absent (0); present (1). Changes in scorings of Muizon *et al.* (2018): *Deltatheridium:* ? > 1.
12. **Lower incisors procumbent**: present (0); absent (1)
13. **Lower canine procumbent:** absent (0); present (1).
14. **Shape of canines (F115):** small: upper canine lower than twice the height of P3, lower canine same height or lower than apex of molars protoconid (0); large: upper canine as high as or taller than twice the height of P3, lower canine taller than apex of molars protoconid (1); saber-like upper canines (2). **Ordered.**
15. **Pulp cavity of canines (F116):** closed in adults (0); open in upper canines only (1); open in upper and lower canines (2). **Ordered.**
16. **Roots of canine (F117):** smooth (0); corrugated (1).
17. **Number of roots of upper canine**: two (0); one (1) (Rougier *et al.* 1998).
18. **Number of postcanine tooth family:** eight or more (0); seven or fewer (1) (Rougier *et al.* 1998, modified). Changes in scorings of Muizon *et al.* (2018): *Deltatheroides*: ? > 1.
19. **Number of premolars (F118):** five (0); four (1); three (2), two or fewer (3) (Rougier *et al.* 1998). Changes in scorings of Muizon *et al.* (2018): *Deltatheroides*: ? > 2. .**Ordered.**
20. **Orientation of first upper and lower premolars relative to tooth row (F119, modified):** parallel (0); oblique (1); transverse (2). Changes in scorings of Muizon *et al.* (2018): *Eodelphis*: 0 > 3; *Pucadelphys*: 0&1 > 0. **Ordered.**
21. **First upper premolar strongly asymmetrical in lateral view:** absent or weak (0); distinctly present (1). Changes in scorings of Muizon *et al.* (2018): *Deltatheridium*: 0 > 1; *Eodelphis*: ? > 1.

Comment: in state (0), the apex of the tooth is roughly above the space between the two roots, or the middle of the crown when the tooth is single-rooted. In state (1), the apex of the tooth is above the anterior root, or above anterior edge of the crown when the tooth is single-rooted.

22. **Diastema anterior to first upper premolar (F120):** absent (0); present (1). Changes in scorings of Muizon *et al.* (2018): *Deltatheridium*: 0 > 0&1; *Eodelphis*: ? > 0; *Didelphis, Monodelphis, Metachirus*: 1 > 0.
23. **Diastema posterior to first upper premolar (F121):** absent (0); present (1). Changes in scorings of Muizon *et al.* (2018): *Eodelphis*: ? > 0;
24. **Diastema posterior to first lower premolar (F122):** absent (0); present (1).

Appendix 3. — Continuation.

25. **Shape of premolars (F123):** transversely compressed and uninflated (0); bulbous (1)
26. **Ultimate premolar protocone:** absent (0); small posterolingual bulge or cusp (1); distinct protocone with basin (2). **Ordered.**
27. **Size of penultimate lower premolar (F125 modified):** smaller than ultimate premolar (0); subequal to ultimate premolar (1); larger than ultimate premolar (2). **Ordered.**
28. **Change in height of the lower premolars (F126):** abrupt change in size between antepenultimate premolar and penultimate-ultimate premolar (0); abrupt change in size between antepenultimate-penultimate premolar and ultimate premolar (1).
29. **Roots of lower premolars (F127):** not inflated, as wide as crown (0); bulbous on only one premolar (1); bulbous on all premolars and some molars (2). **Ordered.**
30. **Anterobasal cusp or cingulid on penultimate premolar (F128 modified):** absent (0); present (1). Changes in scorings of Muizon *et al.* (2018): *Deltatheroides*: ? > 0; *Eodelphis* 0 > 1.
31. **Ultimate lower premolar symmetry of main cusp (F129):** absent: anterior edge of cusp more convex than posterior edge (0); present: both edges similar in curvature (1). Changes in scorings of Muizon *et al.* (2018): *Deltatheroides*: ? > 0.
32. **Timing of eruption of ultimate upper and lower premolars relative to ultimate or penultimate upper and lower molars (F130):** ultimate upper and lower premolars with penultimate or antepenultimate upper and lower molars (0); ultimate upper and lower premolars with ultimate upper and lower molars (1).
33. **Size of molars (upper and lower) increases posteriorly (F132):** moderate (0); marked (1). Changes in scorings of Muizon *et al.* (2018): *Mayulestes, Allqokirus, Patene, Hondadelphys*: 0 > 1.

Comment: concerning the upper molars, the ultimate molar is not considered in the size increase. Furthermore, in the case of deltatheroidans, the last lower molar is not considered either. The changes in the scorings of the four sparassodont genera above is justified by the fact that their posterior molar increase is at the least as pronounced as in deltatheroidans, which are scored 1.

34. **Width (labiolingual) of ultimate relative to penultimate upper molar (F133 modified):** narrower (0); subequal or wider (1). Changes in scorings of Muizon *et al.* (2018): *Mayulestes*: 1 > 0.

Comment: Contra Muizon et al. *(2018) the M4 of* Mayulestes *is in fact slightly narrower than the M3 and therefore this taxon is scored 0 for this character.*

35. **Width of stylar shelf (on penultimate molar), (F151, modified):** uniform in width (0); slightly reduced labial to paracone (1); strongly reduced labial to paracone (2); vestigial to absent (3); reduced labial to metacone (4). Changes in scorings of Muizon *et al.* (2018): *Deltatheridium, Deltatheroides*: 0 > 4. **Ordered.**

Comment: a fifth state has been added to this character to take into account the condition in deltatheroidans, in which the stylar shelf of penultimate molar is distinctly reduced labial to metacone.

36. **Stylar shelf vs tooth width (on penultimate or antepenultimate molar), (F151, modified):** 50% of transverse width or more (0); less than 50% of transverse width (1).
37. **Deep ectoflexus (F152, modified):** present on one or more teeth (0); absent on any tooth (1). See Ladevèze & Muizon (2007 ch. 20) for comments on the definition of this character as defined here vs. that of Rougier *et al.* (1998) and Forasiepi *et al.* (2015).

*Comment: the depth of the ectoflexus has been shown to be highly variable for the same dental locus in some fossil and extant metatherians (*e.g., Pucadelphys andinus, Peratherium elegans, Marmosa murina*; see Ladevèze* et al. *2011, 2012).*

38. **Postmetacrista (on antepenultimate or penultimate molar), (F148 modified):** subequal or shorter than preparacrista (0); distinctly longer than preparacrista (1).
39. **Carnassial notch in postmetacrista at posterolabial base of metacone**: Absent (0); Present (1).
40. **Stylar cusp A (F153):** distinct but smaller than B (0); subequal to larger than B (1).
41. **Stylar cusp B (F154, modified):** present but smaller than paracone (0); subequal to or approaching the size of the paracone (1); Vestigial to absent (2).
42. **Anterolabial cingulum on upper molars**: absent (0); present (1).

Comment: stylar cusps A and B are present but poorly individualized and integrated in a variably developed anterolabial cingulum.

43. **Stylar cusp C (F155):** absent or tiny (0); present (1).

C*omment: this feature has been evidenced as highly variable in some fossil and extant metatherians (*e.g., Pucadelphys andinus, Peratherium elegans, Marmosa murina*; see Ladevèze* et al. *2011, 2012).*

44. **Relative size of Stylar cusp B and D:** B smaller or subequal to D (0); B larger than D (1). Changes in scorings of Muizon *et al.* (2018): *Deltatheroides*: 0 > 1.
45. **Stylar cusp E (F157):** present and distinct (0); indistinct or tiny (1). Changes in scorings of Muizon *et al.* (2018): *Deltatheroides*: ? > 1.

APPENDIX 3. — Continuation.

46. **Relative size of paracone vs metacone (on penultimate or antepenultimate molar), (F134 modified):** subequal or slightly larger (0); slightly smaller in volume and height (*c.* 10%) (1); distinctly smaller in volume and height (*c.* 30% smaller); (2); much smaller (*c.* 50% or less) (3); absent or simple bulge on the anterior edge of metacone (4). **Ordered.**
47. **Shape of paracone and metacone (F136):** conical (0); triangular (flat labial face) (1).
48. **Metacone and paracone contact (F137 modified):** separated – i.e. point of junction of premetacrista and postparacrista approximately at the level of the floor of trigon and/or stylar shelf basin (0); adjoined at base (on, at least, half of their height) – i.e. point of junction of premetacrista and postparacrista well below the level of the floor of the trigon and stylar shelf basin (1); adjoined on most of their height; apices of cusps only are separated (2). **Ordered.**
49. **Metacone on last molar (F139):** present and distinct (0); extremely reduced (1), absent (2). Changes in scorings of Muizon *et al.* (2018): *Deltatheridium*: 0 > 1. **Ordered.**
50. **Centrocrista (F138):** straight (0); V-shaped (1).
51. **Relative lengths of preparacristae of penultimate and ultimate molars (F147):** preparacrista of ultimate molar shorter than that of penultimate molar (0); preparacrista of ultimate molar subequal to longer than that of penultimate molar (1).
52. **Orientation of preparacrista (on penultimate or antepenultimate molar), (F146 modified):** transverse (0); anterolabial (1).
53. **Conules (F143):** present (0); absent (1).
54. **Conules wing-like cristae (F144):** present (0); absent (1).
55. **Conules labiolingual position (on penultimate or antepenultimate molar), (F145):** at or lingual to mid-point between protocone and para/metacone (0); closer to para/metacone (1).
56. **Trigon basin:** absent (0); present (1).
57. **Protocone size (on penultimate or antepenultimate molar), (F 141, modified):** absent or very small (0); small and anteroposteriorly narrow (1); anteroposteriorly expanded (2); with posterolingual projection (3). **Ordered.**
58. **Protocone height (F142, modified):** approximately half the height of metacone or less (0); only slightly lower than metacone (1); almost the size of metacone or higher (2). **ordered**
59. **Roots on ultimate molar (F140):** 3 (0); 2 or 1 (1).
60. **Paracingulum (on penultimate or antepenultimate molar), (F149):** continuous between stylar margin and paraconule (0); interrupted between stylar margin and paraconule (1); absent (2). **Ordered**
61. **Postprotocrista labial extension:** does not extend labially past the base of the metacone (0); extends labially past the base of metacone (1).
62. **Precingulum (on penultimate or antepenultimate molar):** absent or weak (0); present (1).
63. **Postcingulum (on penultimate or antepenultimate molar), (F150):** absent or weak (0); present (1).
64. **Size of ultimate lower molar (F158):** subequal or smaller in height and/or length than penultimate molar (0); larger in height and/or length than penultimate molar (1).
65. **Ventral extent of the enamel above posterior root lower than above anterior root on labial side of the crown of lower molars (F159):** absent (0); present only on first and second molars and weakly developed (1); on the first three molars and strongly developed (2). Changes in scorings of Muizon *et al.* (2018): *Deltatheroides*: ? > 0.
66. **Lingual opening of trigonid basin on penultimate molar when possible (162, modified):** wide open: angle between protocristid (or postprotocristid when metaconid is lost) and paracristid more than 45°; (0); less open: angle proto-paracristid between *c.* 45° and 15° (1); anteroposteriorly compressed: cristids subparallel (2). Changes in scorings of Muizon *et al.* (2018): *Deltatheroides*: 0 > 1. **Ordered.**
67. **Trigonid basin floor**: sub-horizontal (0); sloping lingually (1); lost (2).
68. **Trigonid proportions:** wider than long (0); as wide as long (1); longer than wide (2). Changes in scorings of Muizon *et al.* (2018): *Deltatheroides*: ? > 1. **Ordered.**
69. **Trigonid height (on penultimate or antepenultimate molar), (F167, modified):** much higher than talonid (more than twice), (0); moderately higher than talonid (twice or less), (1).

Comment: When the talonid is extremely reduced or lost, this character is scored as inapplicable.

70. **Trigonid vs talonid width (on penultimate or antepenultimate molar), (F166):** wider than talonid (0); as wide as talonid (1); narrower than talonid (2).

Comment: taxa with incomplete trigonid (lack of metaconid) are scored as inapplicable.

71. **Protoconid labial expansion:** the labial edge of the protoconid at mid-height is strongly convex, protruding labially and overhangs the base of the crown; as a consequence, the apex and base of the trigonid are more lingual than the mid-height region of the cusp and the trigonid is therefore wider at mid-height than at its base (see Fig. 14); present (0); absent (1). Changes in scorings of Muizon *et al.* (2018): *Deltatheroides*: ? > 0.

Comments: state (1) corresponds to a protoconid regularly widening towards the base of the cusp, which is therefore wider at its base than at mid-height.

Appendix 3. — Continuation.

Lotheridium *is scored absent for this character,* contra *Bi* et al. *(2015) on the basis of a personal communication of Shundong Bi to one of us (CM).*

72. Trigonid vs talonid length (on penultimate or antepenultimate molar), (F165): subequal in length to talonid (0); longer than talonid (1); shorter than talonid (2). Changes in scorings of Muizon *et al.* (2018): Deltatheroides: ? > 1. Ordered.
73. **Talonid:** small heel (0); multicusped basin (1). Changes in scorings of Muizon *et al.* (2018): *Deltatheroides*: ? > 1.
74. **Proportions of talonid basin (F175):** longer than wide (0); as long as wide (1); wider than long (2). **Ordered.**
75. **Relative size and shape of talonid of ultimate vs penultimate molar (F160):** talonid of ultimate molar similar to anterior tooth (0); talonid of ultimate molar reduced and narrower than on anterior tooth (1). Changes in scorings of Muizon *et al.* (2018): *Deltatheroides*: ? > 0.
76. **Paraconid position (on penultimate or antepenultimate molar), (F163, modified):** at anterior edge of the trigonid (0); at anterolingual angle of trigonid (1).

Comment: the wording of this character considers the position of the paraconid on the trigonid rather than the metaconid as in Character 163 of Forasiepi et al. *(2015). Because, implicitly, it is the relative position of the two cusps, which is considered, this formulation gives identical results in term of scoring. We prefer to refer to the paraconid because the transverse position of this cusp varies considerably in therian lower molar evolution, while that of the metaconid is less variable. Furthermore, the position of the lingual edge of the metaconid is displaced labially when the metaconid is reduced, a bias which is avoided if considering the paraconid.*

77. **number of cusps on last molar talonid:** three (0); two (1); one (2). **Ordered.**
78. **Vertical keel (ridge) at anterolingual angle of paraconid labially bordered by hypoconulid notch (vertical sulcus at lingual end of precingulid) (F172):** absent (0); present (1).
79. **Orientation of protocristid (or postprotocristid) vs anteroposterior axis of the molar (on penultimate or antepenultimate molar), (F164, modified):** transverse or slightly oblique (i.e., less than 45°) (0); strongly oblique (i.e., more than 45°) or parallel (1).
80. **Paraconid elongated with anterior projection of the paraconid keel (ridge) mostly in the ventral half of the cusp:** absent (0); present (1); (Marshall *et al.* 1990, modified).

Comment: as a consequence of the anterior projection of the paraconid keel, the anterior edge of the cusp is markedly convex.

81. **Precingulid (F173):** on protoconid and paraconid (0); on paraconid (1); absent (2). **Ordered**
82. **Height of protoconid (Hpo) relative to length of ultimate or penultimate lower molar (Lm)**: Hpo/Lm < 0.9 (0); Hpo/Lm > 0.9 (1). Changes in scorings of Muizon *et al.* (2018): *Deltatheroides*: ? > 1.
83. **Protoconid height in trigonid (F171):** tallest cusp of trigonid (0); sub-equal to para- and/or metaconid (1).
84. **Height of metaconid vs paraconid (on penultimate molar) (F170, modified):** higher (0); subequal (1); lower (2). **Ordered.**

Comment: taxa in which the metaconid is lost are scored inapplicable.

85. **Volume of the metaconid vs paraconid (on penultimate molar), in occlusal and lingual views**: larger (0); subequal (1); smaller (2).

Comment: taxa in which the metaconid is lost are scored inapplicable.

86. **Metaconid on first molar (F168):** present (0); absent (1).
87. **Metaconid on molars between the first and last molar (F169 modified)**: Present (0); Present, but extremely reduced as a tiny cuspule at the posterior base of the protoconid (1); Absent (2).
88. **Metaconid on ultimate lower molar:** present (0); vestigial or absent (1) Changes in scorings of Muizon *et al.* (2018): *Deltatheroides*: ? > 0.
89. **Relative lengths of para- and protocristid:** subequal (0); paracristid > protocristid (1); protocristid > paracristid (2).
90. **Anterior end of cristid obliqua (F184):** beneath carnassial notch (0); lingual to carnassial notch (1); labial to carnassial notch (2). Changes in scorings of Muizon *et al.* (2018): *Deltatheroides*: ? > 1.

Comment: taxa which lack a metaconid also lack a carnassial notch and are scored as inapplicable.

91. **Carnassial notch in cristid obliqua (F186):** absent (0); present (1).
92. **Hypoconulid position (F180, modified):** in median position (0); shifted lingually, close to entoconid (1); absent (2).
93. **Hypoconulid of last molar (F181, modified):** as tall as or lower than other talonid cusps (0); taller than other talonid cusps (1); absent (2).
94. **Hypoconid position (F176):** middle of labial margin of tooth (0); posterolabial angle of tooth (1); absent (2). Changes in scorings of Muizon *et al.* (2018): *Deltatheroides*: ? > 0.
95. **Shape of entoconid (F177):** conical (0); transversely compressed (1); vestigial to absent (2).
96. **Relative height of entoconid (F178):** lower than hypoconid (0); subequal to taller than hypoconid (1); absent (2).
97. **Position of entoconid relative to trigonid (on antepenultimate or penultimate molar) (F179, modified):**

APPENDIX 3. — Continuation.

at posterolingual corner of tooth (in posterior half of the distance between the posterior base of trigonid and posterior margin of tooth) (0); between posterior edge of trigonid and posterior margin of tooth (mid-way or in anterior half of the distance between the posterior base of trigonid and posterior margin of tooth) (1).

98. **Entocristid (F182, modified):** absent or weakly developed (0); well-developed and sharp (1).
99. **Posthypocristid:** oblique relative to long axis of tooth (0); transverse relative to long axis of tooth (1).
100. **Hypoflexid (F185):** deep (*c.* 40-50% of talonid width) (0); shallow or absent (less than 40% of talonid width) (1).
101. **Labial postcingulid (F187):** absent (0); present (1).
102. **Postcingulid on last molar:** present (0); absent (1).

Mandibular characters

103. **Depth/length of the dentary below molars (F97):** shallow (less than 0,15) (0); intermediate (between 1,5 and 2) (1); elevated (more than 2) (2). **Ordered.**

Comment: In the case of Mayulestes*, because the ramus mandibularis (vertical ramus) is missing in the only specimen known, the length of the dentary has been estimated on the basis of the position of the postglenoid process and articular condyle, when the lower tooth row of the dentary is in occlusion with the upper tooth row*.

104. **Ventral margin of the dentary behind last molar continuous to condyle (F98):** straight (0) or gently curved (1); angled (2).
105. **Mandibular symphysis (F99):** unfused (0); fused (1).
106. **Anteroventral edge of mandibular symphysis:** slanting and forming a small angle with tooth row (< 25°) (0); less slanting, forming an angle > 25° (1).
107. **Posteriormost mental foramen (F100):** below last premolar or anterior (0); at last premolar/m1 embrasure (1); below first molar (2); posterior to first molar (3). **Ordered.**
108. **Masseteric fossa:** restricted dorsally by crest reaching condyle (0); extended ventral to lower margin of dentary (1), (Rougier *et al.* 1998: ch. 67).
109. **Posterior shelf of masseteric fossa:** absent (0); present (1), (Rougier *et al.* 1998: ch. 68).
110. **Labial mandibular foramen (F102):** present (0); absent (1).
111. **"Coronoid" facet:** present (0); absent (1), (Rougier *et al.* 1998: ch. 76).
112. **Angle between coronoid process and tooth row (F104):** subvertical between 95° and 105° (0); Between 106° and 125° (1); more than 125° (2). **Ordered.**

Comment: The condition in Patene *has been measured on the left mandible of IML-PV 2618, in which the ramus mandibularis is in correct position relative to the corpus mandibularis. On the right dentary, the ramus is not in anatomical position and, in medial view, it is slightly rotated clockwise. Because of this incorrect position of the ramus, the angle of the coronoid process of the right dentary is distinctly greater than on the left dentary.*

113. **Retromolar space (F101):** absent (0); present (1).
114. **Angular process medially inflected:** absent (0); present (1), (Rougier *et al.* 1998: ch. 73, modified).
115. **Morphology of medially inflected angular process (F103):** shelf-like (ASL/AL>0.81) (0); intermediate (0.72<ASL/AL <0.81) (1); rod-like (ASL/AL < 0.72) (2). ASL: angular process shelf length, AL: angular process length. **Ordered**
116. **Anteroposterior position of mandibular foramen (F105):** posterior to mid-point of coronoid process (0); at mid-point of coronoid process (1); anterior to mid-point of coronoid process (2). **Ordered.**
117. **Morphology of mandibular condyle (F106):** subspherical (0); cylindrical (1).
118. **Condyle vertical position vs tooth row (F107):** approximately at the same level or slightly below (0); above (1).

Comment: The condition in Patene *has been scored on the left mandible of IML-PV 2618, in which the ramus mandibularis is in correct position relative to the corpus mandibularis. On the right dentary, the ramus is not in anatomical position and, in medial view, it is slightly rotated clockwise. Because of this incorrect position of the ramus, the condyle appears to be almost at the level of the tooth row, as stated by Goin* et al. *(1986). On the left dentary, in which the position of the ramus is correct, the condyle is located well above the tooth row.*

Cranial characters

119. **Length of the skull (F1):** short (less than twice width at the level of zygomatic arch), (0); long (more than twice width at level of zygomatic arch), (1).
120. **Length of the rostrum (F2):** less than (or equal to) ⅓ total length of the skull (0); between ⅓ and ½ total length of the skull (1); more than ½ total length of the skull (2).

Comment: The length of the rostrum of Allqokirus *has been estimated because the only skull known (MHNC 8267) is that of a subadult individual in which the M4 and m 4 are not fully erupted. The correction applied is the length of the m4 (*c. *3.5 mm). With this correction, Allqokirus is scored 1 for this character.*

121. **Expanded apex of the rostrum with concave tooth rows and lateral edges of the rostrum between canine and infraorbital foramen**: absent (0); present (1).
122. **Width of the braincase versus maximum postorbital width (F3)**: braincase at base of zygomatic arches wider than maximum postorbital width (0); braincase narrower than maximum postorbital width (1).

Appendix 3. — Continuation.

123. **Proportions of the braincase (F4 modified)**: almost as wide as long (0); distinctly wider than long (1); longer than wide (2).
124. **Level of the palate relative to basicranium (F 5)**: palate lower than basicranium (0); palate and basicranium at the same level (1).
125. **Anterolateral process of the maxilla in the paracanine fossa (F6 modified)**: present: the anterolateral process of the maxilla closes the fossa laterally; the paracanine fossa is composed of the maxilla and premaxilla (0); absent: the fossa is opened laterally; the paracanine fossa is composed of the premaxilla only (1).
126. **Paracanine fossa morphology**: not extended dorsally: longer (anteroposteriorly) than high (dorsoventrally) (0); extended dorsally: higher dorsoventrally than (or as high as) long (anteroposteriorly) (1).
127. **Precanine notch (F7):** absent (0); present (1).

Comment: in dorsal or ventral view, the presence of a precanine notch results in a transverse constriction of the rostrum just anterior to the canine. The precanine notch is scored present in Allqokirus *and* Mayulestes *because the weak but distinct concavity observed anterior to the canine is regarded as an incipient development of this character (see Figs 3 and 4).*

128. **Lateral palatal process of the premaxilla (F8 modified):** anterior to anterior border of canine alveolus (0); just reaches anterior border of canine alveolus (1); posterior to anterior border of canine alveolus (2). **Ordered.**
129. **Posterior border of incisive foramen (F9):** anterior to or just reaches anterior border of canine alveolus (0); posterior to anterior border of canine alveolus (1).
130. **Dorsoventral position of the medial palatal process of the premaxilla (F10):** horizontal (0); with posterior end shifted dorsally, forming an incisive fossa (1).
131. **Distinct narial tubercle or process at the anterodorsomedial angle of the premaxilla (F11):** absent (0); present and small (narrower than I1) (1); present and very large (wider than I1) (2). Changes in scorings of Muizon *et al.* (2018): *Didelphodon* 1 > 2; *Pharsophorus* ? > 1; *Australohyaena*: 1 > 0;
132. **Posterior end of the facial (posterodorsal) process of the premaxilla (F12 Modified):** above canine or anterior (0); above P1 or P2 (1); posterior to P2 (2). **Ordered.**
133. **Anterior parabolic protrusion of nasals, which overhangs nasal aperture (F13):** present (anterior protrusion is approximately as long as width of the nasal at the level of anteriormost point of the nasal-premaxilla suture) (0); absent (1).

Comment: Mayulestes *has been scored 1 for this character in spite of statement by Muizon (1998: 34) that these "bones extend anteriorly beyond the anteriormost point of the nasal-premaxilla suture". In fact, this statement is biased by the distortion (dorsoventral compression) of the specimen. The distortion has pushed the nasal ventrally and the maxillae dorsally. More important, the distortion also shows a slight anteroposterior component, which has pushed the maxillae and premaxillae posteriorly. This condition is evidenced on the posterior part of the Na-Mx suture, where the maxillae clearly overlap the nasals (in the anterolateral portion of the posterior expanded region of the nasals). In this respect, the reconstruction of Muizon (1998: fig 6A) is clearly inaccurate. Given that, although the anterior edge of the nasals of* Mayulestes *is slightly convex anteriorly, their condition is clearly more similar to those of* Thylacinus *and* Arctodictis *than to those of* Didelphis *and* Pucadelphys. *In these taxa, the anterior extension of the nasal is at least as large as the width of the nasal at the level of the anterior end of the nasal-premaxilla suture. This is certainly not the case in* Mayulestes. *In contrast,* Callistoe*, in which the nasals distinctly protrude anteriorly, has been scored 0.*

134. **Anterior end of the nasals:** V-shaped (or parabolic) (0); transverse or slightly convex anteriorly (1); notched (V-shaped posteriorly) (2). **Ordered.**
135. **Shape of naso-frontal suture (F14, modified):** acute W- or V-shaped (0); wide open W or posteriorly convex (1).
136. **Nasofrontal suture with medial process of the frontals wedged between the nasals:** Present (0); Absent (1), (Rougier *et al.* 1998: ch. 84).
137. **Postorbital process (F15, modified):** absent (0); weak tuberosity (1); conspicuous protruding process (2). **Ordered.**
138. **Orbital crests (F35)**: absent (0); present (1).
139. **Naso-lacrimal contact (F16):** present (0); absent (1).
140. **Facial process of the lacrimal (F30, modified):** large triangular and pointed anteriorly (0); small crescentic and rounded anteriorly (1).
141. **Lacrimal tubercle (F31 modified):** present, knob-like (0); present, crest-like (1); absent (2).
142. **Lateral wall of ventral or lateral lacrimal foramen (F32, modified):** distinctly anterior to medial wall (foramen exposed on face and faces laterally or posterolaterally) (0); at the same anteroposterior level as the medial wall (foramen not exposed on face and faces posteriorly) (1); intermediate (one foramen on face, the other in the orbit) (2).
143. **Number of lacrimal foramina (F33):** two (0); one (1).
144. **Infraorbital foramen position (F18, modified):** above penultimate premolar (0); above ultimate premolar (1); above M1 or posterior (2). Changes in scorings of Muizon *et al.* (2018): *Eodelphis*: ? > 1. **Ordered.**
145. **Flaring of maxillary cheek posterior to infraorbital foramen (F19):** present (0); absent (1).

APPENDIX 3. — Continuation.

Comment: Callistoe *has been scored 0 contra Forasiepi* et al. *(2015), because the holotype in ventral view presents a small but distinct flaring of the maxillae behind the infraorbital foramina. Furthermore, it is noteworthy that the skull has suffered some transverse (mediolateral) compression, which suggests that the flaring was even more pronounced than the condition actually observed on the holotype.*

146. **Angle (posterior angle) between maxilla-jugal suture and plane of the tooth row in lateral view (F17):** more than 140° (0); between 140° and 95° (1).
147. **Fossa for the levator labii muscle in the anterior end of the jugal:** absent (0); present mainly in the jugal (1); present mainly in the maxilla (2).
148. **Anterior medial and lateral palatal processes of the maxilla:** both processes approximately of the same size (0); medial process much smaller than the lateral or absent (1).
149. **Number of palatal pits independently of their size (F21, modified):** none (0); one (between ultimate and penultimate molar) (1); two between ultimate, penultimate and antepenultimate molars (2); two pits between first, antepenultimate, and penultimate molars. (3), three between each molar (4). Changes in scorings of Muizon *et al.* (2018): *Eodelphis*: ? > 4. **Unordered**.
150. **Palatal vacuities (F22):** absent (0); present (1). Changes in scorings of Muizon *et al.* (2018): *Eodelphis*: ? > 1;
151. **Major palatine foramen (F23):** well individualied, within maxilla and/or palatine (0); multiple small foramina in palatine and/or maxilla (1).
152. **Minor palatine foramen (F24, modified):** present and complete (closed posteriorly) (0); incomplete (open posteriorly) or absent (1).
153. **Palatal expansion with regard to ultimate molar (F25, modified):** posterior (0); even with (1); anterior (2). **Ordered.**
154. **Posterior palatine spine (F26, modified):** weak or absent and posterior edge of the palate concave posteriorly (0); absent and posterior edge of the palate straight (1); prominent and posterior edge of the palate double-arched (2), (see Wible *et al.* 2009: ch. 192).
155. **Size of foramen or groove in lateral edge of postpalatine torus:** absent (0); present and small (less than half the diameter of the minor palatine foramen or groove), (1); present and large (approximately half the diameter of the minor palatine foramen or more (2). **ordered**

Comment: state (1) present in didelphids corresponds to the postpalatine torus foramen of Wible (2003: fig. 9 p. 144).

156. **Morphology of the postpalatine torus foramen**: totally or almost totally enclosed in the palatine (0); wide-open groove (the section is approximately half a circle or less) (1).
157. **Palatine enters the posterior opening of the infraorbital canal (maxillary foramen) (F27):** present (0); absent (1).
158. **Position of sphenopalatine foramen (F28):** posterior to the level of the posterior border of lacrimal (0); anterior to the level of the posterior border of lacrimal (1).
159. **Anteroposterior position of the sphenopalatine foramen relatively to the molars**: above penultimate or antepenultimate molar (0); above ultimate molar or posterior (1).
160. **Development of pterygoids (F29):** well-developed and expanded on medial side with midline contact (0); well developed and expanded on medial side but no midline contact (1); reduced, not expanded on medial side (2). **Ordered.**
161. **Posterior process of pterygoids, which covers the alisphenoid-basisphenoid suture:** present (0); absent (1).
162. **Orbitotemporal canal:** present (0); absent (1), (Rougier *et al.* 1998: ch. 103).
163. **Optic foramen (F48):** well separated from sphenorbital fissure (0); confluent with sphenorbital fissure (1).
164. **Interparietal (F36):** present (0); absent (or fused to parietals) (1).
165. **Frontoparietal suture (F37):** with posterior wedge of the frontals (0); with anterior wedge of the parietals (1); no wedge, roughly straight (2).
166. **Parietal-alisphenoid or fronto-squamosal contact (F38):** parietal-alisphenoid (0); fronto-squamosal (1).
167. **Foramina for temporal rami (F95 modified):** present (0); absent (1).
168. **Anterior lamina of the petrosal**: present with large exposure on lateral braincase wall to (0); rudimentary with small exposure on lateral braincase wall (1); rudimentary without exposure on lateral braincase wall (2); absent and totally lost (Marshall & Muizon, 1995; Ladevèze & Muizon, 2007: ch. 123; Rougier *et al.* 2015). Changes in scorings of Wilson *et al.* (2016): *Didelphodon*: 2 > 1. **Ordered.**

Comments: The addition of Vincelestes*, which has a well-developed anterior lamina exposed on the lateral braincase wall required the addition of an additionalcharacter state. Furthermore, we reconsidered this character to take into account not only the size of the anterior lamina but also its participation to the braincase wall as discussed in the formulation of this character in Rougier* et al. *(2015) matrix (Character 108: Anterior lamina exposure on lateral braincase wall).* Vincelestes *and* Prokennalestes *are respectively scored 0 and 1for this character.*

On the digital rendering of the petrosal of Didelphodon *provided by Wilson* et al. *(2016: supplementary figure 8 a, b) the fossa on the dorsolateral aspect of the petrosal, labelled "petrosal contribution to cavum epiptericum" (cep) (named trigeminal*

Appendix 3. — Continuation.

fossa in Muizon et al. *2018 and in this paper) is identical to the condition observed in* Allqokirus *and* Andinodelphys *and is regarded here as a rudimentary anterior lamina. Furthermore, on supplementary fig 8 b of Wilson* et al. *(2016) the dorsal edge of the figure is totally straight, thus indicating some missing part of the lamina probably due to difficulty in the segmentation of the petrosal. We estimate that the rudimentary anterior lamina of* Didelphodon *was probably at least as large as in* Allqokirus *and* Andinodelphys. *Therefore, in our matrix, we scored this character 2 (rudimentary without exposure on lateral braincase wall) rather than "absent" as in Wilson* et al. *(2016).*

The scoring of Pediomys *follows here that of Rougier* et al. *(2015), because we have not seen the specimen FMNH PM 53907, on which it is based. However, because this isolated petrosal is very slightly damaged, we strongly suspect that the anterior region of the "part of petrosal in middle cranial fossa" (mcf) of Wible (1990), which we regard as an equivalent of the "petrosal contribution to cavum epiptericum" (cep) of Wilson* et al. *(2016: suppl. fig. 8 a, b) and of our trigeminal fossa (Muizon* et al. *2018 and this paper) bore a vestigial anterior lamina as is observed in the Tiupampan fossils and that such a delicate structure has been broken off during fossilisation.*

169. Nuchal crest (F73): at or posterior to the level of the condyles (0); anterior to condyles (1).
170. Sagittal crest (F72): extending to frontals (0); restricted to parietals (1); absent (2). **Ordered.**
171. Glenoid process of the jugal (F34): with articular facet (0); without articular facet (1).
172. Postorbital (frontal) process of the jugal: absent (0); present (1).
173. Width of the glenoid fossa (F39): less than twice anteroposterior length (0); more than twice anteroposterior length (1), (Rougier *et al.* 1998: ch. 115, modified).
174. Preglenoid process of the squamosal (F40): absent (0); present (1).
175. Proportions of the postglenoid process (F41, modified): higher than wide and roughly parabolic (0); as wide as high (1); very low and wider than high (2). **Ordered**
176. Width of the postglenoid process: as wide as glenoid fossa (0); narrower than glenoid fossa (1).
177. Location of postglenoid foramen (F42): posterior to postglenoid process (0); medial to postglenoid process (1); anterior to postglenoid process (2); absent (3).

Comment: because of the condition in Vincelestes*, which lacks a postglenoid foramen, we added a new state to this character: absent (2).*

178. Suprameatal foramen (F43 modified): absent (0); below postzygomatic crest (1); at the same level or above postzygomatic crest (2).

Comment: Dromiciops *is scored as "non-applicable" because the postzygomatic crest does not reach the level of the suprameatal foramen posteriorly.*

179. Paroccipital process of exoccipital: low tubercle or absent (0); long process with diameter at apex smaller than proximodistal length (1).
180. Glenoid process of alisphenoid (F47): absent (0); present, does not contribute to glenoid fossa (1); present, contributes to glenoid fossa.

Comment: A conspicuous glenoid process is generally absent in sparassodonts other than Mayulestes *and* Allqokirus*, although a small projection of the alisphenoid toward the glenoid fossa is observed in* Prothylacynus*,* Arctodictis, Borhyaena*, and* Lycopsis*. This condition is interpreted here as a vestigial (or incipiently developed) glenoid process of the alisphenoid.*

181. Transverse canal (F49): absent (0); present (1).
182. Tympanic process of the alisphenoid (F50): absent (0); present (1).
183. Hypotympanic sinus (F51): absent (0); formed by squamosal, alisphenoid and petrosal (1); formed by alisphenoid alone or alisphenoid and petrosal (2).

Comment: The Gurlin Tsav Skull is scored 1 for this character following Rougier et al. *(2015).*

184. Dorsal epitympanic expansion of the hypotympanic sinus above the glenoid fossa: absent (0); present (1).
185. Medial process of the squamosal, which extends into the middle ear and forms part of the roof of the tympanic cavity (F52): absent (0); present (1). Changes in scorings of Muizon *et al.* (2018): *Eodelphis*: ? > 0.

Comments:

1) When a hypotympanic sinus is present, the medial process of the squamosal is part of the cavity (generally with the alisphenoid and the petrosal).

2) In the data matrix, we have changed the scoring of Forasiepi et al. *(2015) for* Prothylacinus, Arctodictis, *and* Australohyaena, *because in these three taxa the squamosal-petrosal suture distinctly enters the hypotympanic sinus. Therefore, the squamosal is part of the sinus (with the petrosal and alisphenoid) and consequently projects medially within the middle ear cavity. As a matter of fact, this condition is clearly mentioned by Forasiepi el al (2015: 510) in* Australohyaena*, although the authors scored the medial process of the squamosal absent in this genus.*

3) We also observed a medial process of the squamosal in Borhyaena *(YPM-PU 15120). However, because we have not observed all the available skulls of this genus, we cautiously*

APPENDIX 3. — Continuation.

follow Forasiepi et al. *(2015), who scored this character as polymorphic for this taxon.*

4) Lotheridium *is scored present for this character,* contra *Bi* et al. *(2015) on the basis of a personal communication of Shundong Bi to one of us (CM).*

5) The Gurlin Tsav Skull is scored 1 for this character following Rougier et al. *(2015).*

186. **Intratympanic sinus excavated in the exoccipital:** absent (0); present (1).
187. **Intratympanic sinus in the pars mastoidea**: Absent (0); present (1)
188. **Anterior expansion of the middle ear sinus within the lateral wall of the braincase**: absent (0); present (1), (Muizon 1999: ch. 14; Babot *et al.* 2002: ch. 13).

Comment: in Paraborhyaena, Thylacosmilus *and* Callistoe, *in addition to the spherical dorsal expansion, the hypotympanic sinus has a narrow and pointed anterior extension (not dorsal as stated by Muizon 1999), which inserts in the lateral wall of the braincase, affecting the squamosal and alisphenoid.*

189. **Squamosal extratympanic sinus excavated in the roof of the external acoustic meatus:** absent (0); present (1).
190. **Pneumatization of the squamosal with air cells present at the posterior base of the zygomatic process (F55):** absent (0); present (1).
191. **Notch or foramen in alisphenoid for greater petrosal nerve (F59):** present (0); absent (1).
192. **Primary foramen ovale (F57, modified):** between petrosal and alisphenoid (0); In alisphenoid or between alisphenoid and squamosal (1); in petrosal (2). **Ordered**

Comment: Didelphodon *is coded (?) contra Wilson* et al. *(2016) because the foramen ovale coded by Wilson is in fact a secondary foramen ovale, which is bordered ventrally by the tympanic process of the alisphenoid. The primary foramen ovale is hidden by the tympanic process of alisphenoid and is not observable on Wilson's digital renderings.*

Because of the condition in Vincelestes *we added a new state to this character: "in petrosal (2)".*

193. **Secondary foramen ovale totally enclosed in the alisphenoid (F58):** absent (0); present (1).

Comment: Didelphodon *is coded present*

194. **Carotid foramen position (F60):** well anterior to basioccipital-basisphenoid suture (0); in basisphenoid at the level of basioccipital-basisphenoid suture (1).
195. **Hypoglossal foramen number (F61, modified):** confluent with jugular foramen (0); two or more (1); one (2). **Ordered.**
196. **Groove between hypoglossal foramina and foramen for inferior petrosal sinus (F62):** absent or faint (0); present and deep (1).
197. **Jugular foramen vs inferior petrosal sinus:** separated from foramen for inferior petrosal sinus (0); confluent with foramen for inferior petrosal sinus, (Rougier *et al.* 1998: ch. 150).
198. **Size of jugular foramen relative to fenestra cochleae:** subequal or slightly larger (0); much larger, at least three times larger (1). (Ladevèze & Muizon 2007).
199. **Median keel on basioccipital (F65):** absent (0); present (1).
200. **Midline rod-shaped eminence on basisphenoid (F66, modified):** absent (0); present (1), (Wible *et al.* 2009: ch. 240).
201. **Dorsoventral position of petrosal (F76):** at the level of the basioccipital (0); distinctly dorsal to the basioccipital (1).
202. **Orientation of the pars cochlearis of the petrosal: plane defined by the apex of the promontorium-fenestra vestibuli-fenestra cochleae:** sub-horizontal or slightly oblique (0); sub-vertical (1), (Muizon 1999: ch. 20, modified; Babot *et al.* 2002: ch. 18, modified).

Comment: In this character, the axis of rotation of the pars cochlearis is oriented anteromedially-posterolaterally but remains in a roughly horizontal plane. The rotation is clockwise on the left side.

203. **Orientation of the major axis of the petrosal (axis subarcuate fossa- internal acoustic meatus):** subhorizontal to slightly oblique (0); oblique to subvertical (1); vertical (2), (Muizon 1999: ch. 20, modified; Babot *et al.* 2002: ch. 18, modified). **ordered**

Comment: in this character, the axis of rotation is oriented anterolaterally-posteromedially, approximately horizontal, i.e. *at 90° to the axis of rotation of character 202.*

204. **Anteromedial flange (= epitympanic wing) (F83):** present (0); absent (1).

Comment: the epitympanic wing, or anteromedial flange of Wible (2003), is a medially expanded crest which borders the anterior and anteromedial edge of the promontorium and which contacts the basioccipital medially. It forms the floor of the groove for the inferior petrosal sinus.

205. **Cavum epiptericum (F79, modified):** floored by petrosal alone (0); floored by petrosal and alisphenoid (1); floored primarily or exclusively by alisphenoid (2); Open as a pyriform fenestra (3). **Ordered.**

Comment: Didelphodon *is coded (1) taking into account that the petrosal contributes to the floor of the cavum epiptericum,*

Appendix 3. — Continuation.

as indicated in the supplementary figures 8 a and b of Wilson et al. *(2016).*

Regarding Pediomys *it is noteworthy that, in Wible (1990: fig 2E, G), the region labelled mcf (part of petrosal in middle cranial fossa) is likely an equivalent of our trigeminal fossa or of the cep (petrosal contribution to cavum epiptericum) of Wilson* et al. *(2016: suppl. fig. 8 a, b). Therefore, it is probable that the cavum epiptericum of the petrosal described by Wible (1990) and commonly accepted to be referred to* Pediomys, *was actually floored by, both, the petrosal and the alisphenoid. We therefore question the scoring of Rougier* et al. *(2015) (2, floored primarily or exclusively by the alisphenoid). However, because we have not seen the specimen FMNH PM 53907, we follow their scoring here.*

Furthermore, because this petrosal is very slightly damaged, it is likely that the anterior region of the "mcf-cep-trigeminal fossa" bore a vestigial anterior lamina as in observed in Tiupampa fossils, and that such a delicate structure has been broken off during fossilisation. See comment above on character 168.

206. **Medial expansion of the crista petrosa that forms a thin and straight lamina covering the anterolateral part of the fossa subarcuata:** absent (0); present (1), (Ladevèze & Muizon 2007: ch. 122)
207. **Internal acoustic meatus (F80):** deep with thick prefacial commissure (0); shallow with thin prefacial commissure (1).
208. **Internal acoustic meatus (IAM) and subarcuate fossa:** subequal and separated by sharp wall (0); IAM narrower than the opening of the subarcuate fossa and separated by a thick wall (1) (Ladevèze & Muizon 2007: ch. 125).
209. **Fossa subarcuata (F81, modified):** deep: greatest diameter larger than aperture (spherical) (0); intermediate: greatest diameter subequal to aperture (cylindrical) (1); wide open: greatest diameter is the aperture (conical) (2); very shallow or absent: just a depression (3). **Ordered.**
210. **Deep groove for internal carotid artery excavated in medial side of promontorium apex ventrally (F82):** absent (0); present (1).

*Comment: in some taxa with a subvertical promontorium, the groove is located at the anterior end of the apex of the promontorium (*i.e. Borhyaena, Pharsophorus, Arctodictis,*) rather than on the ventral aspect of the apex as in taxa in which the promontorium is not subvertical (*i.e. Notogale, Cladosictis, Sipalocyon*). In* Arctodictis*, the structure referred by Forasiepi (2009) as a possible fossa for the tensor tympani muscle is identified here as the carotid groove. Because of the function of the tensor tympani muscle, this fossa is generally located on the lateral edge of the promontorium, anterior to the secondary facial foramen. Given the morphology of the petrosal of* Arctodictis*, a position of the tensor tympani fossa at the anteromedial apex of the promontorium is unlikely.*

4) Lotheridium *is scored absent for this character* contra *Bi* et al. *(2015) on the basis of a personal communication of Shundong Bi to one of us (CM).*

211. **Prootic canal (F84):** present (0); absent (1). Changes in scorings of Muizon *et al.* (2018): *Herpetotherium*: 1 > 0.

Comment: the prootic canal of Mayulestes, Notogale, Siplaocyon *and* Borhyaena *has been observed on CT data (see Muizon* et al. *2018). The scoring of* Thylacinus *and* Sminthopsis *follows Archer (1976a) and Wroe* et al. *(2000: 1024, see comment on character 77).*

A careful re-examination of the CT data of Herpetotherium *has allowed to observed a small prootic canal in* Herpetotherium, contra *Horovitz* et al. *(2008)*

212. **Prootic canal morphology:** large with endocranial opening (0); reduced with intramural opening (1), (Ladevèze & Muizon 2007: ch. 148). Changes in scorings of Muizon *et al.* (2018): *Herpetotherium*: 1 > 0.
213. **Rostral tympanic process of petrosal (F85, modified):** absent or low ridge of smooth tubercle (0); erected process (1); distinct ridge restricted to posterior half of promontorium (2); tall ridge reaching apex of promontorium (3).

Comment: two supplementary states have been added to this character following states 1 and 2 of character 85 of Forasiepi et al. *(2015).*

214. **Tensor tympani fossa:** smooth and shallow area (0); distinct elongated fossa at anterolateral edge of promontorium (1); long and narrow groove bordering the anterolateral edge of promontorium (2) (Geisler 2001: ch 14; Ladevèze & Muizon 2007: ch. 128).
215. **Eustachian foramen in posteroventromedial petrosal sinus (F56, modified):** absent (0); present (1).

*Comment: This foramen is observed at the junction of the rostral tympanic process and the tympanic process of the alisphenoid. The rostral tympanic process greatly develops, ventrally and laterally and floors the whole promontorium (*e.g., *in* Dasyurus*) anteroventrally and forms a ventromedial sinus, closed ventrally by its contact with the alisphenoid process. The exit of the Eustachian tube from the middle ear is through a foramen anteriorly at the junction of the alisphenoid and rostral tympanic processes.*

216. **Rostral tympanic process anterolaterally directed wing:** absent (0); wing restricted to posterior region of promontorium (1); wing extend over the whole length of promontorium and contacts the alisphenoid tympanic process anteriorly (2), (Ladevèze & Muizon 2007: ch. 134). **Ordered.**

APPENDIX 3. — Continuation.

217. Petrosal plate: absent (0); present (1), (MacPhee 1981; Ladevèze & Muizon 2007: ch. 142).

Comment: The petrosal plate is formed by the ventral junction of the rostral and caudal tympanic processes of the petrosal.

218. Caudal tympanic process anterior extension: absent (0); present (1), (Ladevèze & Muizon 2007: ch. 141).

Comment: In state 1, the caudal tympanic process extends anteriorly and totally floors the postpromontorial sinus.

219. Relative size of posttympanic and paroccipital processes (F45): paroccipital process longer (0); both processes are similar in size (1).

220. Orientation of the posttympanic and/or paroccipital processes (F46): ventrally projected (0); anteroventrally projected (1).

*Comment: when the processes are anteroventrally projected, they tend either to contact the tympanic process of the alisphenoid when present (*Notogale, Cladosictis*, and* Sipalocyon*) or to contact the medial region of the posterior wall of the postglenoid process or the anterior wall of the external auditory meatus (*Lycopsis, Paraborhyaena*). An extreme condition is found in* Thylacosmilus*, in which the postmeatal and paroccipital processes contact the alisphenoid and squamosal anteriorly, medial to the glenoid fossa. Since* Thylacosmilus *has no tympanic process of the alisphenoid, the tympanic cavity is floored ventrally by the postmeatal and paroccipital processes only.*

221. Diameter of stapedius fossa (F94): approximately twice the size of that of fenestra vestibuli (0); distinctly less than twice the size of that of the fenestra vestibuli (=small and shallow) (1).

222. Mastoid process (= paroccipital process of Rougier *et al.* 1998); (F86, modified): proximodistally long and vertical (0); small nodular tubercle on posterolateral border of stylomastoid notch (1); indistinct or absent (2), (Ladevèze & Muizon 2007: ch. 139).

223. Hiatus Fallopii (F87, modified): on dorsal (cerebellar) face of petrosal (0); intermediary (i.e. neither visible in dorsal nor in ventral views) (1); ventral (tympanic) face of petrosal (2). **Ordered.**

224. Exit of facial nerve (F88): stylomastoid notch (0); stylomastoid foramen (1).

225. Floor of cavum supracochleare (F89): absent (0); present (1).

226. Roof of cavum supracochleare: Open dorsally in cavum epiptericum (0); Closed (1), (Rougier *et al.* 1998: ch. 128).

227. Tympanic petrosal crest (= petrosal crest of Archer, 1976 and Muizon, 1999), (F93): absent (0); present (1). Changes in scorings of Muizon *et al.* (2018): *Didelphodon*: ? > 1.

228. Tuberculum tympani: Absent (medial and lateral ends of tympanic petrosal crest equally developed) (0); Moderately developed (lateral end of tympanic petrosal crest larger than medial one) (1); expanded in a sharp anteroventrally directed process (triangular in lateral view (2).

Comment: an additional state has been added in order to better define this character and to better exemplify the development of the lateral end of the tympanic petrosal crest, which forms the tuberculum tympani.

229 – Contribution of squamosal to epitympanic recess (F91, modified): squamosal part as large as petrosal one (0); squamosal part distinctly smaller than petrosal one (1); squamosal part distinctly larger than petrosal one (2); squamosal contribution absent (3).

Comment: an additional state (absent) has been added to take into account the condition of Vincelestes.

230. Fossa incudis and epitympanic recess (F92): continuous (0); separated by distinct ridge (1).

231. Stapedial ratio (F90): subcircular (less than 1.8) (0); elliptical (more than 1.8) (1).

Comment: Measurements taken in extant marsupials (Segall 1970; Horovitz et al. *2008) show very variable values within a genus or even a species. For instance,* Monodelphis *exhibits values of stapedial ratio from 1.25 to 2.00 and* Philander *from 1.23 to 1.88 (Horovitz* et al. *2008). The stapedial ratio in* Andinodelphys *and* Mayulestes *are scored "?" because the fenestra vestibuli has suffered* post-mortem *distortion, being generally dorsoventrally compressed.*

232. Mastoid exposure (F77, modified): large on occiput (0); narrow (1); mastoid internal, wedged between the squamosal and exoccipital (2). **Ordered.**

233. Posttemporal notch or foramen (F96): present (0); absent (1).

234. Posttemporal sulcus on squamosal surface of petrosal: present (0); absent (1), (Ladevèze & Muizon 2007: ch. 152). Changes in the scorings of Muizon *et al.* (2018): *Pucadelphys* and *Andinodelphys*: 1 > 0 & 1.

235. Stapes (F74): collumelliform (not perforated) (0); bicrurate (perforated) (1).

236. Ectotympanic shape (F75): ring-shaped (0); transversely expanded (1)

237. Ectotympanic attachment to the skull: loose connection (no marked ridges and grooves on the skull) (0); tight attachment with marked ridges and grooves (1); fused to rostral tympanic process of petrosal (2), (Muizon, 1999: ch. 4; Babot *et al.* 2002: ch. 3). **Ordered.**

238. Squamosal at external acoustic meatus: squamosal not thickened at meatus (0); squamosal thickened at mea-

Appendix 3. — Continuation.

tus with mediolateral width mediolateral width shorter than anteroposterior length (1); squamosal thickened at meatus with mediolateral width mediolateral width longer than anteroposterior length (2), (Muizon, 1999: ch. 16; Babot *et al.* 2002: ch. 15). **Ordered.**

239. **Ascending canal:** present (0); absent (1), (Rougier *et al.* 1998: ch. 152).
240. **Contribution of squamosal to occiput**: absent or small (0); large (1), (Muizon 1999: ch. 21; Babot *et al.* 2002 ch. 19).
241. **Dorsal margin of the foramen magnum (F67)**: formed by exoccipitals, which contact medially (0); formed by the supraoccipital medially and exoccipitals, which do not contact medially (1).
242. **Connection between condylar articular facets on ventral edge of foramen magnum (F69):** absent (0); present (1).

Post-cranial characters:

243. **Atlantal foramen (F188)**: absent (0); present (1).
244. **Atlas transverse foramen (F189)**: absent (0); present (1).
245. **Ventral foramen at the base of the transverse process of the atlas (F190)**: absent (0); present (1).
246. **Posterior extent of transverse processes of the atlas (F191)**: anterior or just reach caudal facets for axis (0); extend caudally beyond level of caudal facet for axis (1).
247. **Shape of the transverse processes of the atlas**: proximodistaly short and roughly circular or quadrate (0); distinctly elongated (proximodistal length longer than transverse width) (1).
248. **Shape of the cranial facets of atlas (F193)**: concavity is roughly constant along the whole height of the facet (0); dorsal third of the facet much more concave than the ventral two thirds and strongly inflected medially (1).
249. **Atlas and intercentrum (F194)**: unfused (0); fused (1).
250. **Axis transverse foramen (F195)**: absent represented by a notch (0); present, enclosed (1).
251. **Axis, posterior extension of the neural process (F196)**: shorter or subequal than anterior extension (0); distinctly longer than anterior extension (1).

Comment: in state (1) the spinous process bears a sharp finger-like posterior process, which overhangs the C3 posteriorly and in some cases almost reaches the posterior edge of the centrum of C3.

252. **Ventral sagittal crest of axis**: roughly straight (0); distinctly concave because of the development of a robust ventral process posteriorly (1).
253. **C3-C4 ventral sagittal process (F197)**: absent (0); present (1).
254. **C5 transverse process heads in lateral view (F198 modified)**: ventral head enlarged in a ventral lamina with the dorsal head as a tubercle, dorsal to the posterior part of the ventral lamina (0); ventral (anteroventral) head triangular to rod-like and anteriorly projected with the dorsal (posterodorsal), head rod-like, posteriorly elongated, and widely separated from the anterior head; the posterodorsal head is either almost at the same level as the anteroventral one or slightly dorsal (in lateral view) and never overhangs the ventral head (1).

Comment: The two states of this character, as reformulated, more clearly describe the states originally defined by Horovitz & Sánchez-Villagra (2003). Note that state 0 is state 1 of Horovitz & Sánchez-Villagra (2003) and vice versa.

255. **C5 and T1 body length (F199)**: C5 subequal or longer than T1 (0); C5 shorter than T1.
256. **C6 spinous process (F200)**: absent or protuberance (0); lamina (1).
257. **C7 transverse foramen (F201)**: absent (0); represented by a notch (1); complete foramen (2). **Ordered.**
258. **First thoracic vertebra with a (relative to other vertebrae) tall spinous process (F203)**: T1 (0); T2 (1); T3 (2).
259. **Anticlinal vertebra (F204)**: on lumbar (0); on thoracic (1); no anticlinal vertebra (2).
260. **Foramen on dorsal arch of last lumbar vertebra (F205)**: absent (0); present (1).
261. **Mammillary processes (metapophyses) in third lumbar vertebra anterior to the last lumbar (F206)**: absent or weak (0); present (1).
262. **Ventral median keel on anterior lumbar vertebrae (F207, modified)**: absent (0); present (1).
263. **Auricular process of the sacrum (F208)**: developed on two sacral vertebrae (0); developed on one sacral vertebra (1).
264. **Size of sacral spinous process (F209):** shorter than last lumbar (0); taller than last lumbar (1).
265. **Length of the tail (F210)**: shorter than twice the length of the precaudal vertebral column (0); longer than twice the length of the precaudal vertebral column (1).
266. **Angle between scapular spine and dorsal border of infraspinatus fossa (F211)**: acute or almost right (between 80° and 95°) (0); obtuse (more than 95°) (1).
267. **Coracoid process (F212)**: large (extends beyond medial border of glenoid fossa) (0); small (just reaches medial border of glenoid fossa) (1).
268. **Distal extension of acromion process (F213)**: extends distally beyond glenoid fossa (0); does not extend distally beyond glenoid fossa (1).
269. **Anterior extension of the acromion process**: posterior to anterior edge of glenoid fossa (0); anterior or just lateral to anterior edge of glenoid fossa (1).
270. **Width of infraspinatus fossa (F214)**: less than ¼ its length (0); more than ¼ its length (1).
271. **Width of the acromion process at the level of the neck (F215)**: wider than infraspinatus fossa (0); narrower (1).

APPENDIX 3. — Continuation.

272. **Infraspinous/supraspinous fossa width at the level of the neck (F216)**: supraspinous fossa subequal of wider (0); supraspinous fossa narrower (1).
273. **Scapular notch (F217)**: more than 130° (0); between 90 and 130° (1).
274. **Clavicle (F218)**: present (0); absent (1).
275. **Medial process or rugosity for the teres major on humeral diaphysis (F219)**: absent (0); present (1).
276. **Tricipital line of humerus (F220)**: absent (0); ridge or small crest (1); massive crest continuous with deltopectoral crest (2).
277. **Capitulum for radius on humerus (F221)**: spherical (0); cylindrical (1).
278. **Entepicondylar foramen (F222)**: present (0); absent (1).
279. **Laminar supinator crest (ectepicondylar crest) (F224)**: large: proximolateral angle expanded (0); intermediate: proximolateral angle not expanded (1); absent (2).

Comment: In state 0, the angle between the proximal and lateral margins of the supinator crest is subequal or inferior to 130°. In state 1, the angle is superior to 130°.

280. **Greater tuberosity height relative to humeral head height (F225)**: subequal or lower (0); higher (1).
281. **Development of greater tuberosity in proximal view (F226)**: small (less than half the anteroposterior length of head) (0); large (greater than or equal to half the anteroposterior length of the head) (1).
282. **Extension of the deltoid crest (F227)**: restricted to proximal half of the humerus (0); reaches distal half of the humerus (1).
283. **Distal end of deltoid crest (F228)**: merging with diaphysis (0); forming a distinct angle or process (1).
284. **Relative heights of the trochlea and capitulum in anterior view (F229, modified)**: proximal extension of capitulum longer (0); subequal (1); proximal extension of trochlea longer (2).
285. **Humerus medial epicondyle size (F230)**: large (0); small (1).
286. **Humerus distal end size (F231)**: large (0); small (1).

Comment: this character is based on the ratio of transverse width of distal epiphysis without entepicondyle/transverse width of proximal epiphysis. A ratio > 0.9 is large (state 0); a ratio < 0.9 is small (state 1) (Horovitz & Sánchez-Villagra, 2003; Forasiepi, 2009).

287. **Lateral extension of capitulum (F232, modified)**: absent: capitulum rounded and regularly sloping laterally (0); present: straight with a flat shelf and/or a salient crest (1).
288. **Depth of humeral trochlea (intercondylar notch) (F233)**: wide and relatively shallow concave (0); narrow and concave posteriorly (1).
289. **Curvature of posterior border of the humeral shaft (F234)**: curved (0); straight (1).
290. **Medial development of ulnar anconeal process (F235)**: does not protrude beyond medial border of olecranon process (0); medially protruding (1).
291. **Medial curvature of the ulna (F236, modified)**: present (0); absent (1).
292. **Posterior border of the proximal half of the ulna (F237)**: convex posteriorly (0); straight or concave posteriorly (1).
293. **Shape of articular facet for the humerus on the radius (F238)**: anteroposteriorly compressed (0); circular (1).
294. **Distal shaft of the radius (F239)**: oval (wider than long) (0); rounded (almost as wide as long) (1).
295. **Prepollex (F240):** absent (0); present (1).
296. **Distolateral process of scaphoid (F241)**: absent (0); present but does not separate lunate from magnum (1); present but separates lunate from magnum (2).
297. **Number of plantar tubercles (distal heads) on trapezium (F242)**: two (0); one (1).
298. **Angle between transverse axis of proximal and distal epiphyses of metacarpal V (F243)**: absent (0); present (1).
299. **Orientation of ilium relative to ischium in lateral view (F244)**: deflected dorsally (0); aligned with ischium (1).
300. **Tuberosity for the rectus femoris muscle (F245)**: absent (0); protuberance (1); depression (2).
301. **Length of the iliac neck (F246)**: long, 15% or more the total pelvis length (0); short, less than 15% the total pelvis length (1).
302. **Greater sciatic notch (F247)**: obtuse angle (0); right or acute angle (1).
303. **Iliac and gluteus fossae (F248)**: no fossa (0); two fossae subequal in size (1); gluteous fossa larger (2).
304. **Epipubic bones (F249)**: present (0); absent (1).
305. **Proximal size of epipubic bones (F250)**: short (0); long (1).
306. **Torsion between proximal and distal epiphyses of femur (F251)**: present (0); absent (1).

Comment: The scoring of Mayulestes *is not simple because the distal epiphysis of the left femur is incomplete and the right is known by its distal epiphysis only. Furthermore, in distal view, the elevation of the lateral trochlear crest is misleading because it is distinctly higher than the medial one. Therefore, a reference line for the distal epiphysis could be the line joining the attachment area of the lateral and medial femorotibial ligaments. The attachment of the femorotibial ligament is not preserved on the left femur of the holotype, but it is present on the distal extremity of the right bone. Its position can thus be estimated on the left femur. Given that, there is apparently no significant torsion in* Mayulestes*, which is scored 1.*

307. **Height of greater trochanter relative to femoral head (F252)**: lower or subequal in height (0); higher (1).

Appendix 3. — Continuation.

308. **Lesser trochanter of femur (F253)**: present, large and blade-like (0); knob-like or absent (1).
309. **Femoral condyles (F254)**: Lateral condyle wider than medial (0); subequal (1); medial condyle wider than lateral (2). **Ordered**
310. **Ossified patella (F255)**: absent (0); present (1).
311. **Parafibula (F256)**: present (0); absent (1).
312. **Femorofibular articulation (F257)**: present (0); absent (1).
313. **Tibial length relative to femur length (F258)**: subequal to longer (0); shorter (1).
314. **Proximal dimensions of tibia (F259)**: larger mesdiolaterally than anteroposteriorly (0); subequal (1); larger anteroposteriorly than mediolaterally (2). **Ordered.**
315. **Tibia shape (F260)**: sigmoid (0); straight (1).
316. **Torsion between proximal and distal epiphyses of tibia (F261)**: present (0); absent (1).
317. **Tibia, distal articulation type (F 262)**: sagittal (0); spiral (1).

Comments: in state 0, the lateral tibioastragalar facet is curved medially and turns around the medial malleolus. Such a condition allows for some rotation of the pes during flexion-extension movements of the ankle, which tend to give a medial orientation of the plantar face of the pes. In state 1, the lateral tibioastraglar facet is anteroposteriorly oriented and allows for flexion-extension movements in sagittal plane only and the plantar face of the pes faces plantarly or posteroplantarly.

318. **Posterior extension of the lateral astragalotibial facet of tibia in distal view (F263)**: does not extend posteriorly beyond the medial astragalotibial articulation (0); extends posteriorly beyond the medial astragalotibial articulation (1).
319. **Orientation of the lateral edge of the lateral astragalotibial articular facet (in lateral view):** parallel to epiphyseal suture of the tibia (0); oblique to epiphyseal suture of the tibia (1).
320. **Anteroposterior length of the of the medial malleolus of the tibia at base relative to the greatest anteroposterior length of the distal epiphysis (as seen in distal view)**: subequal (0); medial malleolus much shorter (1).
321. **Distal malleolus of tibia (F264)**: absent or weak (0); distinct (1).
322. **Astragalus, angle between medial and lateral astragalotibial facets (F265)**: 90° (0); intermediate (1); 180° (2). **Ordered.**
323. **Astragalus, astragalonavicular facet extends onto ventromedial side of head (F266)**: absent (0); present (1).
324. **Astragalus, width and height of navicular facet in distal view (F267)**: transverse diameter > dorsoplantar diameter (0); transverse diameter < dorsoplantar diameter (1).
325. **Astragalus, visibility of medial plantar tuberosity of the astragalus in dorsal view (F268)**: not visible (0); visible (1).
326. **Astragalus, angle between lateral tibial and fibular facets (F269)**: no angle (0); with angle (1).
327. **Astragalus, medial extent of sustentacular facet (F270)**: does not reach the medial edge of the neck (0); reaches the medial edge of the neck (1).
328. **Astragalus, astragalar canal (F271)**: present (0); absent (1).
329. **Astragalus, width of astragalar neck (F272)**: neck wider than head (0); neck narrower or as wide as head (1).
330. **Malleolar shelf of the astragalus (F274)**: absent (0); present (1).
331. **Astragalus, dorso-distal tuber of the head (F275)**: absent (0); present (1).

Comments: this structure was termed "astragalo-distal tuber" by Forasiepi (2009). We instead use here the term "dorso-distal tuber of the head", which we regard as more descriptive. A dorsal tuber is present on an astragalus (MHNC 8398) *referred to* Mayulestes ferox *because its size and articular calcanear facets perfectly fit the condition oberved on the calcaneus of the holotype (CM, personal observations). Furthermore, a distinct dorsal tuber is also observed in* Pucadelphys *and* Andinodelphys.

332. **Astragalus, connection between astragalo-navicular (or cuboid) facet and sustentacular facet (F276)**: present (0); absent (1).
333. **Astragalo-cuboid facet on astragalar head**: present (0); absent (1).
334. **Calcaneus, longest dimension of ectal facet (F277, modified)**: anteromedial-posterolateral (0); anteroposterior (1); transverse (2); anterolateral-posteromedial (3).
335. **Calcaneus, orientation of the calcaneoastragalar (ectal) facet (F278)**: mostly medial (0); Intermediate (1); mostly dorsal (2). **Ordered.**
336. **Calcaneal peroneal process (F279, modified)**: present as a salient and dorsoplantarly thick protuberance (0); present but reduced to a thin crest (1) absent or faint (2). **Ordered.**
337. **Calcaneus, position of the peroneal process (F280)**: at the level of the edge of the cuboid facet (0); proximal to the level of the edge of the cuboid facet (1).
338. **Calcaneal peroneal groove for the peroneous longus (F281)**: indistinct or weakly developed (0); distinct and deeply grooved (1).
339. **Calcaneus, position of the sustentaculum (F282)**: reaches anterior end of calcaneus (0); subterminal (1).
340. **Calcaneus, outline of sustentacular process (F283)**: triangular or rounded (0); rectangular (1).
341. **Calcaneus, orientation of sustentacular facet in distal view (F284)**: mostly medial (0); mostly dorsal (1).
342. **Calcaneus, orientation of sustentacular facet in medial view (F285)**: fully dorsal (0); *c.* 45° dorsodistally (1).

APPENDIX 3. — Continuation.

Comment: Contra *Horovitz & Sánchez-Villagra (2003), we consider that taxa scored with a medial orientation of the sustentacular facet (state 0) can be scored on the anteroposterior orientation of the sustentacular facet.*

343. **Calcaneus, sustentacular facet morphology (F286)**: slightly concave or flat (0); posteriorly convex (1).
344. **Calcaneus, secondary distal calcaneoastragalar facet (F287)**: absent (0); present (1).
345. **Calcaneus, sustentacular and posterior calcaneoastragalar facets (F288)**: separated (0); merged (1).
346. **Calcaneal facet for fibula (F289)**: present (0); absent (1).
347. **Orientation of the calcaneal facet for the fibula (F290)**: dorsal (0); lateral (1).
348. **Length of the tuber calcis (F291)**: longer than the body (0); as long as or shorter than the body (1).
349. **Medial curvature of the tuber calci (F292)**: present (0); absent (1).
350. **Ventral curvature of the tuber calcis (F293)**: present (0); absent (1).
351. **Calcaneus, Notch for cuboid pivot on calcaneocuboid facet (F294)**: absent (0); present (1).
352. **Calcaneus, angle between proximal and distal areas of calcaneocuboid facet (F295)**: no angle (0); oblique facet (1).
353. **Spatial relationship between navicular and entocuneiform (F296)**: entocuneiform distal to navicular (0); entocuneiform extends proximally and medial to the distal area of the navicular (1).
354. **Angle between navicular and distal metatarsal facets of ectocuneiform (F297)**: oblique (0); parallel to the distal facet (1).
355. **Prehallux (F298)**: absent (0); present (1).
356. **Metatarsal V proximal process (F299)**: does not extend ventral to cuboid (0); extends ventral to cuboid (1).
357. **Proximal ends of metatarsal II and III (F300)**: subequal in length (0); Mt II extends more proximally than Mt III (1).
358. **Ridge on proximal articular facet of metatarsal I (F301)**: absent (0); present (1).
359. **Mt III thickness relative to that of Mt IV (F302)**: Mt III thicker or subequal to Mt IV (0); Mt III thinner (1).
360. **Mt III thickness relative to that of Mt I (F303)**: Mt I thicker or subequal than Mt III (0); Mt III thinner than Mt I (1).
361. **Median keel on palmar/plantar surface of metapodials (F304)**: sharp (0); blunt (1).
362. **Foot ungual phalanx of digit IV in proximal view (F305)**: larger dorsoventrally than mediolaterally (0); larger mediolaterally than dorsoventrally (1).
363. **Ungual phalange (F306)**: uncleft (0); cleft (1).
364. **Dorsal border of ungual phalanges (F307)**: crest-like (0); rounded (1).

APPENDIX 4. — Taxon list, references, and specimens

Aenigmadelphys archeri; casts of OMNH 20120, 20160, 20531, 20612, 22898, 23321, 23375, 23460, 26169; Cifelli & Johanson (1994);
Alcidedorbignya inopinata: MHNC 1210, 8282, 8287, 8290, 8295, 8298, 8300, 8315, 8359-8363, 8371, 8372, 8373, 8399-8463, 13830-13845;
Allqokirus australis: YPFB pal 6188, 6189, 6190, MHNC 8267; Marshall & Muizon (1988), Muizon (1992);
Alphadon spp: Eaton (1993);
Alphadon: A. eatoni: Cifelli & Muizon 1998; *A. marshi* (casts of UCMP 47464, 47497, 51385, 51428, 51585, 52502, 52506); *A. wilsoni* (casts of UCMP 46403, 46885, 52767);
Andinodelphys cochabambensis: MHNC 8264, 8306, 8308, 8370, 13847, 13925 13927, 13928 (Five sub-complete skulls and four subcomplete to partial skeletons); Marshall & Muizon (1988), Muizon (1992), Muizon *et al.* (1997), Muizon & Argot (2003).
Arctodictis sinclairi: MLP 85-VII-3-1; Forasiepi (2009);
Asiatherium reshetovi: cast and original specimen of PIN 3907; Szalay & Trofimov (1996);
Asioryctes nemegtensis: cast of ZPAL MgM-I/56 and I/98; Kielan-Jaworowska (1975a, 1977, 1981, 1984); Horovitz & Sánchez-Villagra (2003); Wible *et al.* (2004, 2009);
Atokatheridium boreni: Kielan-Jaworowska & Cifelli (2001); Davis *et al.* (2008); Davis & Cifelli (2011);
Australohyaena antiqua: Forasiepi *et al.* (2015);
Australopediomys marshalli : Cast of DGM 808-M; Carneiro *et al.* (2018);
Barinya wangala: Wroe (1999);
Barunlestes butleri: Kielan-Jaworowska & Trofimov (1980);
Borhyaena tuberata: YPM-PU 15120, 15701, MACN 2074; Sinclair (1906) Cabrera (1927), Marshall (1981);
Callistoe vincei: PVL 4187; Babot *et al.* (2002);
Caluromys lanatus: MNHN-ZM-MO-1929-650; MNHN-ZM-MO-1929-651; MNHN-ZM-MO-1929-652; MNHN-ZM-MO-1932-2999;
Caluromys philander: MNHN-ZM-MO-1986-140; MNHN-ZM-MO-1986-142; MNHN-ZM-MO-1986-143;
Caluromysiops irrupta: Voss & Jansa (2009);
Chironectes minimus: MNHN-ZM-MO-1995-202, MNHN-ZM-MO-1932-2860; Voss & Jansa (2009);
Cladosictis patagonica: MNHN.F.SCZ143, SCZ146, YPM-PU15170, YPM-PU15702, YPM-PU15705, YPM-PU15046. Sinclair (1906), Cabrera (1927), Patterson (1965), Marshall (1981), Argot (2003);
Cryptonanus spp*:* Voss & Jansa (2009);
Dasycercus byrnei: MNHN-ZM-MO-1897-1489;
Dasyurus hallucatus: MNHN-ZO-MO-1854-99, ZO-MO-1880-1019, ZO-MO-1871-84;
Dasyurus maculatus: MNHN-ZO-AC-A3295, ZM-MO-1994-2140, ZM-MO-1865-32; FMHN 119806, 119805, 119804, 119803;
Dasyurus viverrinus: MNHN-ZM-AC-A2626, ZM-AC-A2627, ZM-AC-A3315, ZM-MO-1882-563, ZM-MO-1883-1537;
Deltatheridium praetrituberculare: casts of ZPAL MgM-I/102, ZPAL MgM-I/91, PSS-MAE 132 and 133; Kielan-Jaworowska (1975b); Kielan-Jaworowska & Nessov (1990); Marshall & Kielan-Jaworowska (1992); Rougier *et al.* (1998);
Deltatheroides cretacicus: Gregory & Simpson (1926); Kielan-Jaworowska (1975b), Rougier *et al.* (2004);
Didelphis albiventris: MNHN-RH24, RH120, RH161, MNHN-RH uncat.;
Didelphis virginiana SL uncat., MNHN-ZM-2007-7, MNHN-ZM-2007-12;
Didelphis marsupialis: MNHN-ZM-MO-1900-581, MNHN-ZM-MO-1900-583, MNHN-ZM-MO-1932-3003, MNHN-ZM-2007-8;
Didelphodon vorax: cast of USNM 2136, UCMP 52326, 46946, 52342, 51419, 46962, 48189, 48581, 52290, 47304, 53181, 52289. CT data of NDGS 431; UWBM 94500, 94084; SCNHM VMMa 20. Clemens (1966, 1968), Fox & Naylor (1986); Wilson *et al.* (2016);
Dromiciops gliroides: IEEUACG 2162, IEEUACG 2167; FMNH 22675, FMNH 134556;
Eodelphis browni: cast of AMNH 14169; Matthew (1916), Fox (1981); Fox & Naylor (2006); Scott & Fox (2015);
Epidolops ameghinoi: Beck (2017);
Gobiconodon ostromi: Luo *et al.* (2003);
Gracilinanus spp: Voss & Jansa (2009);
Haldanodon: Lillegraven & Krusat (1991);
Herpetotherium cf. *fugax*: PIMUZ 2613, MB.Ma 50671, 50672; SMF 2000/168, 2000/169; Gabbert (1998); Horovitz *et al.* (2008, 2009);
Herpetotherium fugax: AMNH 5254; FMNH P25654, P25653, P15329; Fox (1983), Gabbert (1998);
Hondadelphys fieldsi: Photos of UCMP 37960; Marshall (1976b);
Hyladelphys kalinowskii: Voss & Jansa (2009);
Incadelphys antiquus: YPFB Pal 6251;
Itaboraidelphys camposi: casts of DGM 804-M, 814-M, 817-M, 923-M, 926-M; MNRJ 2878-V a and b; Marshall & Muizon (1984);
Kennalestes gobiensis: Kielan-Jaworowska (1969, 1977, 1981); Wible *et al.* (2009), casts of ZPALMgM-I/2 and I/3;
Kokopellia juddi: OMNH 26361, 34200, 33248, 33243, 27639. Cifelli (1993); Cifelli & Muizon (1997);
Kyrptobaatar dashzevegi: Wible & Rougier (2000);
Leptictis dakotensis: AMNH 80213; AMNH FAM 87458; cast of AMNH 108194; Novacek (1986); Rose (1999); Rose (2006); Wible *et al.* (2009);
Lestodelphys halli: Voss & Jansa (2009);
Lotheridium mengi: Bi *et al.* (2015); Bi, personnal communications to CM
Lutreolina crassicaudata: Voss & Jansa (2009);
Lycopsis longirostris: Photos of UCMP 38061; Marshall (1977);
Maelestes gobiensis: PPS-MAE-607, Wible *et al.* (2009);
Marmosa murina: MNHN-ZM-MO-2001-1428, MNHN-ZM-MO-2001-1464, MNHN-ZM-MO-2001-1966, MNHN-ZM-MO-2001-1967;

APPENDIX 4. — Continuation.

Marmosops spp: Voss & Jansa (2009);
Mayulestes ferox: MHNC 1249 (holotype);
Megazostrodon rudnerae: Gow (1986), Luo *et al.* (2007);
Metachirus nudicaudatus: MNHN-RH16, RH81, MNHN-RH uncat., MNHN-ZM-AC-2175, MNHN-ZM-2004-316, MNHN-ZM-MO-2001-1422, MNHN-ZM-MO-1985-1803;
Micoureus demerarae: MNHN-ZM-MO-2001-1481;
Mimoperadectes houdei: USNM 482355. Horovitz *et al.* (2009); *M. labros*: UM 66144
Mizquedelphys pilpinensis: YPFB Pal 6196, MHNC 13917;
Monodelphis brevicaudata: MNHN-ZM-AC-258-M, MNHN-ZM-2004-317, MNHN-ZM-MO-1995-3216, ZM-MO-1967-330. Wible (2003);
Monodelphopsis travassosi: casts of M.N.R.J. No. 1365-V and DGM 807-M;
Morganucodon spp: Kermack *et al.* (1981);
Myrmecobius fasciatus: AMNH 155328, MNHN-ZM-AC-A2564;
Nanocuris improvida: Fox *et al.* (2007), Wilson & Riedel (2010);
Nimbacinus dicksoni: stl files of QMF36357; Wroe & Musser (2001);
Notogale mitis: MNHN.F.SAL94, SAL95, SAL97, SAL271; Petter & Hoffstetter (1983), Muizon (1999);
Notoryctes spp: MNHN-ZM-MO-1962-2587, MNHN-ZM-AC-1931-717; AMNH 202107;
Oklatheridium szalayi: Davis *et al.* (2008), Davis & Cifelli (2011);
Paraborhyaena boliviana: MNHN.F.SAL51. Petter & Hoffstetter (1983);
Patene simpsoni: MNHN.F.ITB1, cast of AMNH 49805, DGM 324-M, DGM 654-M, DGM 655-M, 657-M, DGM 659-M, 656-M, MNRJ 1331-V, MNRJ 1332-V, MNRJ 1341-V, MNRJ 1351-V, photos of PVL 2618. Casts of uncatalogued Itaboraí specimens of DGM, with MNHN catalogue numbers: MNHN.F.ITB8, ITB9, ITB11, ITB63, ITB64. Paula Couto (1952a), Marshall (1981), Goin *et al.* (1986);
Patene coloradensis: Photos of PLV 2618, Goin *et al.* (1986); Rangel *et al.* (2019);
Patene coluapiensis: cast of AMNH 28448; Marshall (1981);
Pediomys spp: Rougier *et al.* (1998), Luo *et al.* (2003), Forasiepi (2009);
Pediomyids: *Pediomys elegans*: cast of UCMP 51406, 47049, 47527, 52719, 47478, 47035, 50293; cast of AMNH 58809, 58768, 58748; *Protolambda hatcheri*: cast of UCMP 46881, 48157, 46847, 53205, 53206; *Protolambda florencae*: cast of UCMP 48384, 47283, 47433, 46344, 51440; *Leptalestes krejcii*: UCMP 47039, 46412, 51390, 51368, 51373; *Leptalestes cooki*: cast of UCMP 47738, 46400, 51613, 51434, AMNH 58756;
Peradectes elegans: cast of AMNH17383; *P. chesteri*: cast of UM71663; Crochet 1980;
Peratherium spp: MNHN.F.AU2370, QU8061.R, QU8062.R, QU8063.R, QU8214, QU13371; Crochet (1980);
Philander opossum: MNHN-ZM-MO-1986-485, MNHN-ZM-MO-2000-215, MNHN-ZM-MO-1998-2264 MNHN-ZM-2012-21;
Planigale spp: Archer (1976b);
Prokennalestes trofimovi: PSS-MAE 136; Kielan-Jaworowska & Dashzeveg (1989); Sigogneau-Russell *et al.* (1992); Wible *et al.* (2001); Lopatin & Averianov (2017)
Protaplphadon lulli: (casts of UCMP 46882, 47047, 47475; AMNH 58758); Clemens (1966);
Prothylacynus patagonicus: MACN 705, 707 (same individual), MACN 642, YPM-PU 15700, MACN 5931; Sinclair (1906), Cabrera (1927), Marshall (1979b);
Pseudantechinus macdonnelensis: MNHN-ZM-MO-1897-1492;
Pucadelphys andinus: MHNC 8265, 8266, 8365, 8376-8395 (all specimens are complete or partial skulls and mandible);
Repenomanus robustus: Hu *et al.* (2005);
Sallacyon hoffstetteri: MNHN.F.SAL92, 93. Petter & Hoffstetter (1983);
Sarcophilus spp: MNHN-ZM-MO-1874-291, MNHN-ZM-2007-15;
Sillustania quechuense: cast of CHU 33, 34;
Sipalocyon gracilis: YPM PU 15373, 15154, 15029, AMNH 9254, MACN 691, 692, Sinclair (1906), Cabrera (1927), Marshall (1981);
Sminthopsis crassicaudata: MNHN-ZM-2007-18, FMNH 60116; FMNH 104788;
Sminthopsis sp.: MNHN-ZO-AC-1919-30, 1892-660;
Sparassocynus heterotopicus: Reig & Simpson (1972);
Sulestes karakshi and *Sulestes* sp.: Kielan-Jaworowska & Nessov (1990), Averianov *et al.* (2010);
Szalinia gracilis: MHNC 8350;
Thylacinus cynocephalus: MNHN-ZM-AC-A2620, ZM-AC-A2621, ZM-AC-A3299, ZM-AC-A3298, ZM-AC-A12413;
Thylacosmilus atrox: cast of FMNH P 14531. Riggs (1934), Turnbull & Segall (1984), Goin & Pascual (1987);
Thylamys elegans: MNHN-ZM-MO-1971-1040, MNHN-ZM-MO-1971-1041, MNHN-ZM-MO-1971-1042, MNHN-ZM-MO-1971-1043;
Tlacuatzin canescens: Voss & Jansa (2009);
Turgidodon spp: *T. rhaister* (casts of UCMP 48221, 50282, 521346, 52413, 52461, 52483); *T. madseni* (casts of OMNH 20538, 20589); *T. lillegraveni* (casts of OMNH 20530, 20540); Cifelli (1990);
Varalphadon spp*: V. wahweapensis* (casts of OMNH 20109, 20115, 20123, 20536, 20587, V4516, V4574); *V. janetae*: Carneiro (2018);
Vincelestes neuquenianus: Cast of MACN-N04; photographs the ear region of this specimen, MACN-N05, and MACN-N09 kindly provided by G. Rougier; Rougier *et al.* (1992); Bonaparte & Rougier (1987);
Wynyardia bassiana: Jones (1930);
Zalambdalestes lechei: PSS-MAE 108, 130, Kielan-Jaworowska (1984); Kielan-Jaworowska & Trofimov (1980); Wible *et al.* (2004, 2009).

APPENDIX 5. — List of genus and species names cited in the text with authorship and year.

Zhangheotherium quinquecuspidens: Hu *et al.* (1997).
Aenigmadelphys Cifelli & Johanson, 1994
Aenigmadelphys archeri Cifelli & Johanson, 1994
Alcidedorbignya Muizon & Marshall, 1987
Alcidedorbignya inopinata Muizon & Marshall, 1987
Allqokirus Marshall & Muizon, 1988
Allqokirus australis Marshall & Muizon, 1988
Alphadon Simpson, 1927
Alphadon lulli Clemens, 1966
Alphadon eatoni Cifelli & Muizon, 1998
Ambolestes Bi, Zheng, Cignetti, Yang, & Wible, 2018
Amphiperatherium Filhol, 1879
Andinodelphys Marshall & Muizon, 1988
Andinodelphys cochabambensis Marshall & Muizon, 1988
Aquiladelphis Fox, 1971
Arctodictis Mercerat, 1891
Arctodictis sinclairi Marshall, 1978
Asiatherium Trofimov & Szalay, 1994
Asiatherium reshetovi Trofimov & Szalay, 1994
Asioryctes Kielan-Jaworowska, 1975
Asioryctes nemegtensis Kielan-Jaworowska, 1975
Atokatheridium Kielan-Jaworowska & Cifelli, 2001
Australohyaena Forasiepi, Babot, & Zimicz, 2015
Australohyaena antiqua Forasiepi, Babot, & Zimicz, 2015
Austropediomys Carneiro, Oliveira & Goin, 2018
Austropediomys marshalli Carneiro, Oliveira & Goin, 2018
Barinya Wroe, 1999
Barinya wangala Wroe, 1999
Borhyaena Ameghino, 1887
Borhyaena tuberata Ameghino, 1887
Callistoe Babot, Powell & Muizon, 2002
Caluromys Allen, 1900
Caluromys lanatus Olfers, 1818
Caluromys philander Linnaeus, 1758
Caluromysiops Sanborn, 1951
Chironectes Illiger, 1811
Chironectes minimus (Zimmermann, 1780)
Cladosictis Ameghino, 1887
Cryptonanus Voss, Lunde & Jansa, 2005
Dakotadens Eaton, 1993
Dasycercus Petters, 1875
Dasyuroides Spencer, 1896
Dasyuroides byrnei Spencer, 1896
Dasyurus Geoffroy Saint-Hilaire, 1796
Dasyurus hallucatus Gould, 1842
Dasyurus maculatus (Kerr, 1792)
Dasyurus viverrinus (Shaw, 1800)
Deltatheridium Gregory & Simpson, 1926
Deltatheridium pretrituberculare Gregory & Simpson, 1926
Deltatheroides Gregory & Simpson, 1926
Deltatheroides cretacicus Gregory & Simpson, 1926
Didelphis Linnaeus, 1758
Didelphis albiventris Lund, 1840
Didelphis marsupialis Linnaeus, 1753
Didelphis virginiana Kerr, 1792
Didelphodon Marsh, 1899
Didelphodon vorax Marsh, 1899
Dromiciops Thomas, 1894
Dromiciops gliroides Thomas, 1894
Eodelphis Matthew, 1916
Eodelphis browni Matthew, 1916
Epidolops Paula Couto, 1952a
Epidolops ameghinoi Paula Couto, 1952a
Gobiconodon Trofimov, 1978
Haldanodon Kühne & Krusat, 1972
Herpetotherium Cope, 1873
Herpetotherium fugax Cope, 1873
Hondadelphys Marshall, 1976
Hyladelphys Voss, Lunde & Simmons, 2001
Iqualadelphis Fox, 1987
Incadelphys antiquus Marshall & Muizon, 1988
Itaboraidelphys Marshall & Muizon, 1984
Itaboraidelphys camposi Marshall & Muizon, 1984
Juramaia Luo, Yuan, Meng, & Ji, 2011
Kennalestes Kielan-Jaworowska, 1968
Kennalestes gobiensis Kielan-Jaworowska, 1968
Kokopellia Cifelli, 1993
Kokopellia juddi Cifelli, 1993
Kryptobaatar Kielan-Jaworowska, 1969
Lestodelphys Tate, 1934
Leptictis Leidy, 1868
Lotheridium Bi, Jin, LI & Du, 2015
Lotheridium mengi Bi, Jin, LI & Du, 2015
Lutreolina Thomas, 1910
Lycopsis Cabrera, 1927
Lycopsis longirostris Marshall, 1976
Maelestes Wible, Rougier, Novacek, & Asher, 2007
Maelestes gobiensis Wible, Rougier, Novacek, & Asher, 2007
Marmosa Gray, 1821
Marmosa murina Linnaeus, 1758
Marmosops Matschie, 1916
Mayulestes Muizon, 1994
Mayulestes ferox Muizon, 1994
Megazostrodon Crompton & Jenkins, 1968
Metachirus Burmeister, 1854
Metachirus nudicaudatus Geoffroy Saint-Hilaire, 1803
Micoureus Lesson, 1842
Micoureus demerarae (Thomas, 1905)
Mimoperadectes Bown & Rose, 1979
Mimoperadectes houdei Horovitz, Martin, Bloch, Ladevèze, Kurz & Sánchez-Villagra, 2009
Mimoperadectes labrus Bown & Rose, 1979
Mizquedelphys Marshall & Muizon, 1988
Mizquedelphys pilpinensis Marshall & Muizon, 1988
Monodelphis Burnett, 1830
Monodelphis brevicaudata (Erxleben, 1777)
Monodelphopsis, Paula Couto, 1952
Monodelphopsis travassosi, Paula, Couto 1952

APPENDIX 5. — Continuation.

Morganucodon Kühne, 1949
Myrmecobius Waterhouse, 1836
Myrmecobius fasciatus Waterhouse, 1836
Nanocuris Fox, Scott & Bryant, 2007
Nimbacinus Muirhead & Archer, 1990
Nimbacinus dicksoni Muirhead & Archer, 1990
Notogale Loomis, 1914
Notogale mitis (Ameghino, 1897)
Notoryctes Stirling, 1891
Oklatheridium Davis, Cifelli & Kielan-Jaworowska, 2008
Pappotherium Slaughter, 1965
Paraborhyaena Hoffstetter & Petter, 1983
Paraborhyaena boliviana Hoffstetter & Petter, 1983
Patene Simpson, 1935
Patene coluapiensis Simpson, 1935
Patene simpsoni Paula Couto, 1952a
Pediomys Marsh, 1889
Peradectes Matthew & Granger, 1921
Peratherium Aymard, 1850
Philander Brisson, 1762
Philander opossum (Linnaeus, 1758)
Planigale Troughton, 1928
Prokennalestes Kielan-Jaworowska & Dashzeveg, 1989
Prokennalestes trofimovi Kielan-Jaworowska & Dashzeveg, 1989
Prothylacynus Ameghino, 1891
Prothylacynus patagonicus Ameghino, 1891
Protolambda Davis, 2007
Protolambda hatcheri (Osborn, 1898)
Pseudantechinus Spencer, 1896
Pseudantechinus macdonnelensis Spencer, 1896
Pucadelphys Marshall & Muizon, 1988
Pucadelphys andinus Marshall & Muizon, 1988
Repenomanus Hu, Meng & Li, 2005
Sallacyon Villarroel & Marshall, 1982
Sallacyon hoffsteteri Villarroel & Marshall, 1982
Sarcophilus Geoffroy Saint-Hilaire & Cuvier, 1837
Sipalocyon Ameghino, 1887
Sipalocyon gracilis Ameghino, 1887
Sminthopsis Thomas, 1887
Sminthopsis crassicaudata (Gould, 1844)
Solenodon Brandt, 1833
Solenodon paradoxus Brandt, 1833
Sulestes Nessov, 1985
Sulestes karakshi Nessov, 1985
Sparassocynus Reig & Simpson, 1972
Swaindelphys: Johanson, 1996
Swaindelphys cifellii: Johanson, 1996
Szalinia Muizon & Cifelli, 2001
Szalinia gracilis Muizon & Cifelli, 2001
Thylacinus Temminck, 1824
Thylacinus cynocephalus (Harris, 1808)
Thylacosmilus Riggs, 1934
Thylacosmilus atrox Riggs, 1934
Thylamys Gray, 1843
Thylamys elegans Waterhouse, 1839
Tlacuatzin Voss & Jansa, 2003
Turgidodon Cifelli, 1990
Varalphadon Johanson, 1996
Varalphadon creber Fox, 1971
Varalphadon janetae Carniero, 2018
Varalphadon wahweapensis
Vincelestes Bonaparte, 1986
Vincelestes neuquenianus Bonaparte, 1986
Wynyardia Spencer, 1901
Wynyardia bassiana Spencer, 1901
Zalambdalestes Gregory & Simpson, 1926
Zalambdalestes lechei Gregory & Simpson, 1926
Zhangheotherium Hu, Wang, Luo & Li, 1997